AFML-TR-76-244
Part I

ADA041490

BIAXIAL TESTING OF GRAPHITE/EPOXY COMPOSITES CONTAINING STRESS CONCENTRATIONS

IIT RESEARCH INSTITUTE
10 W. 35th STREET
CHICAGO, ILLINOIS 60616

DDC

JUL 11 1977

DECEMBER 1976

TECHNICAL REPORT AFML-TR-76-244
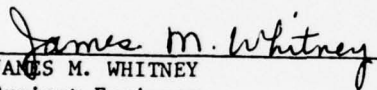FINAL REPORT FOR PERIOD APRIL 1975 - SEPTEMBER 1976

AU No.
DDC FILE COPY

AIR FORCE MATERIALS LABORATORY
AIR FORCE WRIGHT AERONAUTICAL LABORATORIES
AIR FORCE SYSTEMS COMMAND
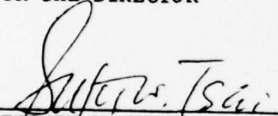WRIGHT-PATTERSON AIR FORCE BASE, OHIO 45433

JAMES M. WHITNEY
Project Engineer

FOR THE DIRECTOR

STEPHEN W. TSAI, Chief
Mechanics & Surface Interactions Branch
Nonmetallic Materials Division

REPORT DOCUMENTATION PAGE		READ INSTRUCTIONS BEFORE COMPLETING FORM
1. REPORT NUMBER AFML-TR-76-244 - Part I	2. GOVT ACCESSION NO.	3. RECIPIENT'S CATALOG NUMBER
4. TITLE (and Subtitle) Biaxial Testing of Graphite/Epoxy Composites Containing Stress Concentrations. Part I		5. TYPE OF REPORT & PERIOD COVERED Final- Part I 4/1/75 - 9/30/76
		6. PERFORMING ORG. REPORT NUMBER
7. AUTHOR(s) I.M. Daniel		8. CONTRACT OR GRANT NUMBER(s) F33615-75-C-5113
9. PERFORMING ORGANIZATION NAME AND ADDRESS IIT Research Institute 10 W. 35th Street Chicago, Illinois 60616		10. PROGRAM ELEMENT, PROJECT, TASK AREA & WORK UNIT NUMBERS 73400398
11. CONTROLLING OFFICE NAME AND ADDRESS Air Force Materials Laboratory (AFML/MBM) Air Force Wright Aeronautical Laboratories Wright-Patterson AFB, Ohio 45433		12. REPORT DATE December 1976
		13. NUMBER OF PAGES 238
14. MONITORING AGENCY NAME & ADDRESS(if different from Controlling Office) Wright-Patterson Air Force Base, Ohio 45433		15. SECURITY CLASS. (of this report) Unclassified
		15a. DECLASSIFICATION/DOWNGRADING SCHEDULE

16. DISTRIBUTION STATEMENT (of this Report)

Approved for public release, distribution unlimited

17. DISTRIBUTION STATEMENT (of the abstract entered in Block 20, if different from Report)

18. SUPPLEMENTARY NOTES

19. KEY WORDS (Continue on reverse side if necessary and identify by block number)
Graphite/Epoxy composites, stress concentrations, biaxial testing, holes, cracks, failure criteria, failure modes, notch size effect, crack propagation, strength reduction, strain gages, photoelastic coatings, moire, strain distributions.

20. ABSTRACT (Continue on reverse side if necessary and identify by block number)
An experimental program was conducted to study the behavior under uniaxial and biaxial tensile loading of quasi-isotropic graphite/epoxy plates with circular holes and through-the-thickness cracks and to determine the influence of notch size on failure. Experimental stress analysis techniques used were strain gages, photoelastic coatings and moire grids. Recorded failure strains at the notch have exceeded twice the ultimate strain of the unnotched laminate. In specimens with circular holes failure initiates ———

DD FORM
1 JAN 73 1473   EDITION OF 1 NOV 65 IS OBSOLETE   UNCLASSIFIED

20.   ABSTRACT (Cont'd)

cont ───> at characteristic points of high strain concentration with
nonlinear response located at 22.5-deg. from some or all
fiber directions. Failure at the crack tip in the form of
a damage zone propagates usually along one of the fiber
directions. Failure occurs when this damage zone reaches
some critical value. There also seems to exist a threshold
notch size below which the laminate becomes notch-insensitive.
At least under uniaxial loading, it was found that the
notch strength for the laminate studied is independent of
notch geometry. Notch size effect can be satisfactorily
explained and predicted using as a failure criterion the
stresses averaged over a distance of 3-5 mm from the notch
boundary. The strength reduction of plates with holes under
equal biaxial loading is approximately 30 percent lower than
under uniaxial loading and the two cases represent upper
and lower bounds. Biaxial tests of plates with cracks
reveal the important contribution to failure of the far-field
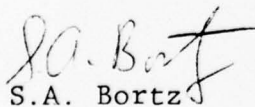shear component.
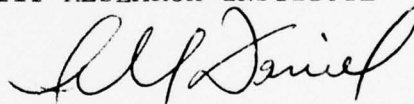
FOREWORD

This is the Final Report on IIT Research Institute Project D6108, "Biaxial Testing of Graphite/Epoxy Composites Containing Stress Concentrations," prepared by IITRI for the Air Force Materials Laboratory, under Contract No. F33615-75-C-5113. The work described in this report was conducted in the period April 1, 1975 to September 30, 1976. Dr. J.M. Whitney, AFML/MBM, was the project engineer. Dr. I.M. Daniel of IITRI was the principal investigator. Additional contributions to the work reported herein were made by Dr. T. Liber and Messrs. W. Hartrick, L. Korso, R. LaBedz, T. Niiro, B. Nowak, M. Senninger and T. Todner.

Respectfully submitted,
IIT RESEARCH INSTITUTE

I.M. Daniel
Science Advisor
Mechanics of Materials Division

APPROVED:

S.A. Bortz
Assistant Director
Mechanics of Materials Division

iii

TABLE OF CONTENTS

TABLE OF CONTENTS
(Continued)

ILLUSTRATIONS

ILLUSTRATIONS
(Continued)

ILLUSTRATIONS
(Continued)

ix

ILLUSTRATIONS
(Continued)

ILLUSTRATIONS
(Continued)

ILLUSTRATIONS
(Continued)

xiii

ILLUSTRATIONS
(Continued)

ILLUSTRATIONS
(Continued)

xv

ILLUSTRATIONS
(Continued)

xvii

ILLUSTRATION
(Continued)

xix

ILLUSTRATIONS
(Continued)

ILLUSTRATIONS
(Continued)

TABLES

SECTION I

INTRODUCTION

Advanced filamentary composites are finding increasing
applications in more critical aircraft components such as
fuselage, wing, control surface panels and engine fan blade
and containment structures. While composites offer significant
potential strength and weight advantages, it is necessary that
they also meet current Air Force design criteria of damage
tolerance. In order to employ these composites in design with
more confidence it is necessary to evaluate their tolerance to
flaws and stress concentrations.

The problem of stress distribution around a cutout in a
composite plate has been treated analytically using linear
anisotropic elasticity (References 1,2) and finite element
methods (References 3-8). The latter can be used to account
for material inhomogeneity, nonlinearity, and inelasticity.
Related analytical failure studies have been limited. Experimental
methods using strain gages, photoelastic coatings and moire
grids have proven very useful in verifying theoretical solutions
in the linear range and complementing them in the nonlinear
range (References 9-14). Experimental methods are especially
useful in studying failure modes.

Most of the failure analyses of composites with stress
concentrations, such as holes or cracks, are based on the
assumption of linear material behavior and on failure criteria
carried over from isotropic materials.   Greszczuk (Reference 15),
for example, used a form of the Hill criterion based on distortion
energy to determine the ultimate load and location of failure
on the hole boundary. Waddoups, Eisenmann and Kaminski
(Reference 16) analyzed failures in composite plates with holes

1

using linear elastic fracture mechanics and assuming the existence of two fictitious Griffith type cracks on the boundary of the hole. No physical interpretation was given to these fictitious cracks. Cruse (Reference 17) analyzed a similar problem by modeling the circular hole with a straight crack having an equivalent stress distribution near its tip. Recently, Whitney and Nuismer (Reference 18) proposed simplified stress fracture criteria which explain discontinuity size effects without applying linear elastic fracture mechanics. They are based on the actual stress distributions near the discontinuity and assume the existence of a characteristic dimension. According to one criterion proposed, failure occurs when the average stress over this characteristic dimension equals the unnotched tensile strength of the material. Comparison with results from uniaxial tensile tests showed satisfactory agreement between predicted and measured strengths for a narrow range of values of the characteristic dimension.

Most of the analytical and experimental work above is limited to uniaxially loaded laminates. Very little work has been reported on the behavior of such laminates with stress concentrations under biaxial states of stress. The inhomogeneity of the material, the nonlinearity of response near failure and the complex interaction of failure modes near notches make it very difficult to predict biaxial behavior on the basis of uniaxial response. An experimental approach dealing directly with biaxial loading of composite plates with stress concentrations is therefore very important.

The objective of this investigation was to study experimentally the deformation and failure under biaxial tensile loading of graphite/epoxy plates containing circular holes and cracks of various sizes and to determine the influence of notch size on failure. This study was limited to a quasi-isotropic laminate.

2

The program consisted of testing uniaxial unnotched and notched specimens and biaxial notched specimens. The approach used was to measure deformations by means of experimental strain analysis techniques, determine strain concentrations, strain distributions failure modes and strength reduction ratios. Whenever possible results are compared with analytical predictions.

SECTION II

MATERIAL QUALIFICATION AND CHARACTERIZATION

1. MATERIAL QUALIFICATION

The graphite/epoxy system selected was the SP-286T300 manufactured by the 3M Company. It is made of Thornel 300 fibers impregnated with SP-286 resin. A quantity of 50 lb of 12 in. wide and 0.005 in. thick prepreg tape was procured.

The graphite/epoxy material received was qualified by determining its flexural and interlaminar shear strengths from unidirectional coupons. The prepreg material was cured according to the following curing cycle:

1) Insert bagged layup into cold autoclave and apply full vacuum.

2) Pressurize autoclave to 690 kPa (100 psi).

3) Raise temperature at 2.8 degK (5°F) per minute to 393 degK (250°F).

4) Release vacuum.

5) Raise temperature at 2.8 degK (5°F) per minute to 448 degK (350°F) and hold for 2 hours.

6) Allow to cool to room temperature.

7) Postcure at 478 degK (400°F) for 6 hours in air circulating oven.

A 15.2 cm x 15.2 cm (6 in. x 6 in.) unidirectional plate, 15-plies thick, was fabricated for qualification testing. Flexural strength coupons were 10.2 cm (4 in.) long, 1.3 cm (0.5 in.) wide with a 6.3 cm (2.5 in.) span length. Interlaminar

4

shear strength coupons were 1.5 cm (0.6 in.) long, 0.6 cm (0.25 in.) wide with a 1 cm (0.4 in.) span length. These specimens were subjected to three-point bending. Results of these qualification tests are tabulated below:

TABLE I

QUALIFICATION FLEXURE TESTS FOR GRAPHITE/EPOXY SP-286T300

Specimen Number	Thickness cm (in.)	Width cm (in.)	Flexural Strength MPa (ksi)
1	0.188 (0.074)	1.265 (0.498)	1660 (241)
2	0.196 (0.077)	1.262 (0.497)	1730 (251)
3	0.196 (0.077)	1.265 (0.497)	1735 (251)
4	0.193 (0.076)	1.270 (0.500)	1755 (254)
5	0.190 (0.075)	1.262 (0.497)	1695 (245)
6	0.196 (0.077)	1.260 (0.596)	1700 (246)
		Average:	1710 (248)

TABLE II

QUALIFICATION INTERLAMINAR SHEAR TESTS FOR GRAPHITE/EPOXY SP-286T300

Specimen Number	Thickness cm (in.)	Width cm (in.)	Shear Strength MPa (ksi)
1	0.193 (0.076)	0.625 (0.246)	88.6 (12.8)
2	0.193 (0.076)	0.620 (0.244)	87.9 (12.7)
3	0.193 (0.076)	0.630 (0.248)	91.2 (13.2)
4	0.193 (0.076)	0.627 (0.247)	92.3 (13.4)
5	0.193 (0.076)	0.622 (0.245)	91.2 (13.2)
6	0.191 (0.075)	0.615 (0.242)	89.8 (13.0)
		Average:	90.1 (13.1)

The results above were judged satisfactory since they exceed the highest data available from the manufacturer for the comparable material SP-286T2.

5

2. CHARACTERIZATION OF UNIDIRECTIONAL MATERIAL

Unidirectional tensile properties were obtained by testing 2.54 cm x 22.9 cm (1 in. x 9 in.) 8-ply coupons. Four specimens of each were tested. Typical stress-strain curves as well as modulus, Poisson's ratio and strength obtained from these tests are shown in Figures 1-4. Strains in the 0-deg. direction are linear to failure. Axial strains in the 90-deg. specimens are linear up to a stress of approximately 21 MPa (3 ksi) corresponding to a strain of 0.002, thereafter they increase at a faster rate.

Compressive properties were obtained using the IITRI-designed compression test fixture which represents an improved modification of the Celanese fixture. The IITRI fixture uses trapezoidal wedges as opposed to the conical grips of the Celanese fixture. The trapezoidal wedges permit surface-to-surface contact at all positions and apply lateral compression to the specimen tabs to prevent slippage. The longitudinal coupons were 13.5 cm x 0.64 cm (5.3 in. x 0.25 in.) and 15-plies thick (1.93 mm; 0.076 in.) with a gage length of 9.5 mm (0.375 in.). The transverse coupons were 16-plies thick and had a gage length of 6.4 mm (1/4 in.). The gage sections of these specimens were instrumented with axial gages on both sides, primarily to monitor strains during loading and confirm the axiality of compressive loading up to failure. Stress-strain curves to failure for the unidirectional compressive specimens are shown in Figures 5-8. Also shown in these figures are the modulus and strength obtained from these data. Both 0-deg. and 90-deg. specimens show nonlinear strain behavior not associated with buckling. The 0-deg. specimens show a modulus somewhat lower than that obtained from corresponding tensile specimens but this difference is not regarded as significant and may be due to the early nonlinear behavior of the material. Their compressive strength is appreciably lower than the 0-deg. tensile strength. The modulus for the 90-deg. specimens is the same as for the 90-deg.

6
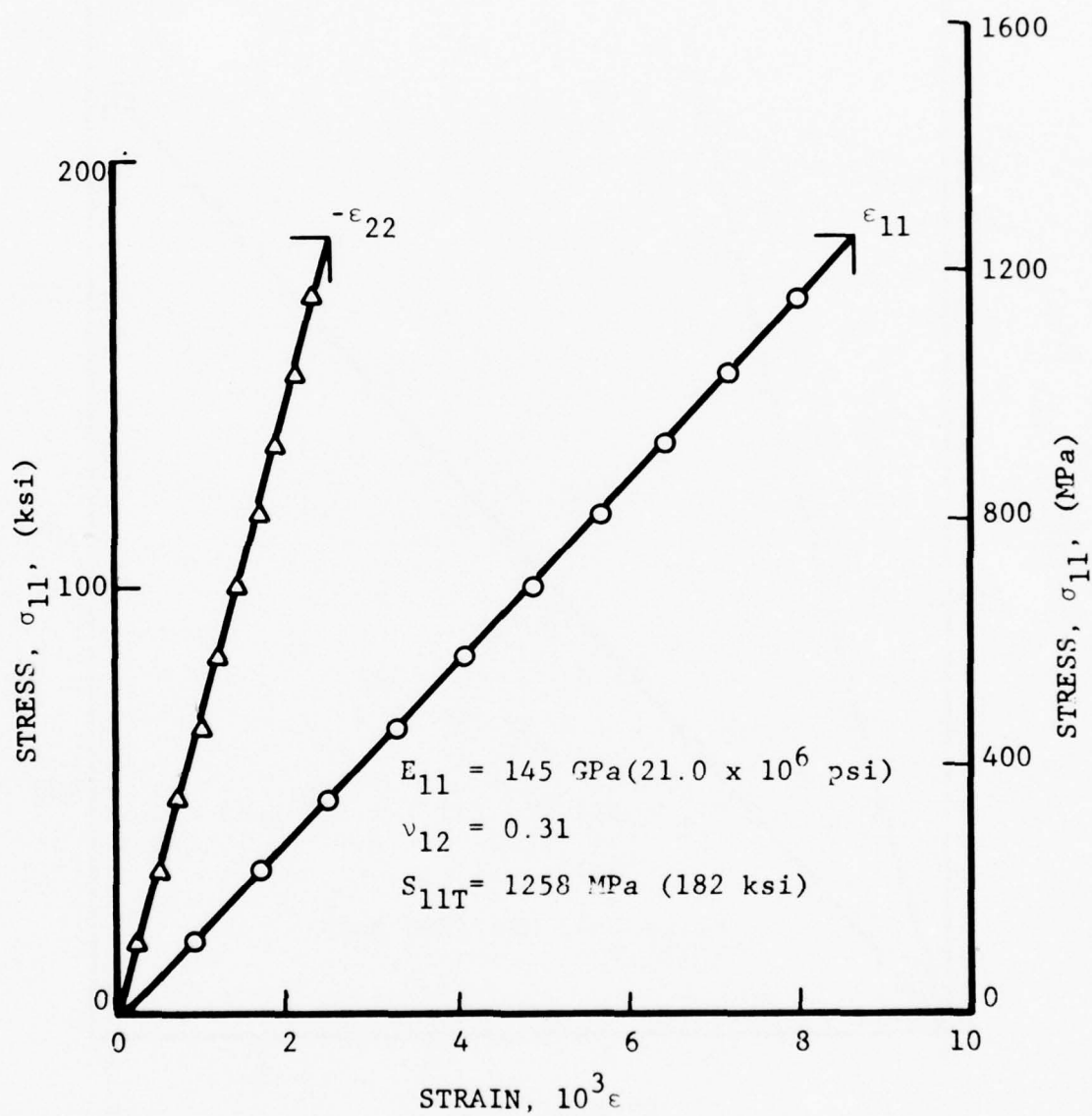
Figure 1.   Stress-Strain Curves for Unidirectional
0-Degree Specimen Under Tensile Loading

7
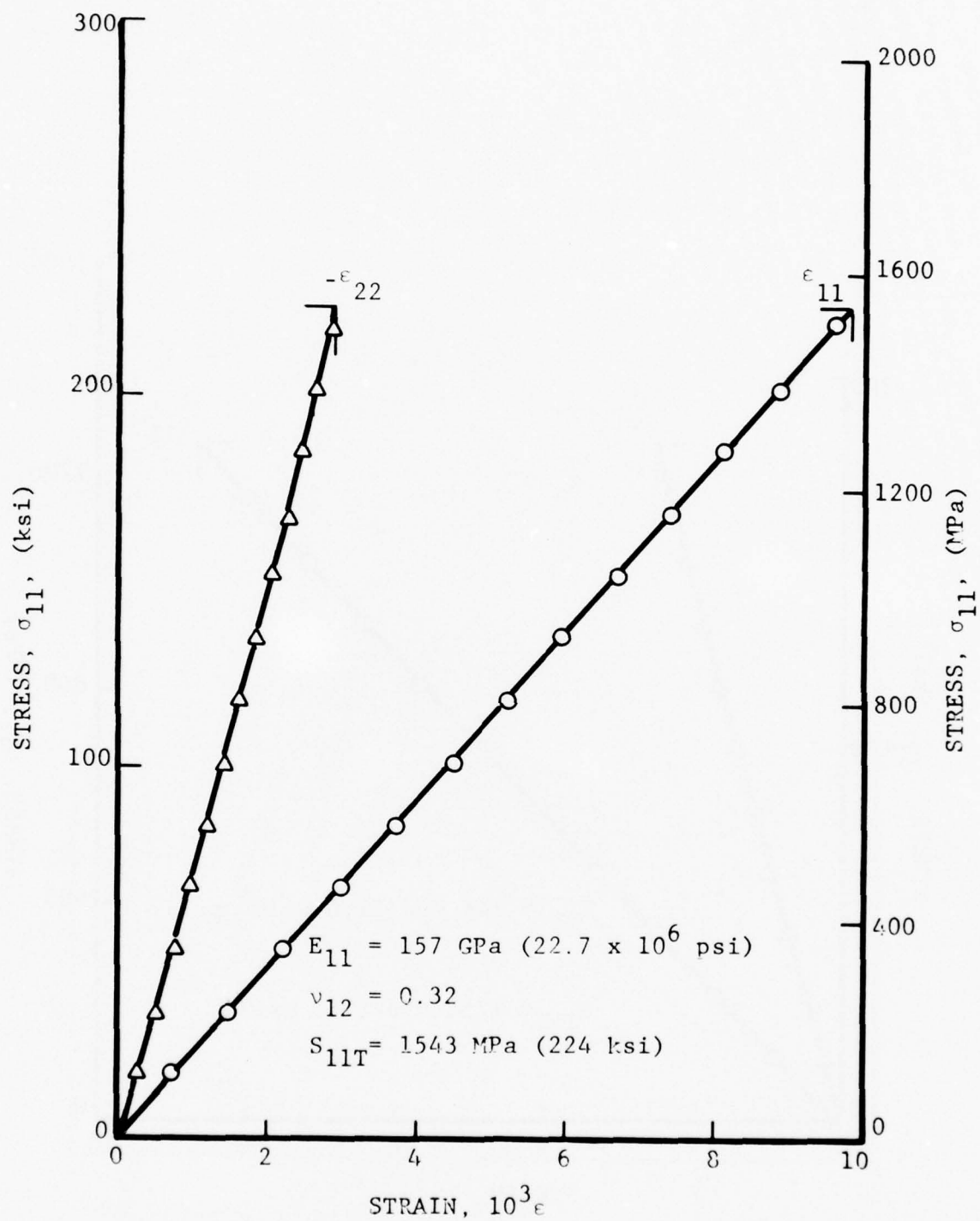
Figure 2. Stress-Strain Curves for Unidirectional
0-Degree Specimen Under Tensile Loading

8
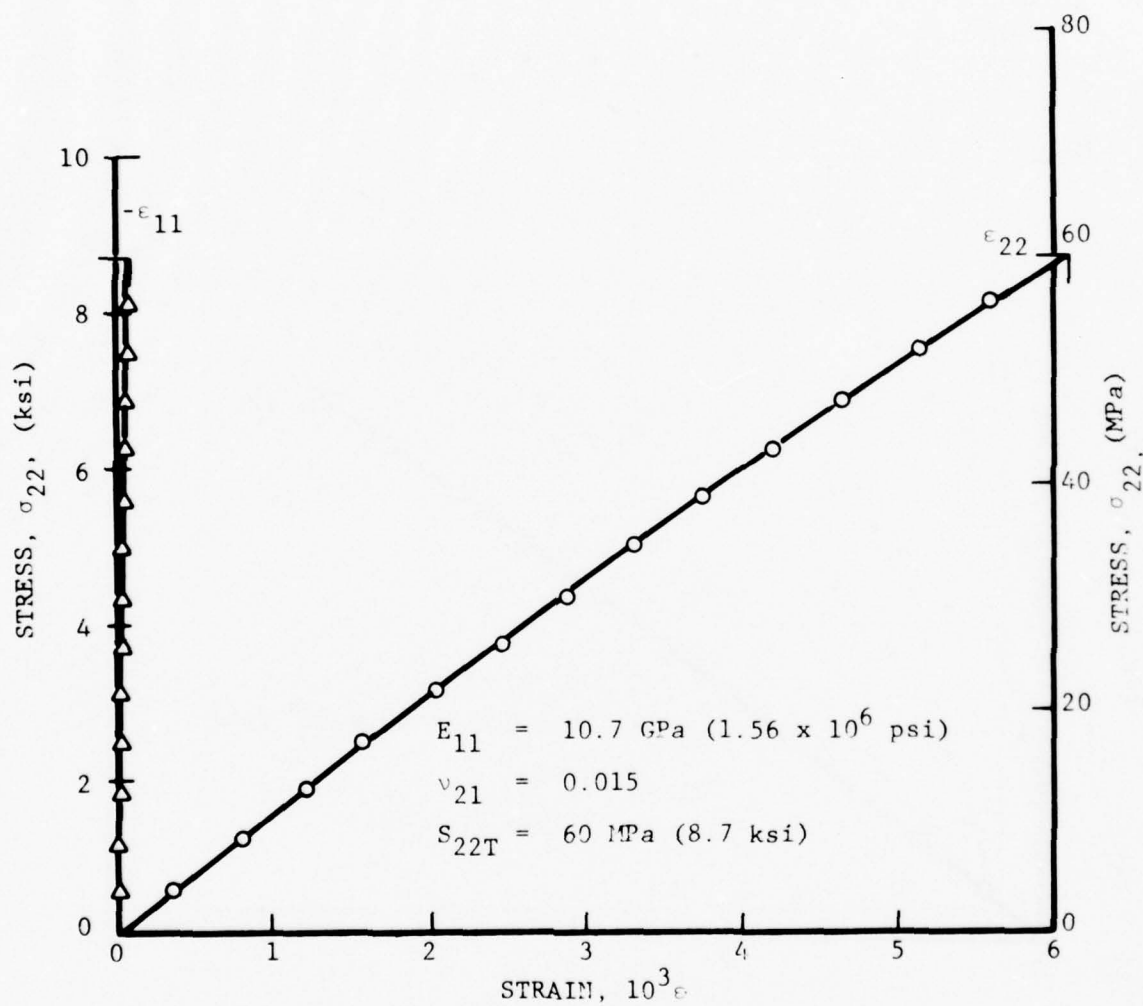
Figure 3. Stress-Strain Curves for Unidirectional 90-Degree
Specimen Under Tensile Loading

9
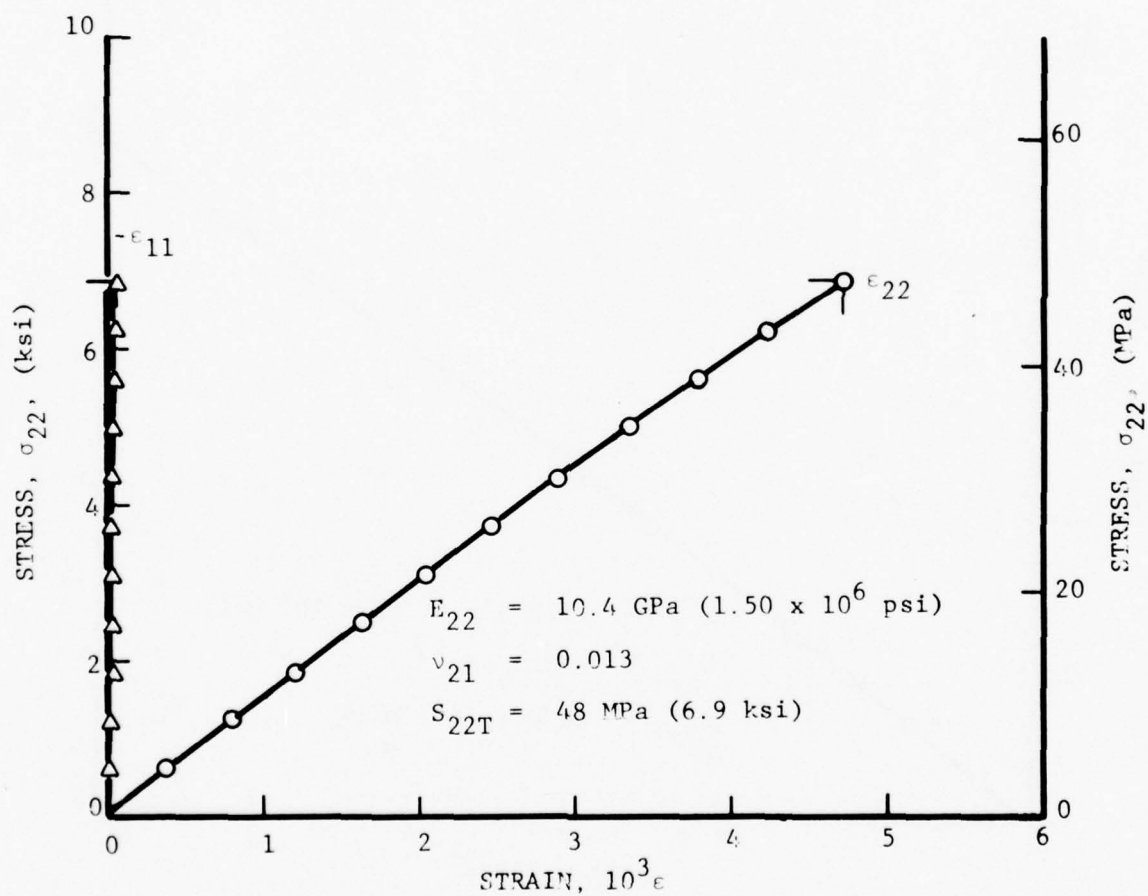
Figure 4.   Stress-Strain Curves for Unidirectional 90-Degree
Specimen Under Tensile Loading

10
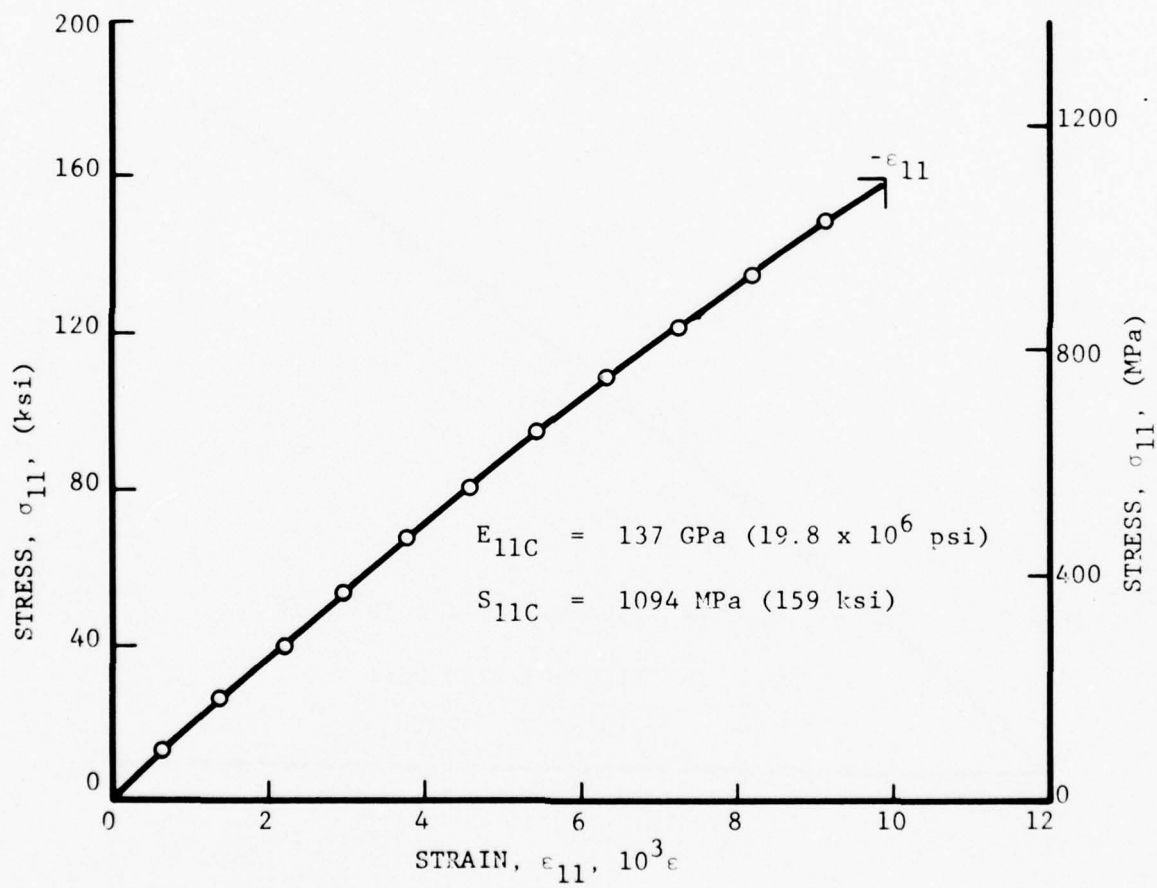
Figure 5. Stress-Strain Curve for Unidirectional 0-Degree
Specimen Under Compressive Loading

11

200

160

120

STRESS, σ_{11}, (ksi)

80

40

0

$-\varepsilon_{11}$

E_{11C} = 134 GPa (19.4 x 10^6 psi)

S_{11C} = 1169 MPa (169 ksi)

0   2   4   6   8   10   12

STRAIN, ε_{11}, $10^3\varepsilon$

1200

800

400

0

STRESS, σ_{11}, (MPa)
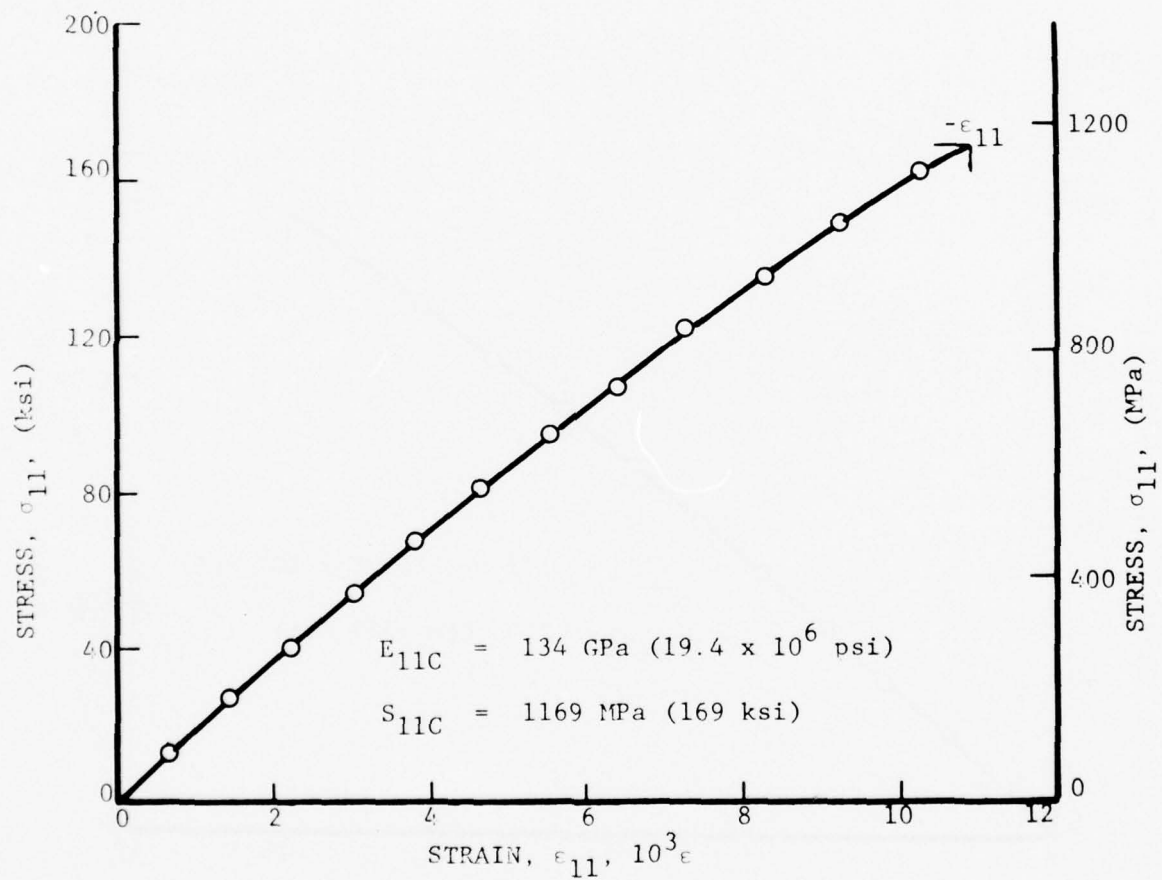
Figure 6.   Stress-Strain Curve for Unidirectional 0-Degree
Specimen Under Compressive Loading

12
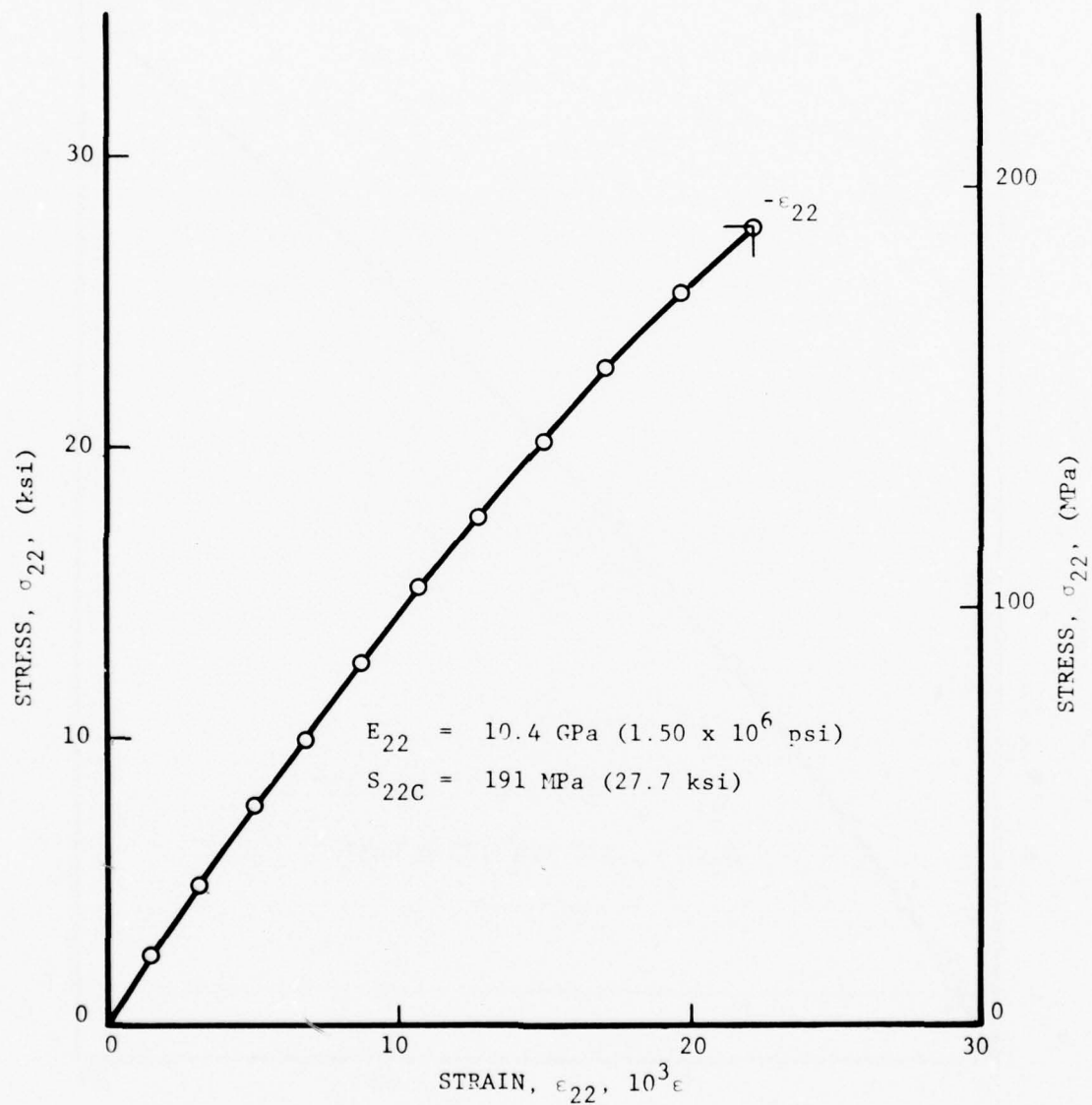
Figure 7. Stress-Strain Curve for Unidirectional 90-Degree
Specimen Under Compressive Loading

13

$E_{22} = 10.8$ GPa (1.57×10^6 psi)

$S_{22C} = 230$ MPa (33.4 ksi)
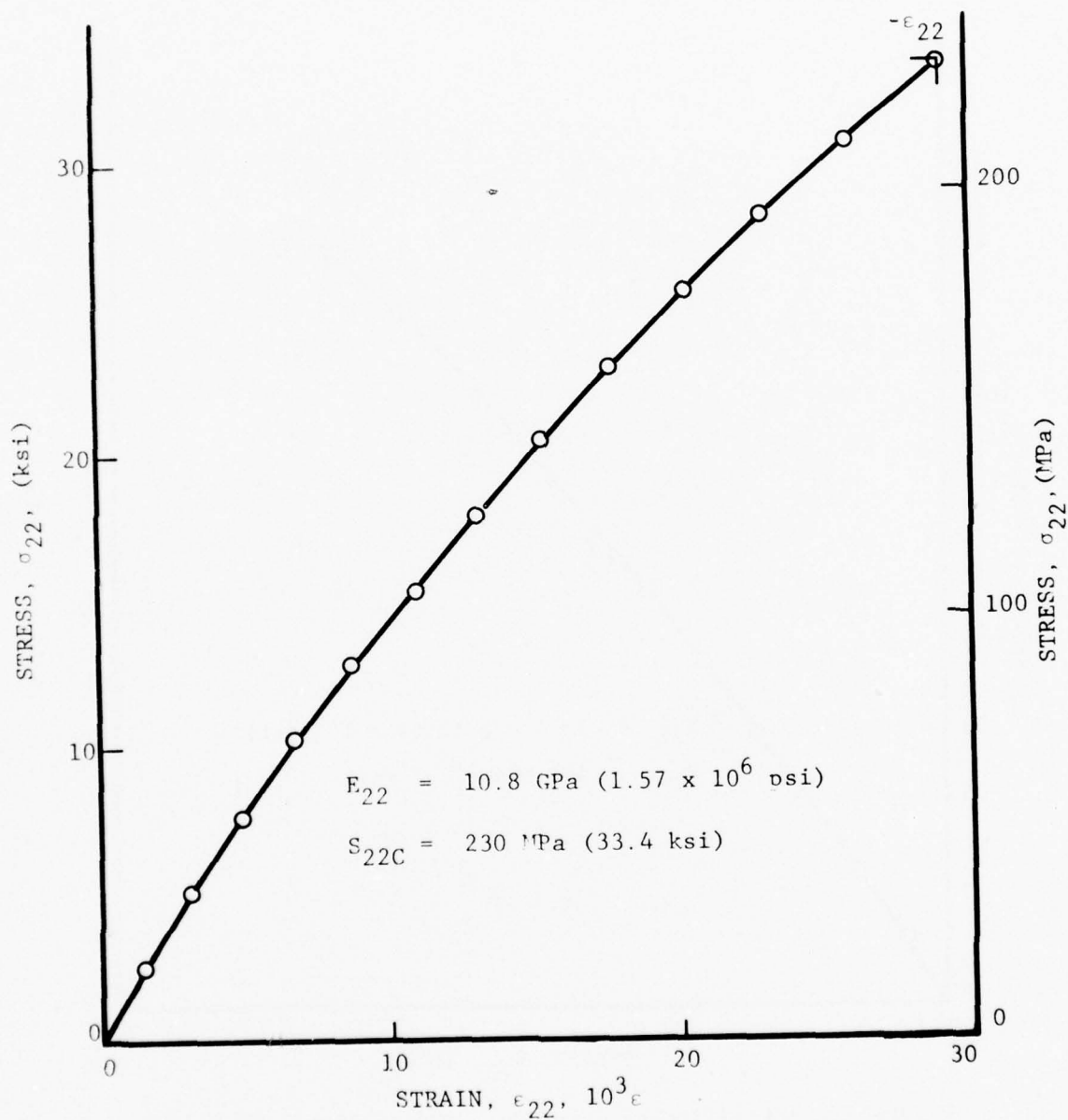
Figure 8.   Stress-Strain Curve for Unidirectional 90-Degree
Specimen Under Compressive Loading

14

tensile specimens. The compressive strength is more than four times the tensile strength as is always the case.

In-plane shear properties were determined by two different methods, by testing 10-deg. off-axis unidirectional specimens and $[\pm 45]_{2s}$ uniaxial specimens. In the first method the specimens were 1.27 cm (0.5 in.) wide, 6-ply thick and 25.4 cm (10 in.) long. They were instrumented with a three-gage strain gage rosette on each side. Shear stress and shear strain computed from the measured data are plotted in Figures 9 and 10. The in-plane shear modulus and shear strength obtained from the data are also shown in the figures. In the second method two $[\pm 45]_{2s}$ eight-ply coupons were prepared, instrumented with two-gage rosettes on each side and loaded to failure under uniaxial tension. The in-plane shear stress and shear strain were computed from the axial stress and the measured axial and transverse strains as follows:

$$\tau_{12} = \frac{\sigma_{xx}}{2}$$

$$\gamma_{12} = \epsilon_{xx} - \epsilon_{yy}$$

where σ_{xx} = axial stress

$\epsilon_{xx}, \epsilon_{yy}$ = axial and transverse strains, respectively

Shear stress versus shear strain are plotted in Figures 11 and 12 for the two specimens. The average values of the modulus and shear strength obtained are:

$$G_{12} = 6.1 \text{ GPa} (0.89 \times 10^6 \text{ psi})$$

$$S_{12} = 72 \text{ MPa} (10.5 \text{ ksi})$$

The value for the modulus is somewhat lower than that obtained from unidirectional 10-degree off-axis tests and the shear strength is appreciably higher than the value obtained in those tests.

15
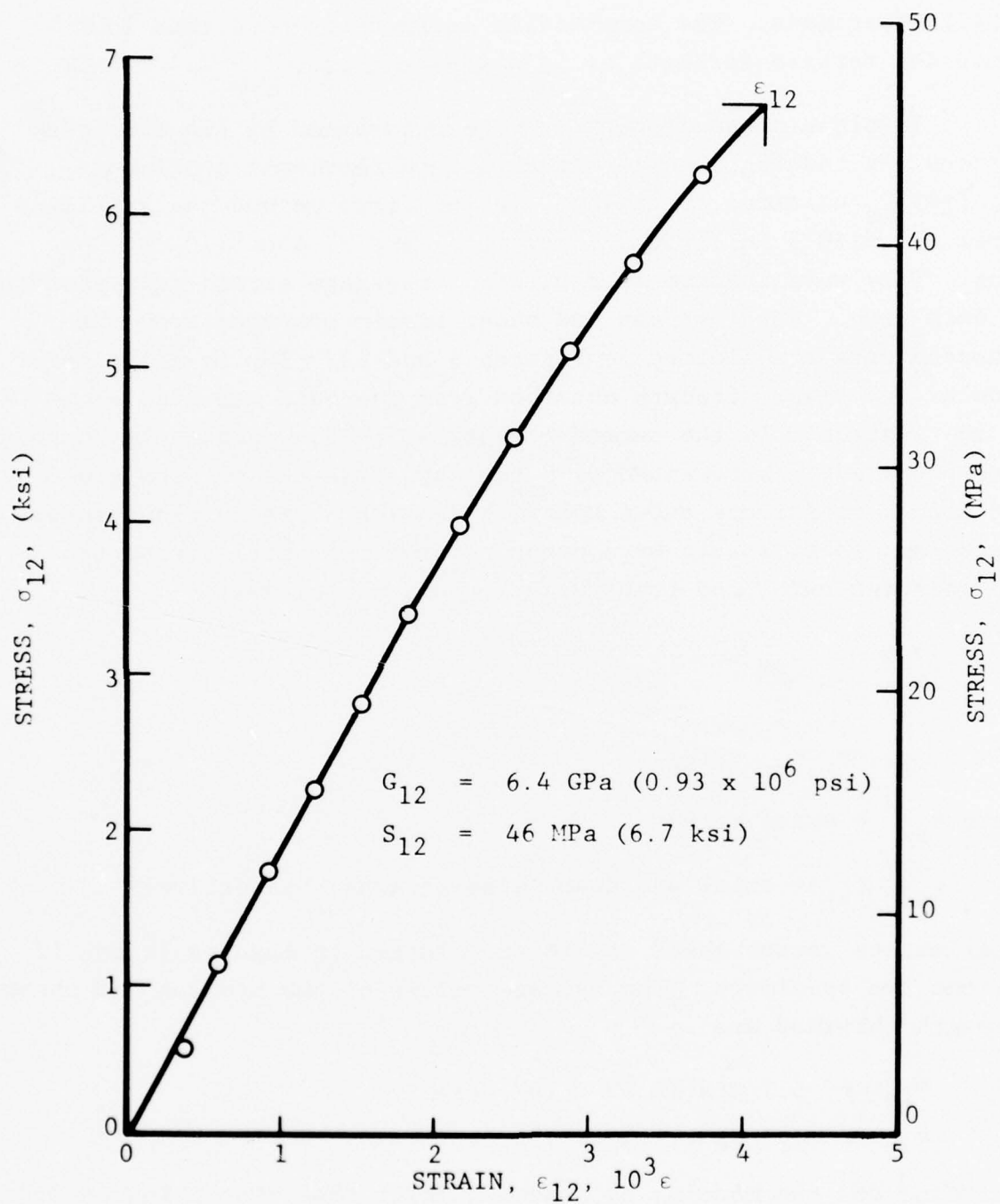
Figure 9.   Shear Stress Versus Shear Strain for 10-
Degree Off-Axis Unidirectional Specimen

16

G_{12} = 6.8 GPa (0.98 x 10^6 psi)

S_{12} = 47 MPa (6.8 ksi)

STRAIN, ε_{12}, $10^3 \varepsilon$
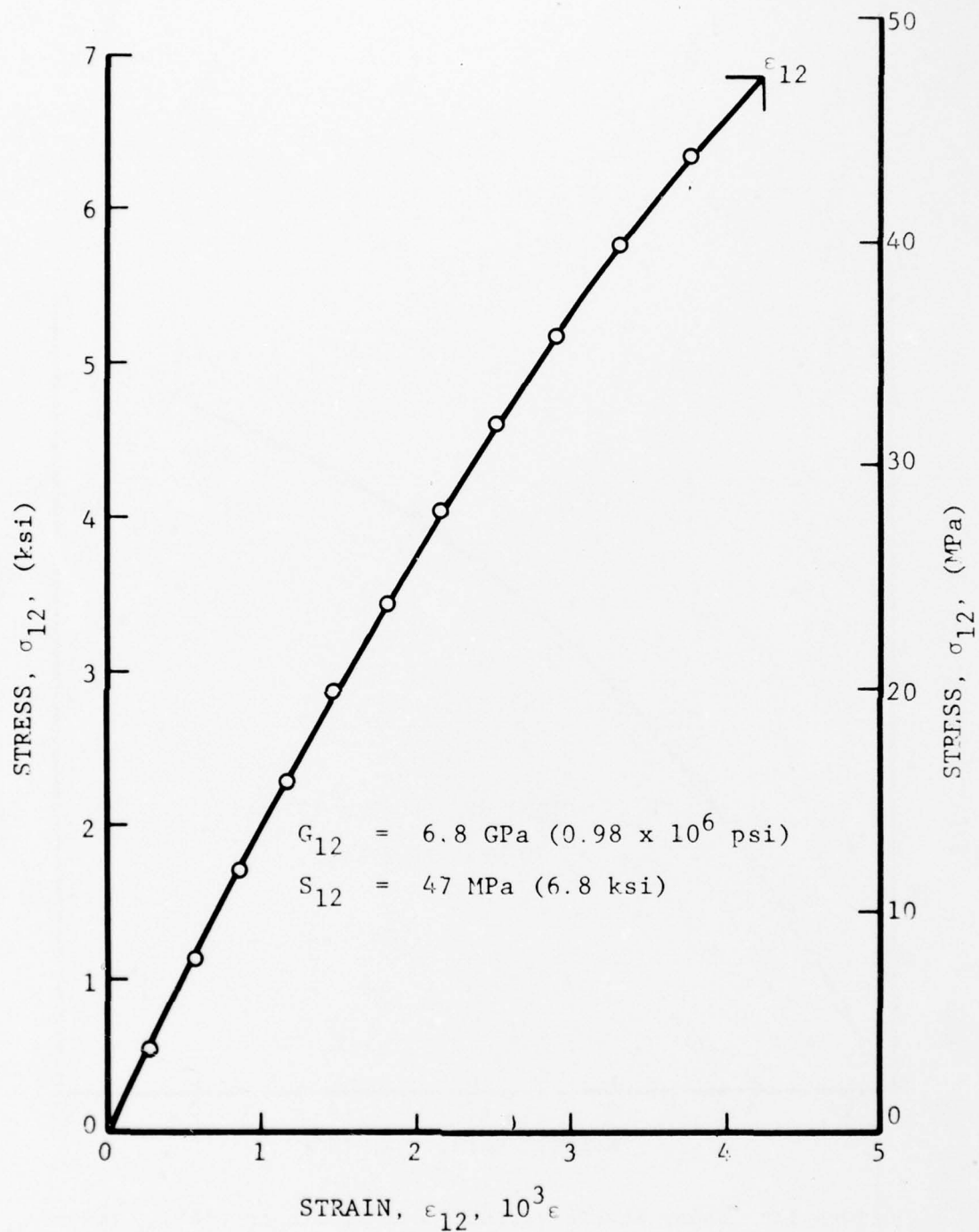
Figure 10.   Shear Stress Versus Shear Strain For 10-Degree Off-Axis Unidirectional Specimen

17
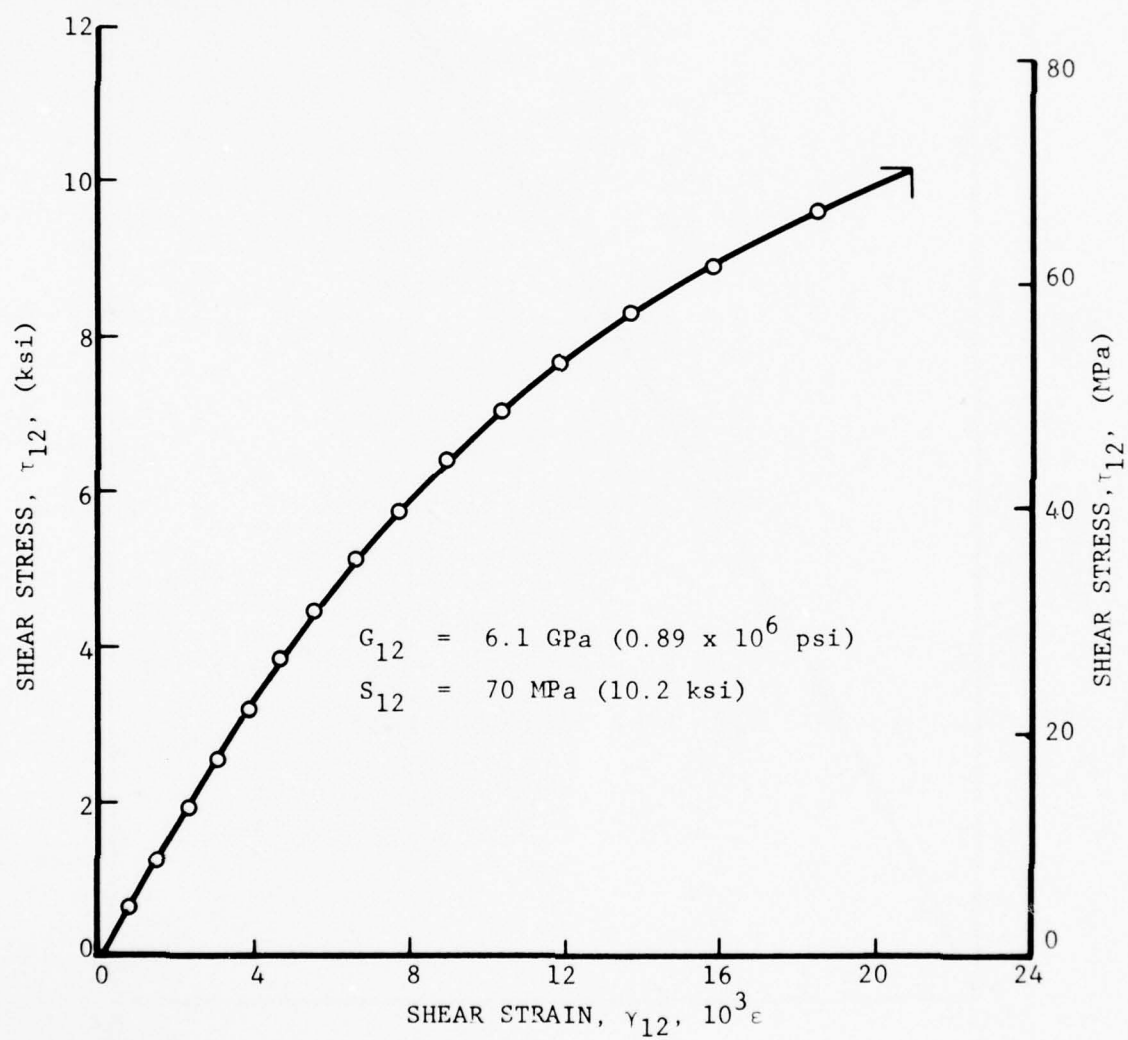
Figure 11.   Shear Stress Versus Shear Strain in $[\pm 45]_{2s}$ Specimen

18
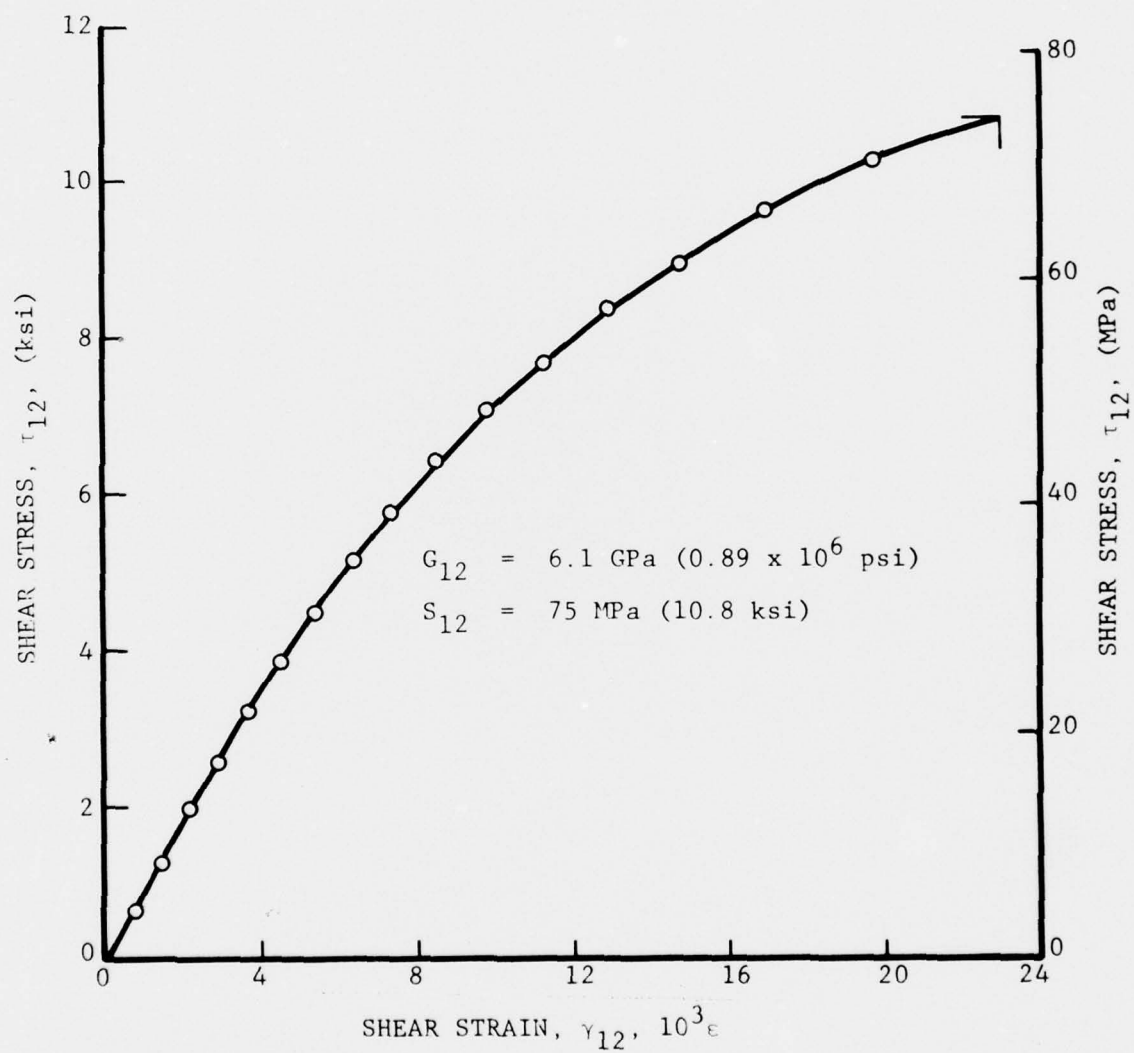
Figure 12. Shear Stress Versus Shear Strain in $[\pm 45]_{2s}$ Specimen

19

Results from the characterization tests above are tabulated in Table III. All values are higher than the manufacturer's data for the comparable material SP-286T2.

TABLE III

PROPERTIES OF UNIDIRECTIONAL GRAPHITE/EPOXY
SP-286T300

Property	Value
Ply Thickness	0.130 mm (0.0051 in.)
Longitudinal Modulus, E_{11}	149 GPa (21.6×10^6 psi)
Transverse Modulus, E_{22}	10.6 GPa (1.53×10^6 psi)
Shear Modulus, G_{12}	6.4 GPa (0.93×10^6 psi)
Major Poisson's Ratio, ν_{12}	0.31
Minor Poisson's Ratio, ν_{21}	0.014
Longitudinal Tensile Strength, S_{11T}	1477 MPa (214 ksi)
Ultimate Longitudinal Tensile Strain, ε_{11T}^u	0.00972
Longitudinal Compressive Strength, S_{11C}	1132 MPa (164 ksi)
Ultimate Longitudinal Compressive Strain, ε_{11C}^u	0.01040
Transverse Tensile Strength, S_{22T}	54 MPa (7.8 ksi)
Ultimate Transverse Tensile Strain, ε_{22T}^u	0.00541
Transverse Compressive Strength, S_{22C}	211 MPa (30.6 ksi)
Ultimate Transverse Compressive Strain, ε_{22C}^u	0.02565
In-plane Shear Strength, S_{12}	72 MPa (10.5 ksi)
Ultimate Shear Strain, ε_{12}^u	0.0110

21

SECTION III

UNIAXIAL TESTS OF UNNOTCHED LAMINATE

Basic properties were determined of the quasi-isotropic $[0/\pm45/90]_s$ laminate used in subsequent tests with notched specimens. Uniaxial tensile properties were determined in the 0-deg. and 90-deg. directions with respect to the outer fibers. The specimens were standard 2.54 cm x 22.9 cm (1 in. x 9 in.) coupons instrumented with two-gage rosettes on each side. Stress-strain curves to failure are shown in Figures 13-16. The strain response is linear up to approximately 240 MPa (35 ksi) corresponding to an axial strain of approximately $4 \times 10^{-3} \epsilon$. This is a little higher than the strain at which the response of the 90-degree unidirectional specimens becomes nonlinear (Figures 3 and 4). Although the number of specimens tested is very small, the influence of stacking sequence is apparent. The strength of the $[90/\pm45/0]_s$ specimens is approximately 7.5% higher than that of the $[0/\pm45/90]_s$ specimens. This is probably due to the fact that the interlaminar normal stresses near the edges between the outer 90-degree plies and the inner plies in the $[90/\pm45/0]_s$ layup are compressive.

Additional tests were conducted on the quasi-isotropic laminate above at 30-deg. to the outer fibers, to characterize it closer in the loading direction of subsequent biaxial specimens with cracks. Typical stress-strain curves for such a specimen are shown in Figure 17. The modulus and Poisson's ratio are the same as for specimens tested in the 0-deg. and 90-deg. directions, however, the strength is lower.

Results of all uniaxial tensile tests on the unnotched laminate are summarized in Table IV.

22
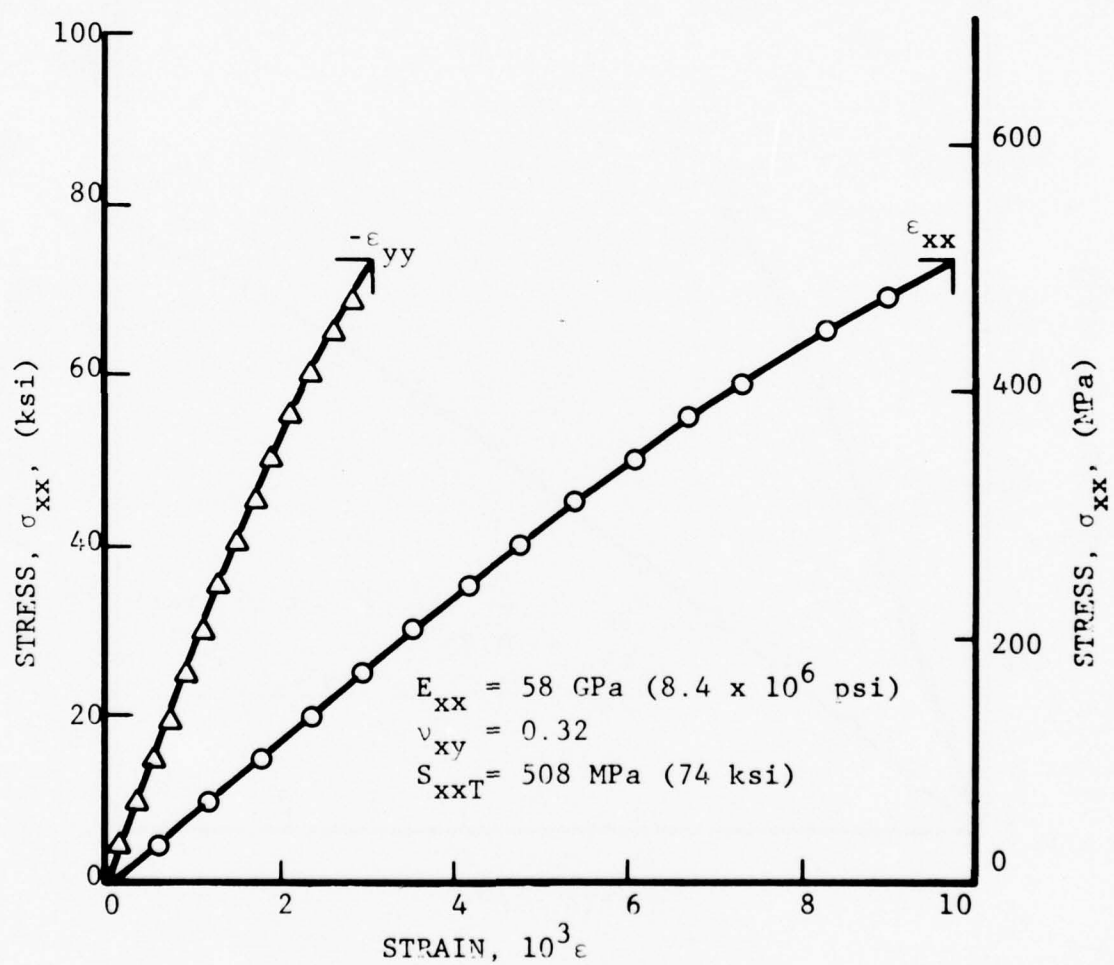
Figure 13.   Strains in $[0/\pm45/90]_s$ Specimen Under
Uniaxial Tensile Loading

23
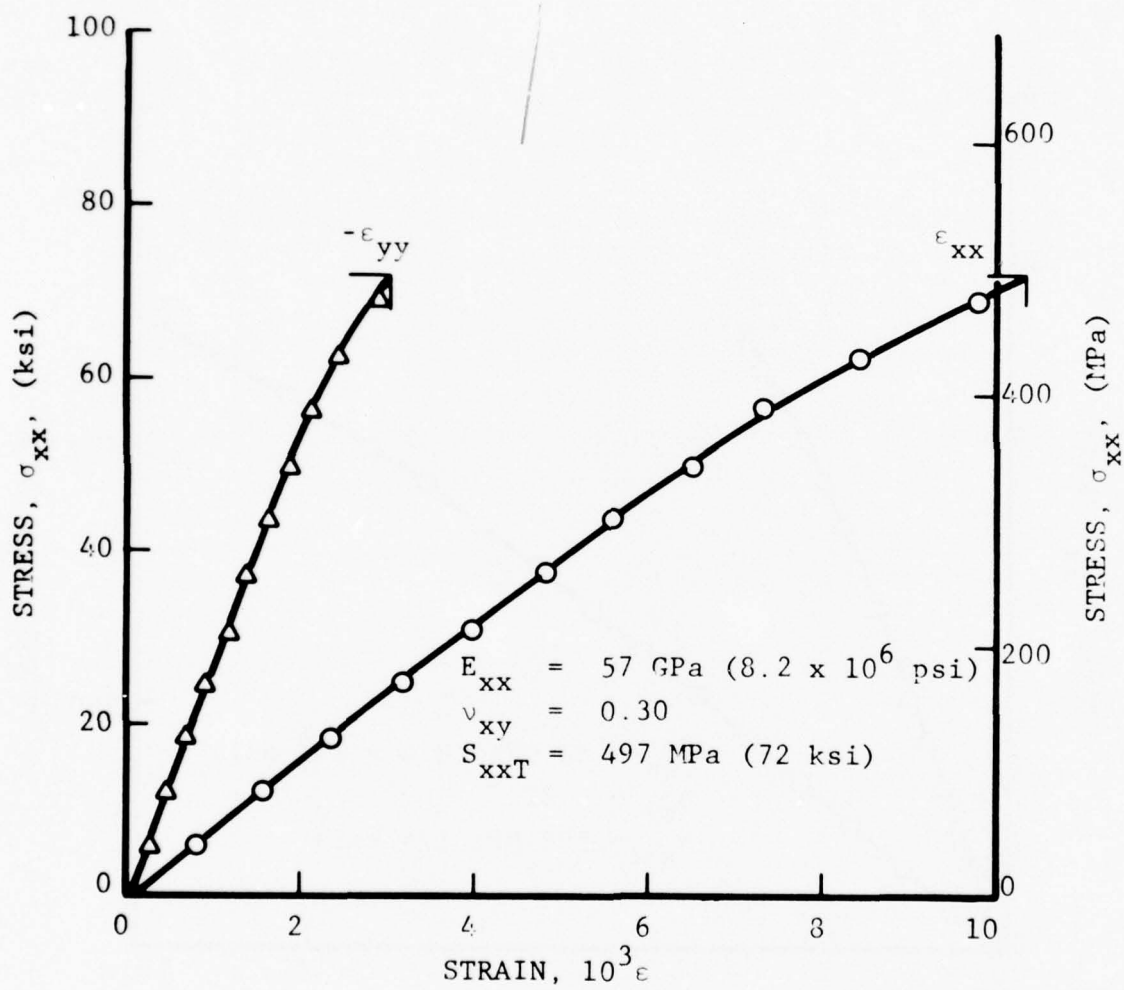
Figure 14.   Strains in $[0/\pm45/90]_s$ Specimen Under
Uniaxial Tensile Loading

24
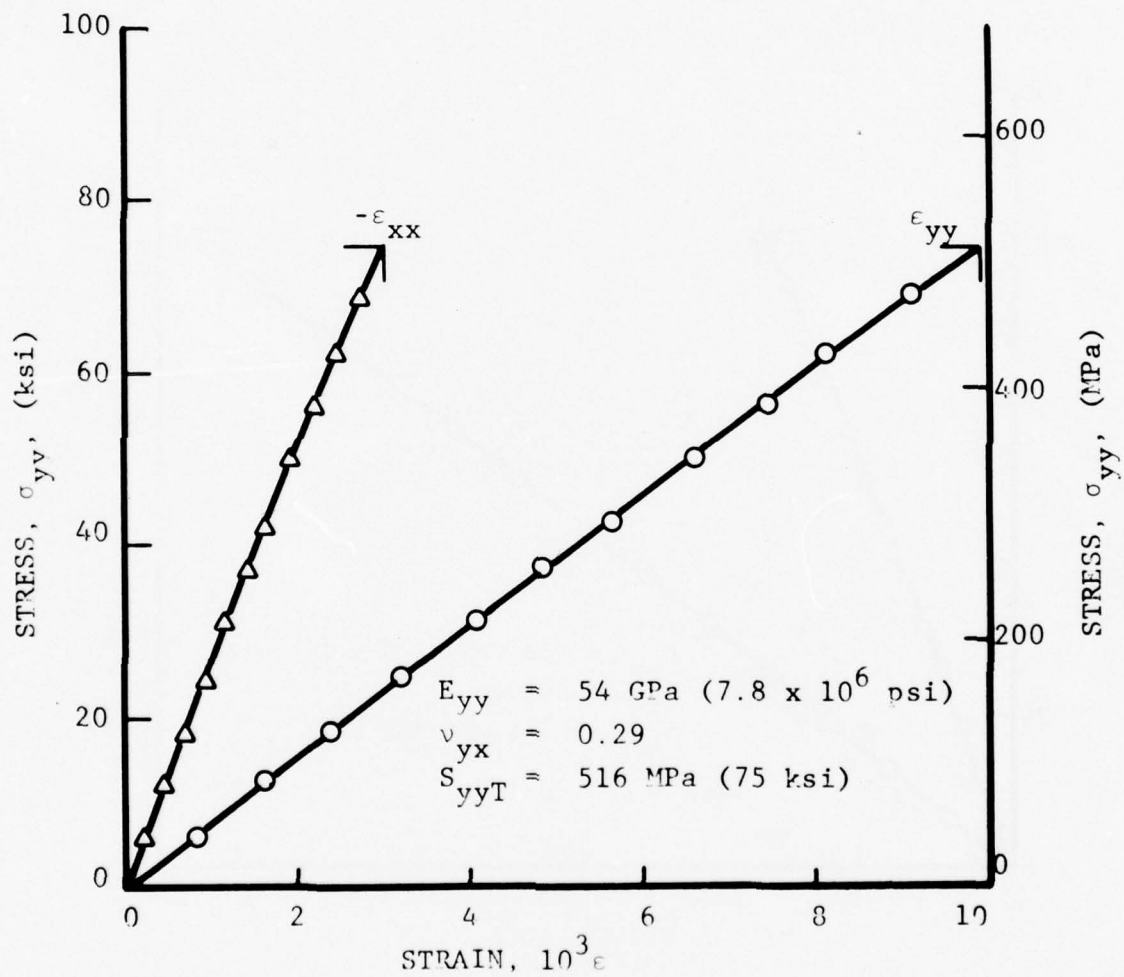
Figure 15.   Strains in $[90/\pm 45/0]_s$ Specimen Under
Uniaxial Tensile Loading

25
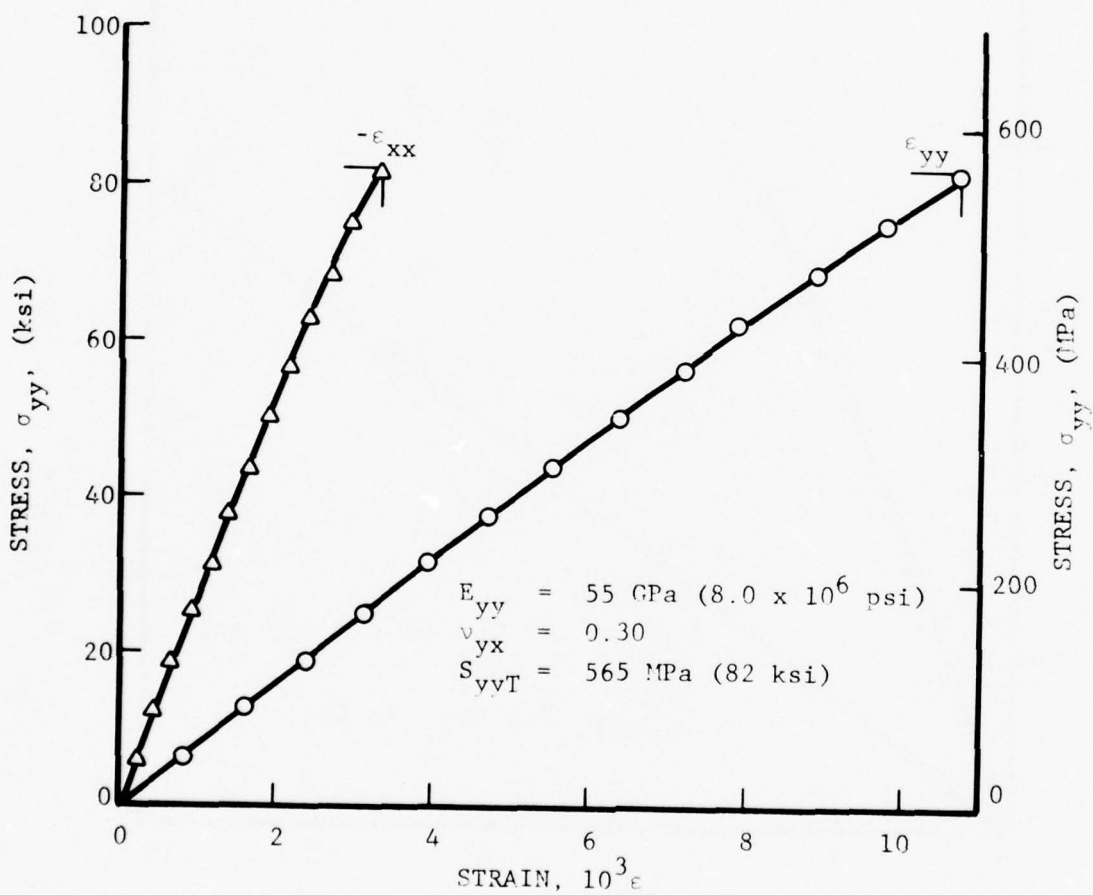
Figure 16.   Strains in $[90/\pm45/0]_s$ Specimen Under Uniaxial Tensile Loading

The figure shows stress σ_{yy} (ksi and MPa) vs strain $10^3\varepsilon$, with curves for $-\varepsilon_{xx}$ and ε_{yy}, and annotations:

E_{yy} = 55 GPa (8.0×10^6 psi)
ν_{yx} = 0.30
S_{yyT} = 565 MPa (82 ksi)

26
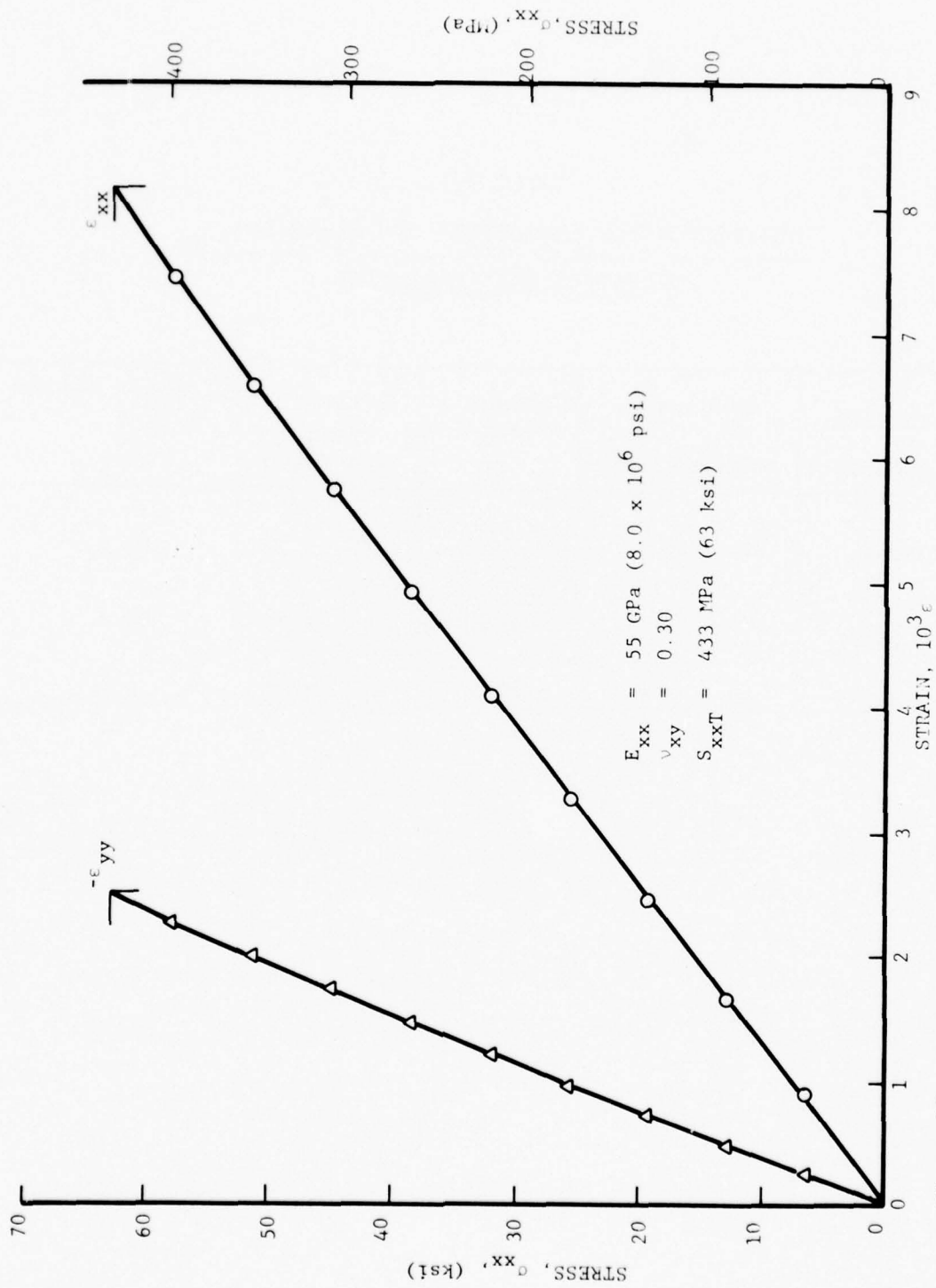
Figure 17. Strains in [0/+45/90]s Laminate Under Uniaxial Tensile Loading at 30-deg.
With Outer Fibers

E_{xx} = 55 GPa (8.0 x 10^6 psi)
ν_{xy} = 0.30
S_{xxT} = 433 MPa (63 ksi)

TABLE IV

STATIC TENSILE PROPERTIES OF $[0/\pm45/90]_s$

GRAPHITE/EPOXY LAMINATES

Direction of Loading	Modulus E_{xx} GPa(10^6 psi)	Poisson's Ratio ν_{xv}	Strength S_{xxT} MPa (ksi)	Ultimate Strain ε^u_{xxT} ($10^3 \varepsilon$)
0-deg.	55 (8.0)	0.30	502 (73)	10.0
90-deg.	55 (7.9)	0.30	541 (78)	10.3
30-deg.	54 (7.8)	0.30	414 (60)	8.0

SECTION IV

UNIAXIAL TESTS OF NOTCHED LAMINATE

1. SPECIMENS

The specimens were 8-ply $[0/\pm45/90]_s$ laminates 12.7 cm
(5 in.) wide and 56 cm (22 in.) long and were tabbed with glass/
epoxy tabs as shown in Figure 18. These tabs were made from
11-ply glass/epoxy crossply (3M 1007 Scotchply). A fixture was
made for aligning the test laminate with the precut tabs, bonding
the tabs onto the laminate and drilling three 1.27 cm (0.500 in.)
through holes at each end (Figure 19). The same fixture was used
to locate and drill central circular holes. All holes were drilled
with diamond core drills. Central transverse through-the-thickness
cracks were machined ultrasonically.

The crack geometry selected is illustrated in Figure 20.
The overall length of the crack was varied but the width at the
center and the end geometry were constant. The crack had tapered
ends (13°) terminating in a 0.076 mm (0.003 in.) radius fillet.
The uniformity of the crack geometry makes comparison of the final
results more valid.

Four hole diameters and four crack lengths, 2.54 cm (1 in.),
1.91 cm (0.75 in.), 1.27 cm (0.50 in.) and 0.64 cm (0.25 in.), were
investigated. The configuration of the notched uniaxial specimens
is outlined in Figure 21. Two specimens were tested for each
notch type and size.

2. STRAIN MEASUREMENT

Deformations and strains were recorded at various load
increments using strain gages, birefringent coatings and moire
grids. Strain gages were mounted near the notch and along the

29

Figure 18. Uniaxial Tensile Specimen with Stress Concentration
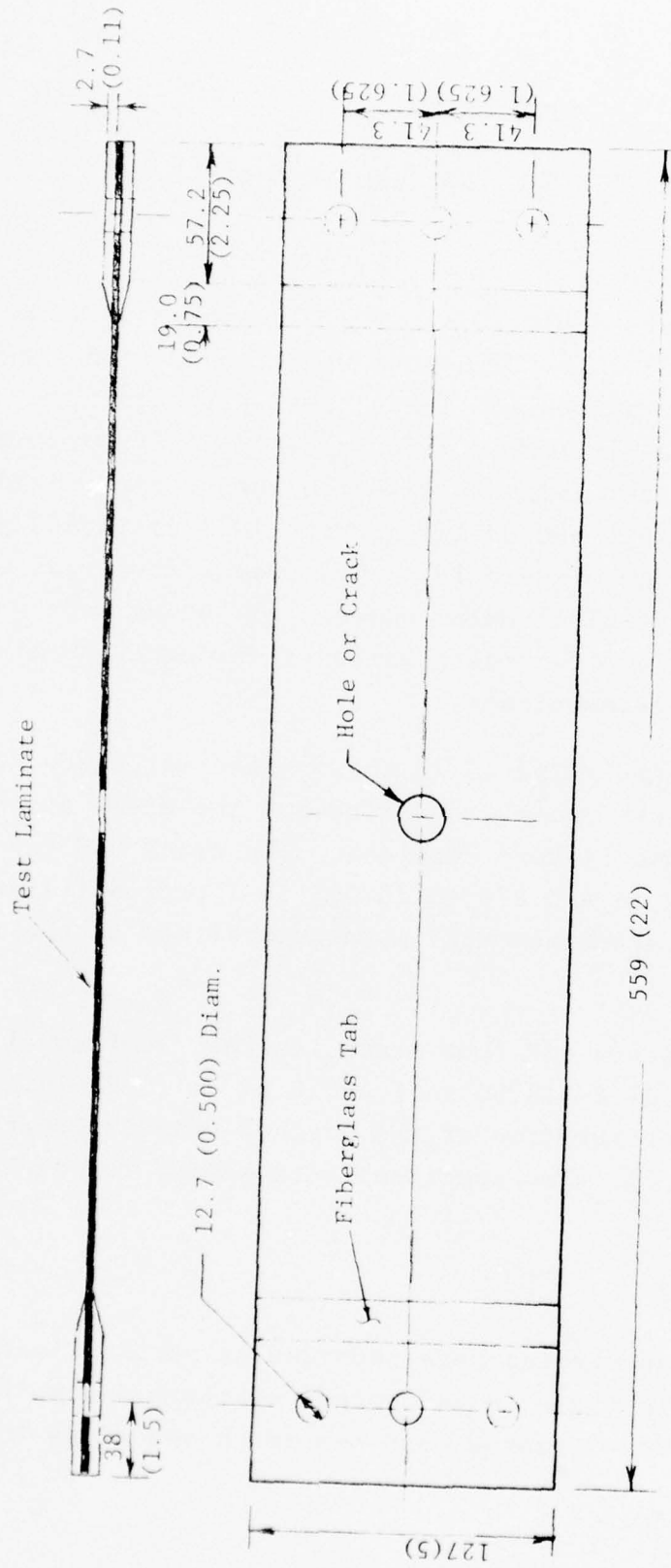
Note: Dimensions are in millimeters and inches.
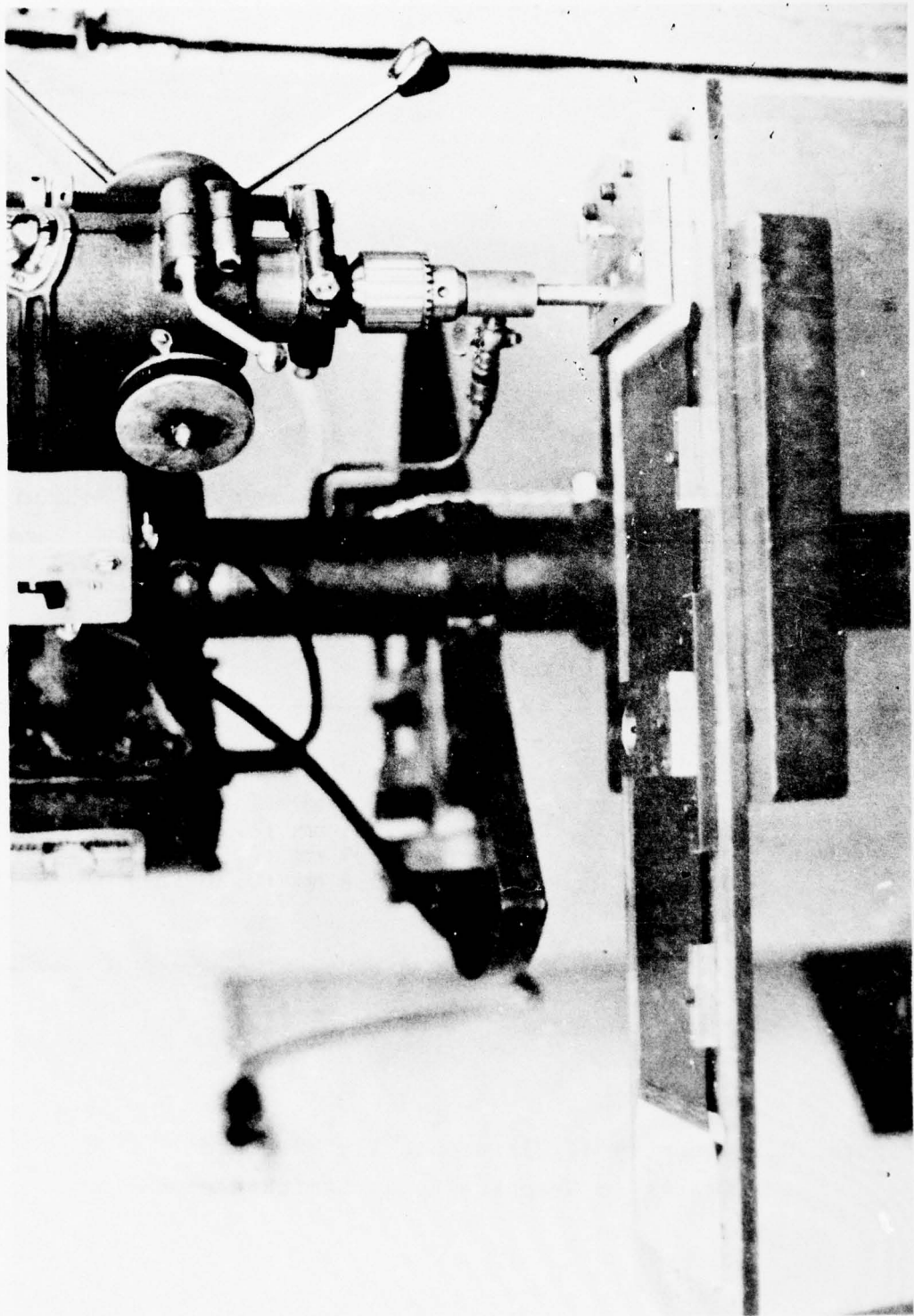
Figure 19. Fixture for Tab Alignment and Drilling of Holes

31
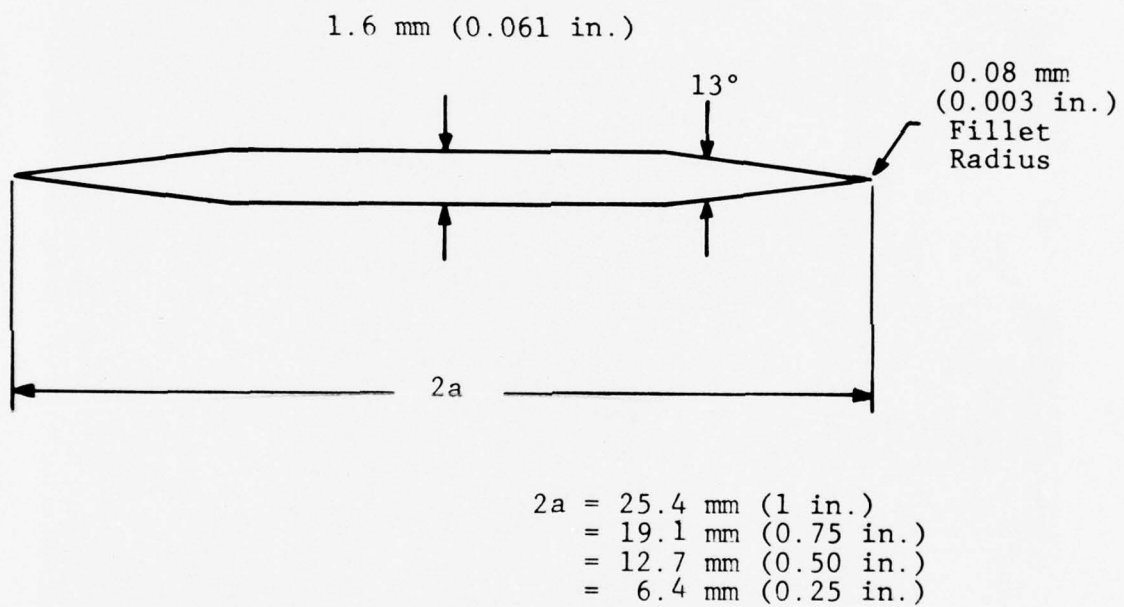
Figure 20. Geometry of Ultrasonically Machined
Cracks in Graphite/Epoxy Laminates

σ₁

2a
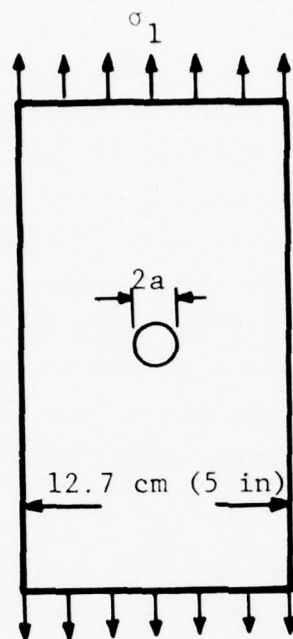
2a, cm (in.)

2a, cm	(in.)
2.54	(1.00)
1.91	(0.75)
1.27	(0.50)
0.64	(0.25)

12.7 cm (5 in)

σ₁

2a

2.54	(1.00)
1.91	(0.75)
1.27	(0.50)
0.64	(0.25)

12.7 cm (5 in)

σ₁
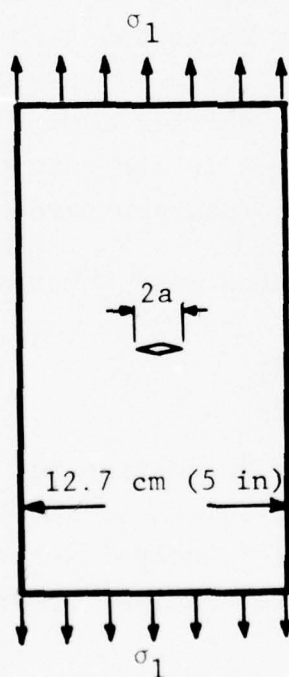
Figure 21. Notched Uniaxial Tensile Specimens
of $[0/\pm 45/90]_s$ Laminate

33

horizontal (normal to loading) axis. They include single gages and two-gage rosettes of various sizes. In the case of specimens with holes miniature gages of 0.38 mm (0.015 in.) gage length were bonded on the curved edge of the hole. A photograph of a typical gage layout near the hole is shown in Figure 22. Specimens with cracks were instrumented with strain gages along the horizontal (crack) axis with miniature gages in the vicinity of the crack tip. Typical gage layouts around cracks are shown in Figures 23 and 24. The strain gage output was recorded by means of a digital data acquisition system, which gave a printout directly in strains.

In many cases birefringent coatings were bonded to one side of the specimen to obtain full-field strain information. Commercial coatings with a reflective backing (Photolastic, Inc.) ranging in thickness between 0.25 mm (0.01 in.) and 1 mm (0.04 in.) were used. The thinnest coating was used on specimens with cracks. Coatings 0.5 mm (0.02 in.) thick were used on all but the specimen with 2.54 cm (1 in.) diameter hole, where the thicker 1 mm (0.04 in.) coating was applied. The isochromatic fringes in the coating were observed with a reflection polariscope and recorded photographically.

Photoelastic coating fringes were interpreted on the basis of the strain-optic law

$$\varepsilon_1^c - \varepsilon_2^c = \varepsilon_1^s - \varepsilon_2^s = \frac{Nf_\varepsilon}{2h}$$

where superscripts c and s refer to coating and specimen, respectively, N is fringe order, h the coating thickness and f_ε the strain fringe value, a material constant. The principal strain along a stress-free boundary where the directions of principal stress and principal strain coincide is given by

$$\varepsilon_1^s = \frac{Nf_\varepsilon}{2h} \cdot \frac{1}{1+\nu^c}$$

34
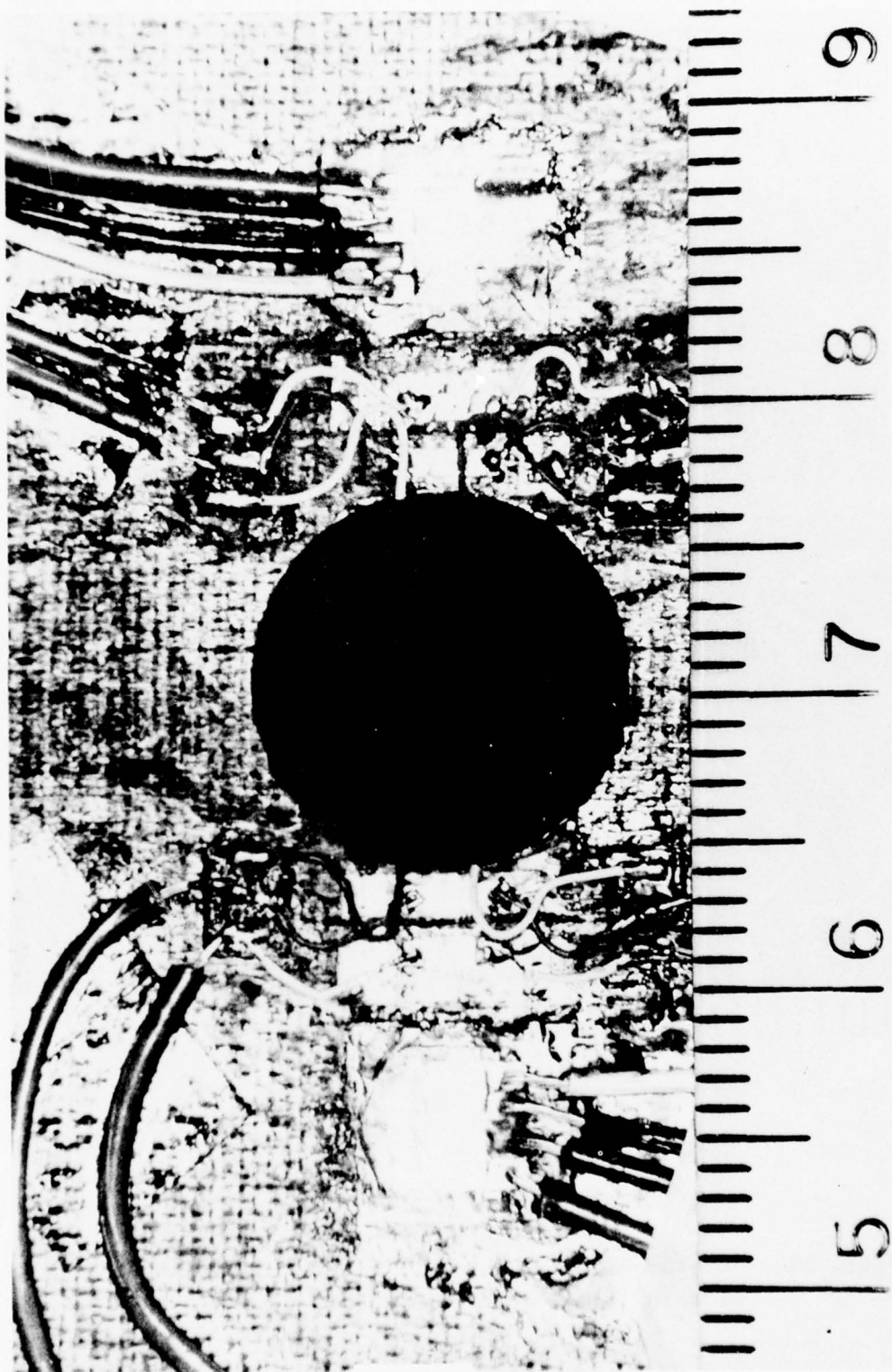
Figure 22. Photograph of Strain Gage Layout Near Hole (Scale is in cm)

35
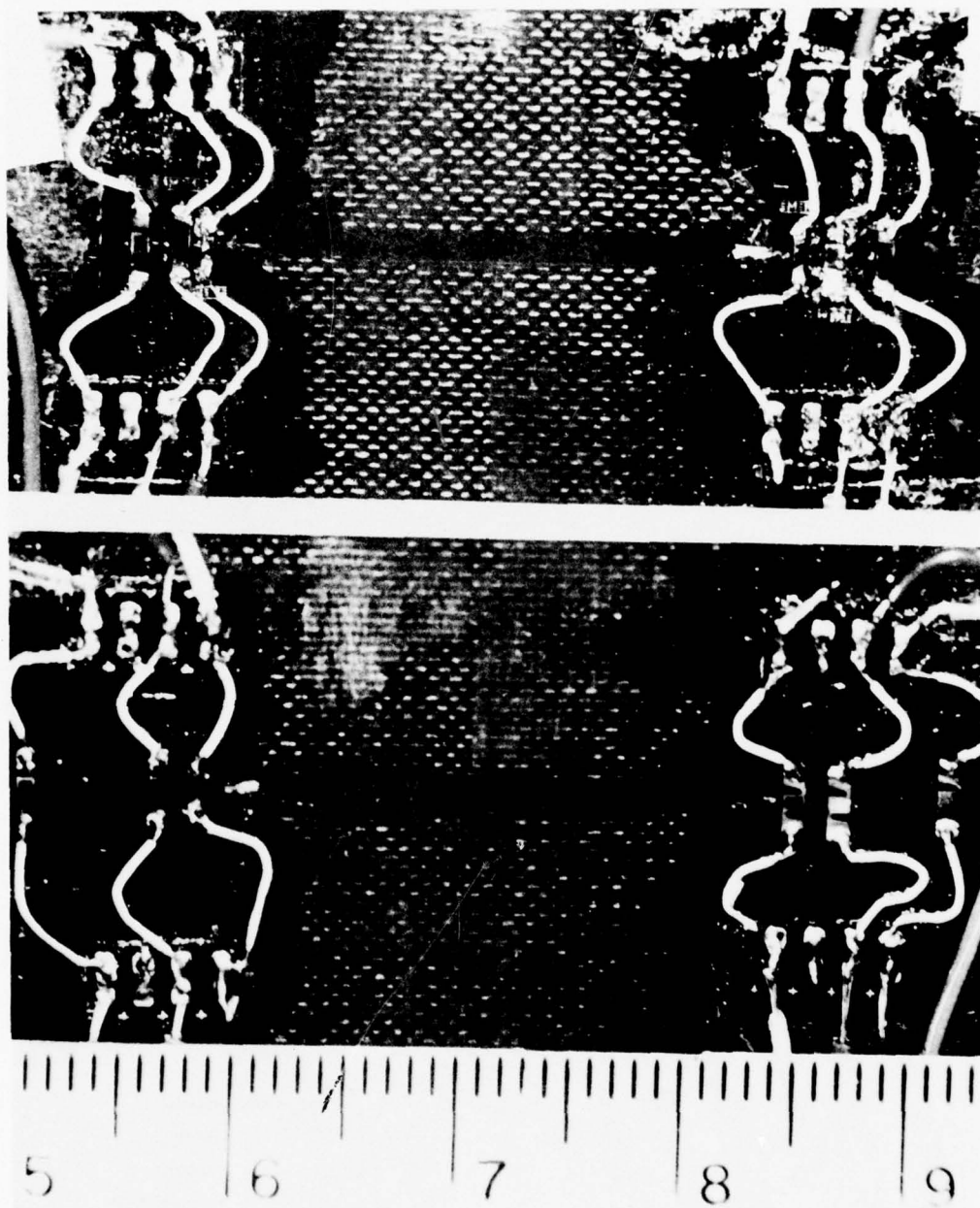
Figure 23.   Strain Gage Layout in the Vicinity of Crack on Two
Sides of Specimen (Scale in cm)

36
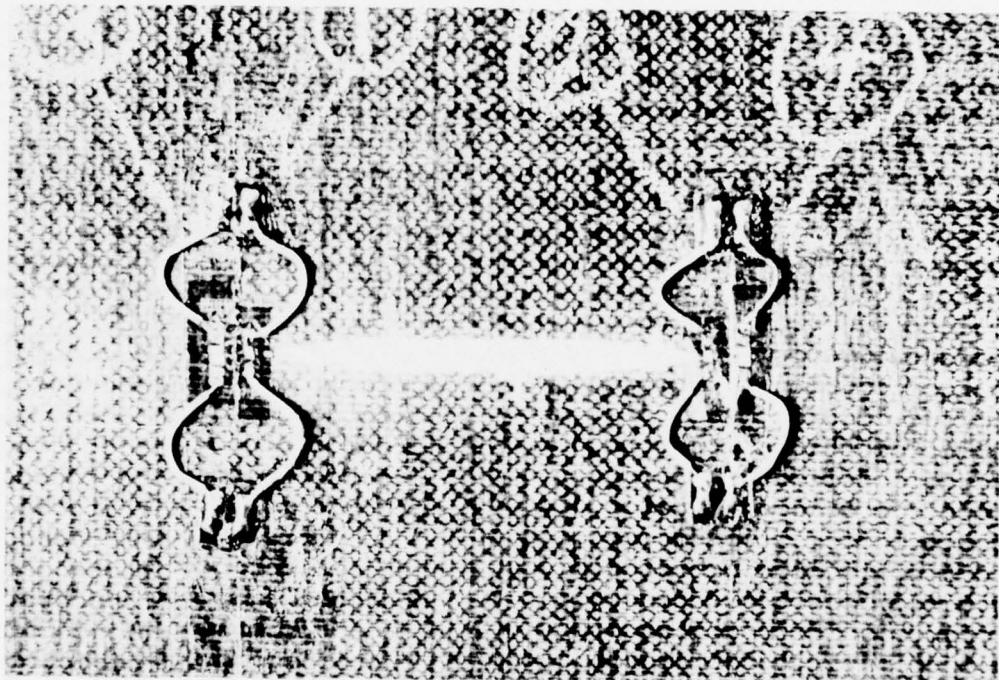
Figure 24.   Strain Gage Layout Around Crack on One Side of
              Specimen.   Other Side Had Birefringent Coating.

The effect of Poisson's ratio mismatch was not great because Poisson's ratio for the quasi-isotropic laminate is not very different from that of the coating.

Moire techniques were used in some cases to obtain full-field information of the in-plane surface displacements. Application of these techniques to composites have been discussed before (References 9 and 19). Arrays of 400 lines/cm (1000 lines/in.) were applied to the specimen surface around the notch. The specimen surface was made reflective by depositing a thin coating of epoxy dyed white with Titanium dioxide. The film with the array of lines was then bonded on this white reflective surface. During testing, a similar film with the same array of lines was placed in contact with the specimen array by means of a film of oil. Deformation of the specimen produces interference fringes which represent loci of constant component of displacement normal to the specimen array. Differentiation of these displacement loci yields strains.

3. LOADING

Uniaxial notched specimens were loaded mainly through friction by bolting gripper plates lined with emery cloth to the tabbed ends, Figure 25. The specimens were loaded in increments in a 120,000 lb Riehle testing machine at a crosshead rate of 1 mm/min (0.04 in/min). At every load level strains were recorded with a digital data acquisition system and photoelastic and moire fringes recorded photographically.

4. RESULTS FOR SPECIMENS WITH HOLES

Specimen No. 4-1 had a 0.64 cm (0.25 in.) diameter hole. It was instrumented with a few gages near the hole boundary and in the far-field. Strain distributions are shown in Figure 26. The far-field strains are nearly linear to failure, whereas those near the

38
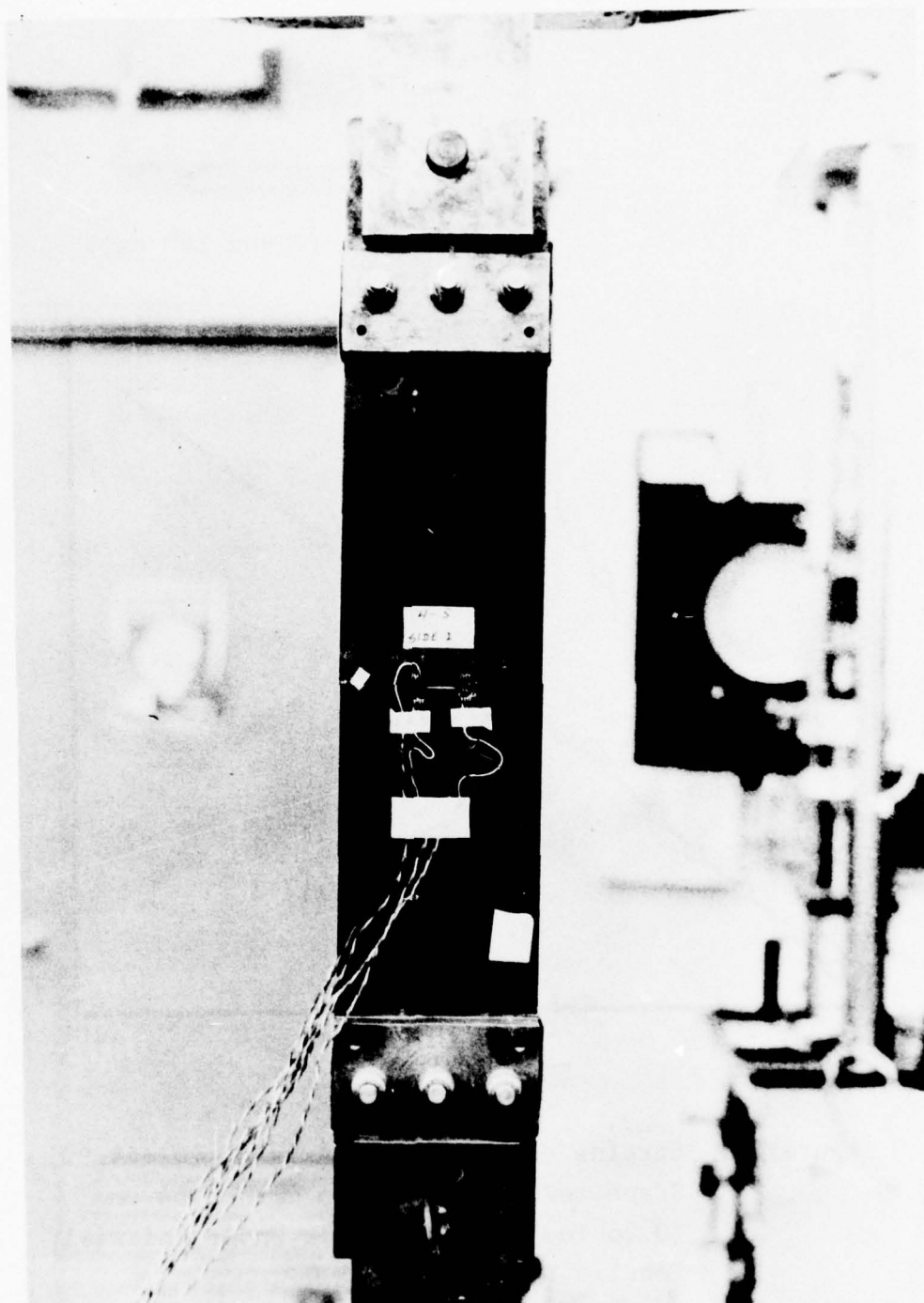
Figure 25. Uniaxial Tensile Loading of Notched Specimen

39
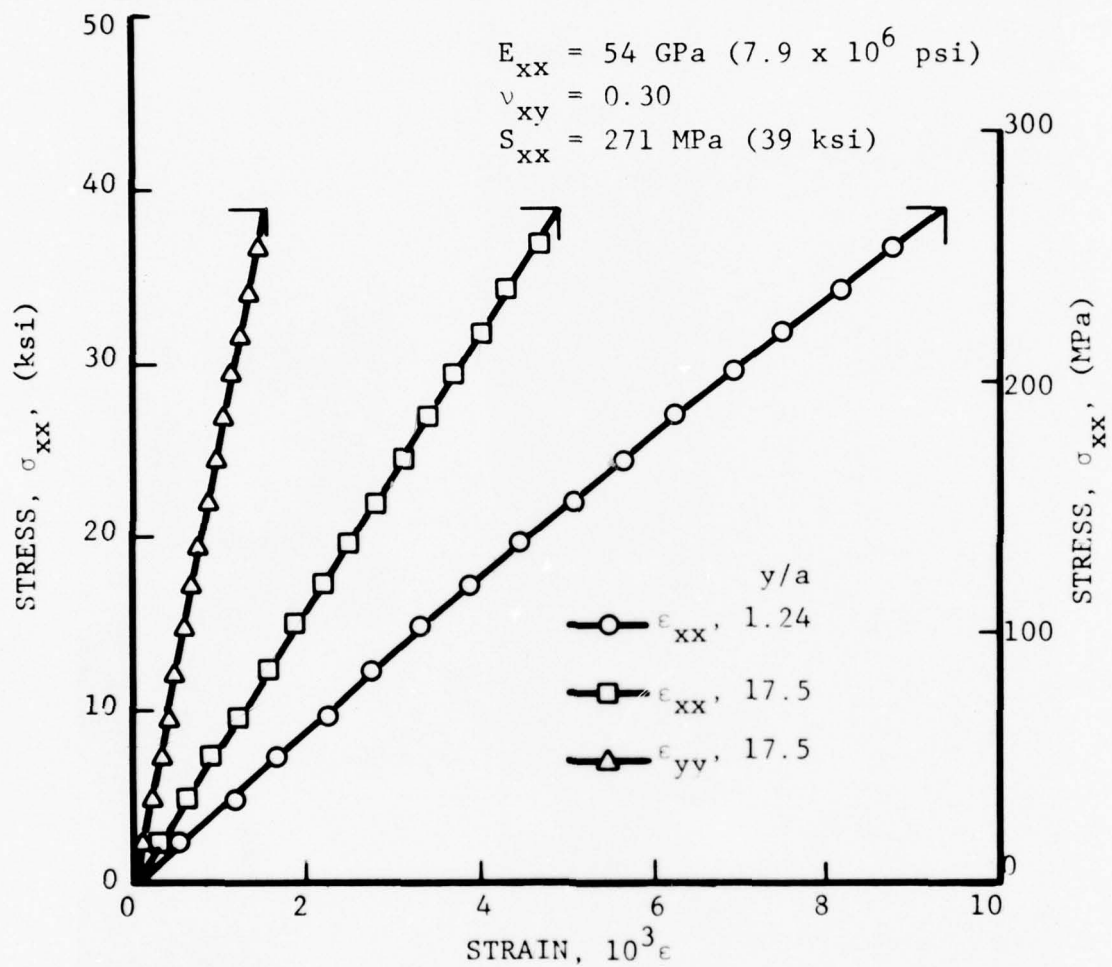
Figure 26.   Strains on Horizontal Axis of $[0/\pm45/90]_s$
Graphite/Epoxy Specimen with 0.64 cm
(0.25 in.) Circular Hole Under Uniaxial
Tensile Loading

hole become nonlinear at a stress level of 140 MPa (20 ksi).
Failure initiated on the hole boundary at points off the
horizontal axis and propagated across the width of the plate
in a nearly horizontal direction. The average failure stress,
based on the gross section, was S_{xxT} = 271 MPa (39 ksi).

Specimen No. 4-2, a replicate of the above, had a 0.64 cm
(0.25 in.) diameter hole and was instrumented with strain gages
and a 0.5 mm (0.020 in.) photoelastic coating. Gages were bonded
on the curved boundary of the hole and at various locations along
the horizontal axis. Results are shown in Figure 27. Strains along
the transverse (horizontal) axis as a function of applied stress are
plotted. The far-field strains are linear for the most part, up
to an applied stress of approximately 210 MPa (30 ksi). Thereafter,
they become slightly nonlinear up to failure. The onset of nonlinear
response occurs earlier as one approaches the hole. The strains at
the two symmetric locations on the hole boundary are nearly equal
to each other up to an applied stress of approximately 100 MPa
(15 ksi). Thereafter, the strain at one point continues to increase
in a slightly nonlinear manner wheras the strain at the symmetric
point increases very rapidly. The latter may be due to some localized
failure in the area of the gage. Values for the modulus, Poisson's
ratio, strength and strain concentration factor obtained from the
measured and plotted data are:

$$E_{xx} = 56 \text{ GPa } (8.1 \times 10^6 \text{ psi})$$

$$\nu_{xy} = 0.25$$

$$S_{xx} = 282 \text{ MPa (41 ksi)}$$

$$k_\epsilon = 2.96$$

The measured value of the strain concentration factor compares well
with the theoretical value of 3. Failure initiated on the hole
boundary off the horizontal axis and propagated across the width of

41
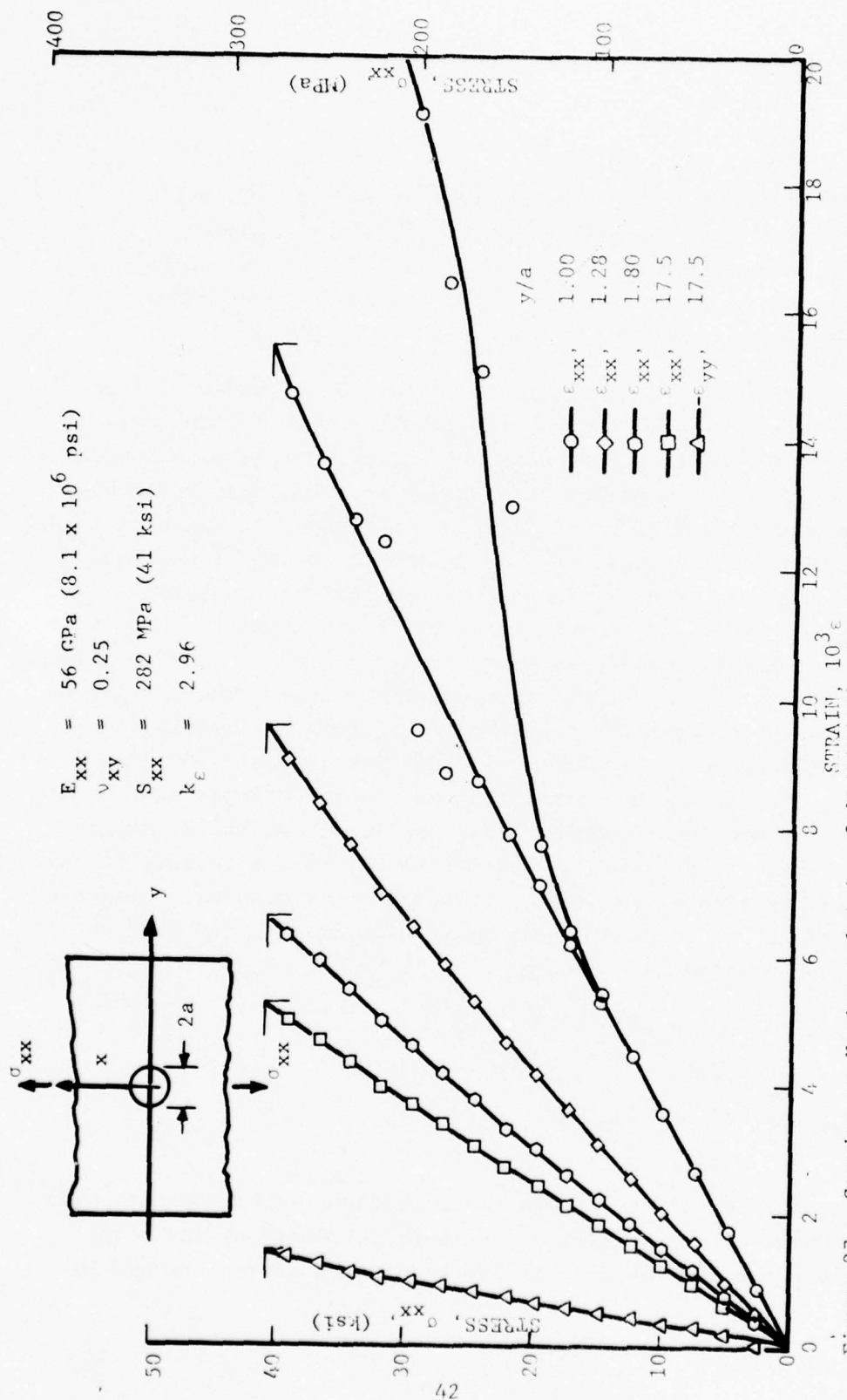
Figure 27. Strains on Horizontal Axis of [0/±45/90]s Graphite/Epoxy Specimen with 0.64 cm (0.25 in.) Circular Hole Under Uniaxial Tensile Loading (Spec. No. 4-2).

the plate. Extensive delamination accompanied this fracture pro-
pagation. The average failure stress, based on the gross section,
was 282 MPa (41 ksi).

Results for specimen No. 4-3 with a 1.27 cm (0.50 in.)
diameter hole are shown in Figures 28 and 29. The far-field strains
are for the most part linear. The strains at the two symmetric
locations on the hole boundary are nearly equal to each other up
to an applied stress of approximately 83 MPa (12 ksi). Thereafter,
the strain at one point increases at a decreasing rate and the
strain at the symmetric point continues to increase linearly up to
an applied stress of approximately 138 MPa (20 ksi). The onset
of failure beyond this point is evident. Values for the modulus,
Poisson's ratio, strength and strain concentration factor are:

$$E_{xx} = 54 \text{ GPa } (7.9 \times 10^6 \text{ psi})$$

$$\nu_{xy} = 0.31$$

$$S_{xx} = 247 \text{ MPa } (36 \text{ ksi})$$

$$k_\varepsilon = 2.96$$

Results for specimen No. 4-4, which was a replicate of
specimen No. 4-3 above, are shown in Figure 30. The far-field
strains are linear to failure. Strains on the hole boundary are
linear up to an applied stress of approximately 103 MPa (15 ksi).
Thereafter they increase nonlinearly at a slower rate. This
unusual trend continues up to failure. Values for the elastic and
strength constants for this specimen are:

$$E_{xx} = 56 \text{ GPa } (8.2 \times 10^6 \text{ psi})$$

$$\nu_{xy} = 0.30$$

$$S_{xx} = 263 \text{ MPa } (38 \text{ ksi})$$

$$k_\varepsilon = 2.64$$

43
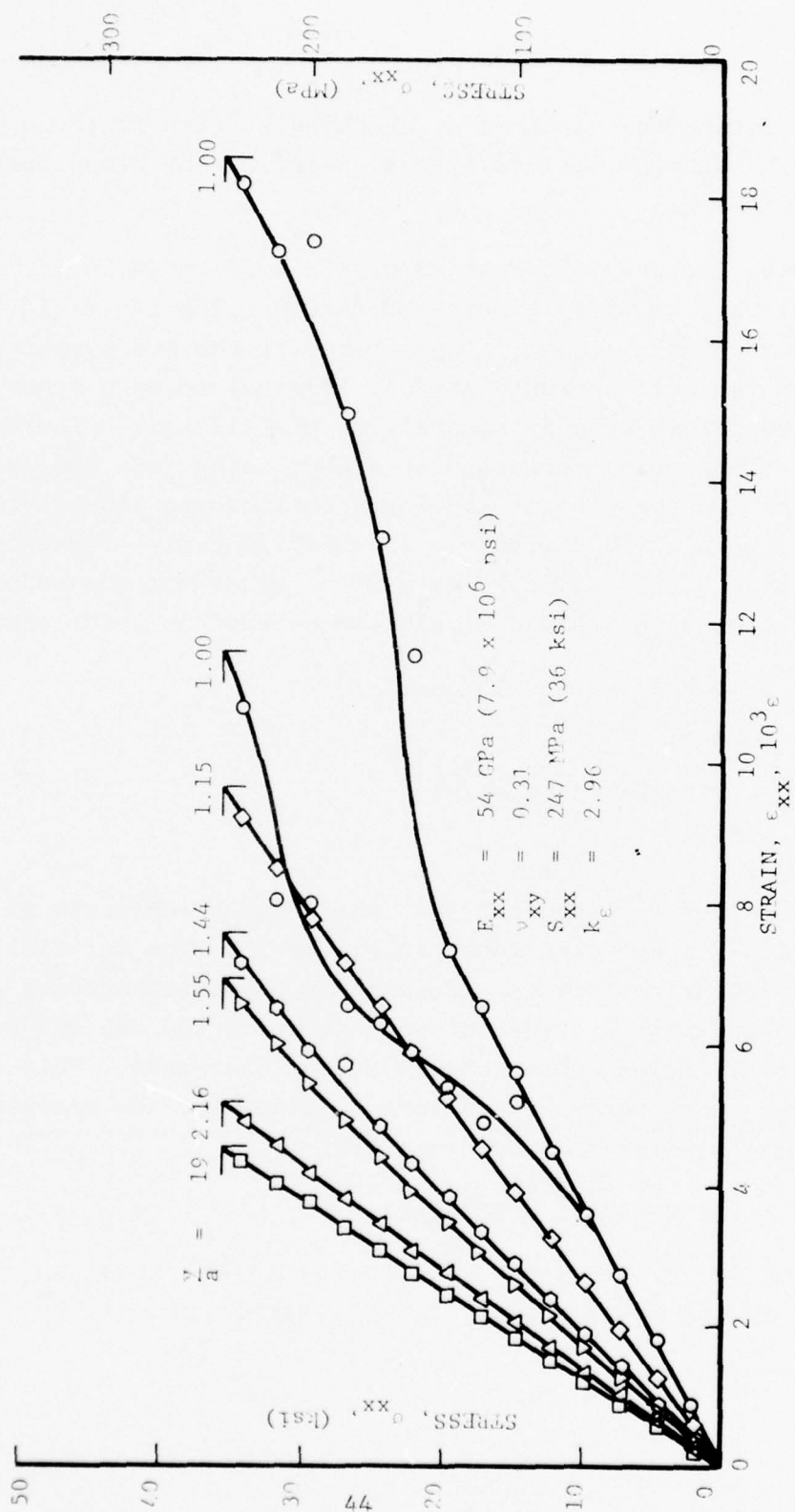
Figure 28. Vertical Strains Along Horizontal Axis of $[0/\pm45/90]_s$ Graphite/Epoxy Specimen With 1.27 cm (0.50 in.) Diameter Hole Under Uniaxial Tensile Loading (Spec. No. 4-3).
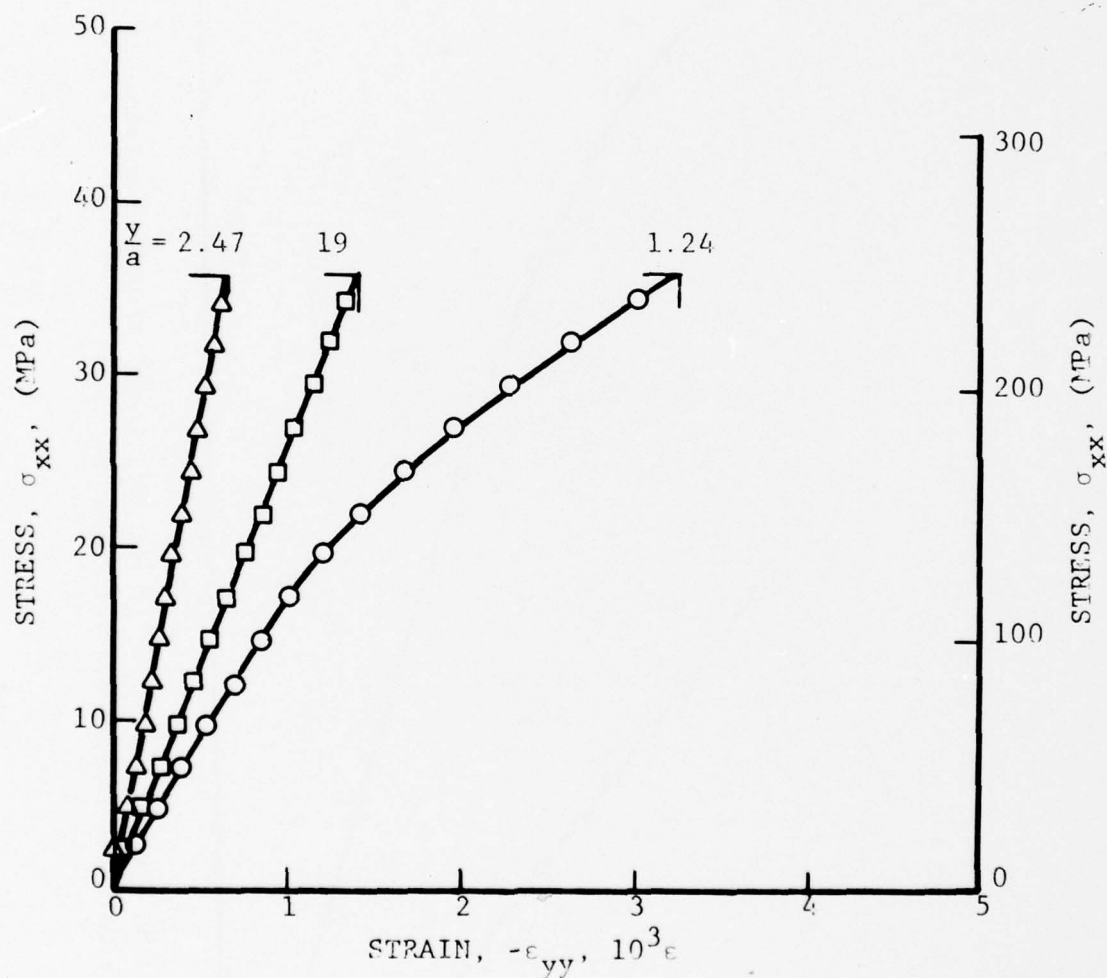
Figure 29. Horizontal Strains Along Horizontal
Axis of $[0/\pm45/90]_s$ Graphite/Epoxy
Specimen With 1.27 cm (0.5 in.)
Diameter Hole Under Uniaxial Tensile
Loading (Spec. No. 4-3).

45
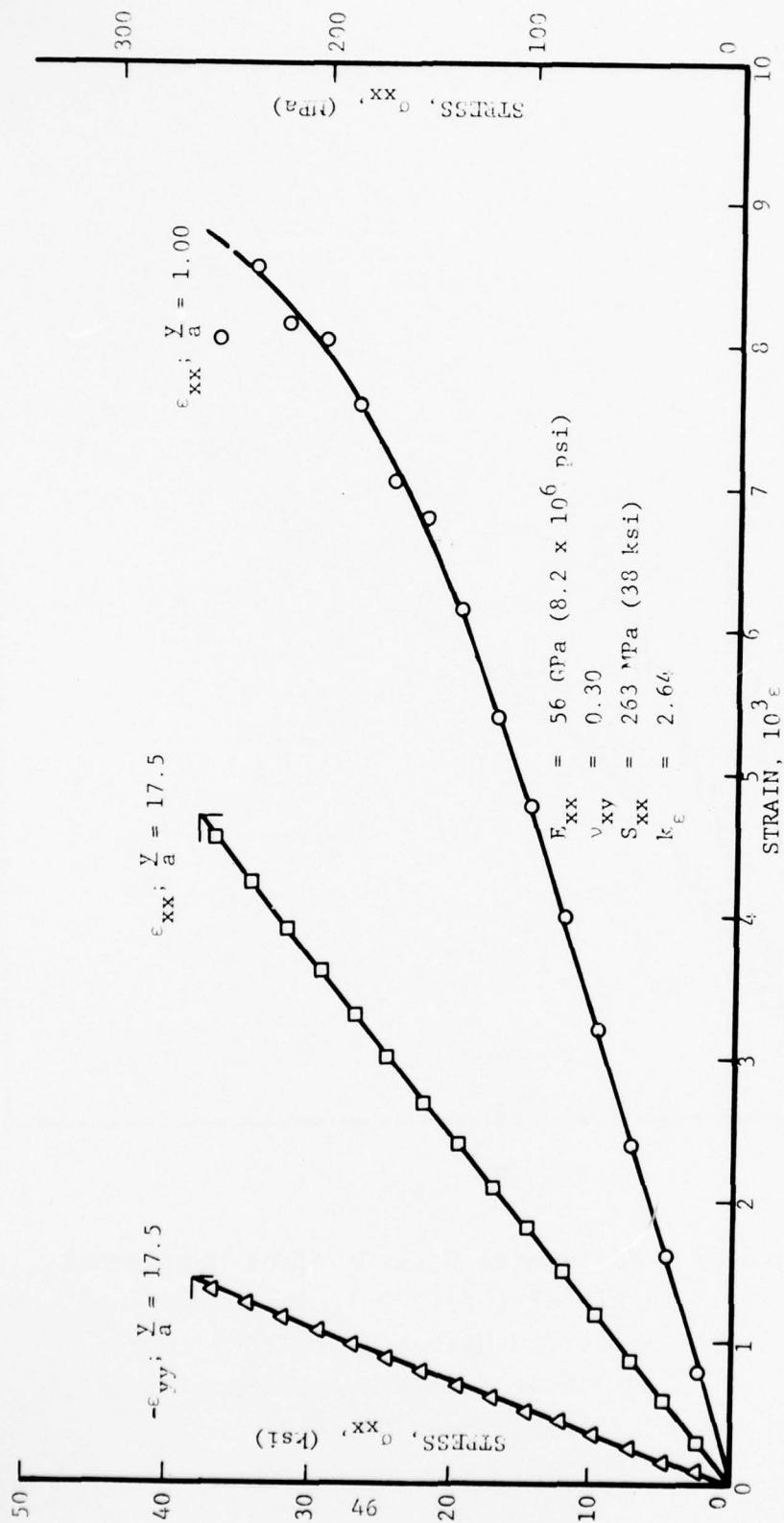
Figure 30. Strains Along Horizontal Axis of $[0/\pm 45/90]_s$ Graphite/Epoxy Specimen With 1.27 cm (0.5 in.) Hole Under Uniaxial Tensile Loading (Spec. No. 4-4).

The strain concentration factor is substantially lower than the theoretical value and previously obtained experimental values.

Specimen No. 4-9 had a 1.91 cm (0.75 in.) diameter central circular hole. It was instrumented with a 0.51 mm (0.020 in.) thick photoelastic coating and strain gages. Strain distributions obtained from strain gages are plotted in Figure 31. Strain readings on the boundary of the hole were erratic for the most part and are not shown. Values for the modulus, Poisson's ratio, and strength are:

$$E_{xx} = 56 \text{ GPa } (8.1 \times 10^6 \text{ psi})$$
$$\nu_{xy} = 0.28$$
$$S_{xx} = 243 \text{ MPa } (35 \text{ ksi})$$

The strains near the hole boundary ($\frac{y}{a} = 1.06$) are linear up to an applied stress of approximately 140 MPa (20 ksi).

Photoelastic fringe patterns on the photoelastic coating used on this specimen are shown in Figure 32. The points of tangential strain concentration off the horizontal axis become evident at higher loads. In this case these points are located at an angle of 71-degrees from the loading axis. The variation of fringe order and tangential strain at the 0-, 71- and 90-degree locations on the hole boundary is shown in Figure 33. The fringe order at the 0-degree location, corresponding to the compressive strain at that point, varies linearly to failure. The birefringence at the 90-degree location varies linearly up to an applied stress of approximately 110 MPa (16 ksi) corresponding to a tangential strain of approximately 0.006ε. The latter corresponds to the failure strain of the 90-degree plies. The fringe order, hence the tangential strain, at the 71 degree location becomes nonlinear at a lower stress, approximately 83 MPa (12 ksi). Thereafter it
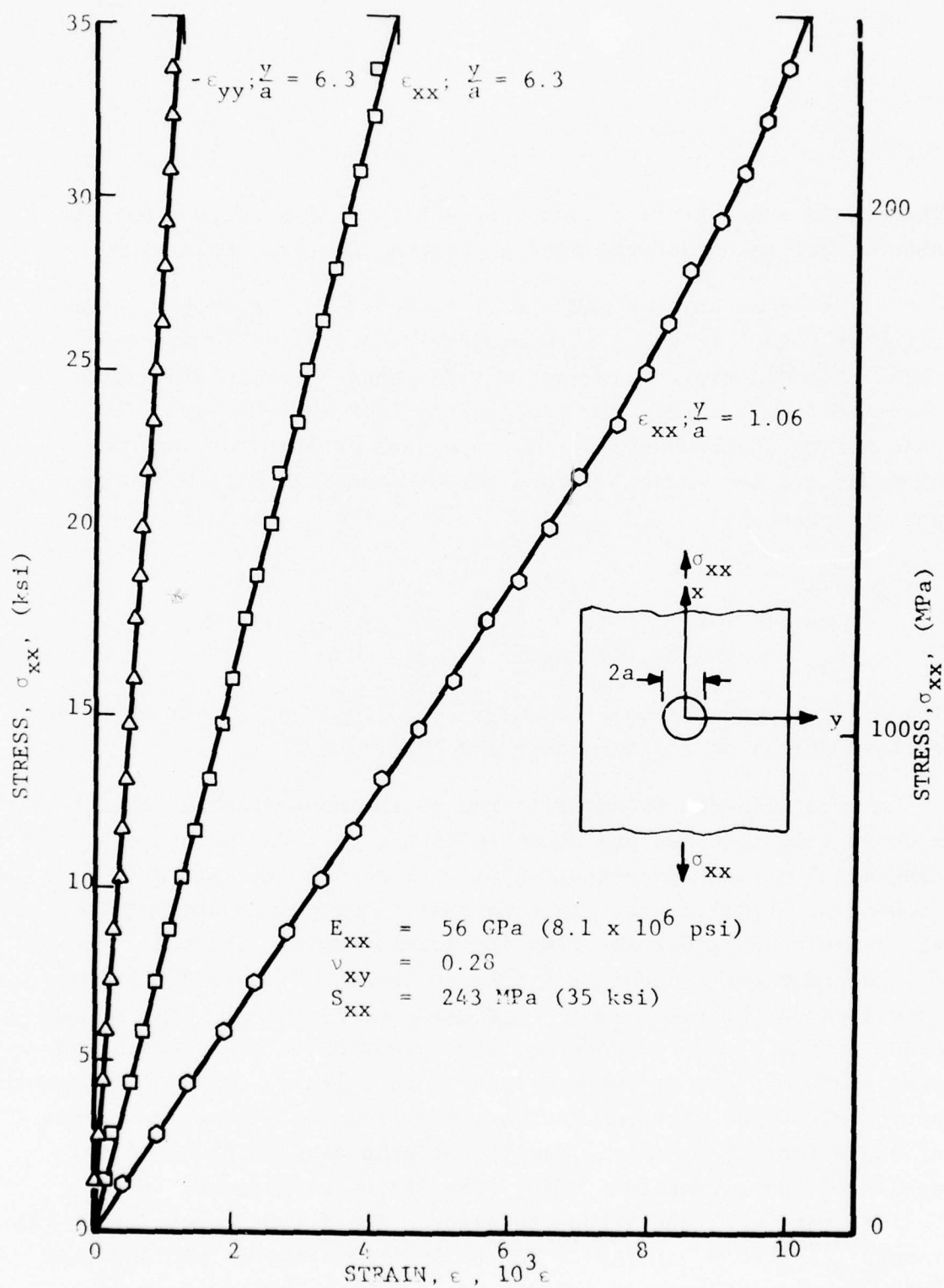
Figure 31. Strains Along Horizontal Axis of $[0/+45/90]_s$ Graphite/
Epoxy Specimen With a 1.91 cm (0.75 In.) Diameter Circular
Hole Under Uniaxial Tensile Loading (Spec. No. 4-9).

48
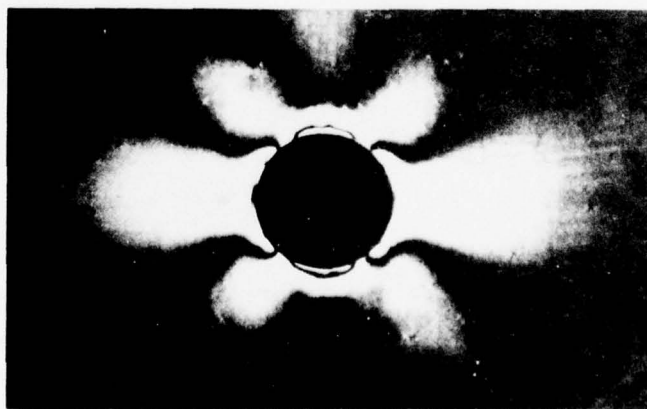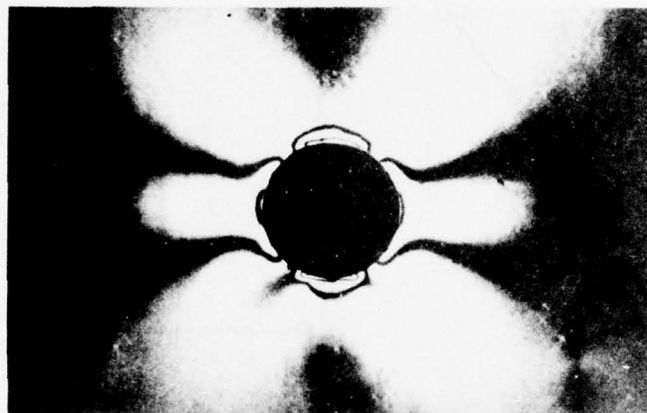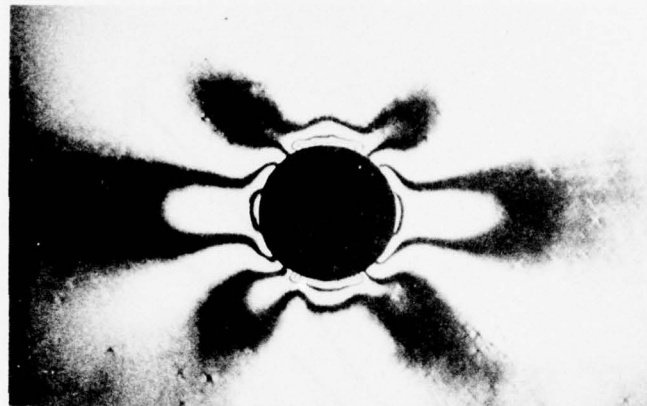
Figure 32. Isochromatic Fringe Patterns in Photoelastic Coating on
[0/±45/90]_s Graphite/Epoxy Specimen with 1.91 cm
(0.75 in.) Diameter Circular Hole Under Uniaxial Tensile
Loading at Three Levels of Applied Stress: (a) 142 MPa
(20.5 ksi), (b) 182 MPa (26.4 ksi) and (c) 223 MPa
(32.3 ksi), (Spec. No. 4-9).

49
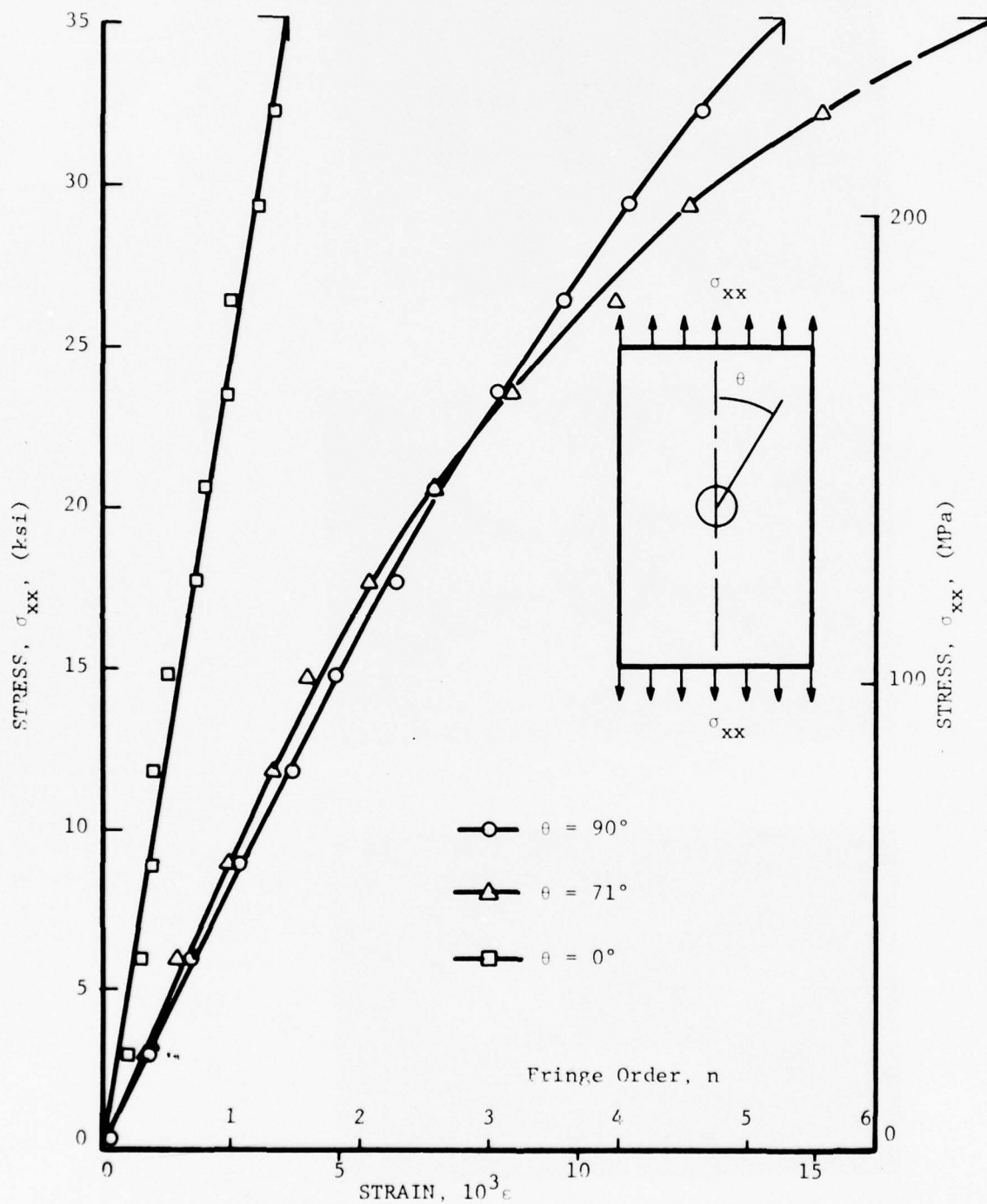
Figure 33. Fringe Order and Tangential Strain at Three Locations
on the Hole Boundary for [0/+45/90]$_s$ Graphite/Epoxy
Specimen with a 1.91 cm (0.75 in.) Diameter Circular
Hole Under Uniaxial Tensile Loading (Spec. No. 4-9).

50

increases at a faster rate overtaking and exceeding the fringe order (strain) at the 90-degree location. Failure initiated at these off-axis points.

Specimen No. 4-10 was a replicate of No. 4-9 above. It was extensively instrumented with strain gages. Strain variations to failure are shown in Figures 34 and 35. Strains on the hole boundary are linear up to an applied stress of approximately 83 MPa (12 ksi), thereafter they tend to show a stiffening effect. This may not be realistic since it was observed that the gages tended to debond at that point due to splitting of the laminate at the edge as a result of interlaminar tensile stresses. This interlaminar tensile failure near the edge affects in a similar manner the strain readings at a distance of 1.06 radii from the center of the hole. Strains farther away from the hole remain linear to higher applied stresses. The far-field strains appear linear to failure. Failure initiated at the characteristic off-axis points discussed before. Values for the modulus, Poisson's ratio, strength and strain concentration factor are:

$$E_{xx} = 52.5 \text{ GPa } (7.6 \times 10^6 \text{ psi})$$

$$\nu_{xy} = 0.29$$

$$S_{xxT} = 219 \text{ MPa } (32 \text{ ksi})$$

$$k_\varepsilon = 2.90$$

Specimen No. 4-11 had a 2.54 cm (1 in.) diameter hole. It was instrumented with a 1 mm (0.04 in.) thick photoelastic coating on one side and strain gages on the other side. Strain distributions obtained from strain gages are plotted in Figure 36. Strains on the boundary of the hole are linear up to an applied stress of approximately 117 MPa (17 ksi), thereafter the strain at one point of the hole boundary increased at a much faster rate whereas the

Figure 34. Vertical Strains Along Horizontal Axis of [0/+45/90]s Graphite/Epoxy Specimen with a 1.91 cm (0.75 In.) Diameter Circular Hole Under Uniaxial Tensile Loading (Spec. No. 4-10).

52
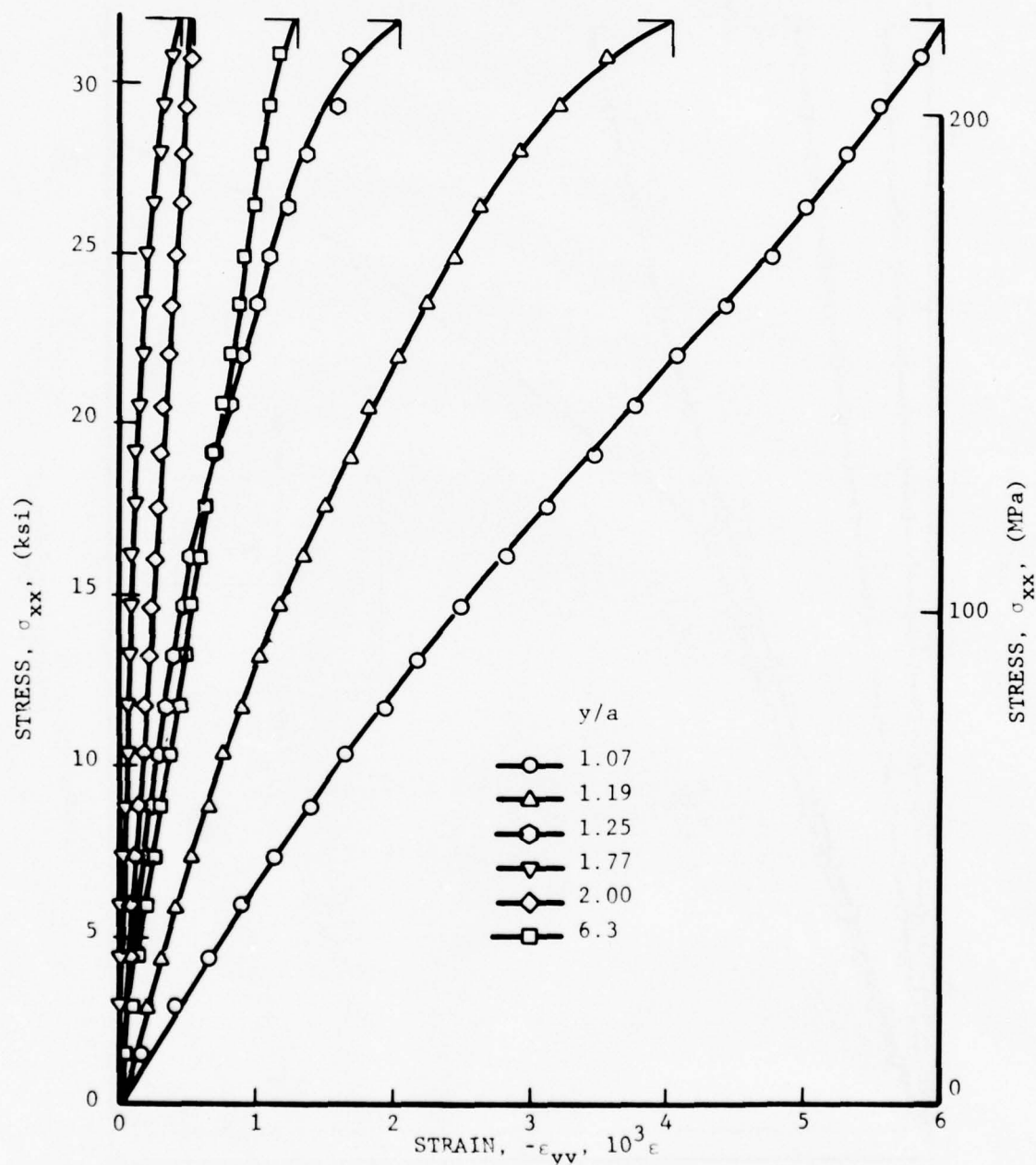
Figure 35. Horizontal Strains Along Horizontal Axis of $[0/+45/90]_s$ Graphite/Epoxy Specimen with a 1.91 cm (0.75 in.) Diameter Circular Hole Under Uniaxial Tensile Loading (Spec. No. 4-10).
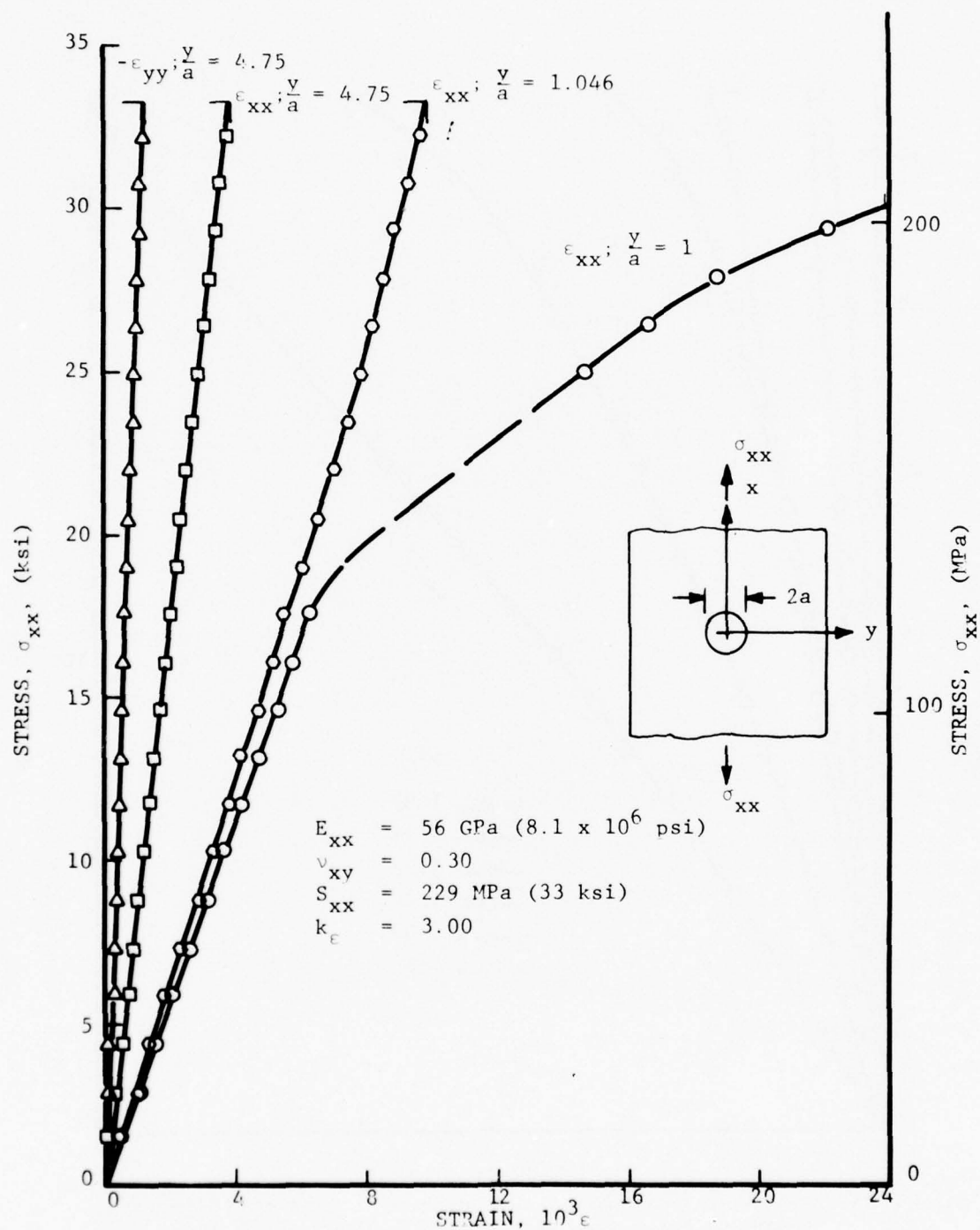
Figure 36. Strains Along Horizontal Axis of $[0/+45/90]_s$ Graphite/Epoxy Specimen With a 2.54 cm (1 in.) Diameter Circular Hole Under Uniaxial Tensile Loading (Spec. No. 4-11).

54

rate of increase at the symmetric point decreased. This may be due
to some asymmetric failure initiation. Values for the modulus,
Poisson's ratio and strength are:

$$E_{xx} = 56 \text{ GPa } (8.1 \times 10^6 \text{ psi})$$
$$\nu_{xy} = 0.30$$
$$S_{xx} = 299 \text{ MPa } (33 \text{ ksi})$$

Fringe patterns on the photoelastic coating used were analyzed at
the 0-degree and 90-degree locations. The fringe order variation
and that of the tangential strain at these two locations are shown
in Figure 37. The birefringence at the 90-degree location varies
linearly up to an applied stress of approximately 110 MPa (16 ksi)
corresponding to the 90-degree ply failure strain of approximately
0.006ε.

Specimen No. 4-12 was a replicate of No. 4-11 above. It
was extensively instrumented with strain gages. Strain variations
to failure are shown in Figures 38 and 39. Strains on the hole
boundary and near the boundary show a stiffening effect which is
due to some delamination on the boundary. Values for the modulus,
Poisson's ratio, strength and strain concentration factor are:

$$E_{xx} = 54.5 \text{ GPa } (7.9 \times 10^6 \text{ psi})$$
$$\nu_{xy} = 0.30$$
$$S_{xxT} = 209 \text{ MPa } (30 \text{ ksi})$$
$$k_{\varepsilon} = 3.00$$

To extend the study of hole size effect, another set of
specimens with hole diameters of 4.76 mm (0.1875 in.), 1.59 mm
(0.0625 in.), 0.406 mm (0.016 in.) and 0.20 mm (0.008 in.) were
prepared and tested. These specimens were 2.54 cm (1 in.) wide

55
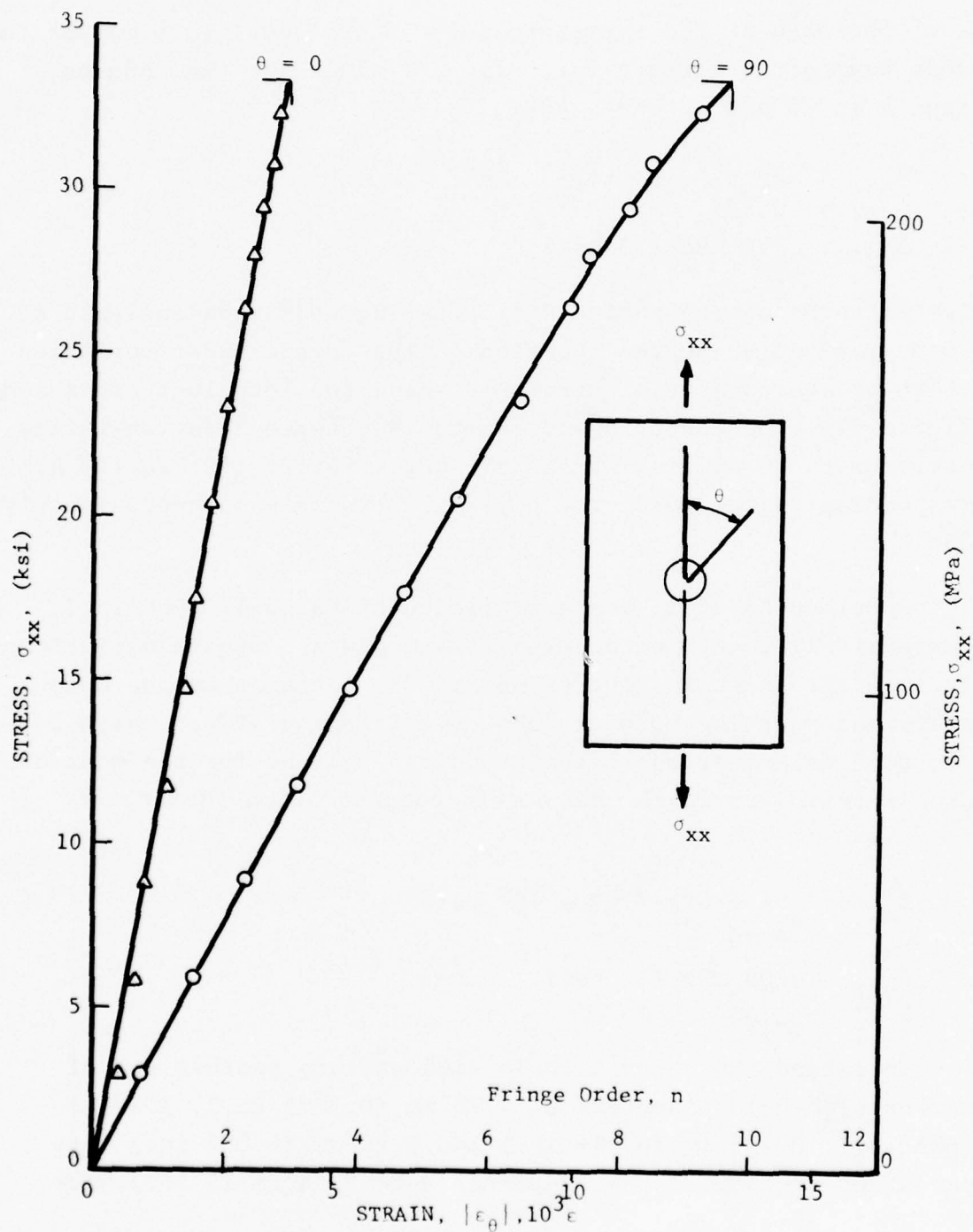
Figure 37. Fringe Order and Tangential Strain at Two Locations on the Hole Boundary for $[0/\pm45/90]_s$ Graphite/Epoxy Specimen with a 2.54 cm (1 in.) Diameter Hole Under Uniaxial Tensile Loading (Spec. No. 4-11).

56
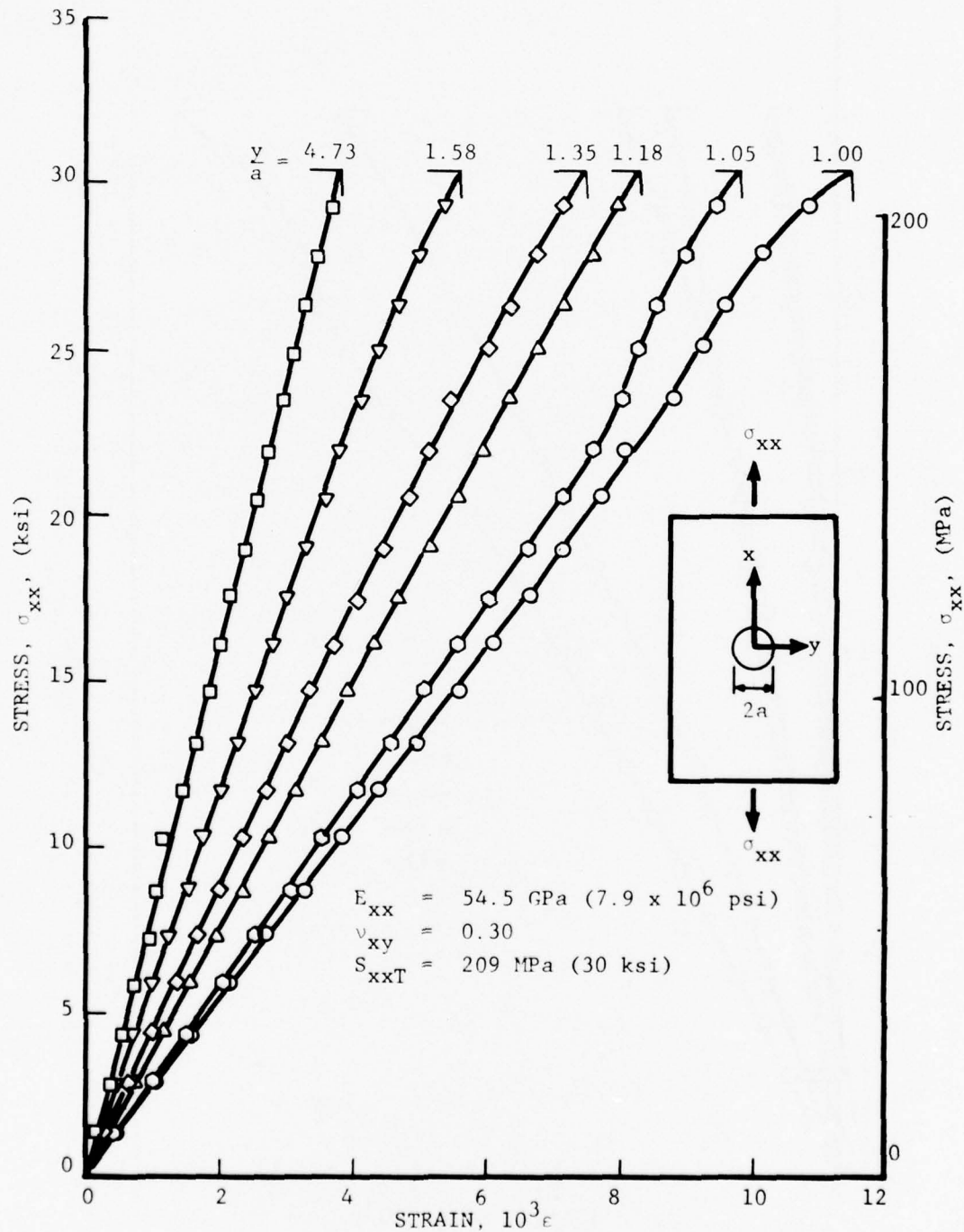
Figure 38. Vertical Strains Along Horizontal Axis of [0/+45/90]$_s$ Graphite/Epoxy Specimen with a 2.54 cm (1 in.) Diameter Circular Hole Under Uniaxial Tensile Loading (Spec. No. 4-12).

57
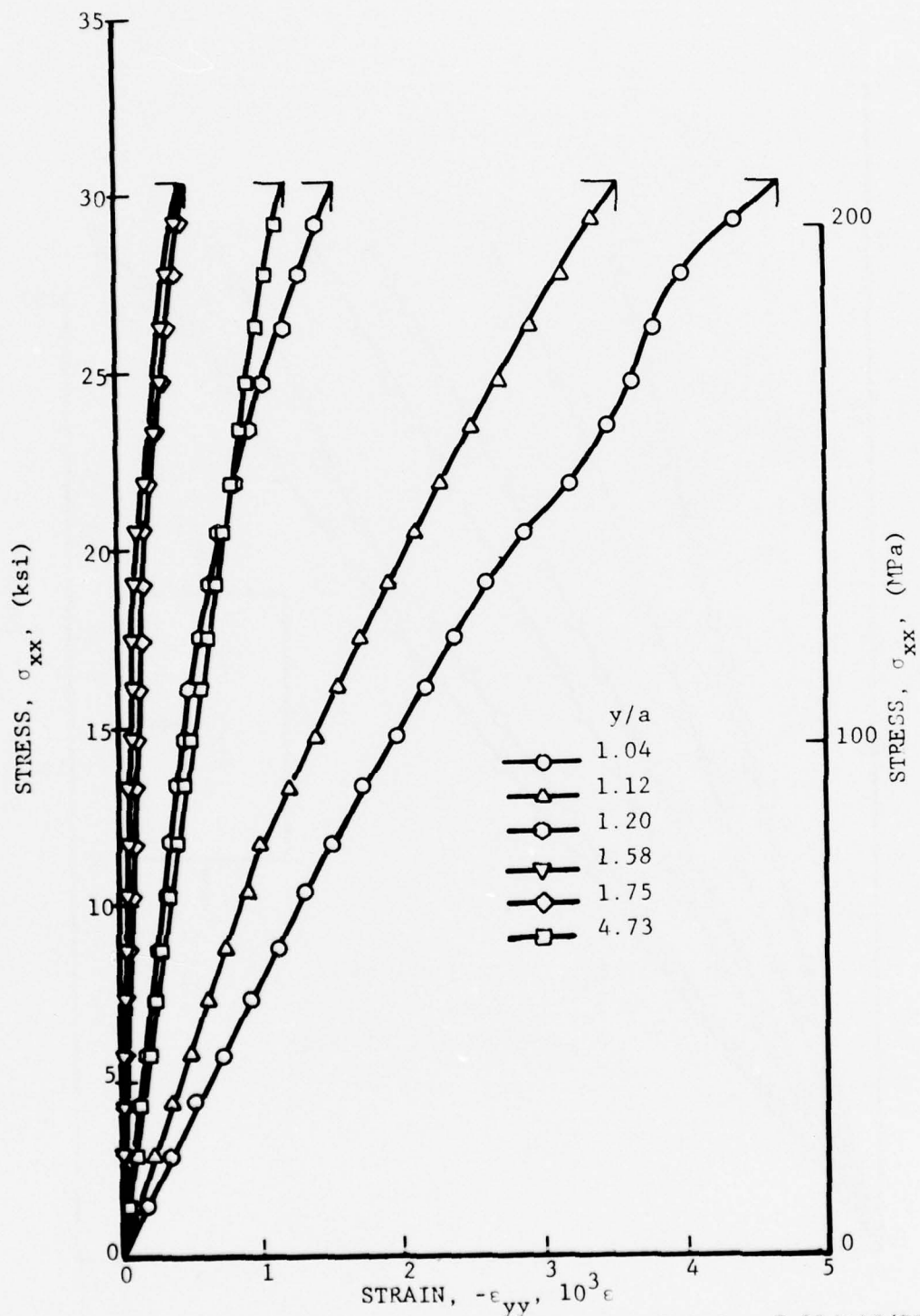
Figure 39. Horizontal Strains Along Horizontal Axis of $[0/\pm45/90]_s$ Graphite/Epoxy Specimen with a 2.54 cm (1 in.) Diameter Circular Hole Under Uniaxial Tensile Loading (Spec. No. 4-12).

58

and 22.9 cm (9 in.) long coupons. The specimens were uninstrumented
and tested to failure to determine the strength reduction due to
the presence of the hole. Two specimens for each hole size were
tested. The four specimens with the two smallest holes did not
fail through the hole. The average strength of these four specimens
was taken as the basic unnotched strength for comparison with the
notched strength of the other specimens. The latter failed through
the holes with failure initiation at the characteristic off-axis
points.

Typical failure patterns of specimens with holes of various
diameters are shown in Figure 40. They illustrate the off-axis
failure initiation and not too straight fracture across the width
of the specimen.

5. EFFECT OF HOLE DIAMETER

Results for all uniaxial specimens with holes are summarized
in Table V. The last column in this table shows the strength reduction
ratio, i.e., the ratio of the strength of the notched specimen to
that of the unnotched specimen. The average values of the measured
modulus and Poisson's ratio computed from the far-field strains
agree well with the values determined from uniaxially loaded
unnotched specimens. The average value for the strain concentration
is 2.90 which is slightly lower than the theoretical value of 3.
Measured peak strains at failure exceed twice the ultimate strain
of the unnotched laminate.

The strength reduction ratio is plotted versus hole diameter
in Figure 41. The point stress and average stress criteria proposed
by Whitney and Nuismer (Reference 18) for uniaxial loading of plates
with holes were used. According to the point stress criterion failure
occurs when the axial (σ_y) stress at some distance d_o from the hole
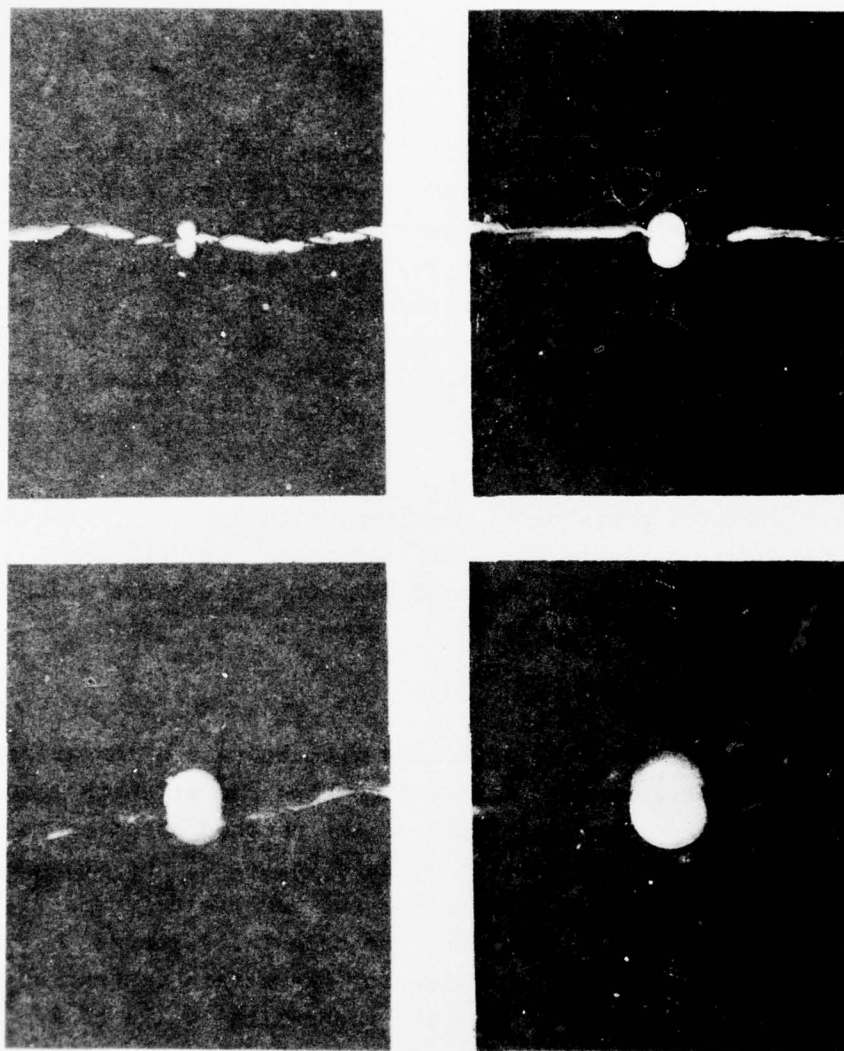
Figure 40.   Failure Patterns in Uniaxially Loaded $[0/\pm45/90]_s$
Graphite/Epoxy Plates with Holes of Various Diameters
(Hole Diameters are: 0.64 cm (0.25 in.), 1.27 cm
(0.50 in.), 1.91 cm (0.75 in.) and 2.54 cm (1.00 in.)

60

TABLE V

UNIAXIAL [0/±45/90]$_s$ LAMINATES WITH CIRCULAR HOLES

Spec. No.	Hole Diameter 2a cm (in)		Modulus E$_{xx}$ GPa (10^6 psi)		Poisson's Ratio ν$_{xy}$	Strain Conc. Factor k$_ε$	Strength S$_{xx}$ MPa (ksi)		Maximum Strain at Failure (10^{-3} ε)	Strength Reduction, S$_{xx}$/S$_o$
4-11	2.54	(1.00)	56	(8.1)	0.30	3.00	229	(33)	>22	0.455
4-12	2.54	(1.00)	54	(7.9)	0.30	3.00	209	(30)	11.5	0.416
4-9	1.91	(0.75)	56	(8.1)	0.28	2.85	243	(35)	18.5	0.482
4-10	1.91	(0.75)	53	(7.6)	0.29	2.90	219	(32)	-	0.436
4-3	1.27	(0.50)	54	(7.9)	0.31	2.96	247	(36)	18.6	0.493
4-4	1.27	(0.50)	56	(8.2)	0.30	2.64	263	(38)	-	0.521
4-1	0.64	(0.25)	54	(7.9)	0.30	-	271	(39)	>9.4	0.534
4-2	0.64	(0.25)	56	(8.1)	0.25	2.96	282	(41)	19	0.562
4-17	0.48	(0.187)					309	(45)		0.658
4-18	0.48	(0.187)					286	(41)		0.608
4-19	0.16	(0.062)					381	(55)		0.811
4-20	0.16	(0.062)					388	(56)		0.825
4-21	0.04	(0.016)					463	(67)		1
4-22	0.04	(0.016)					434	(63)		1
4-23	0.02	(0.008)					505	(73)		1
4-24	0.02	(0.008)					478	(69)		1

61
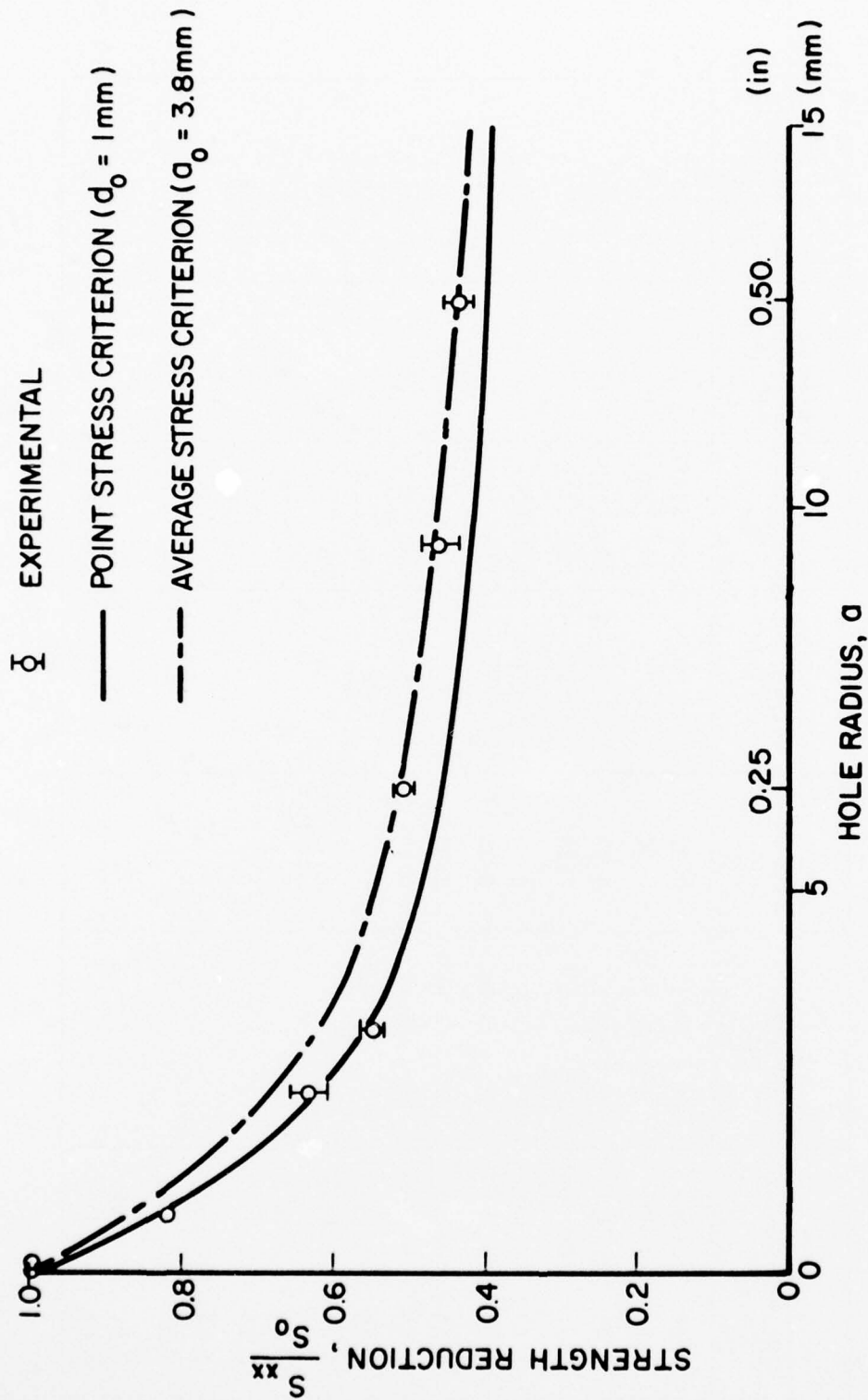
Figure 41. Strength Reduction as a Function of Hole Radius for $[0/\pm45/90]_s$ Graphite/Epoxy Plates with Circular Holes Under Uniaxial Tensile Loading

62

boundary on the horizontal (x-) axis equals the uniaxial strength of the unnotched material (Figure 42). The strength reduction ratio predicted by this criterion is expressed as

$$\frac{S_{yy}}{S_o} = \frac{2}{2+\xi_1^2+3\xi_1^4}$$

where $\xi_1 = \frac{a}{a+d_o}$

d_o = characteristic length dimension (~1 mm)

S_{yy}, S_o = strengths of notched and unnotched laminates, respectively

According to the average stress criterion failure occurs when the axial (σ_y) stress averaged over some length a_o from the hole boundary on the horizontal (x-) axis equals the uniaxial strength of the unnotched material (Figure 43). The strength reduction ratio predicted by this criterion is expressed as

$$\frac{S_{yy}}{S_o} = \frac{2}{(1+\xi_2)(2+\xi_2^2)}$$

where

$\xi_2 = \frac{a}{a+a_o}$

a_o = characteristic length dimension (~4 mm)

Experimental results for the strength reduction ratio were compared with curves based on the two criteria above. The agreement seems to be satisfactory for characteristic dimensions of d_o = 1 mm and a_o = 3.8 mm. One phenomenon observed experimentally, which is not predicted by these curves, is that there is a critical hole diameter below which the laminate becomes insensitive to the notch and fracture is as likely to occur through the notched as through the unnotched section.
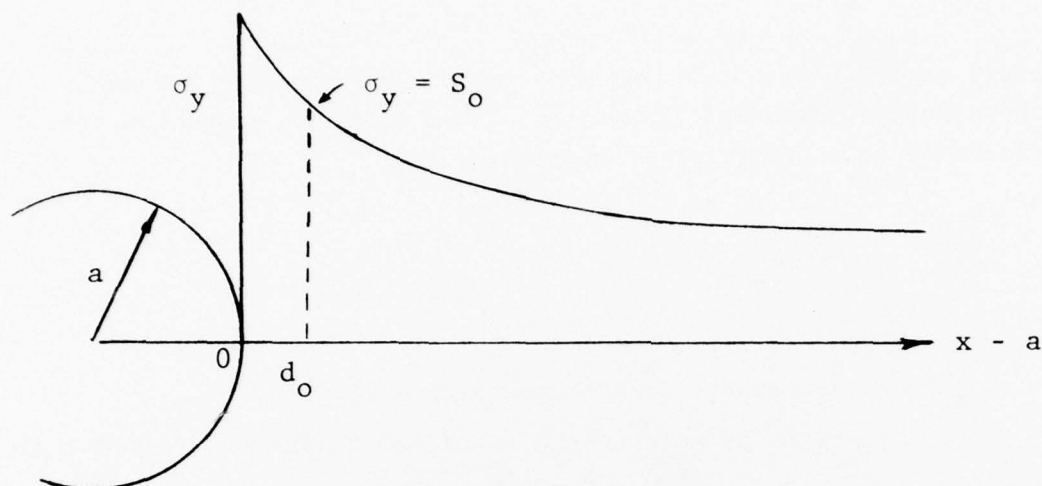
63

$$\frac{S_{yy}}{S_o} = \frac{2}{2 + \xi_1^2 + 3\xi_1^4}$$

$$\xi_1 = \frac{a}{a + d_o}$$

d_o = characteristic length dimension (~ 1 mm)

S_{yy}, S_o = strengths of notched and unnotched laminates, respectively

Figure 42. Strength Reduction of Uniaxially Loaded Plate with Circular Hole According to Point Stress Criterion (Reference 18)

64

$$\frac{S_{yy}}{S_o} = \frac{2}{(1+\xi_2)(2+\xi_2^2)}$$

$\xi_2 = \dfrac{a}{a + a_o}$
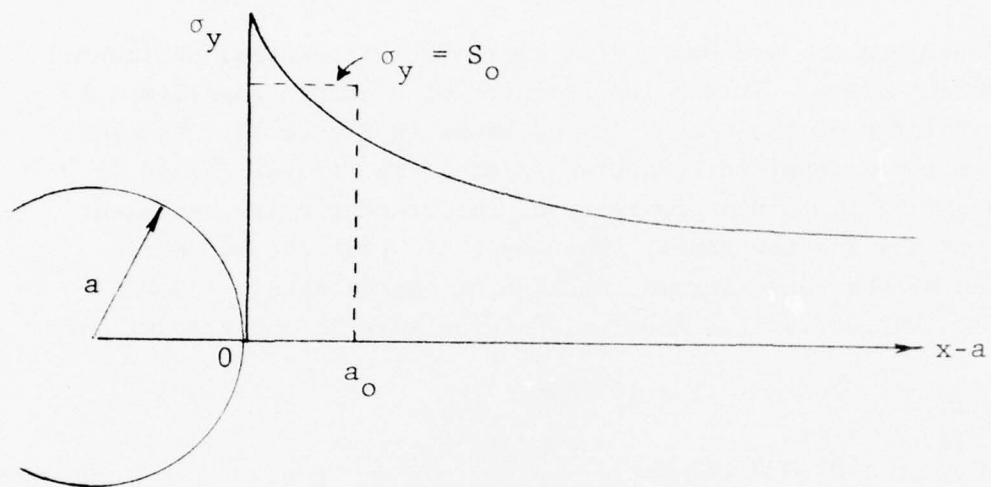
a_o = characteristic length dimension (~ 3.8 mm)

S_{yy}, S_o = strengths of notched and unnotched laminates, respectively.

Figure 43. Strength Reduction of Uniaxially Loaded Plate with Circular Hole According to Average Stress Criterion (Reference 18)

6. RESULTS FOR SPECIMENS WITH CRACKS

Specimen No. 4-5 had a 2.54 cm (1.00 in.) central horizontal (transverse) crack. It was instrumented with strain gages, mostly in the vicinity of the crack tips as shown in Figure 23. Strains as a function of applied stress are plotted in Figures 44 and 45. Strains in the immediate proximity of the crack tip are nonlinear throughout the loading range. The onset of crack extension is evidenced by the rapid strain increase at approximately 138 MPa (20 ksi). Values for the modulus, Poisson's ratio and strength are:

$$E_{xx} = 52 \text{ GPa } (7.5 \times 10^6 \text{ psi})$$
$$\nu_{xy} = 0.27$$
$$S_{xx} = 202 \text{ MPa } (29 \text{ ksi})$$

No strain concentration factor was obtained because the strain cannot be measured precisely at the very crack tip. However, at a distance of $y/a = 1.04$ an initial strain ratio (ratio of local strain to far-field strain) of 3.95 was measured. The transverse strains in the vicinity of the crack are highly nonlinear and show irregular trends, possibly due to strain redistributions.

Specimen No. 4-6 was a replicate of No. 4-5 above. It was instrumented with a 0.25 mm (0.010 in.) thick photoelastic coating on one side and some strain gages on the other. A photograph of the gage layout in the vicinity of the crack is shown in Figure 24. Strain distributions are plotted in Figure 46. Elastic and strength properties obtained are:

$$E_{xx} = 55 \text{ GPa } (7.9 \times 10^6 \text{ psi})$$
$$\nu_{xy} = 0.29$$
$$S_{xx} = 233 \text{ MPa } (34 \text{ ksi})$$

The curve for the strain near the tip of the crack ($y/a = 1.03$) shows two distinct points of slope change, at $\sigma_{xx} = 35$ MPa (5 ksi) and $\sigma_{xx} = 110$ MPa (16 ksi) corresponding to local strains of

Figure 44. Vertical Strains Along, Horizontal Axis of $[0/\pm45/90]_s$ Graphite/Epoxy Specimen With a 2.54 cm (1 in.) Horizontal Crack Under Uniaxial Tensile Loading. (Spec. No. 4-5).
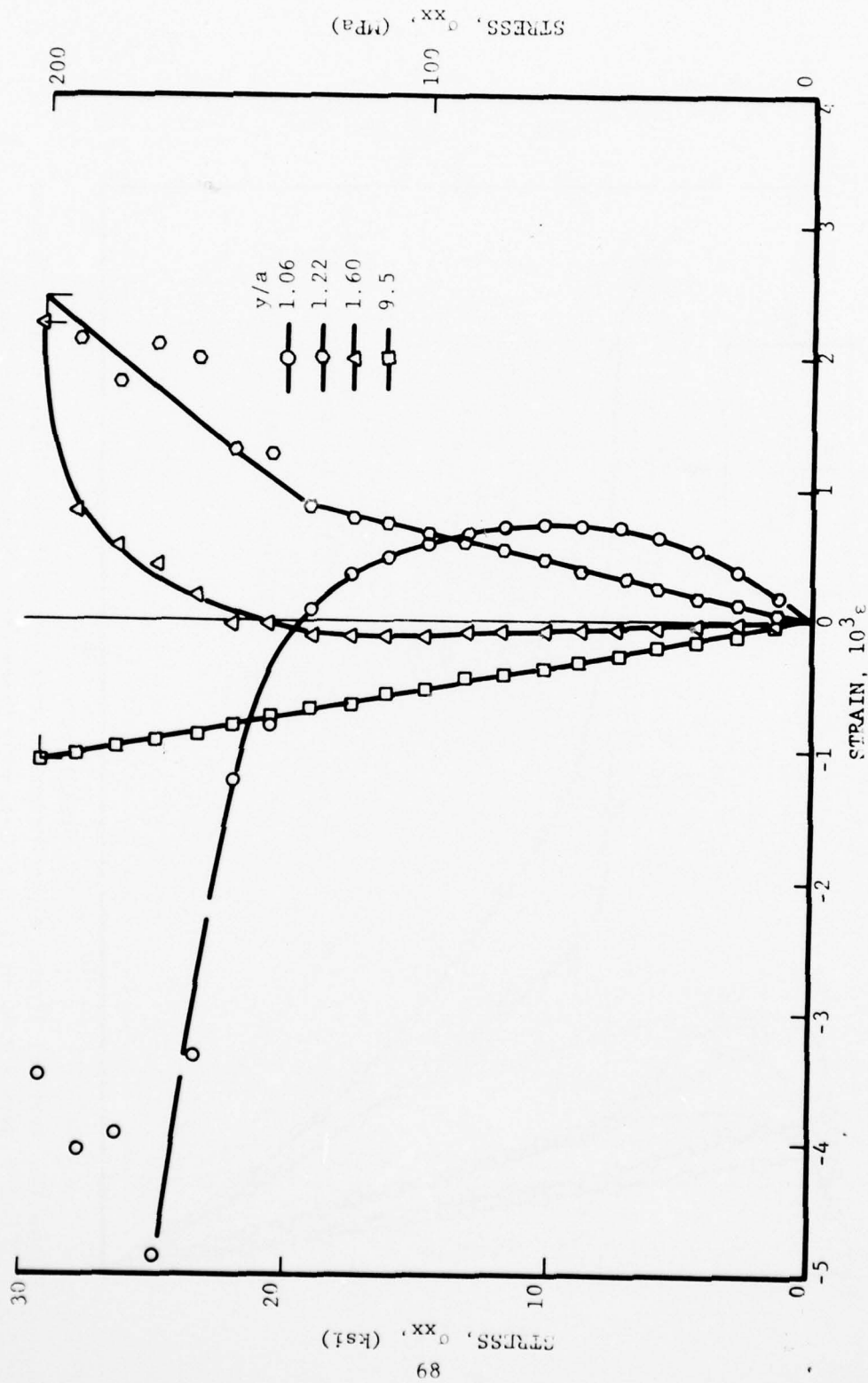
Figure 45. Horizontal Strains Along Horizontal Axis of [0/±45/90]s Graphite/Epoxy Specimen with a 2.54 cm (1 in.) Horizontal Crack Under Uniaxial Tensile Loading (Spec. No. 4-5).
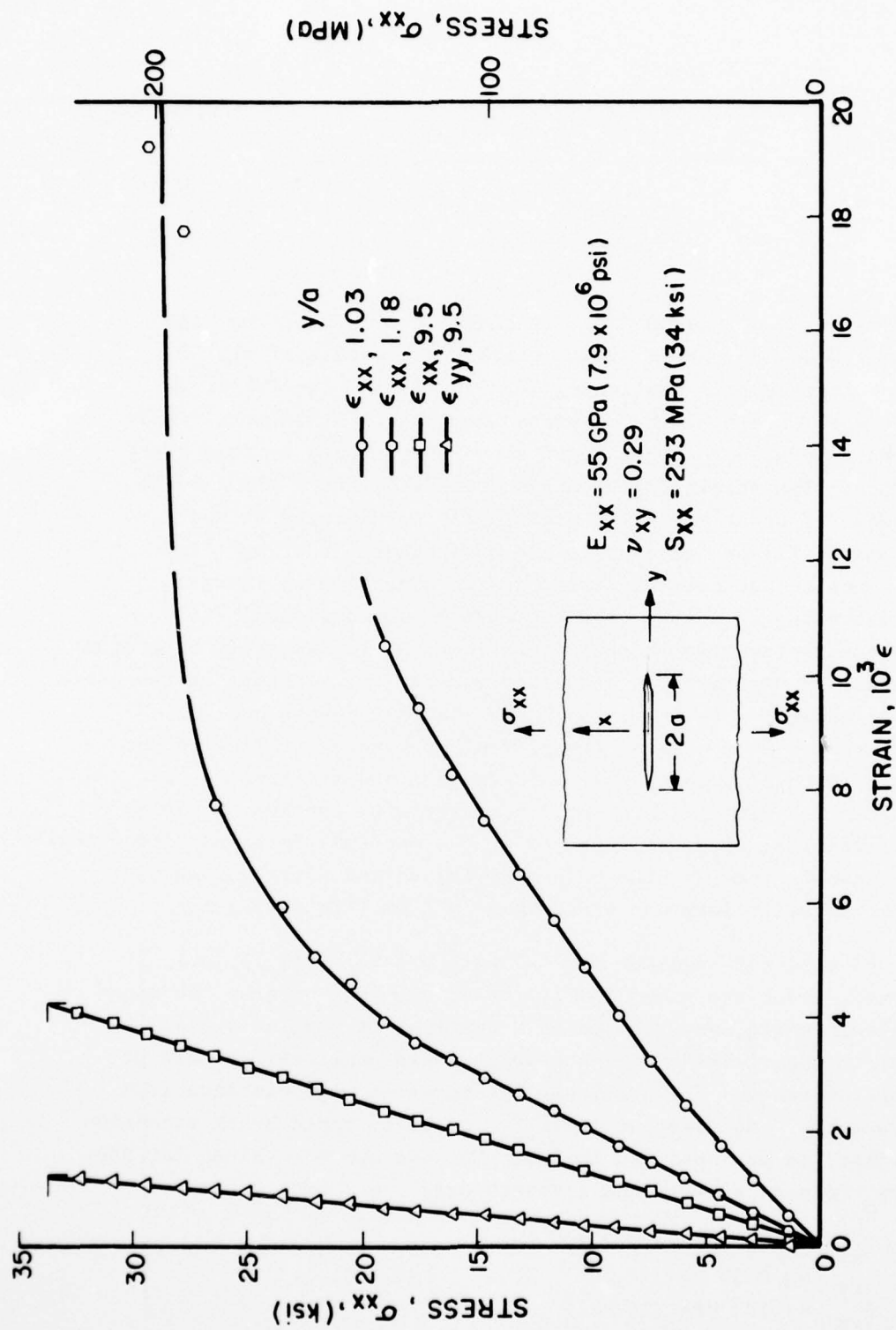
Figure 46. Strains Along Horizontal Axis of [0₂/+45]s Graphite/Epoxy Specimen With a 2.54 cm (1 in.) Horizontal Crack Under Uniaxial Tensile Loading (Spec. No. 4-6)

69

approximately 0.002 and 0.010. It should be recalled that the
former is equal to the strain at which the response of the 90-
deg. specimen becomes nonlinear (Section II) and the latter is
the ultimate strain of the unnotched laminate. It is more likely
then that the higher stress level above corresponds to some crack
extension. The strain distribution around the crack tip and the
phenomenon of crack extension are vividly illustrated by the
isochromatic fringe patterns in the photoelastic coating (Figure
47). A noticeable characteristic is the direction of initial
crack extension at a 45-degree angle with the horizontal axis.
Another characteristic is that there is no sustained crack extension
but rather an extension of a damaged zone in the vicinity of the crack
tip. As observed previously by Mandell et al. (Reference 20),
this damaged zone consists primarily of subcracks parallel to the
fibers of each ply, some local delamination and sometimes fiber
breakage. The size of this zone increases with applied stress up
to some critical size, at which point the specimen fails catastrophically.
In the case in question the mean diameter of the damaged zone just
prior to total failure was approximately 5 mm (Figure 47).

Results for specimen No. 4-7 with a 1.91 cm (0.75 in.)
horizontal crack are shown in Figures 48 and 49. Strains, obtained
from strain gages, are plotted as a function of applied stress.
Strains in the vicinity of the crack tip are nonlinear throughout
the loading range. The nonlinearity decreases with distance from
the crack tip. No clearcut limit for onset of rapid crack extension
is evident, as was observed in spec. No. 4-5 above. Values for the
modulus, Poisson's ratio and strength are:

$$E_{xx} = 53 \text{ GPa } (7.7 \times 10^6 \text{ psi})$$
$$\nu_{xy} = 0.30$$
$$S_{xx} = 180 \text{ MPa } (26 \text{ ksi})$$

70
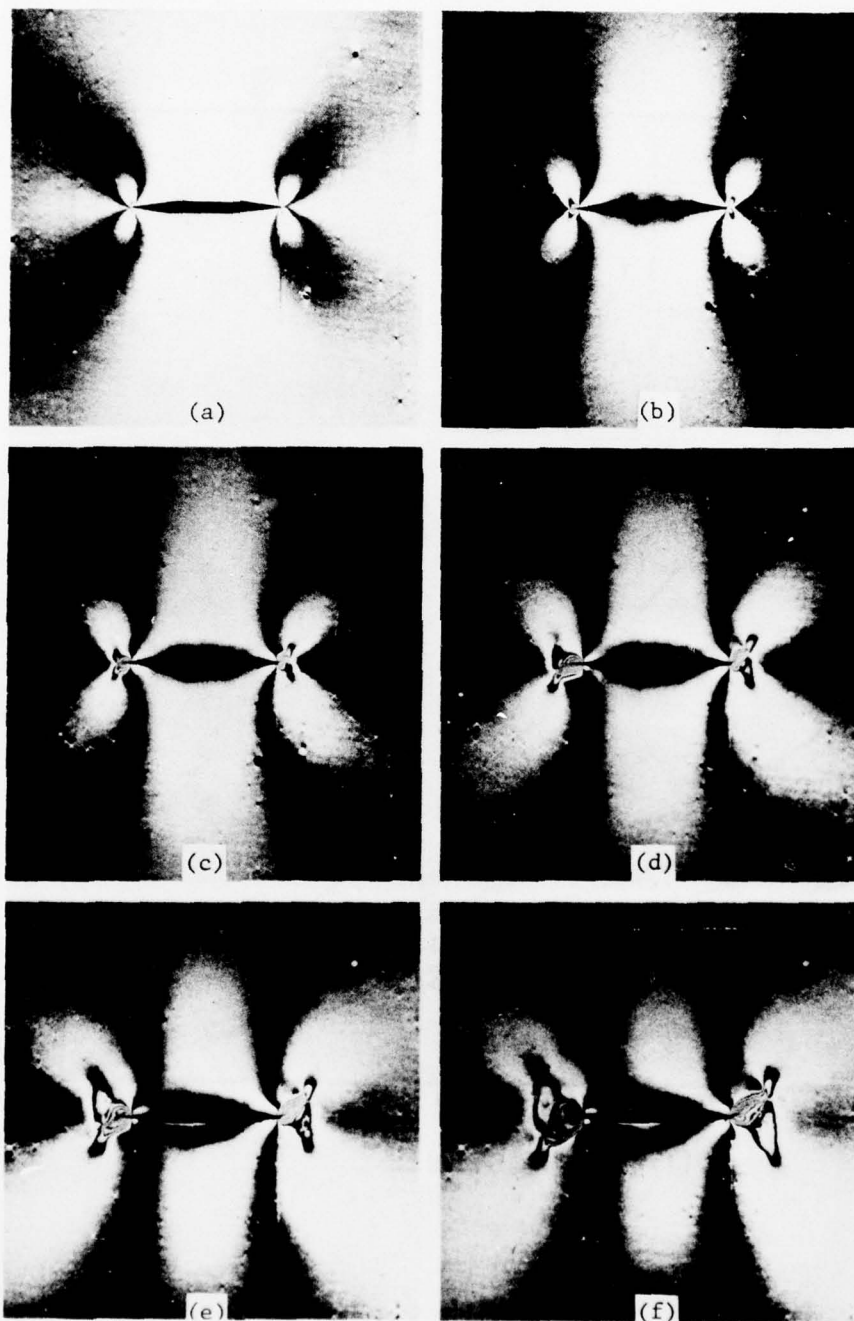
Figure 47. Isochromatic Fringe Patterns in Photoelastic Coating Around Crack of Specimen No. 4-6 at Applied Stress Levels: (a) 121 MPa (17.6 ksi), (b) 152 MPa (22.0 ksi), (c) 172 MPa (24.9 ksi), (d) 192 MPa (27.9 ksi), (e) 212 MPa (30.8 ksi) and (f) 223 MPa (32.3 ksi).

71

STRESS, σ_{xx}, (MPa)

160

120

80

40

0

1.06

σ_{xx}

y

x

2a

σ_{xx}

E_{xx} = 53 GPa (7.7 x 10⁶ psi)

ν_{xy} = 0.30

S_{xx} = 180 MPa (ksi)

STRAIN, 10³ ϵ

14   12   10   8   6   4   2   0

$\frac{y}{0}$ = 12.5 1.78 1.30 1.22

28

24

20

16

12

8

4

STRESS, σ_{xx}, (ksi)
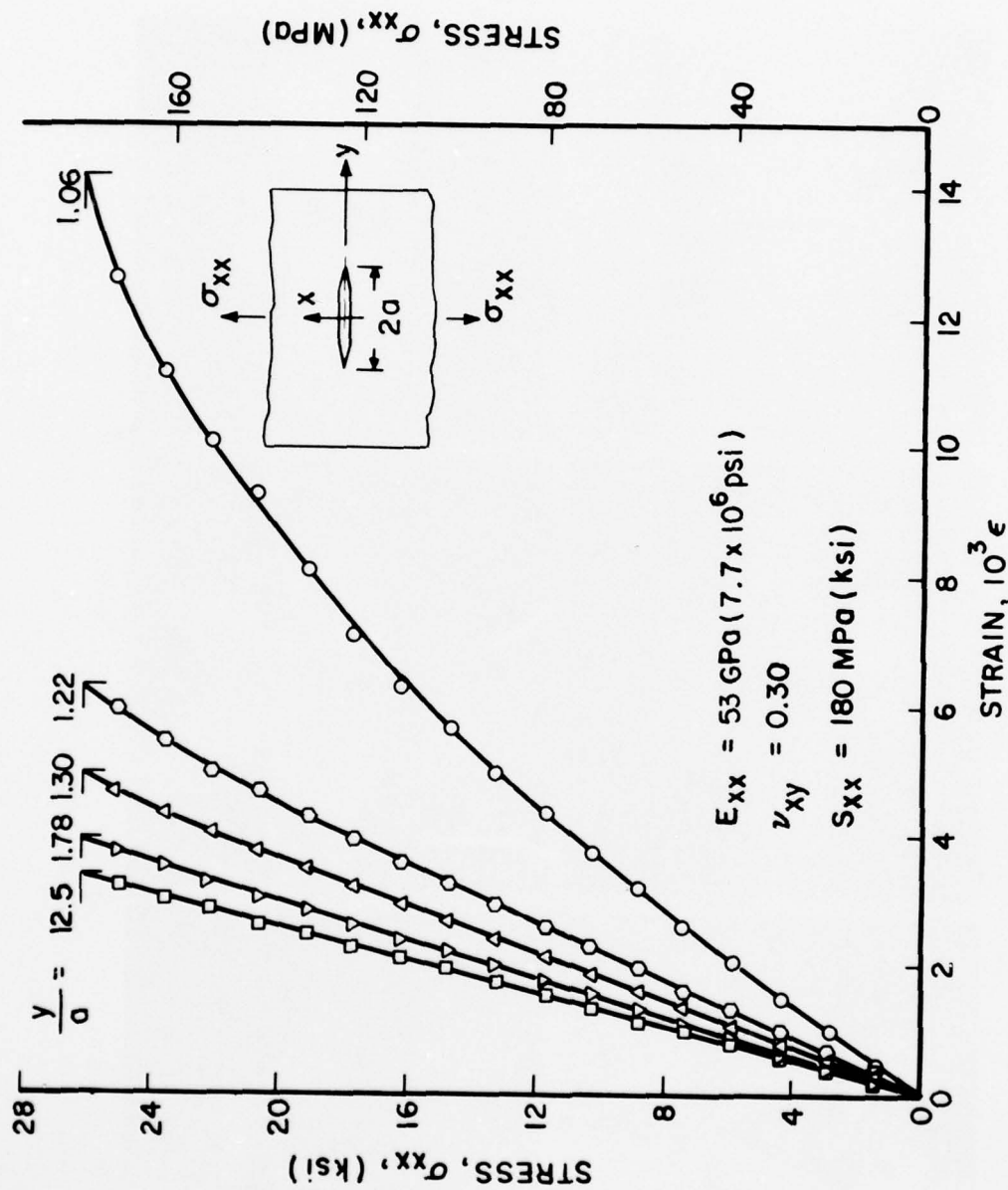
Figure 48.   Vertical Strains Along Horizontal Axis of [0/+45/90]ₛ Graphite/Epoxy
Specimen With a 1.91 cm (0.75 in.) Horizontal Crack Under Uniaxial
Loading (Spec. No. 4-7)
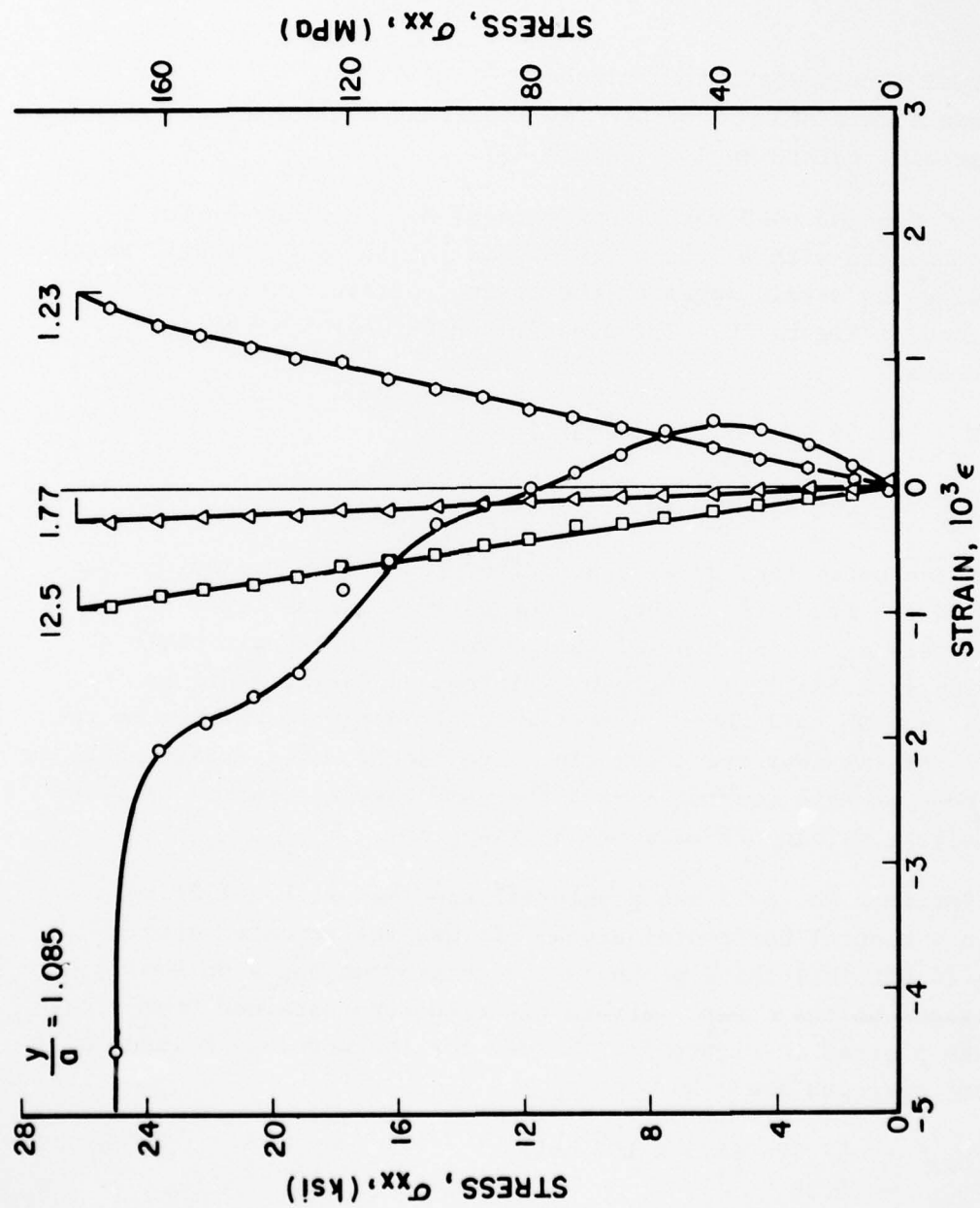
Figure 49. Horizontal Strains Along Horizontal Axis of $[0/\pm45/90]_s$ Graphite/Epoxy Specimen With a 1.91 cm (0.75 in.) Horizontal Crack Under Uniaxial Tensile Loading (Spec. No. 4-7)
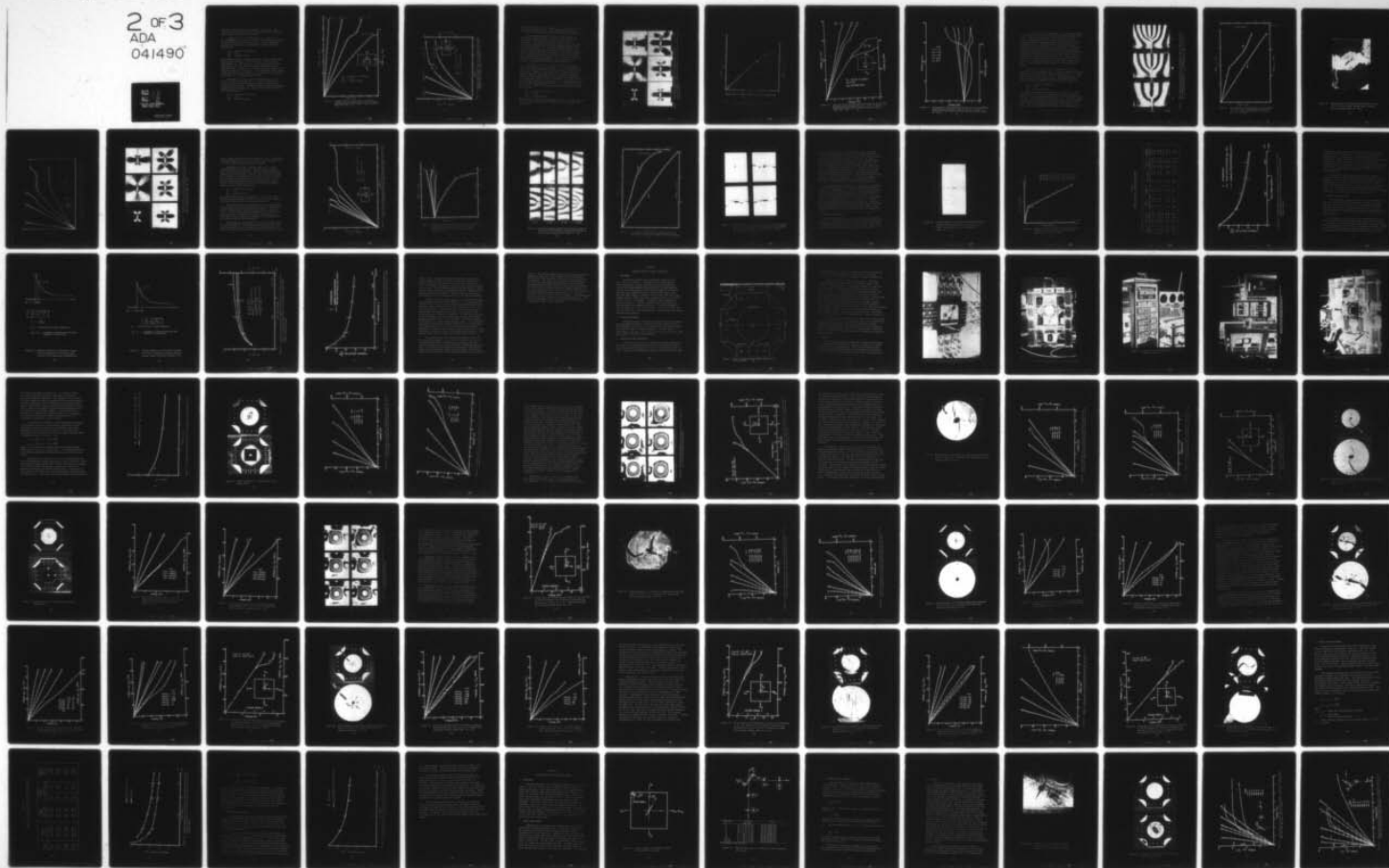
The initial strain ratio at a distance $\frac{y}{a}$ = 1.06 is 2.72. The transverse strain near the crack tip is highly nonlinear, probably due to strain redistribution (Figure 49).

Specimen No. 4-8 was a replicate of No. 4-7 above. It was instrumented with a 0.25 mm (0.010 in.) thick photoelastic coating on one side and strain gages on the other. Strain distributions are plotted in Figure 50. The elastic and strength properties obtained are:

$$E_{xx} = 55 \text{ GPa } (7.9 \times 10^6 \text{ psi})$$
$$\nu_{xy} = 0.30$$
$$S_{xx} = 231 \text{ MPa } (33 \text{ ksi})$$

Rapid damage extension, as evidenced from the strain variation near the tip of the crack ($\frac{y}{a}$ = 1.06), occurred at a stress level of approximately σ_{xx} = 186 MPa (27 ksi). The initial strain ratio at this point is 2.53. This specimen exhibited appreciably higher strength than No. 4-7 above, a fact which is directly related to the measured strains near the crack tip. The isochromatic fringe patterns in the photoelastic coating showed the same characteristics noticed previously, i.e., an off-axis crack extension.

Specimen No. 4-13 was a uniaxial specimen with a 1.27 cm (0.50 in.) central horizontal crack. It was instrumented with a 0.25 mm (0.010 in.) thick photoelastic coating on one side and strain gages on the other. Strain distributions obtained from strain gages are plotted in Figure 51. Values for the modulus, Poisson's ratio and strength are:

$$E_{xx} = 57 \text{ GPa } (8.3 \times 10^6 \text{ psi})$$
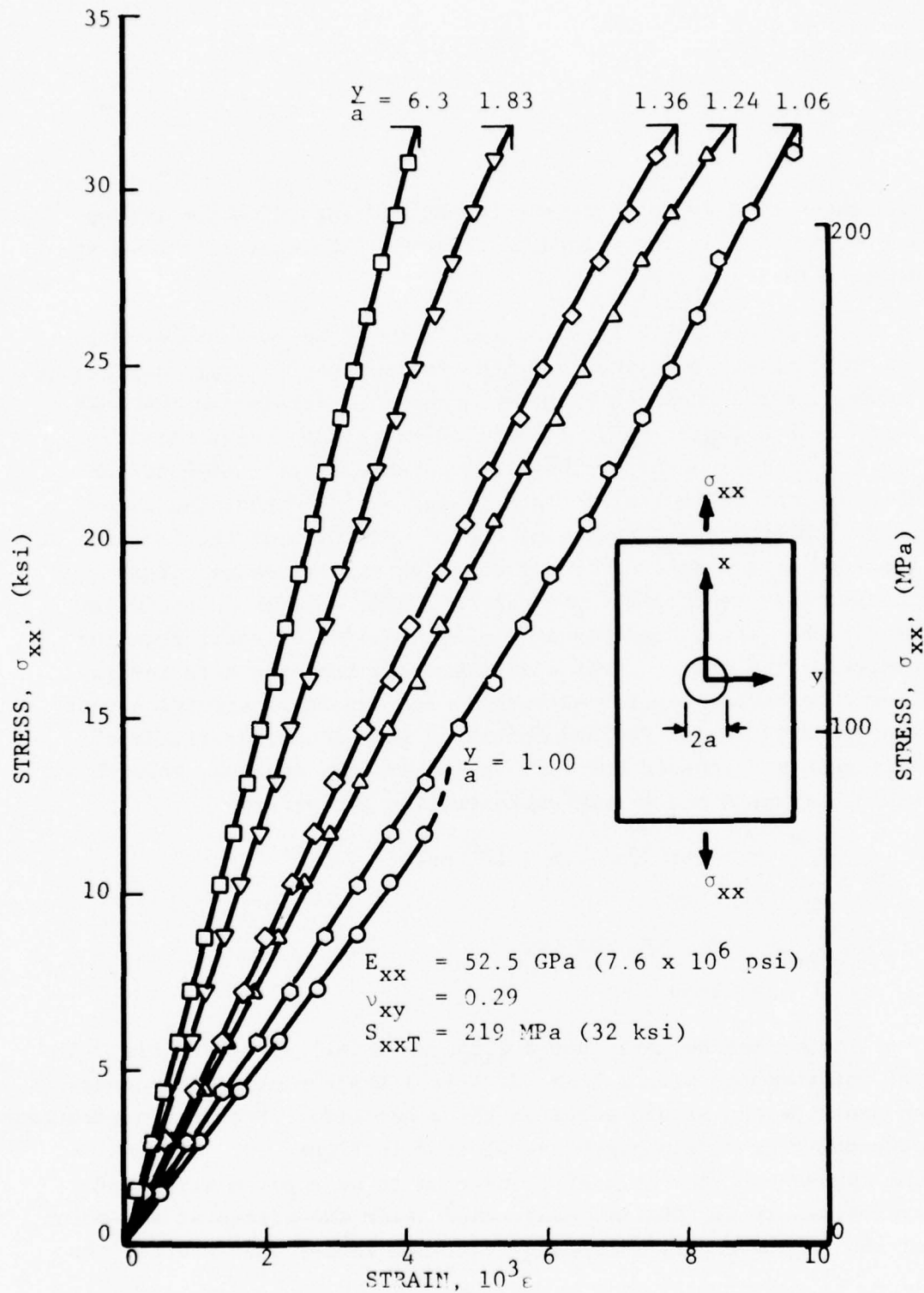$$\nu_{xy} = 0.28$$
$$S_{xx} = 293 \text{ MPa } (42 \text{ ksi})$$

74
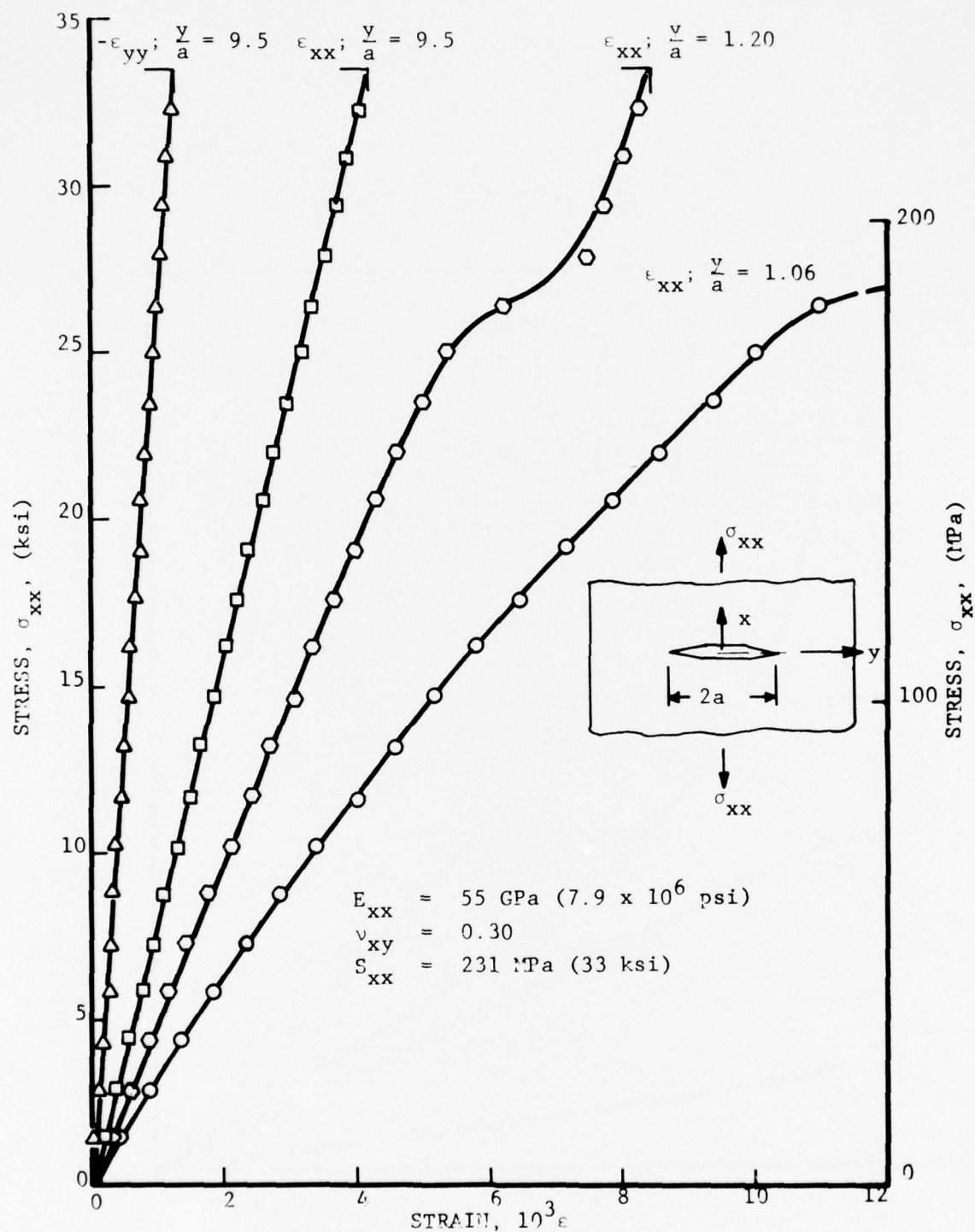
Figure 50. Strains Along Horizontal Axis of $[0/+45/90]_s$ Graphite/Epoxy Specimen With a 1.91 cm (0.75 in.) Horizontal Crack Under Uniaxial Tensile Loading (Spec. No. 4-8)

75

STRESS, $\sigma_{xx'}$ (MPa)

300

200

100

0

ϵ_{xx}; $\frac{y}{a} = 1.34$

ϵ_{xx}; $\frac{y}{a} = 1.08$

ϵ_{xx}; $\frac{y}{a} = 9.5$

$-\epsilon_{yy}$; $\frac{y}{a} = 9.5$

ϵ_{xx}; $\frac{y}{a} = 9.5$

E_{xx} = 57 GPa (8.3 x 10^6 psi)
ν_{xy} = 0.23
S_{xx} = 293 MPa (42 ksi)

STRAIN, $10^3 \epsilon$

14   12   10   8   6   4   2   0

σ_{xx}

2a

σ_{xx}

STRESS, $\sigma_{xx'}$ (ksi)

50   40   30   20   10   0
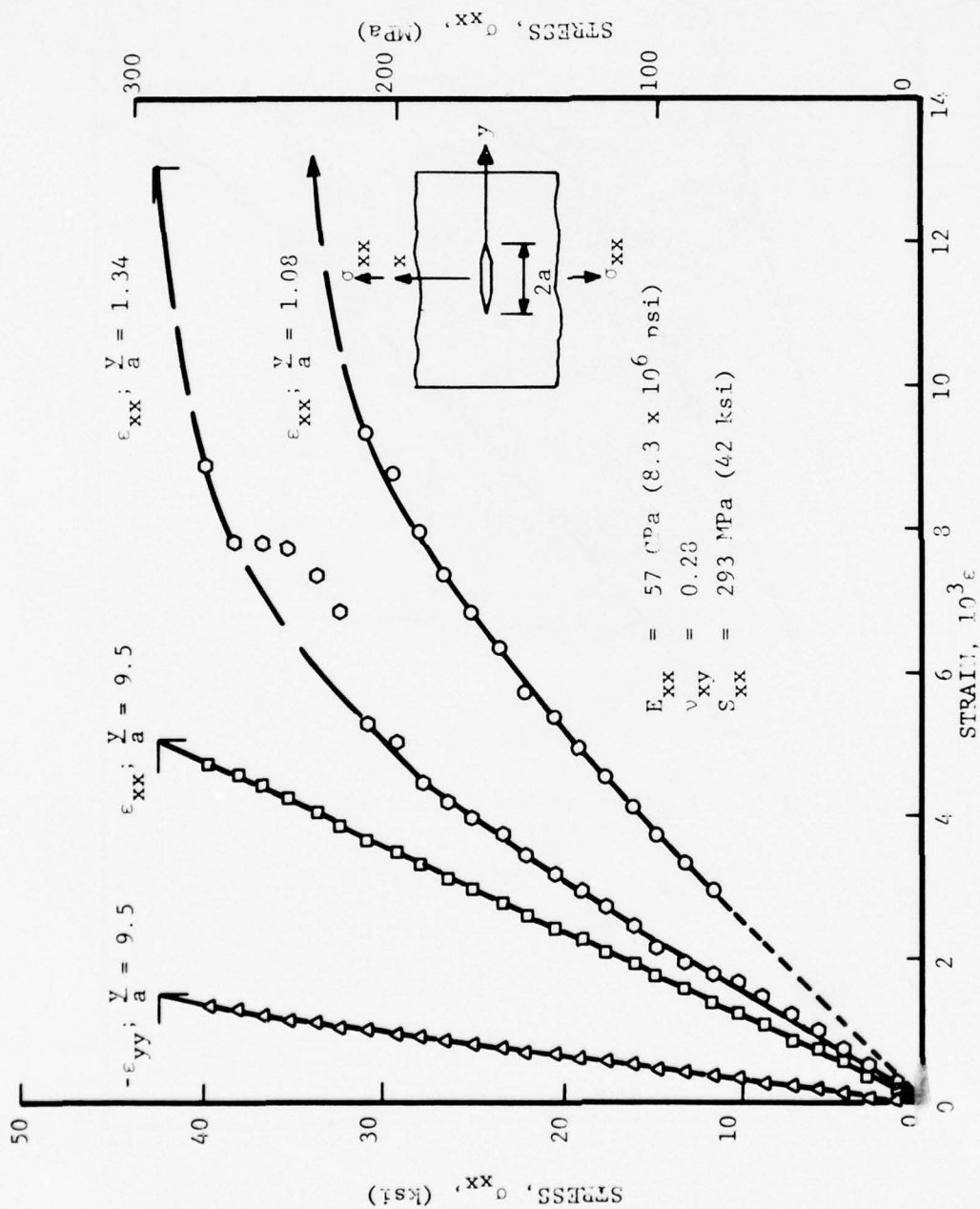
Figure 51. Strains Along Horizontal Axis of $[0/\pm45/90]_s$ Graphite/Epoxy Specimen With a 1.27 cm (0.50 in.) Horizontal Crack Under Uniaxial Tensile Loading (Spec. No. 4-13).

76

The initial strain ratio at a distance $y/a = 1.08$ (ratio of local to far-field strain) is 2.25. The strains near the crack tip are linear up to an applied stress of approximately 152 MPa (22 ksi).

The strain distribution around the crack tip and the phenomenon of damage extension are vividly illustrated by the isochromatic fringe patterns in the photoelastic coating (Figure 52). The maximum fringe order, which occurs at the crack tip off the horizontal axis, and the corresponding maximum strain are plotted in Figure 53 as a function of applied stress. This curve is nearly linear up to the stress level of 180 MPa (26 ksi) when the first cracking noises were heard. The strain concentration factor computed as the ratio of the maximum strain at the crack tip to the far-field axial strain is 5.70. Failure took the form of damage zone growth and extension. The direction of this extension was approximately 40-deg. from the crack axis.

Specimen No. 4-14, with a 1.27 cm (0.050 in.) horizontal crack, was a replicate of No. 4-13 above. It was instrumented with strain gages and a 400 line-per-cm (1000 lpi) moiré ruling parallel to the crack. Results from the strain gage readings are shown in Figures 54 and 55. The strains at the two symmetric points near the crack tip are nearly equal to each other up to an applied stress of approximately 138 MPa (20 ksi). Thereafter, the strain at one of the points increases at an increasing rate. Rapid damage extension occurs at approximately 186 MPa (27 ksi), as in the case of specimen No. 4-8 above. Elastic and strength properties obtained from strain gage data are:

$$E_{xx} = 55 \text{ GPa } (7.9 \times 10^6 \text{ psi})$$
$$\nu_{xy} = 0.28$$
$$S_{xx} = 261 \text{ MPa } (38 \text{ ksi})$$

The initial stress ratio at a distance $\frac{y}{a} = 1.06$ is 2.33. The transverse strain near the crack tip shows the characteristic nonlinearity and sign reversal.

77
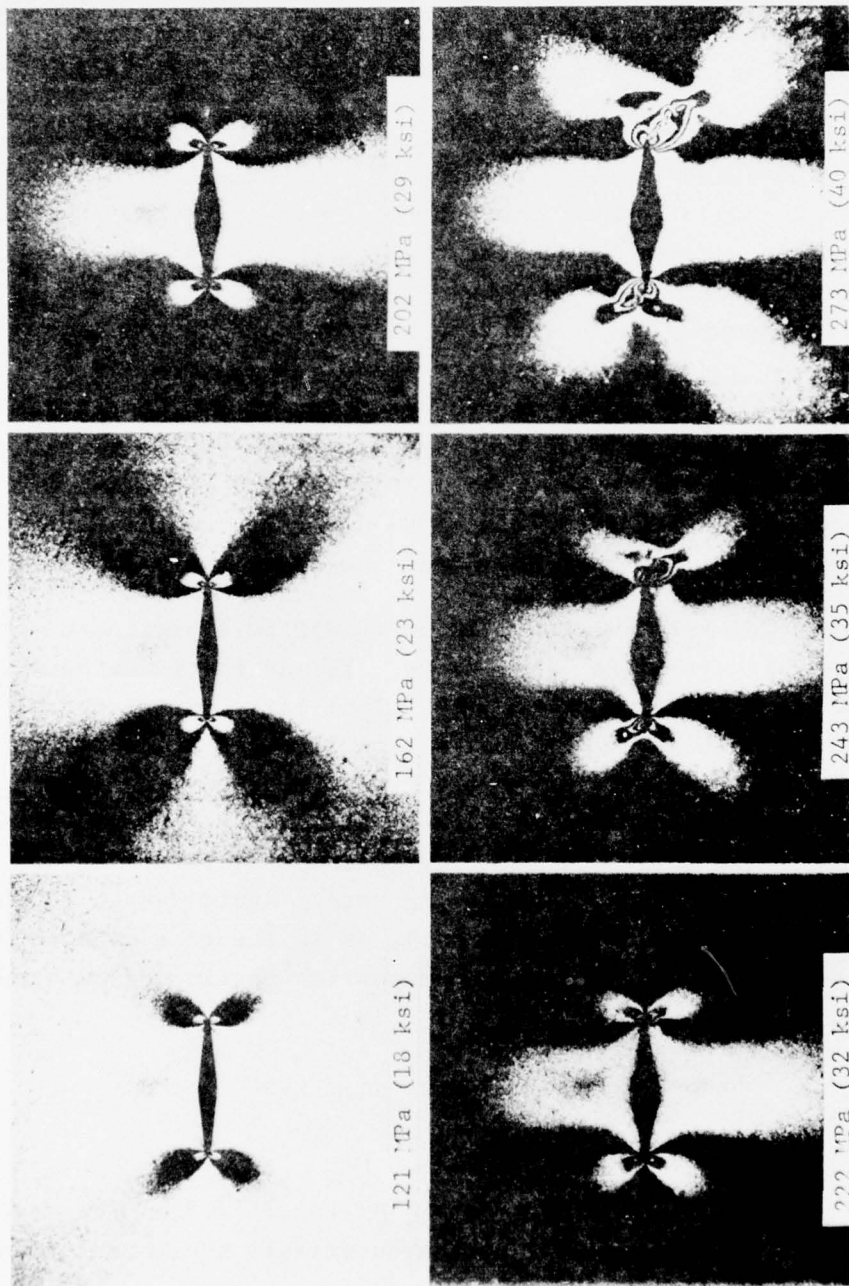
Figure 52. Isochromatic Fringe Patterns in Photoelastic Coating Around 1.27 cm (0.50 in.) Crack of [0/+45/90]ₛ Graphite/Epoxy Specimen at Various Levels of Applied Stress (Spec. No. 4-13)
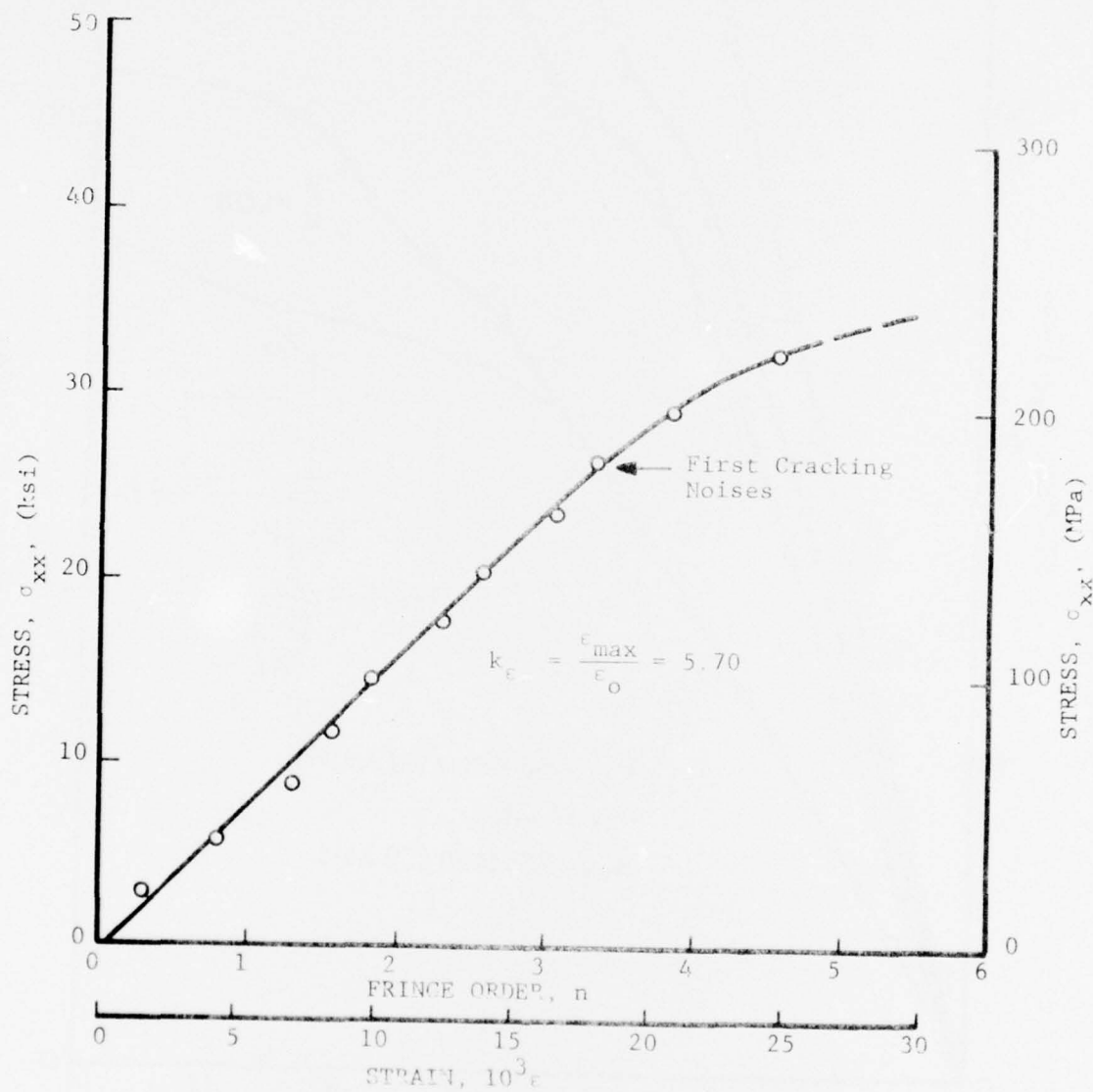
Figure 53. Maximum Fringe Order and Maximum Strain at Crack Tip (Spec. No. 4-13).

79
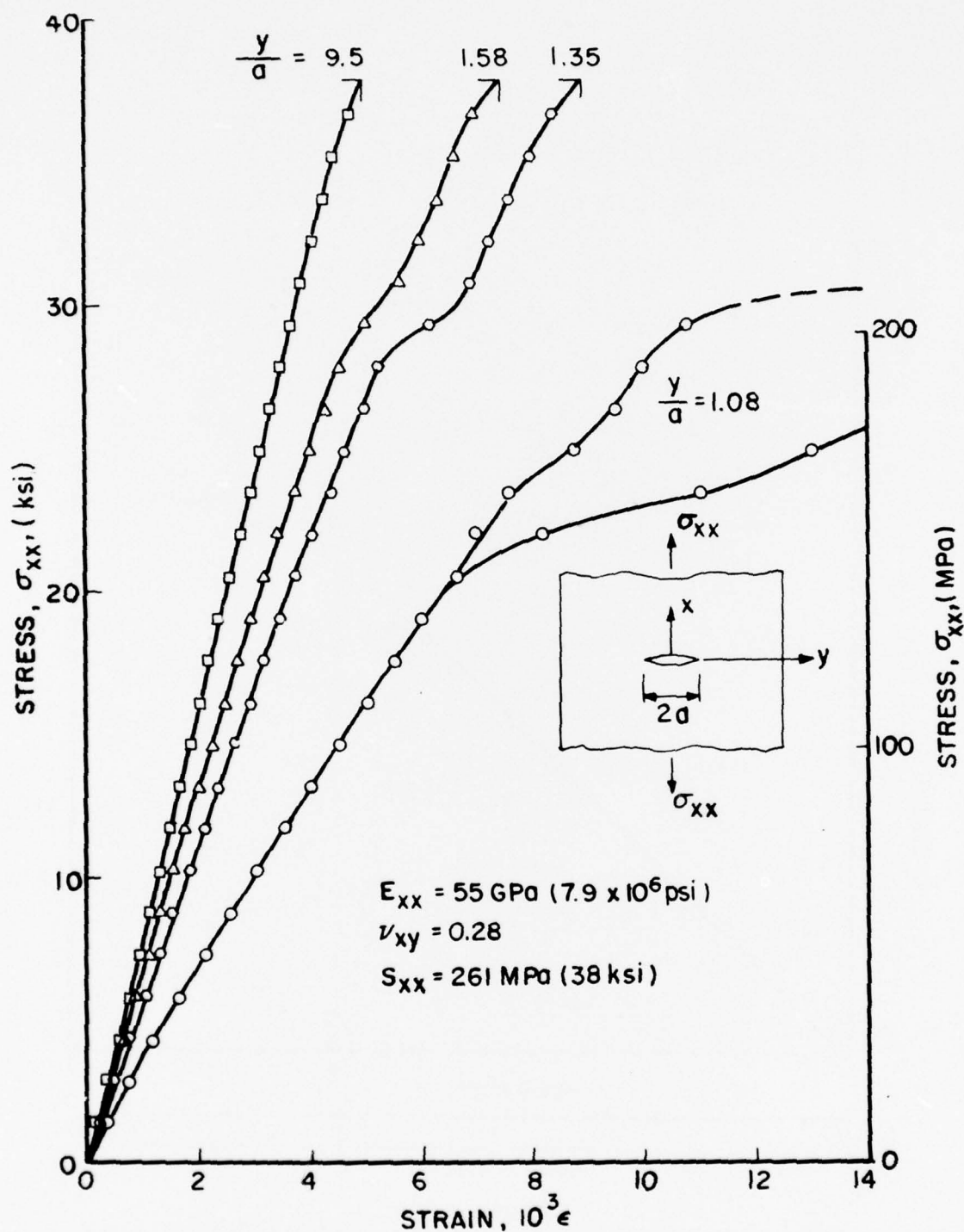
Figure 54. Vertical Strains Along Horizontal Axis of $[0/+45/90]_s$ Graphite/Epoxy Specimen With a 1.27 cm (0.50 $\bar{\text{in}}$.) Horizontal Crack Under Uniaxial Tensile Loading (Spec. No. 4-14)

80
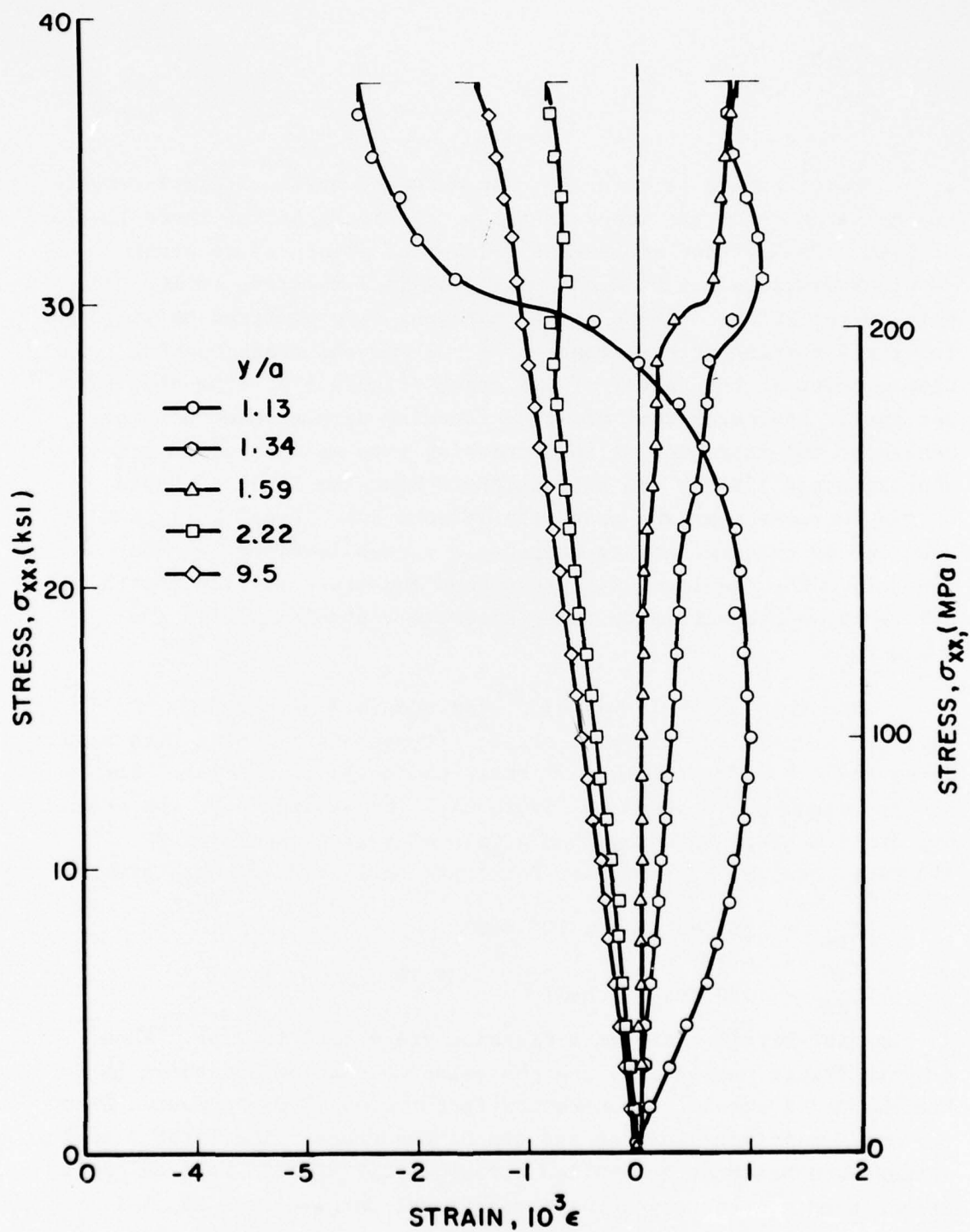
Figure 55.   Horizontal Strains Along Horizontal Axis of $[0/\pm45/90]_s$ Graphite/Epoxy Specimen With a 1.27 cm (0.50 in.) Horizontal Crack Under Uniaxial Tensile Loading (Spec. No. 4-14)

81

Moiré fringe patterns corresponding to vertical displacements
in the vicinity of the crack are shown in Figure 56 for three levels
of load. Each fringe represents a locus of points of constant
vertical displacement of 0.025 mm (0.001 in.) relative to its
neighboring fringe. These fringe patterns were analyzed to yield
far-field strains at a distance of $\frac{y}{a} \cong 3$ and the crack opening
displacement at the center of the crack (Figure 57). The plot for
the latter indicates that the crack opening displacement becomes
nonlinear and increases at an increasing rate at an applied stress of
approximately 138 MPa (20 ksi) which is near the level of rapid
strain increase near the crack tip (Figure 54). Final failure was
preceded by cracking noises heard at a stress level of 172 MPa
(25 ksi). The resulting failure around the crack is illustrated in
Figure 58, where extensive fiber breakage and delamination are
evident.

Specimen No. 4-15 was a similar specimen with a 0.64 cm
(0.25 in.) central horizontal crack. It was instrumented with strain
gages and a 0.25 mm (0.010 in.) thick photoelastic coating. Strain
distributions are plotted in Figure 59. The strains near the crack
tip are linear up to an applied stress of approximately 69 MPa
(10 ksi). Values for modulus, Poisson's ratio and strength are:

E_{xx} = 58 GPa (8.3×10^6 psi)
ν_{xy} = 0.27
S_{xx} = 320 MPa (46 ksi)

The initial strain ratio at a distance y/a = 1.06 is 2.51. Photo-
elastic fringe patterns in the photoelastic coating are shown in
Figure 60. A strain concentration factor of 5.11 was computed from
the maximum fringe order at the tip of the crack. The first cracking
noises were heard at an applied stress of 242 MPa (35 ksi) which is
higher than the corresponding stress level for specimen No. 4-14
above. This is compatible with the lower stress concentration and

(c)

(a)

Figure 56. Moiré Fringe Patterns Around Crack in Uniaxially Loaded [0/±45/90]$_s$ Graphite/
Epoxy Specimen for Three Levels of Applied Stress: (a) σ_{xx} = 152 MPa (22 ksi),
(b) σ_{xx} = 202 MPa (29 ksi), (c) σ_{xx} = 253 MPa (37 ksi) (Spec. No. 4-14).

83
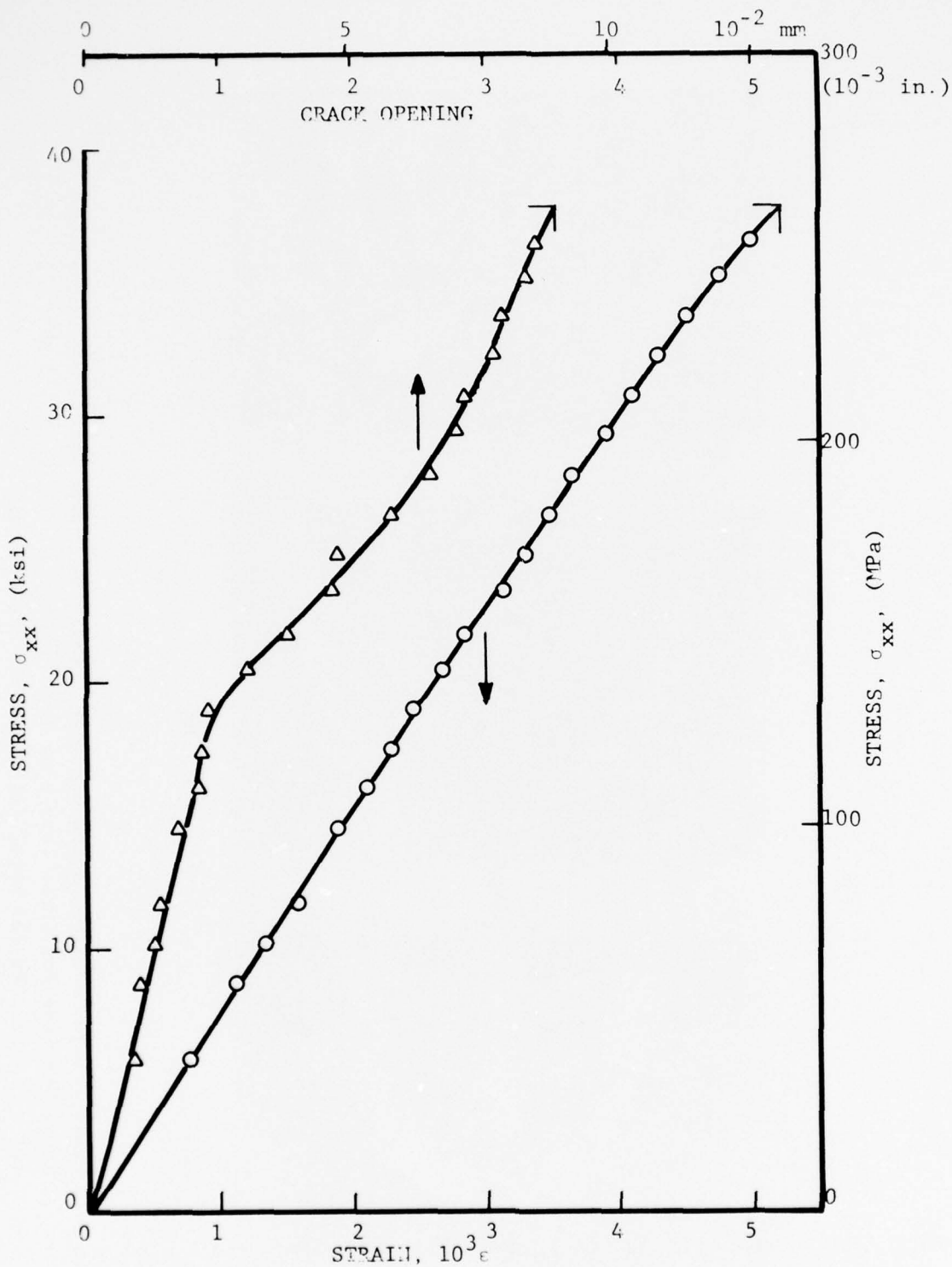
Figure 57. Crack Opening Displacement and Far-Field Strain for [0/+45/90]$_s$ Graphite/Epoxy Specimen With a 1.27 cm (0.50 in.) Horizontal Crack (Spec. No. 4-14; Moire Data)

Figure 58.   Graphite/Epoxy $[0/\pm45/90]_s$ Specimen with 1.27 cm
            (0.50 in.) Crack After Failure Under Uniaxial
            Tensile Loading (Spec. No. 4-14).
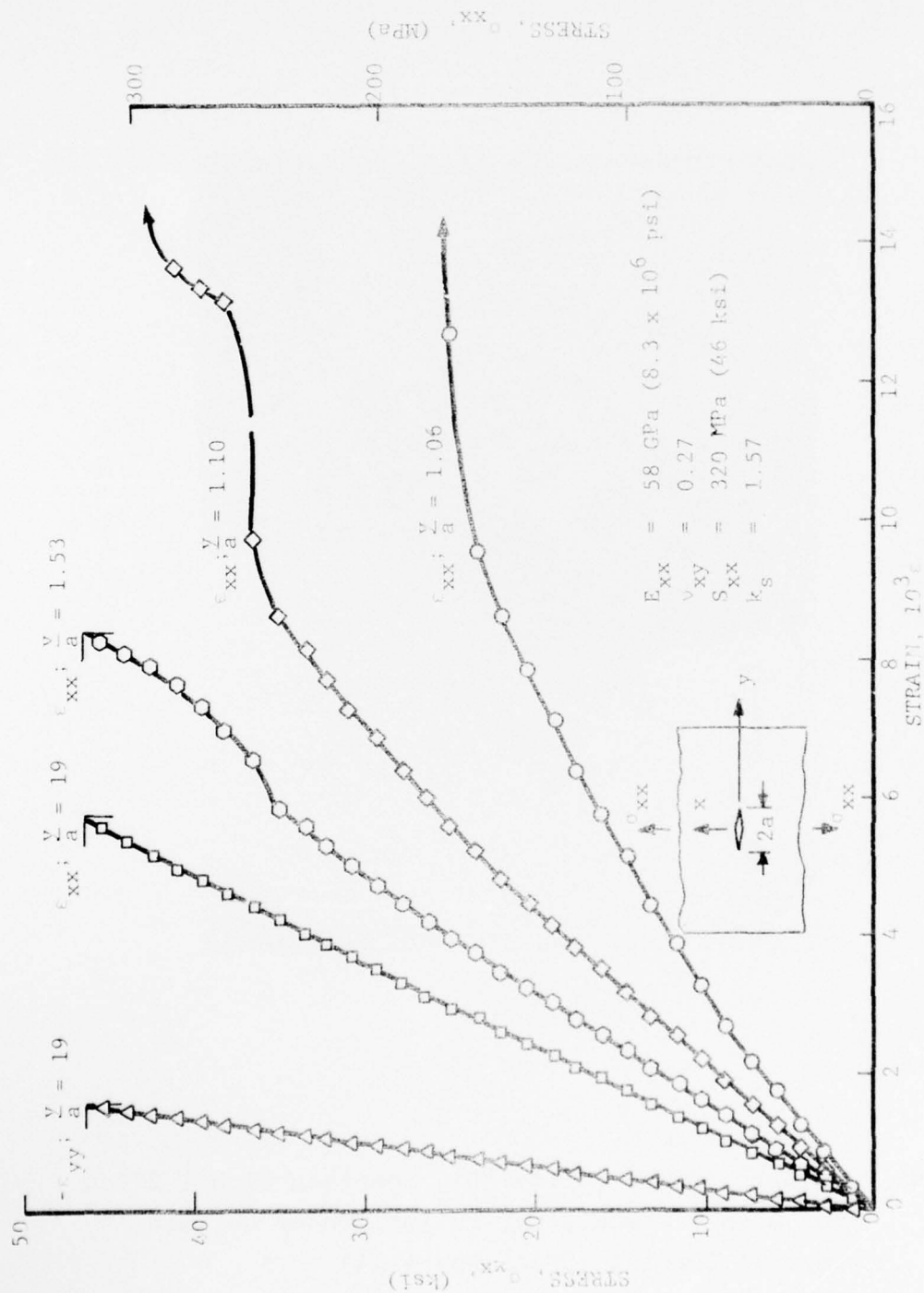
Figure 59. Strains Along Horizontal Axis of [0/±45/90]s Graphite/Epoxy Specimen With a 0.64 cm (0.25 in.) Horizontal Crack Under Uniaxial Tensile Loading (Spec. No. 4-15).

E_{xx} = 58 GPa (8.3 × 10⁶ psi)
ν_{xy} = 0.27
S_{xx} = 320 MPa (46 ksi)
k_s = 1.57

86

242 MPa (35 ksi)

313 MPa (45 ksi)

202 MPa (29 ksi)

303 MPa (44 ksi)

162 MPa (23 ksi)

273 MPa (40 ksi)
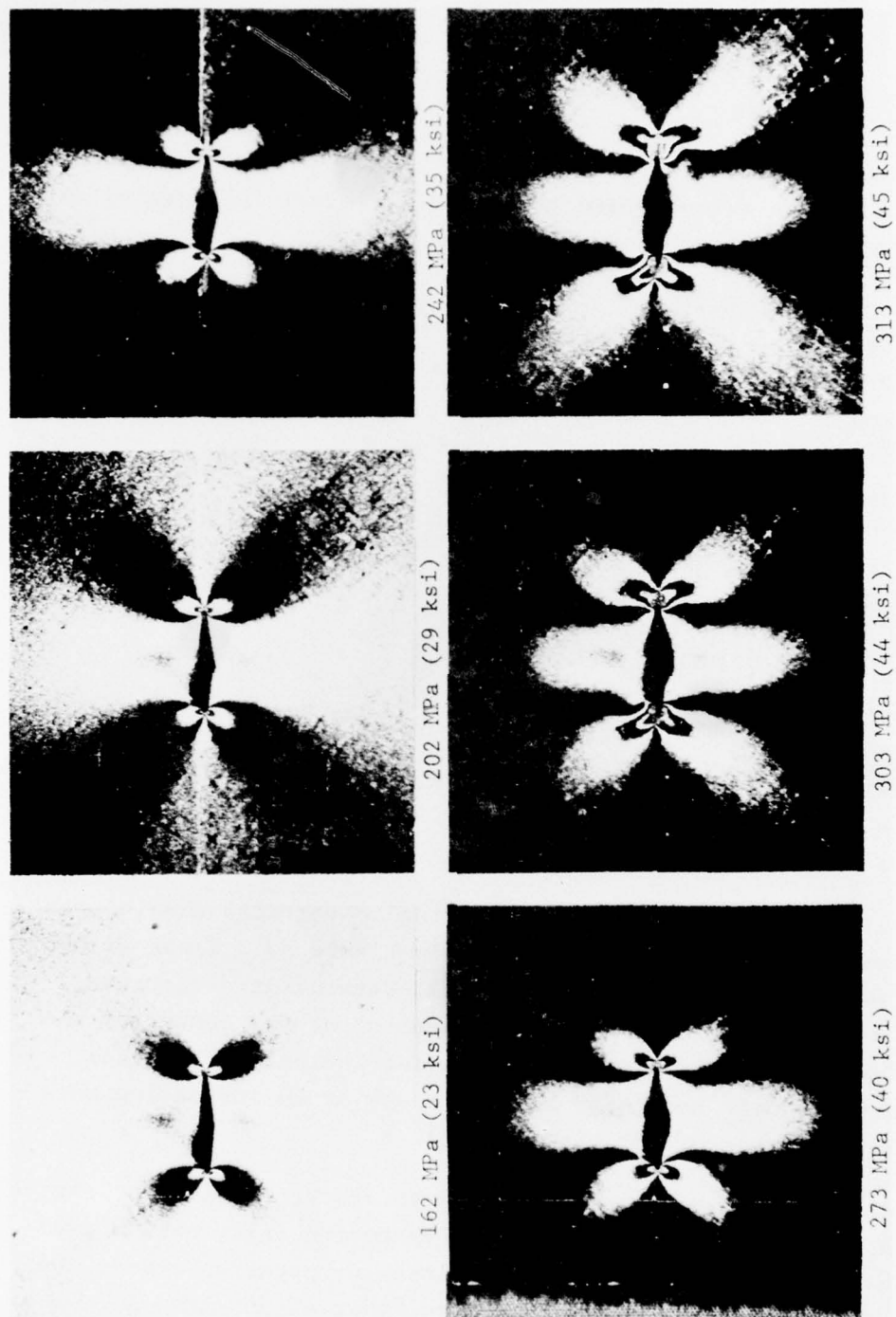
Figure 60. Isochromatic Fringe Patterns in Photoelastic Coating Around 0.64 cm (0.25 in.) Crack of $[0/\pm45/90]_s$ Graphite/Epoxy Specimen at Various Levels of Applied Stress (Spec. No. 4-15).

87

higher strength reduction ratio for specimen No. 4-15. The direction of apparent damage extension in this case was nearly horizontal as can be seen from the isochromatic fringe patterns.

Specimen No. 4-16 was a replicate of No. 4-15. It was instrumented with strain gages and a 400 line-per-cm (1000 lpi) moiré ruling parallel to the crack. Results from the strain gage readings are shown in Figures 61 and 62. The strain near the crack tip is linear up to an applied stress of 69 MPa (10 ksi). Cracking became audible at an applied stress of 250 MPa (36 ksi) which is the level of rapid damage extension as manifested by the strain near the crack tip (Figure 61). Elastic and strength properties obtained from the strain gage data are:

$$E_{xx} = 56 \text{ GPa } (8.1 \times 10^6 \text{ psi})$$
$$\nu_{xy} = 0.30$$
$$S_{xx} = 304 \text{ MPa } (44 \text{ ksi})$$

The initial strain ratio at a distance $y/a = 1.14$ is 1.85. The transverse strain near the crack tip ($y/a = 1.16$) varies similarly as the axial strain at the same location (Figure 62).

Moiré fringe patterns corresponding to vertical displacements in the vicinity of the crack are shown in Figure 63. These fringe patterns were analyzed to yield far-field strains at a distance of $y/a = 3$ and the crack opening displacement at the center of the crack (Figure 64). The plot for the latter indicates that this displacement becomes nonlinear and increases at an increasing rate at an applied stress of 207 MPa (30 ksi).

Failure patterns for specimens with cracks of various lengths are shown in Figure 65. They all show extensive delamination near the crack tips and a not too straight crack propagation across the width of the specimen. Only in one case, that of specimen No. 4-7 with
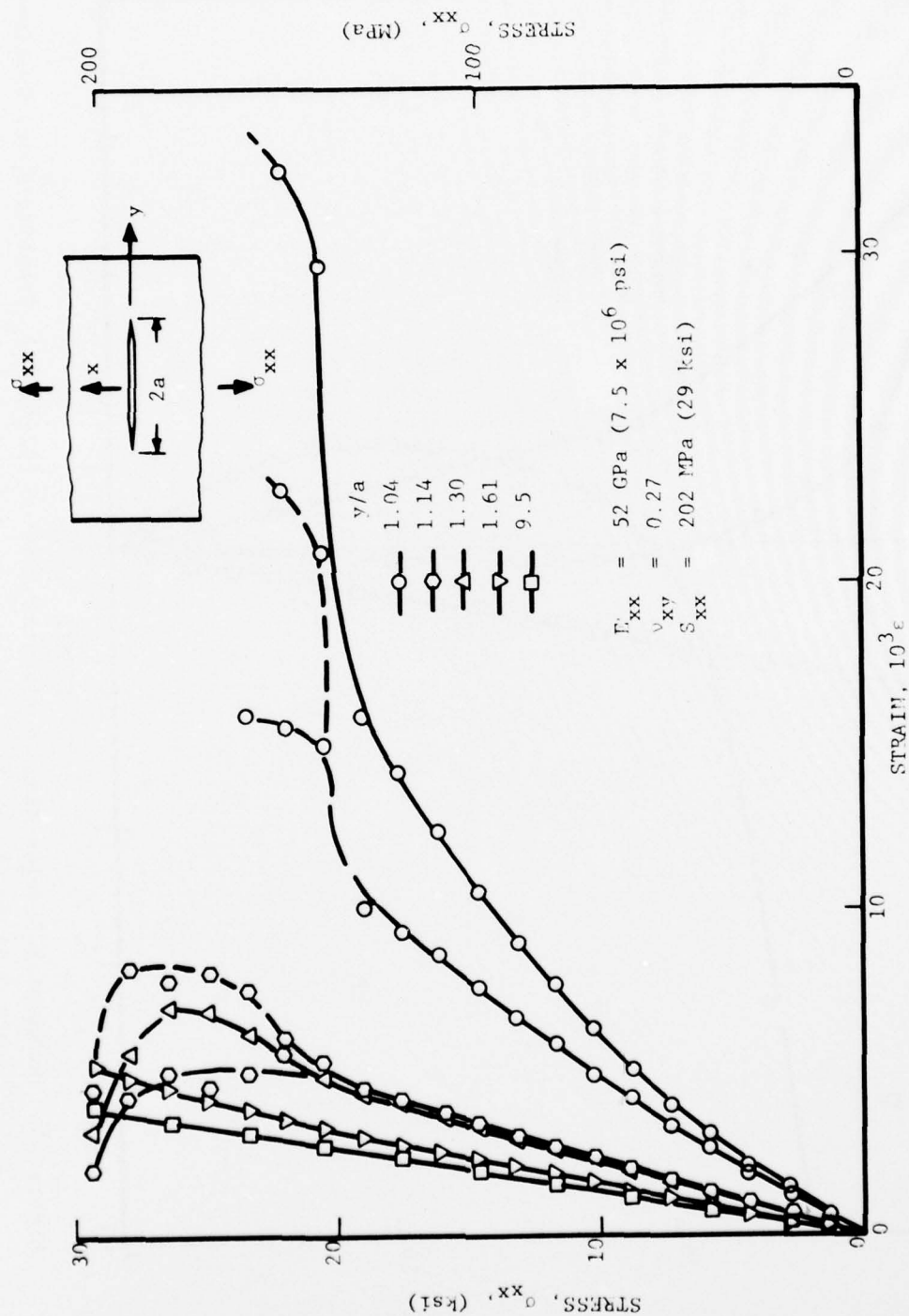
88
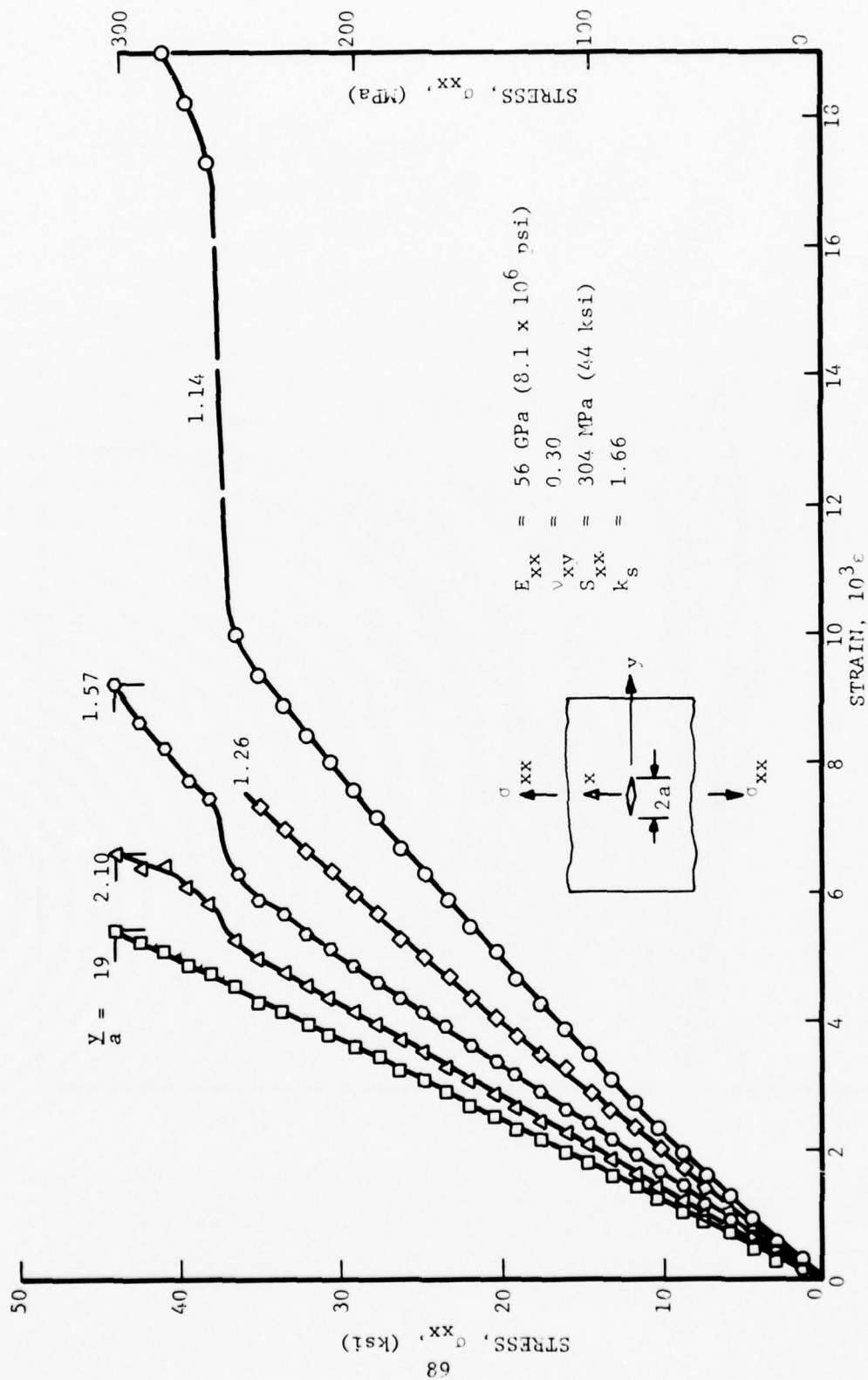
Figure 61. Vertical Strains Along Horizontal Axis of [0/+45/90]s Graphite/Epoxy Specimen With a 0.64 cm (0.25 in.) Horizontal Crack Under Uniaxial Tensile Loading (Spec. No. 4-16).

68
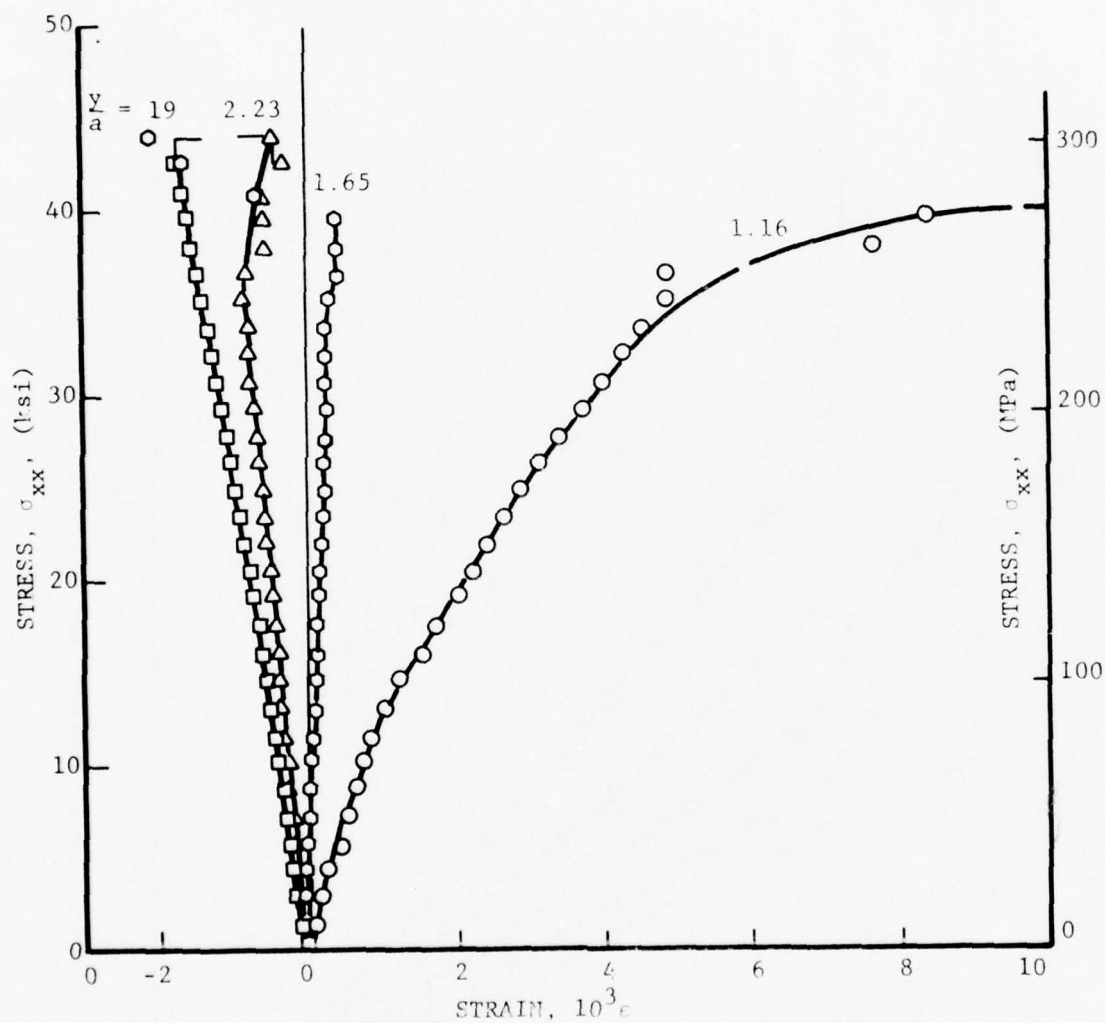
Figure 62. Horizontal Strains Along Horizontal Axis of $\{0/\pm45/90\}_s$ Graphite/Epoxy Specimen With a 0.64 cm (0.25 in.) Horizontal Crack Under Uniaxial Tensile Loading (Spec. No. 4-16).

13 ksi 91 MPa	18 ksi 121 MPa	22 ksi 152 MPa	26 ksi 182 MPa
31 ksi 212 MPa	35 ksi 243 MPa	40 ksi 273 MPa	44 ksi 303 MPa
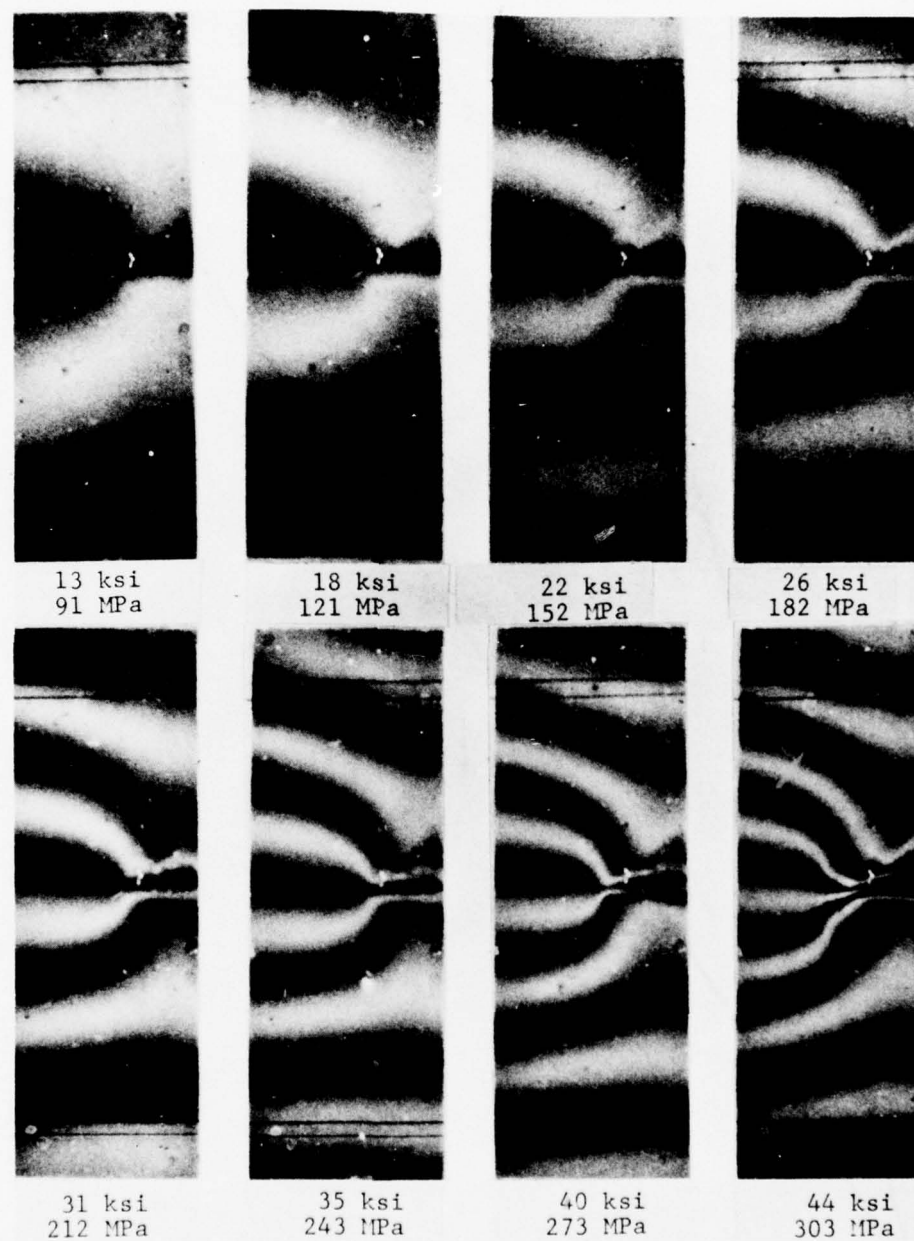
Figure 63. Moiré Fringe Patterns Around 0.64 cm (0.25 in.) Crack in
            Uniaxially Loaded [0/±45/90]$_s$ Graphite/Epoxy Specimen at
            Various Levels of Applied Stress (Spec. No. 4-16).
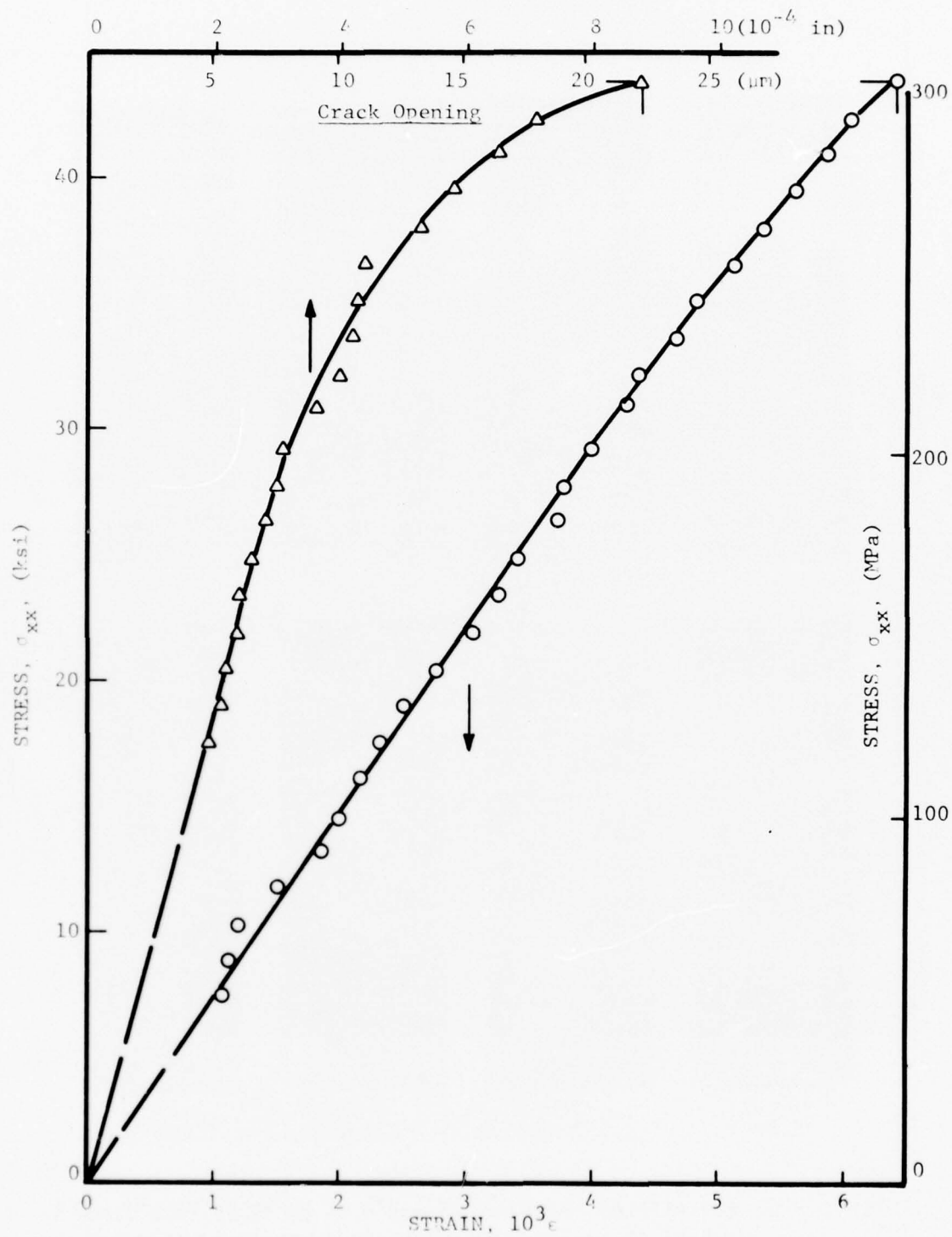
Figure 64. Crack Opening Displacement and Far-Field Strain for [0/±45/90]$_s$ Graphite/Epoxy Specimen With a 0.64 cm (0.25 in.) Horizontal Crack (Spec. No. 4-16; Moire Data)

92
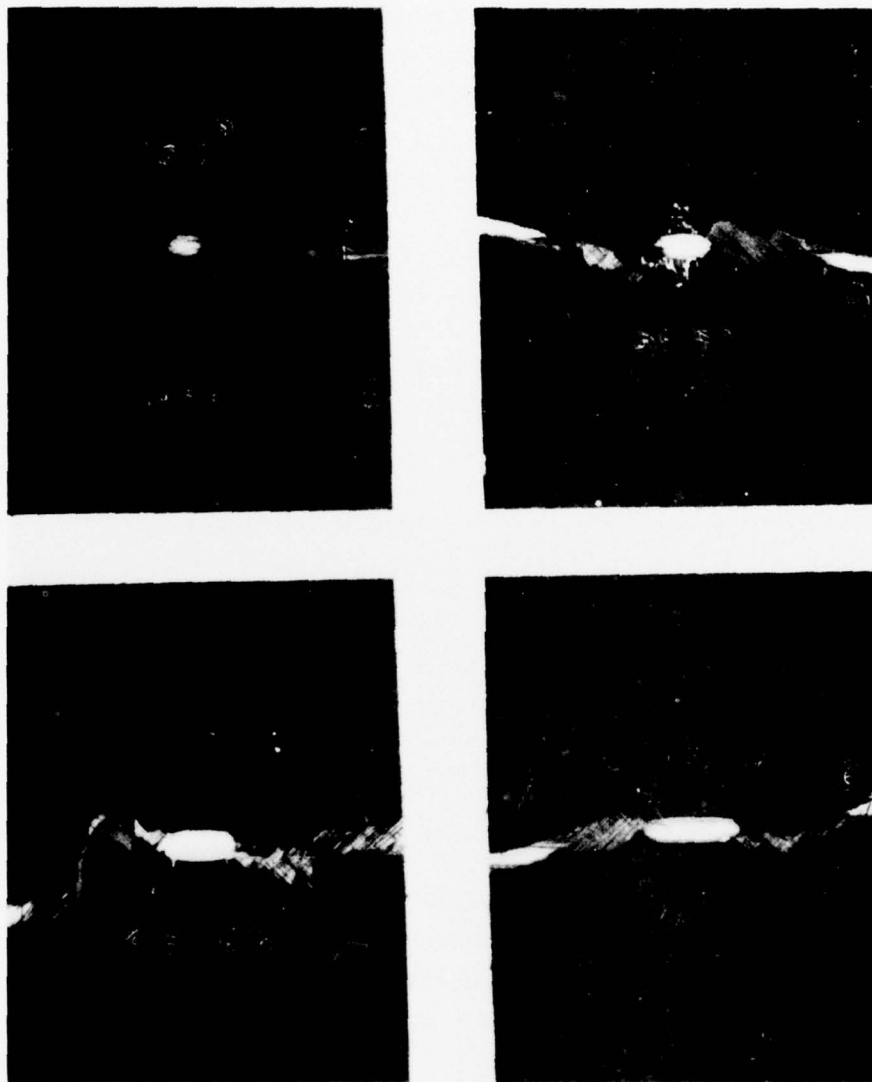
Figure 65. Failure Patterns in Uniaxially Loaded $[0/\pm45/90]_s$ Graphite/
Epoxy Plates with Cracks of Various Lengths (Crack Lengths
are: 0.64 cm (0.25 in.), 1.27 cm (0.50 in.), 1.91 cm
(0.75 in.) and 2.54 cm (1.00 in.)).

a 1.91 cm (0.75 in.) crack, was delamination absent. For some
reason the interlaminar shear strength of the material near the
crack tip was high enough so that the first mode of failure triggered
was tensile fracture due to opening of the crack. The crack
propagated in a near horizontal direction and the specimen failed
catastrophically at a lower than expected load (Figure 66). It
has been observed in several cases of composites with notches that
lack of delamination is accompanied by low strength and vice versa.
When the interlaminar shear strength of the material is such that
local delamination precedes cracking or crack extension around a
notch, then the stress concentration is blunted and the load carrying
capacity of the part is increased. The concept of controlled
delamination for increasing the fracture toughness of notched
composites is also being investigated elsewhere (Reference 21).

An attempt was made to measure the damage zone and correlate
it with the square of the stress intensity factor as was done by
Mandell et al. (Reference 20). The length of the subcracks producing
the damage zone was measured approximately from the photoelastic
fringe patterns for three specimens with crack lengths of 2.54 cm
(1.00 in.), 1.27 cm (0.50 in.) and 0.64 cm (0.25 in.). The subcrack
length varies linearly with K_I^2 up to a value of $K_I \cong 30$ MPa$\sqrt{m}$
(27.5 ksi$\sqrt{in}$) for all three crack lengths (Figure 67). Thereafter,
the subcrack length increases again linearly with K_I^2 but at a faster
rate which is nearly the same for all three crack lengths. This
bilinear nature of the curve is characteristic of notch insensitive
laminates.

7. EFFECT OF CRACK LENGTH

Results for all uniaxial specimens with cracks are summarized
in Table VI. The average values of the measured modulus and Poisson's
ratio computed from the far-field strains agree well with the values
determined from uniaxially loaded unnotched specimens. The strength
reduction ratio was plotted versus crack length in Figure 68.
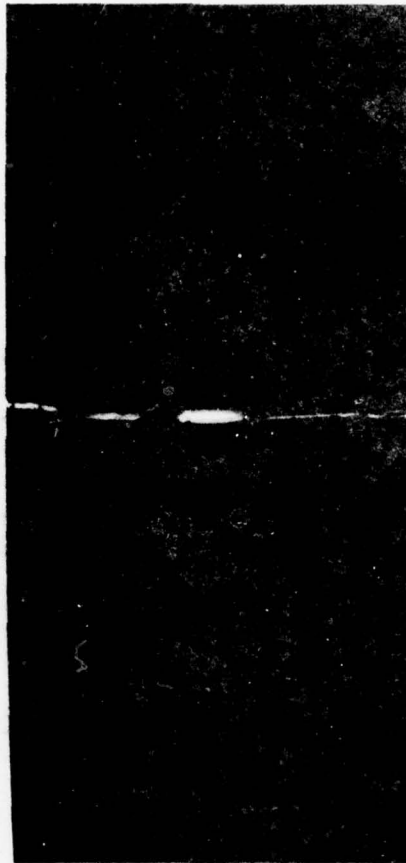
Figure 66. Failure Pattern in Uniaxially Loaded $[0/\pm45/90]_s$
Graphite/Epoxy Plate with 1.91 cm (0.75 in.)
Crack Illustrating Lack of Delamination
(Spec. No. 4-7).

95
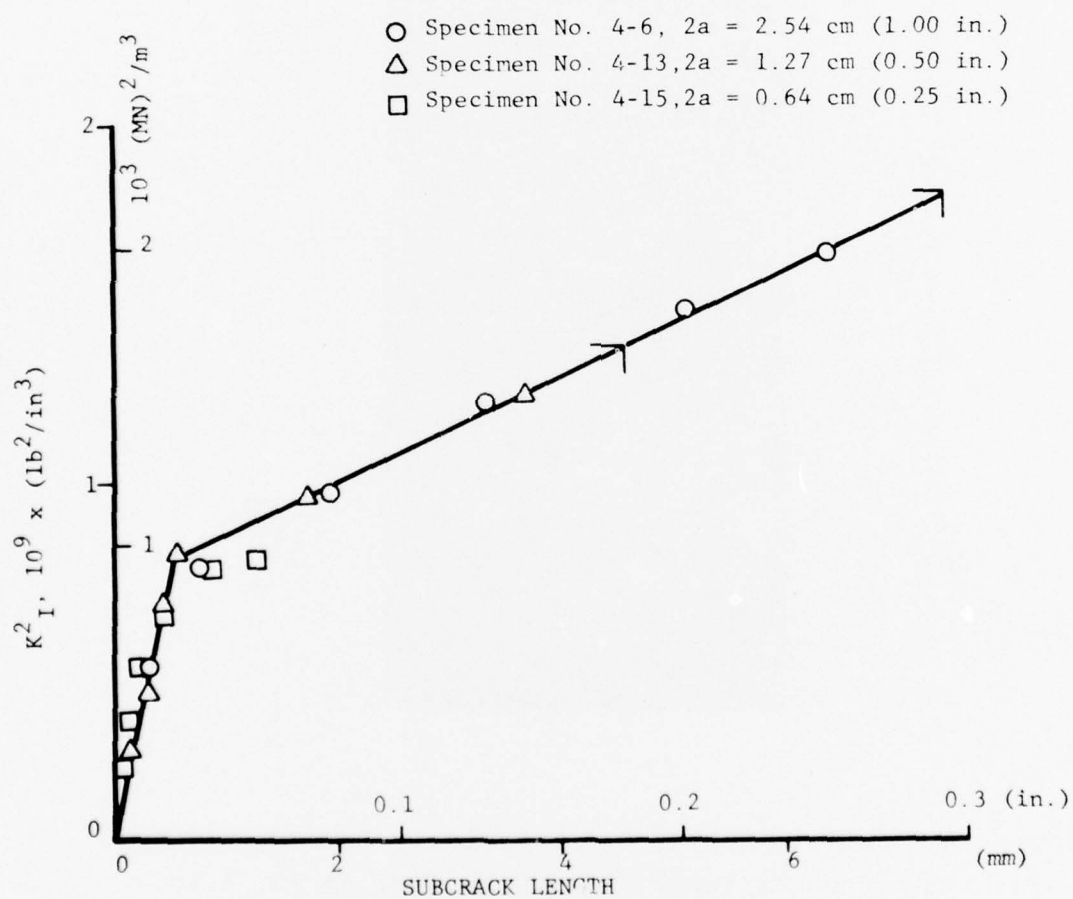
Figure 67. Variation of Length of Subcrack With Square of Stress
Intensity Factor for Uniaxially Loaded [0/±45/90]ₛ
Graphite/Epoxy Plates With Cracks.

96

TABLE VI

UNIAXIAL $[0/\pm45/90]_s$ LAMINATES WITH CRACKS

Spec. No.	Crack Length 2a cm (in)		Modulus E_{xx} GPa (10^6 psi)		Poisson's Ratio ν_{xy}	Strain Ratio $\varepsilon_{max}/\varepsilon_o$	at y/a	Strength S_{xx} MPa (ksi)		Strength Reduction S_{xx}/S_o
4-5	2.54	(1.00)	52	(7.5)	0.27	3.95	1.02	202	(29)	0.397
4-6	2.54	(1.00)	55	(7.9)	0.29	3.25	1.03	233	(34)	0.466
4-7	1.91	(0.75)	53	(7.7)	0.30	2.72	1.06	180	(26)	0.356
4-8	1.91	(0.75)	55	(7.9)	0.30	2.53	1.06	231	(33)	0.452
4-25	1.91	(0.75)	-		-	-	-	224	(32)	0.445
4-13	1.27	(0.50)	57	(8.3)	0.28	2.25	1.08	293	(42)	0.578
4-14	1.27	(0.50)	55	(7.9)	0.28	2.33	1.08	261	(38)	0.521
4-15	0.64	(0.25)	58	(8.3)	0.27	2.51	1.06	320	(46)	0.637
4-16	0.64	(0.25)	56	(8.1)	0.30	1.85	1.14	304	(44)	0.602

97
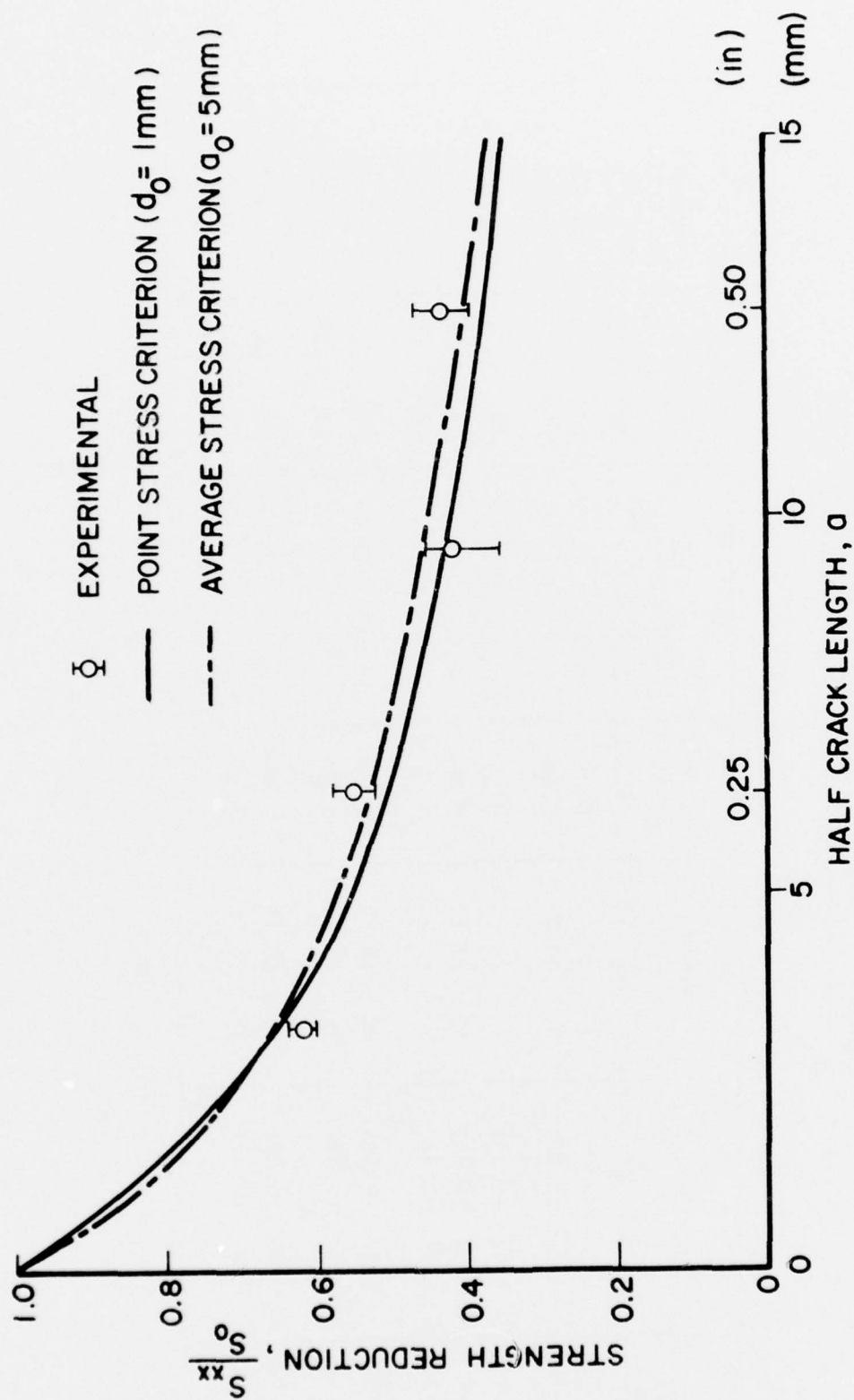
Figure 68. Strength Reduction as a Function of Crack Length for $[0/\pm45/90]_s$ Graphite/Epoxy Plates with Horizontal Cracks Under Uniaxial Tensile Loading

Experimental results agree well with predicted curves using the point stress and average stress criteria using characteristic dimensions of $d_o = 1$ mm and $a_o = 5$ mm for the two criteria, respectively. The definitions of these criteria for the case of a uniaxially loaded plate with a crack are illustrated in Figures 69 and 70. Experimental results as well as predicted ones based on the two criteria above are also presented in terms of the critical stress intensity factor K_Q as a function of crack length (Figure 71).

One somewhat surprising result is that the strength reduction ratios for specimens with holes and cracks are not too different from each other, indicating that the strength may be independent of the stress concentration in this case. Only the size of the discontinuity seems to be of importance. Combined results for all specimens with holes and cracks are shown in Figure 72. The curve for the average stress criterion for circular holes with $a_o = 3.8$ mm seems to give a very good fit.

8. SUMMARY AND CONCLUSIONS

An experimental study was conducted of the deformation and failure of uniaxially loaded $[0/\pm45/90]_s$ graphite/epoxy plates with holes and cracks of various sizes. Experimental methods used were strain gages, birefringent coatings and moiré grids. The notch sizes (hole diameter or crack length) investigated were 2.54 cm (1.00 in.), 1.91 cm (0.75 in.), 1.27 cm (0.50 in.) and 0.64 cm(0.25 in.).

The measured strain concentration around the hole in the linear range was in close agreement with the theoretical value of 3. A value of 5.70 for the stress concentration at the tip of the crack was measured in one case with a photoelastic coating. Strains on and near the hole boundary become nonlinear at a strain level of approximately 0.006 corresponding to initial failure of the

99

$$\frac{S_{yy}}{S_o} = \sqrt{1 - \xi_3^2}$$

$$\xi_3 = \frac{a}{a + d_o}$$
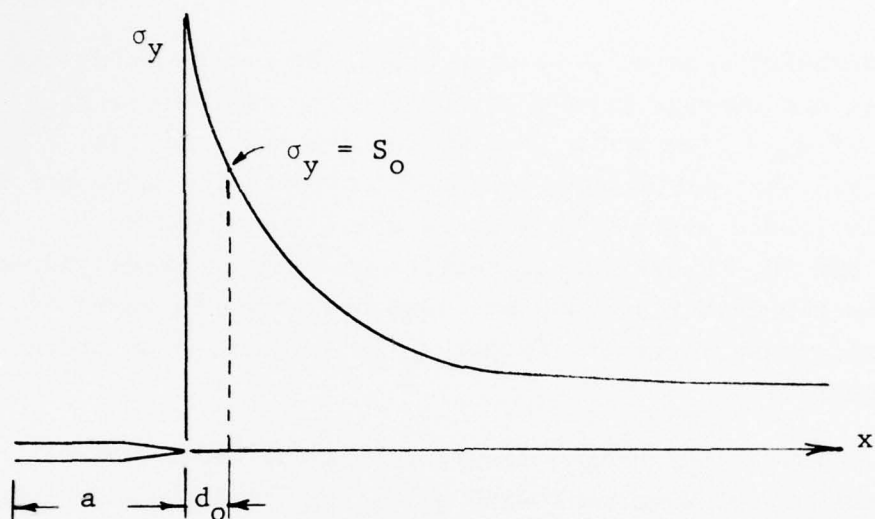
d_o = characteristic length dimension

S_{yy}, S_o = strengths of notched and unnotched laminates, respectively

Figure 69. Strength Reduction of Uniaxially Loaded Plate with Transverse Crack According to Point Stress Criterion (Reference 18)

100
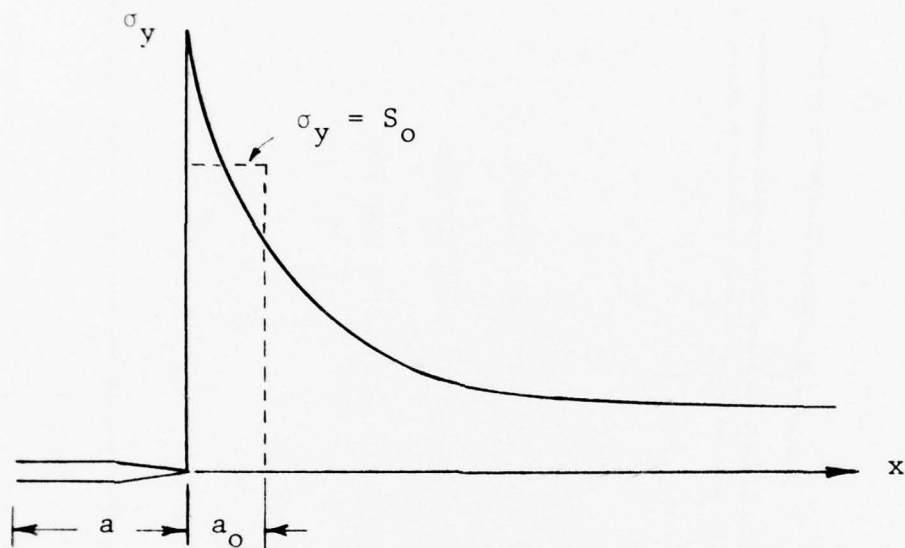
$$\frac{S_{yy}}{S_o} = \sqrt{\frac{a_o}{a_o + 2a}}$$

a_o = characteristic length dimension

S_{yy}, S_o = strengths of notched and unnotched laminates, respectively

Figure 70. Strength Reduction of Uniaxially Loaded Plate with Transverse Crack According to Average Stress Criterion (Reference 18)

101
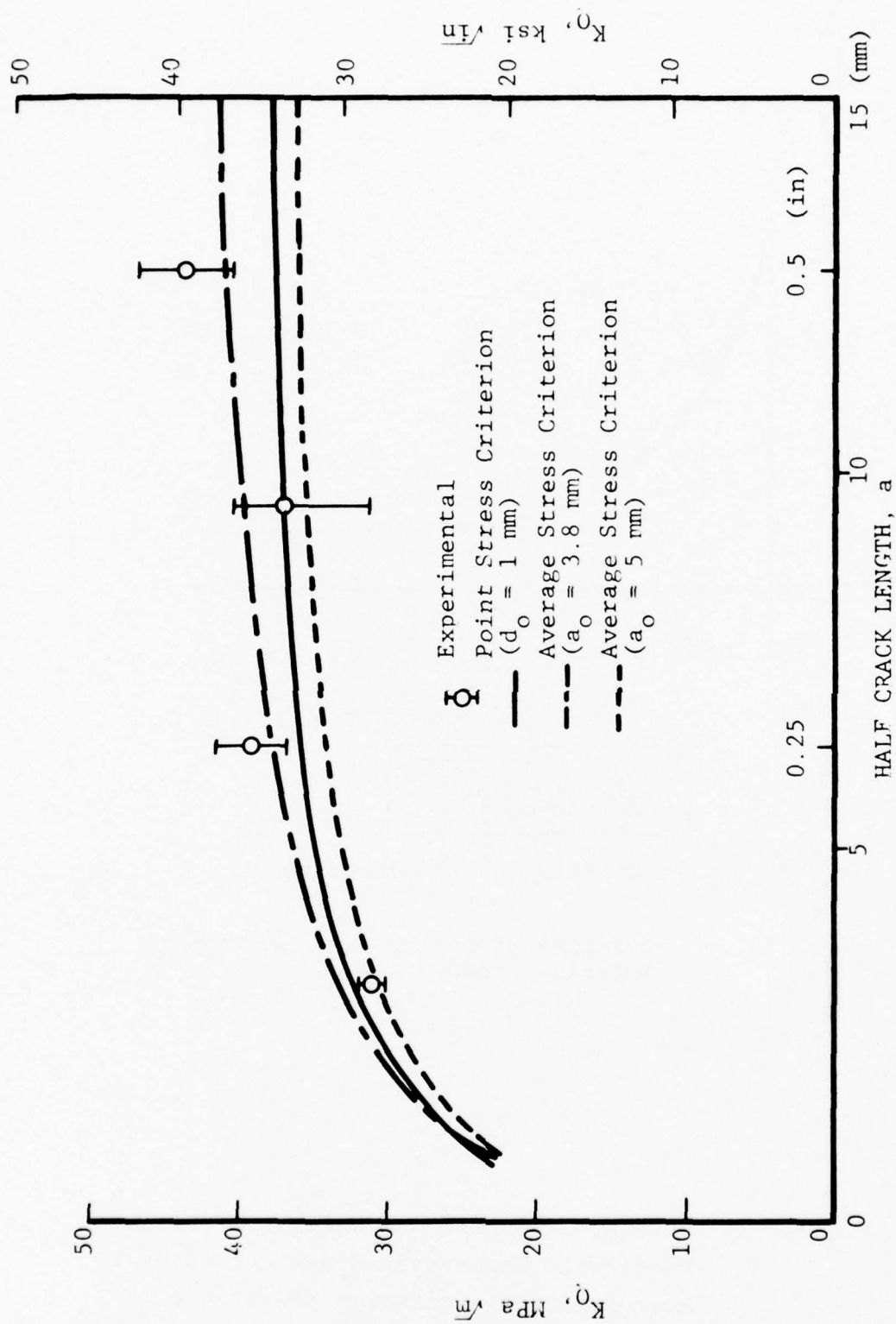
Figure 71. Critical Stress Intensity Factor as a Function of Crack Length for [0/±45/90]s Graphite/Epoxy Plates with Horizontal Cracks Under Uniaxial Tensile Loading
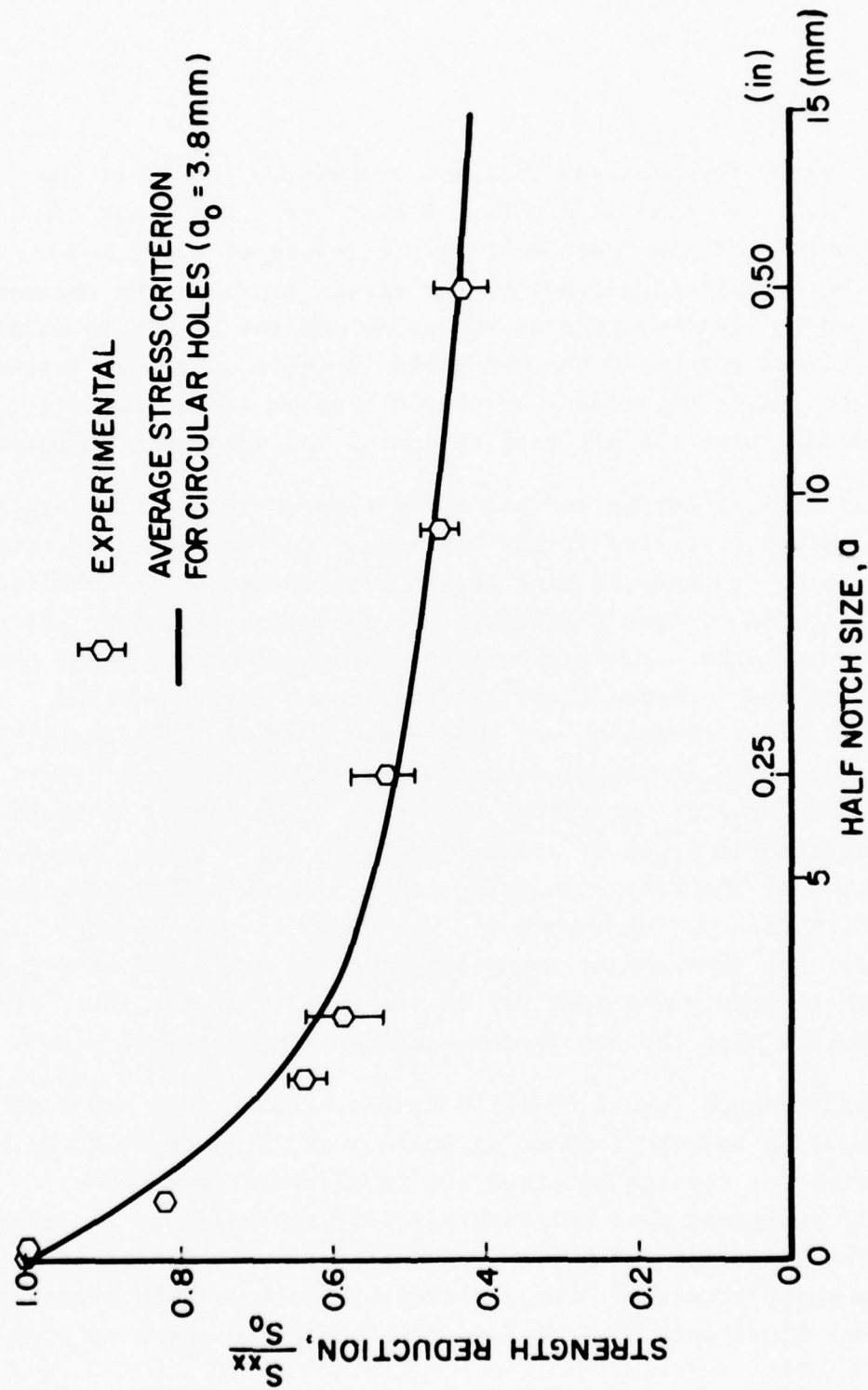
Figure 72. Strength Reduction as a Function of Notch Size for $[0/\pm 45/90]_s$ Graphite/ Epoxy Plates with Circular Holes and Cracks Under Uniaxial Tensile Loading

90-deg. plies. The measured ultimate transverse strain of the unidirectional material is 0.0054. Strains near the crack tip show two points of rate change at strain levels of 0.002 and 0.010. The former corresponds to the strain at which the response of the 90-deg. specimen becomes nonlinear and the latter is equal to the ultimate strain of the unnotched laminate. Maximum strains measured on the hole boundary or near the crack tip at failure have exceeded twice the ultimate strain of the unnotched laminate.

Failure initiation and propagation were vividly illustrated with photoelastic coating fringe patterns. In the specimens with circular holes, regions of high strain concentration with nonlinear response develop at four characteristic locations 22.5-deg. off the horizontal axis. Failure initiates at these points where the interlaminar and membrane shear stresses reach maximum values. No clearcut crack extension was observed. A damage zone consisting of ply subcracking and local delamination with occasional fiber breakage developed at the tip of the crack. This zone propagated at an angle to the crack of approximately 40-deg. It was found that the damage zone increases linearly with K_I^2 up to a certain value of K_I, which does not vary much for the various crack lengths. Thereafter, the damage zone increases linearly again but at a faster rate which is nearly the same for the various crack lengths. Final failure occurs when the damage zone reaches some critical size.

The strength reduction ratio ranged between 0.40 and 0.64 for notch sizes between 2.54 cm (1.00 in.) and 0.64 cm (0.25 in.). The experimental results obtained are in agreement with other previously published data on graphite/epoxy, boron/epoxy and glass/epoxy. The effect of notch size was satisfactorily described by using the point stress or average stress criterion. The average stress over a distance of 4 to 5 mm from the notch seems to give the

104

best fit. The strength reduction for the quasi-isotropic laminate
studied was found to be nearly independent of notch geometry.
Specimens with holes and cracks of the same size had nearly the
same strength. This result is consistent with current findings
at the Air Force Materials Laboratory where it was shown that
for specimens with inclined cracks the main significant parameter
was the horizontal projection of the crack length (Reference 22).
In the case of holes at least, there is a critical notch size below
which the laminate becomes notch insensitive, i.e., failure is
as likely to occur through the hole as elsewhere. Local delamination
near the notch tends to make the laminate notch-insensitive. Lack
of initial delamination at the notch makes the laminate notch-
sensitive and results in lower strength.

SECTION V

BIAXIAL TESTS OF PLATES WITH HOLES

1. SPECIMENS

The specimens were 8-ply $[0/\pm45/90]_s$ plates 40 cm x
40 cm (16 in. x 16 in.). A variety of tab configurations
were tried before a simple and effective one was selected.
In the final configuration selected corners of approximately
5 cm (2 in.) sides were cut off from the composite laminates.
They were then tabbed with 5-ply crossply glass/epoxy tabs
with the outer fibers at +45-deg. and -45-deg. with the 0-deg.
graphite plies. These tabs had a circular cutout at the center
of 20.3 cm (8 in.) diameter. A sketch of this specimen is
shown in Figure 73. Central circular holes were drilled in
the specimens with diamond core drills. Four hole diameters,
2.54 cm (1.00 in.), 1.91 cm (0.75 in.), 1.27 cm (0.50 in.) and
0.64 cm (0.25 in.), were investigated. Two specimens were tested
for each hole diameter.

2. STRAIN MEASUREMENT

Deformations and strains were measured using strain gages
and birefringent coatings. Strain gages were mounted on the
hole boundary, near it and in the far-field along the horizontal
(x-) and vertical (y-) axes of symmetry. In most cases
birefringent coatings 0.5 mm (0.02 in.) and 1 mm (0.04 in.) thick
were used on one side of the specimen.

3. LOADING AND DATA RECORDING

Four 0.95 cm (0.375 in.) diameter holes were provided on
each side of the tabbed specimen for bolting individual pairs
of metal grips approximately 5 cm (2 in.) wide and 10 cm (4 in.)
long. Loading was introduced by means of four whiffle-tree grip

106

203(8)

406(16)

38
(1.5)

Specimen

Glass/Epoxy Tab

9.5
(0.375)

25(1)   51(2)   51(2)   51(2)   25(1)
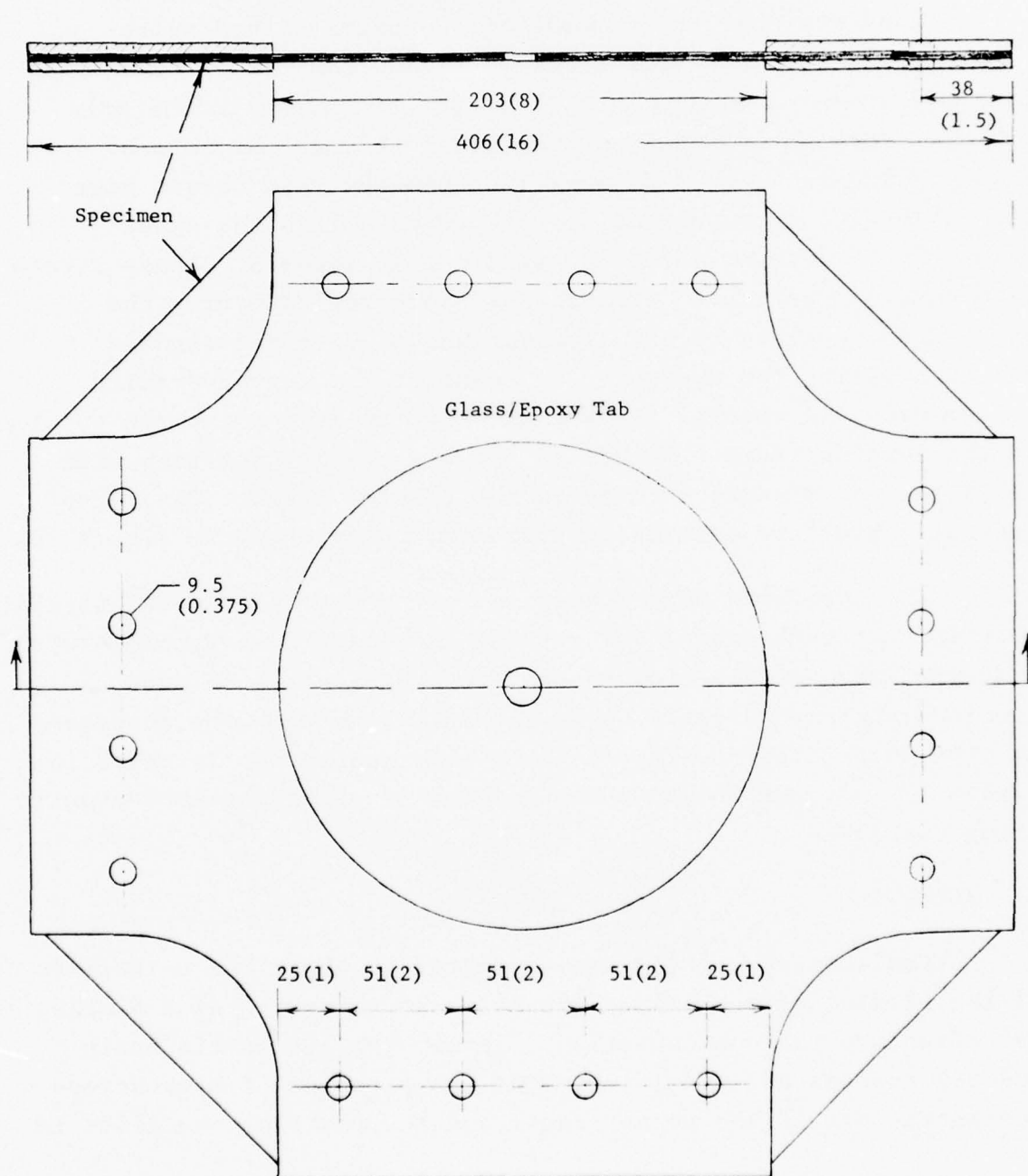
Figure 73.   Sketch of Biaxial Composite Specimen (Dimensions are
in mm and inches)   107

linkages designed to insure that four equal loads were applied to each side of the specimen. A photograph of a biaxial specimen with the loading grip linkages is shown in Figure 74.

Load was applied by means of two pairs of hydraulic jacks attached to the four sides of a reaction frame. The load was transmitted from the hydraulic cylinders to the grip linkages through cylindrical rods going through the bore of these cylinders. The rods were instrumented with strain gages and calibrated in a testing machine to establish the exact relationship between loads and strain gage signals. These strain gage readings were used subsequently both for recording the exact loads applied to the specimen and as feedback signals for controlling the pressures by means of the servohydraulic system used. A special fixture was used to help align the specimen in the loading frame. Figure 75 shows a biaxial specimen with the alignment fixture mounted in the loading frame. The servo-hydraulic pressure control instrumentation is shown in Figure 76.

The specimens were loaded in increments under equal biaxial tension. At each load level strains and loads were recorded with a digital data acquisition system and photoelastic fringes recorded photographically. The loading frame with the specimen and the associated strain recording instrumentation is shown in Figure 77. Figure 78 shows the process of recording photoelastic fringe patterns.

4. RESULTS

Preliminary testing was conducted to check the uniformity of the biaxial stress around the hole and to arrive at a simple but effective tab configuration. Tests with a Columbia Resin (CR-39) transparent model indicated the presence of high stress concentrations at the corner radii and the roots of the slits in
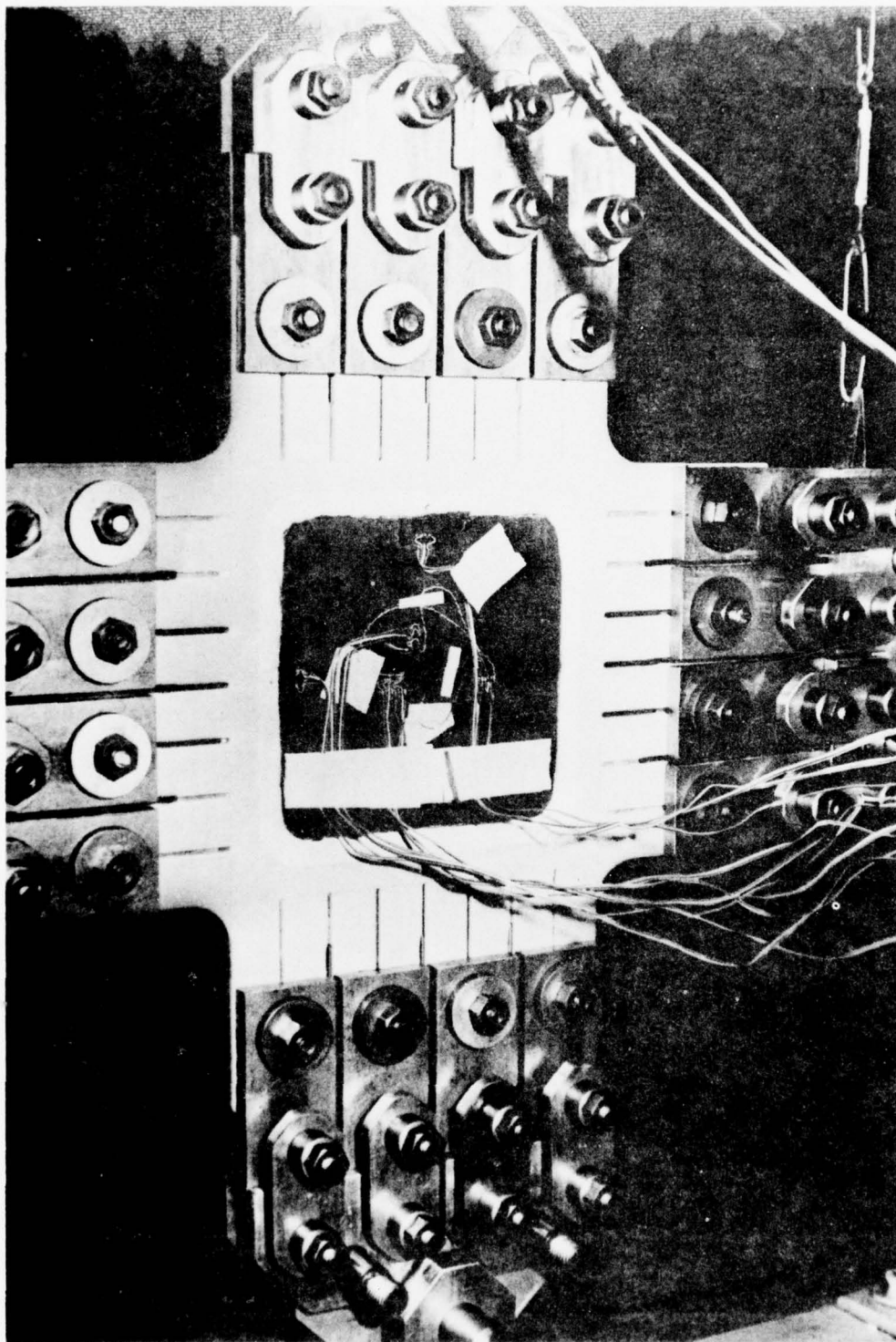
Figure 74. Whiffle-Tree Linkage Grips for Load Introduction
in Biaxial Specimen with Hole.

109
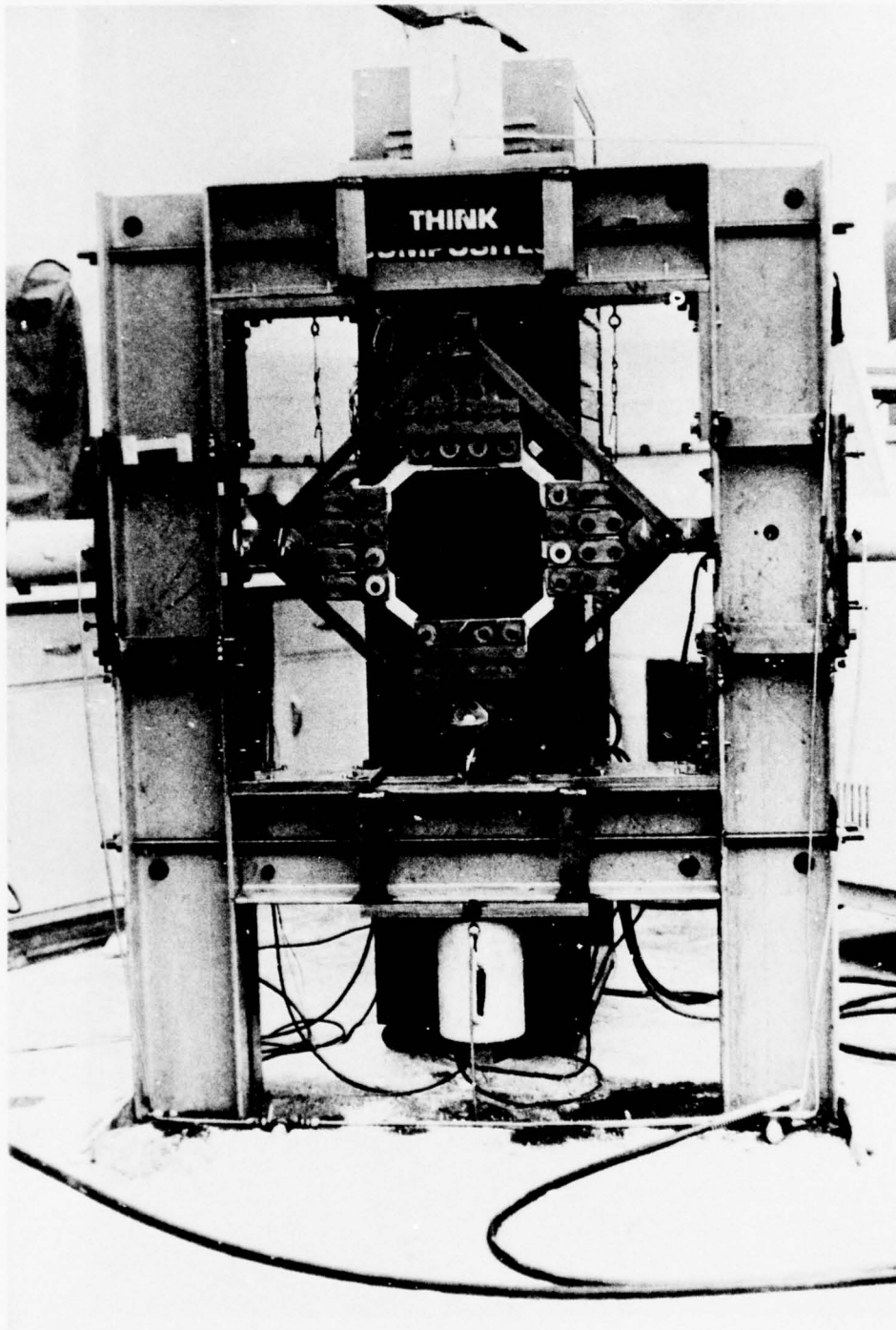
Figure 75.   Biaxial Specimen with Alignment Fixture in Loading Frame

110
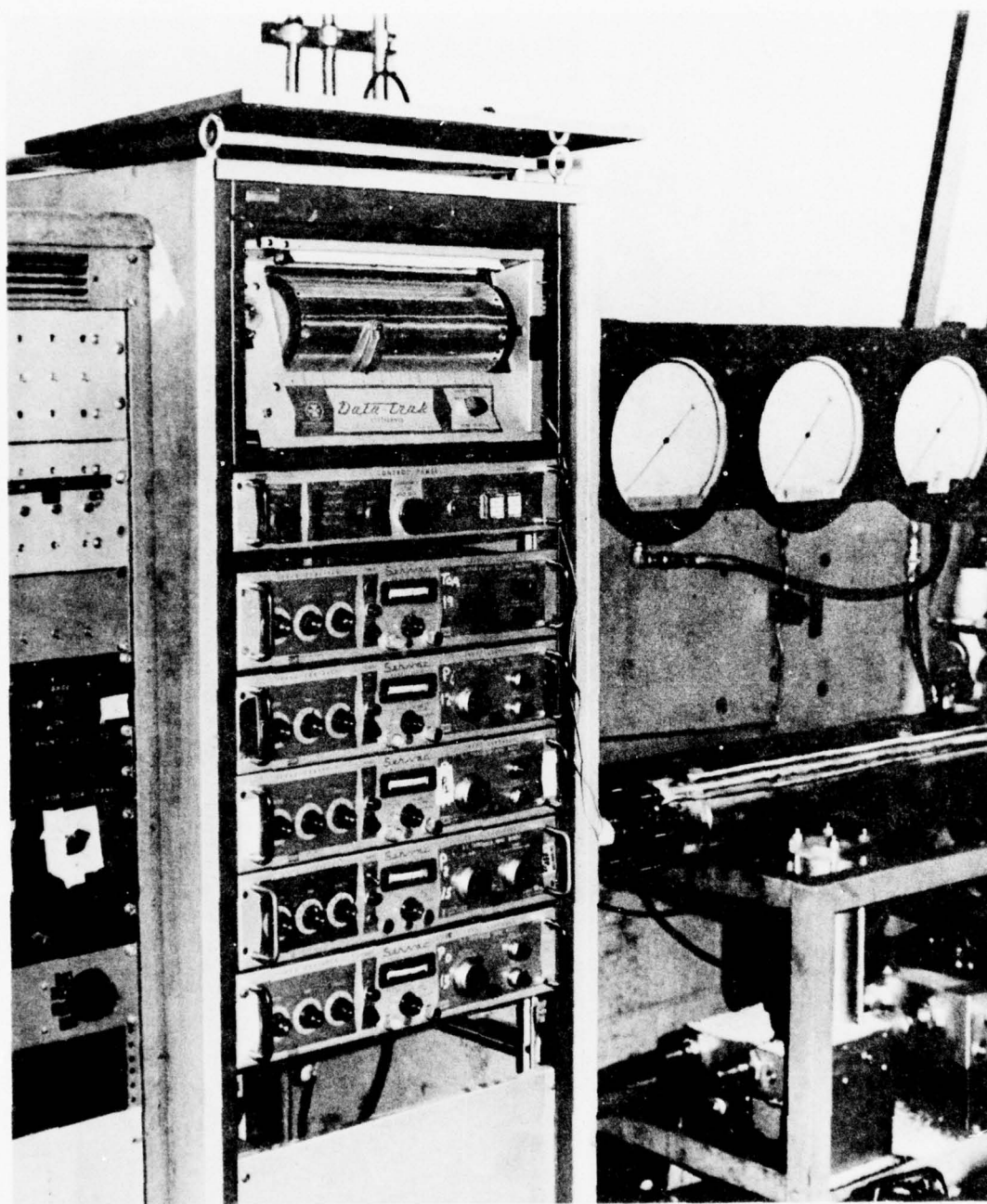
Figure 76.   Pressure Control Instrumentation for Biaxial
Loading of Specimens.

111
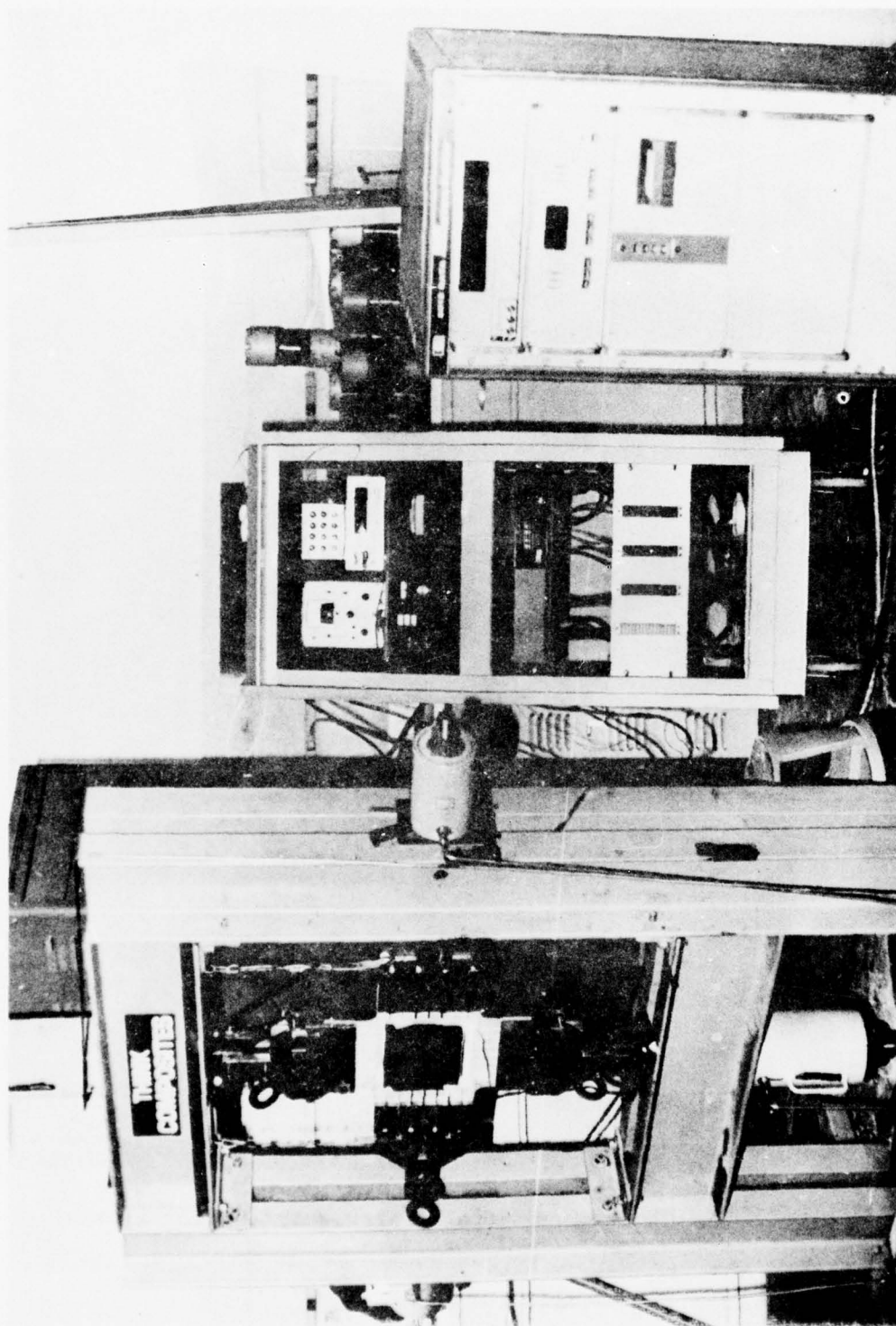
Figure 77. Loading Frame for Biaxial Testing of Flat Laminates and Associated Strain Recording Instrumentation

112
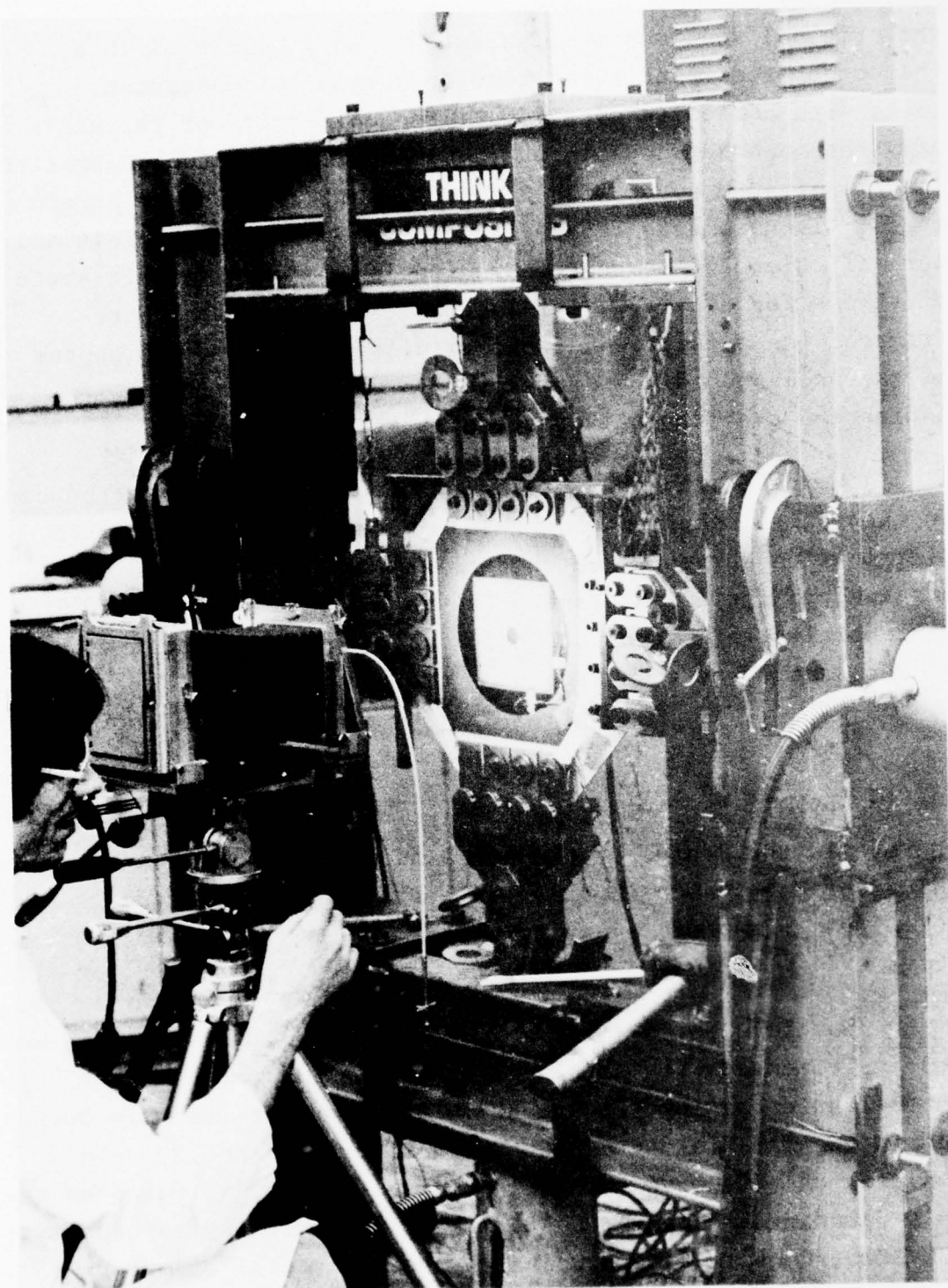
Figure 78.   Recording Fringe Patterns in Photoelastic Coating of
              Biaxial Specimen

113

the original specimen configuration. As a result of this, the corner radii and slits were abandoned in subsequent tests with composite specimens. The uniformity of the state of stress around the hole was checked with an actual composite specimen instrumented with a photoelastic coating and strain gages. Isochromatic fringe patterns around the hole initially were circular and concentric indicating an axisymmetric state of stress for equal biaxial loading. A plot of the bire-fringence as a function of radial distance r from the center of the hole showed that it varied in proportion to $1/r^2$, indicating a hydrostatic state of stress.

To determine the portion of the applied load introduced in the central section of the specimen a theoretical strain distribution curve was matched to experimental data points obtained in the linear range (Figure 79). The radial and tangential strains around a hole in an isotropic material under a hydrostatic state of stress σ_o are:

$$\varepsilon_{\theta\theta} = \frac{\sigma_o}{E} [(1-\nu) + (1+\nu) (\frac{a}{r})^2]$$

$$\varepsilon_{rr} = \frac{\sigma_o}{E} [(1-\nu) - (1+\nu) (\frac{a}{r})^2]$$

where a is the radius of the hole and r the radial distance. Values of E = 55 GPa (8 x 10^6 psi) and ν = 0.30 obtained for the $[0/\pm45/90]_s$ graphite/epoxy laminate were used in the relations above.

Specimen No. 6-7 had a 2.54 cm (1 in.) diameter hole and was instrumented with strain gages and a 1.12 mm (0.044 in.) thick photoelastic coating (Figure 80). Strains near the hole boundary and in the far-field are plotted in Figures 81 and 82 as a function of effective far-field biaxial stress. Strains on the hole boundary are linear up to an applied stress of approximately 138 MPa (20 ksi). The strains on the horizontal diameter measured

114

○ Experimental for $P_x = P_y = 22.2$ kN (5,000 lb)

—— Theoretical for $\sigma_{xx} = \sigma_{yy} = 84$ MPa (12,200 psi)

DISTANCE, $\frac{x}{a}$, $\frac{y}{a}$

STRAIN, $10^3\epsilon$
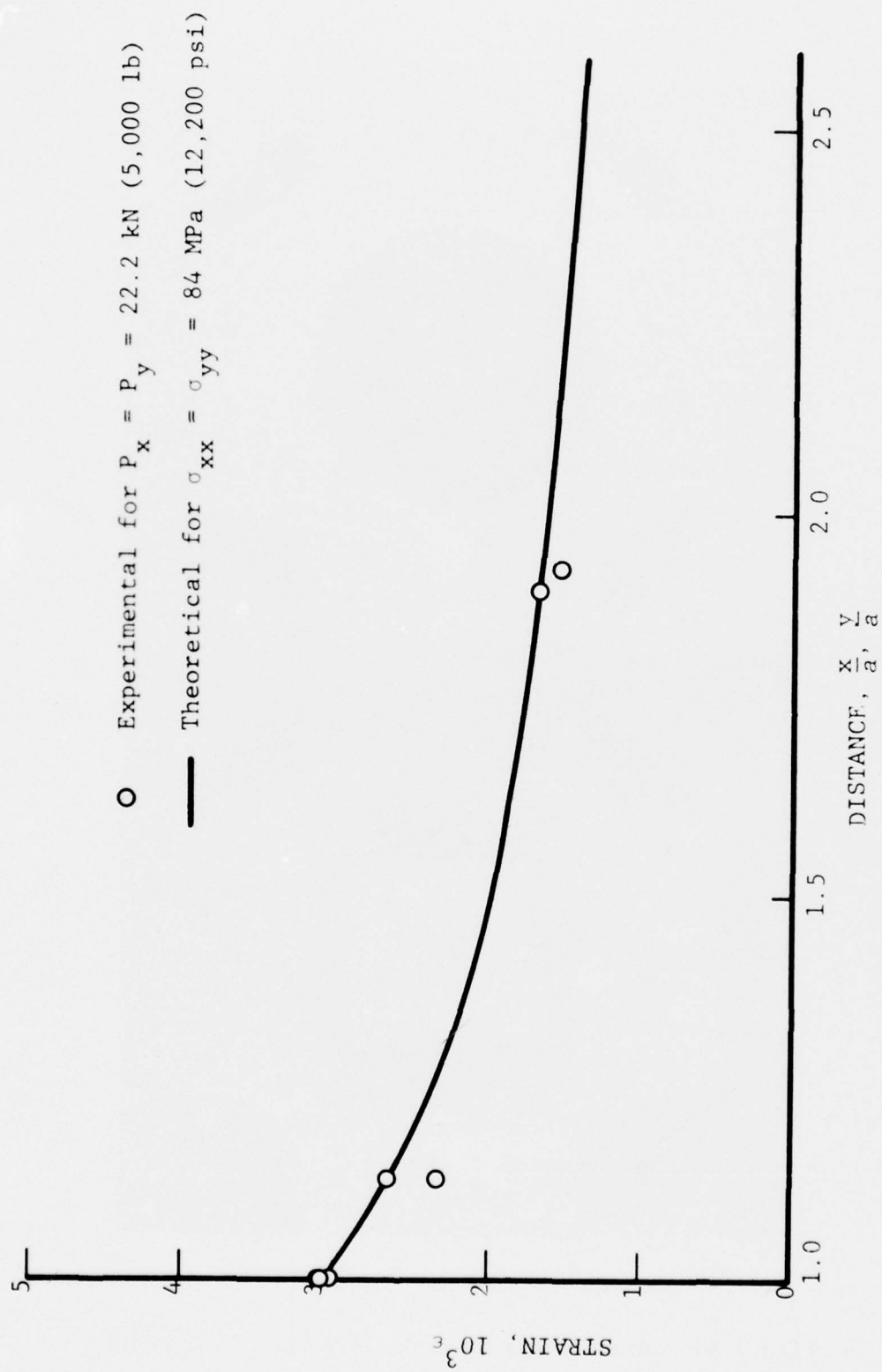
Figure 79. Matching of Theoretical Strain Distribution and Experimental Data

115
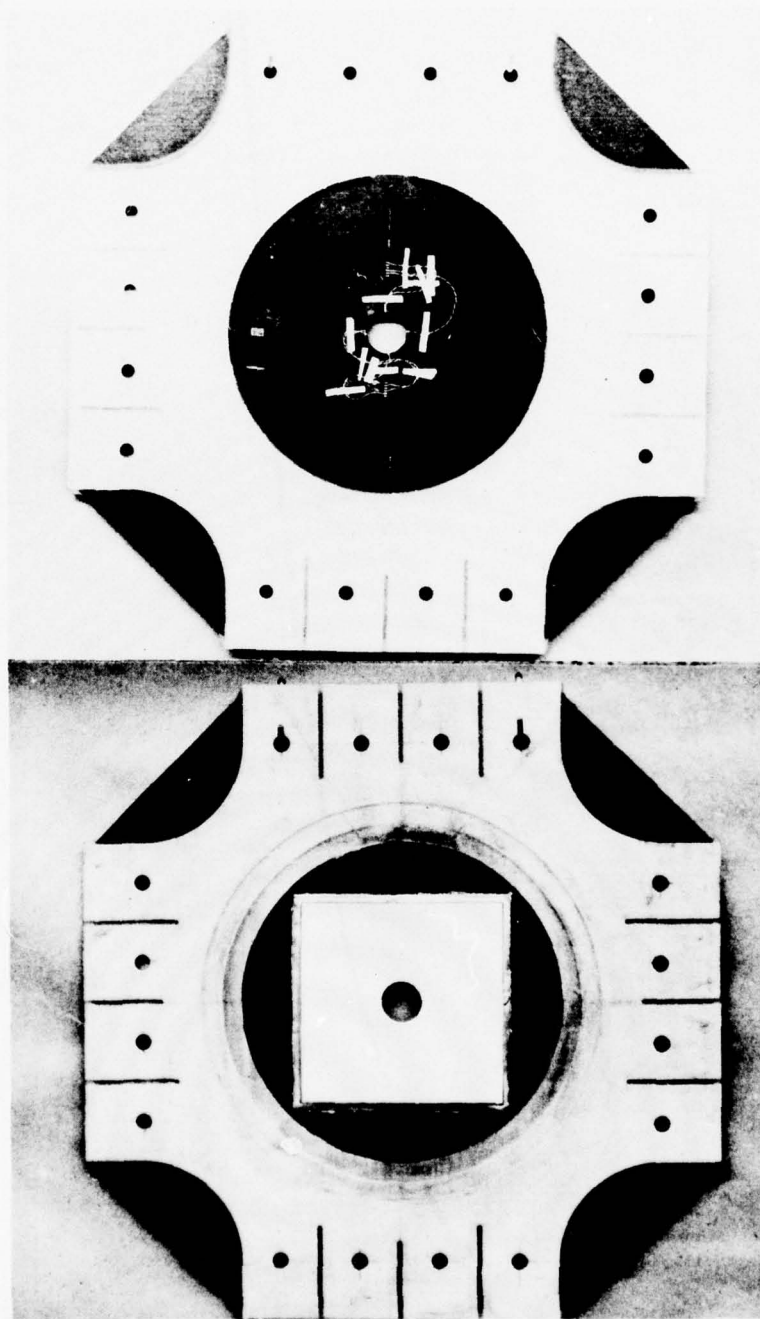
Figure 80.   Biaxial Specimen No. 6-7 with 2.54 cm (1 in.)
Diameter Hole.

116
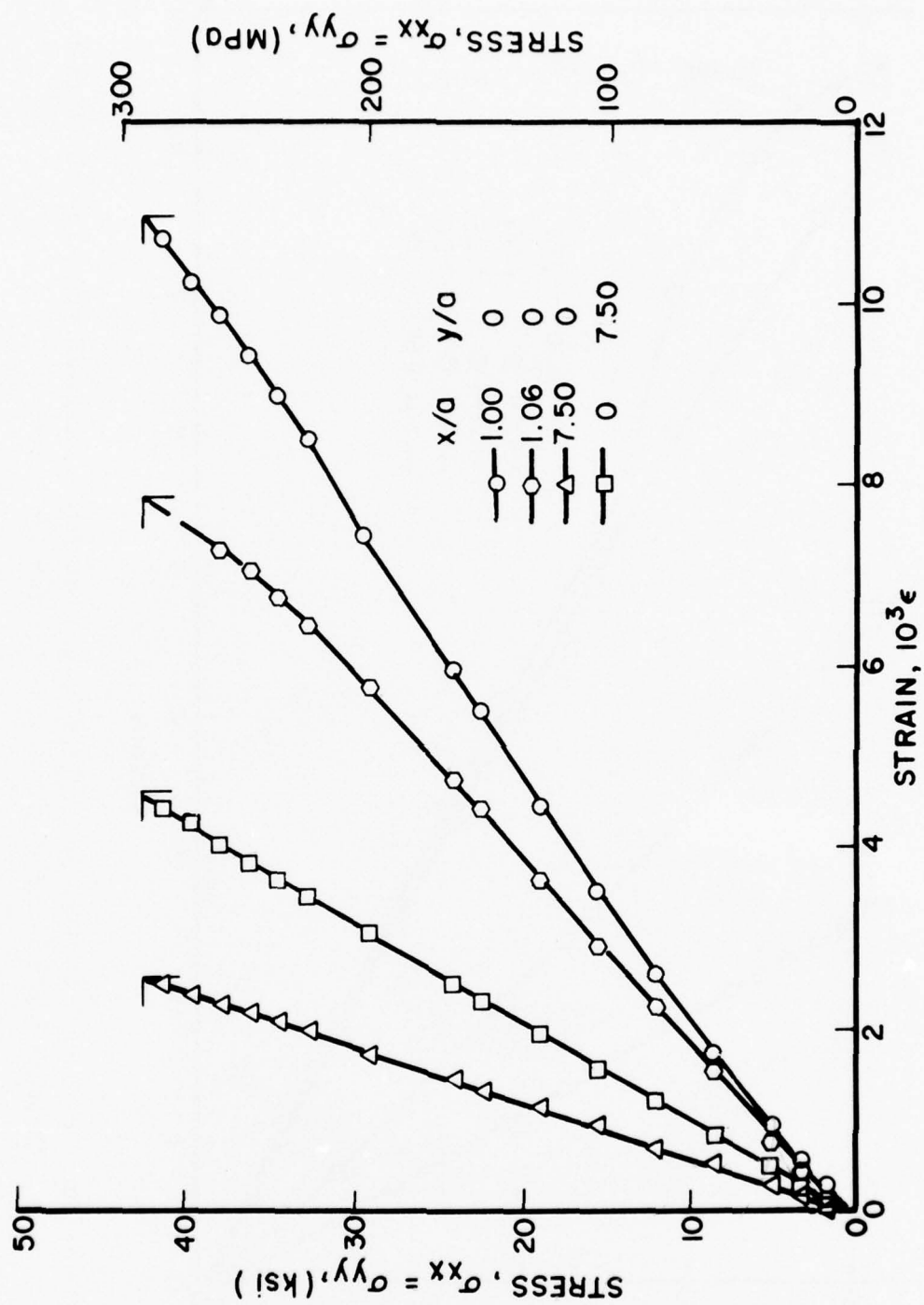
Figure 81. Vertical Strains in $[0/\pm45/90]_s$ Graphite/Epoxy Specimen with 2.54 cm (1 in.) Diameter Hole Under Equal Biaxial Loading (Spec. No. 6-7).

117

Figure 82. Horizontal Strains in [0/±45/90]s Graphite/Epoxy Specimen with 2.54 cm (1 in.) Diameter Hole Under Equal Biaxial Loading (Spec. No. 6-7).

118

with miniature gages located for the most part on the sectioned
90-deg. plies appear to be noticeably higher than the strains on
the vertical diameter. The latter were measured with miniature
strain gages situated on continuous 90-deg. fibers in the middle
of the laminate. These gages are 0.38 mm (0.015 in.) long and
0.51 mm (0.020 in.) wide and they record the deformation of the
middle four plies of the laminate when mounted on the curved
boundary of the hole. Isochromatic fringe patterns around the
hole for three levels of loading are shown in Figure 83. The
pattern initially consists of nearly concentric circular fringes
but at higher loads birefringence concentration appears at eight
characteristic points on the hole boundary. These points are at
angles of 22.5 deg. with all fiber directions. In some cases
these locations of fringe concentration shift toward the 45-deg.
location during fracture initiation. The birefringence variation
with load at two typical characteristic locations on the hole
boundary, at 0-deg. and 22.5-deg.., is plotted in Figure 84. At both
locations the fringe order, hence circumferential strain, is
the same and varies linearly up to an applied stress of approximately
193 MPa (28 ksi). Thereafter, the strain at the critical 22.5-deg.
points increases at an increased rate while at the same time strains
at the 0-deg. and 90-deg. locations show an unloading effect.
This effect was also detected by the strain gages at these
locations. This phenomenon is also visualized physically as the
regions around the 0-deg. and 90-deg. points become more isolated
from load introduction due to the progressive damage in the
adjacent 22.5-deg. and 67.5-deg. regions. The specimen failed
at an applied biaxial stress of 293 MPa (42.5 ksi). Failure
initiated at two points 22.5-deg. off the horizontal axis
(Figure 85).

Specimen No. 6-8 with a 2.54 cm (1 in.) diameter hole
was a replicate of No. 6-7 above. It was instrumented with
strain gages and a 1.12 mm (0.044 in.) thick photoelastic coating.

119

237 MPa (34 ksi)

293 MPa (42 ksi)

202 MPa (29 ksi)

285 MPa (41 ksi)

166 MPa (24 ksi)

261 MPa (38 ksi)
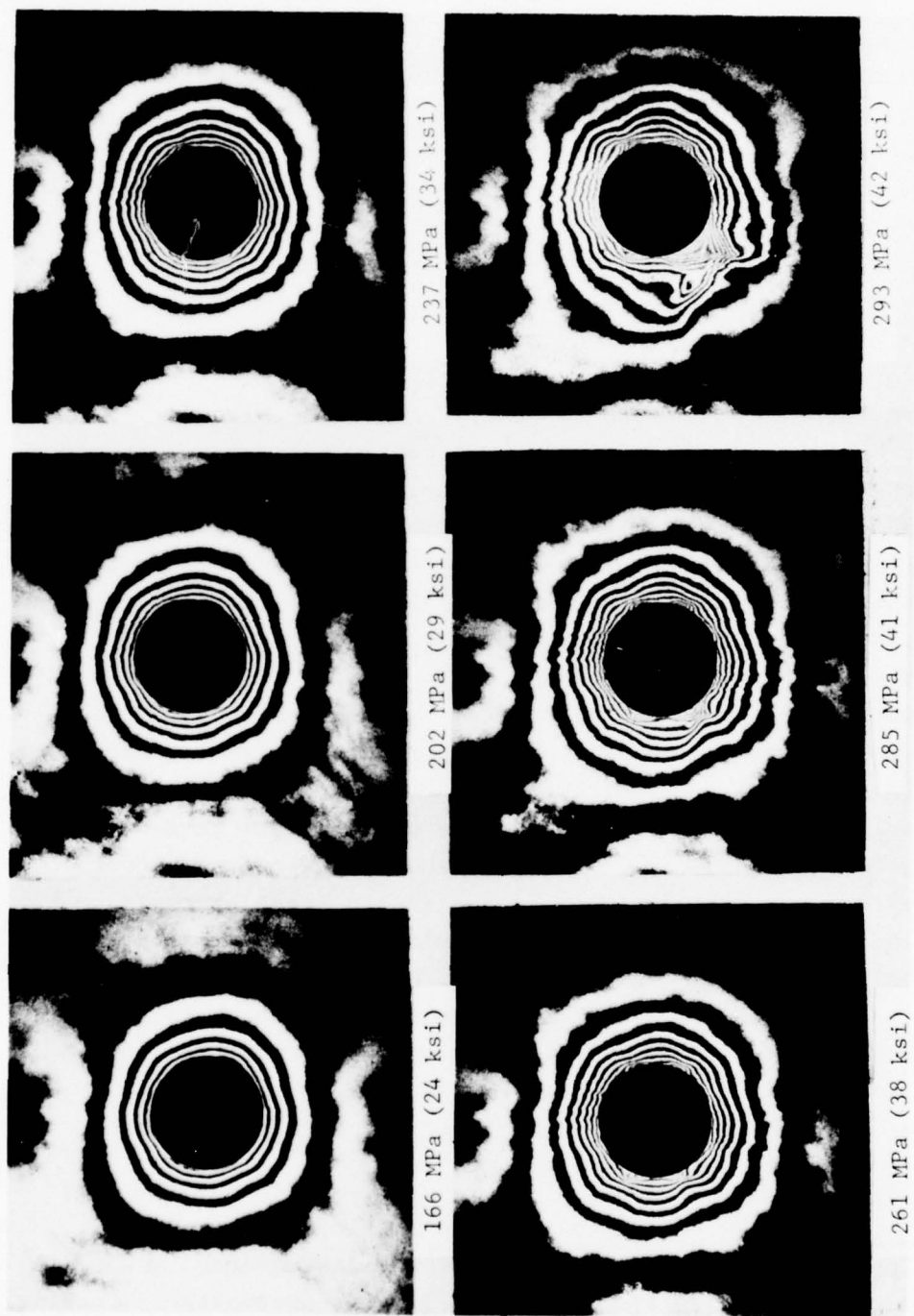
Figure 83. Isochromatic Fringe Patterns in Photoelastic Coating of Specimen
No. 6-7 (Far-Field Biaxial Stress Marked).

120
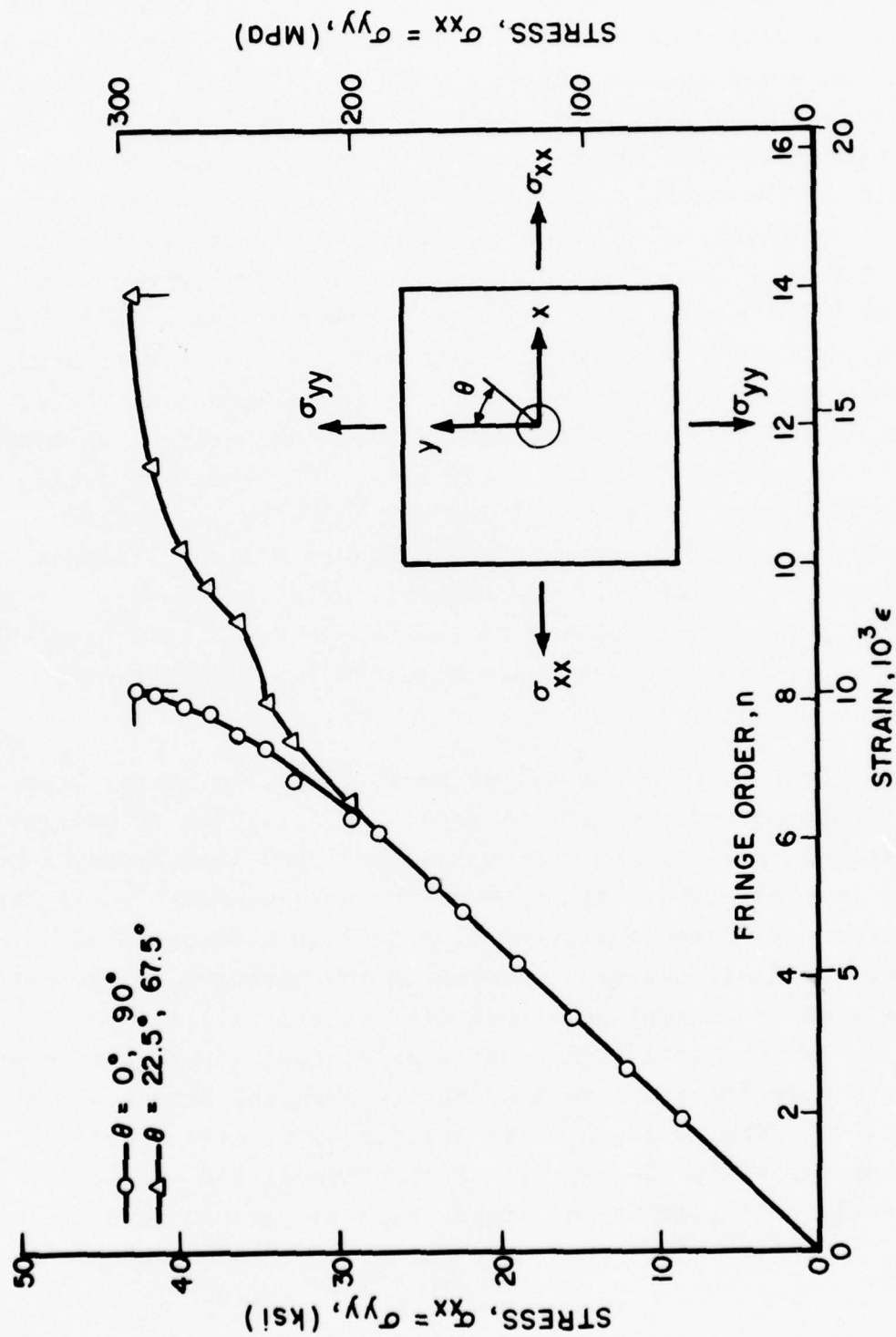
Figure 84. Fringe Order and Circumferential Strain at Two Locations on the Hole Boundary for [0/±45/90]_s Graphite/Epoxy Specimen with 2.54 cm (1 in.) Diameter Hole Under Equal Biaxial Loading (Spec. No. 6-7).

121

The variation of strains with effective far-field biaxial stress is shown in Figures 86 and 87. The strains on the boundary of the hole are linear up to an applied stress of 119 MPa (17 ksi) on the y-axis and up to a stress of 179 MPa (26 ksi) on the x-axis. Far-field strains are linear up to an applied stress of approximately 207 MPa (30 ksi). Isochromatic fringe patterns in the photoelastic coating around the hole were similar to those observed previously with the characteristic fringe concentrations at the 22.5-deg. locations. The variation of fringe order and circumferential strain with effective stress at the 0-deg. and 22.5-deg. locations is shown in Figure 88. At the 0-deg. location the fringe order varies nearly linearly to failure. At the 22.5-deg. location the fringe variation becomes nonlinear at an applied stress of approximately 124 MPa (18 ksi). The specimen failed at an applied biaxial stress of 258 MPa (37.4 ksi). Failure initiated at two points on the hole boundary at two locations approximately 22.5-deg. off the vertical axis (Figure 89). This particular mode may be related to the fact that in this case the outer fibers of the laminate were oriented in the horizontal direction.

Specimen No. 6-6 had a 1.91 cm (0.75 in.) diameter hole and was instrumented with strain gages and a 1.12 mm (0.044 in.) thick photoelastic coating. It was tabbed with glass/epoxy tabs as shown in Figure 90. Strains near the hole boundary and in the far-field are plotted in Figures 91 and 92 as a function of effective far-field stress. Strains on the boundary of the hole are linear up to an applied stress of approximately 131 MPa (19 ksi). Isochromatic fringe patterns in the photoelastic coating around the hole for six levels of applied biaxial stress are shown in Figure 93. The characteristic buildup of fringes occurs at points approximately 25-deg. off the horizontal and vertical axes. Failure initiation and propagation is clearly seen at these points. As failure progresses the points of strain concentration

Figure 85. Failure Pattern in $[0/\pm45/90]_s$ Graphite/Epoxy Specimen
with 2.54 cm (1 in.) Diameter Hole Under Equal Biaxial
Loading (Spec. No. 6-7).

Figure 86. Strains on Horizontal Axis of $[0/\pm45/90]_s$ Graphite/Epoxy Specimen with 2.54 cm (1 in.) Diameter Hole Under Equal Biaxial Loading (Spec. No. 6-8).

124

Figure 87. Strains on Vertical Axis of $[0/\pm45/90]_s$ Graphite/Epoxy Specimen with 2.54 cm (1 in.) Diameter Hole Under Equal Biaxial Loading (Spec. No. 6-8).

125

Figure 88. Fringe Order and Circumferential Strain at Two Locations on the Hole Boundary for $[0/\pm45/90]_s$ Graphite/Epoxy Specimen with 2.54 cm (1 in.) Diameter Hole Under Equal Biaxial Loading (Spec. No. 6-8).

Figure 89.   Failure Pattern in $[0/\pm 45/90]_s$ Graphite/Epoxy Specimen with 2.54 cm (1 in.) Diameter Hole Under Equal Biaxial Loading (Spec. No. 6-8).

127

Figure 90.   Biaxial Specimen No. 6-6 with 1.91 cm (0.75 in.)
             Diameter Hole

128

Figure 91. Strains Along Horizontal Axis in $[0/\pm 45/90]_s$ Graphite/Epoxy Specimen with 1.91 cm (0.75 in.) Diameter Hole Under Equal Biaxial Loading (Spec. No. 6-6).

129

Figure 92. Strains Along Vertical Axis in $[0/\pm45/90]_s$ Graphite/
Epoxy Specimen with 1.91 cm (0.75 in.) Diameter Hole
Under Equal Biaxial Loading (Spec. No. 6-6).
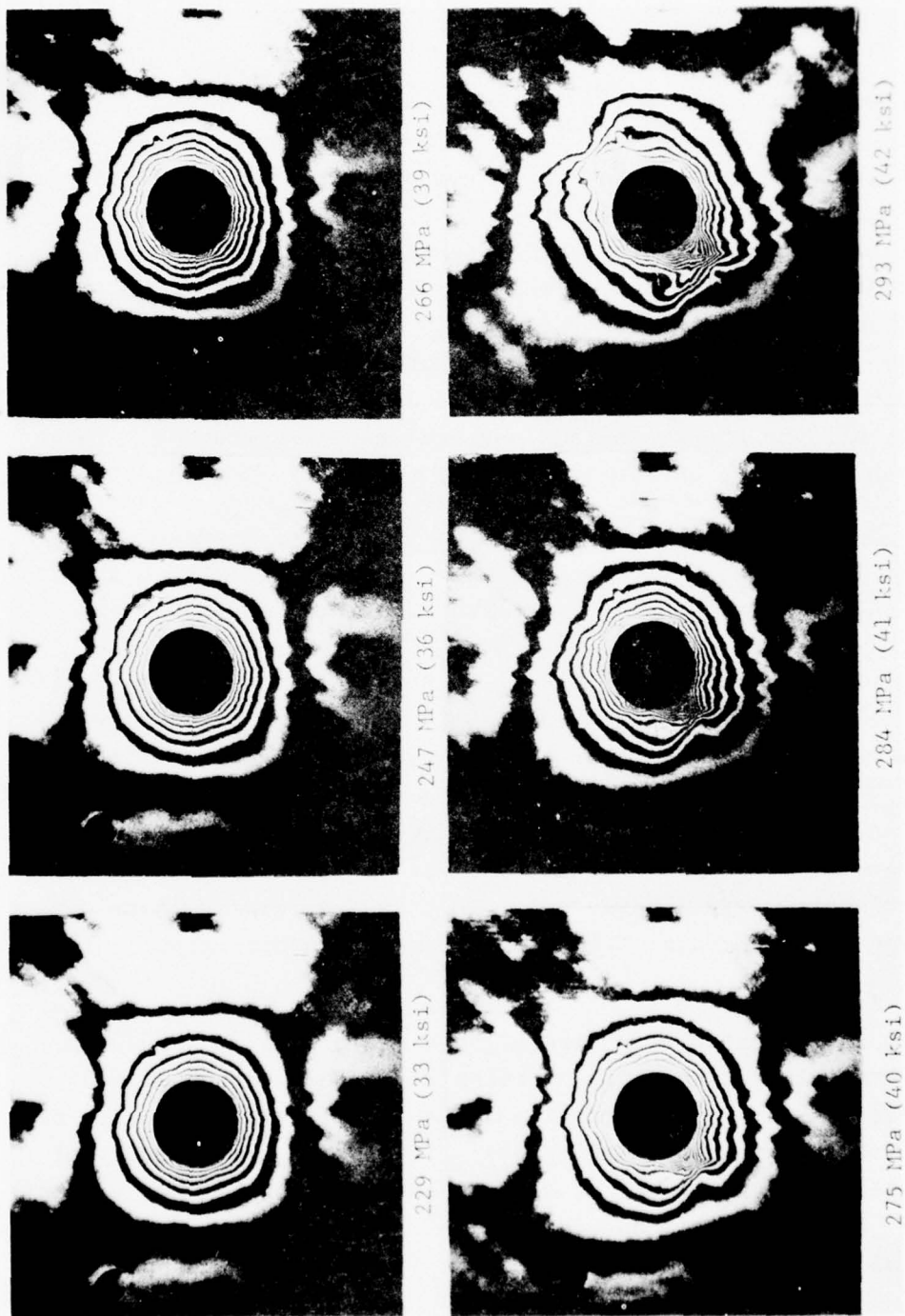
Figure 93. Isochromatic Fringe Patterns in Photoelastic Coating of Specimen No. 6-6 (Far-Field Biaxial Stress Marked).

266 MPa (39 ksi)

293 MPa (42 ksi)

247 MPa (36 ksi)

284 MPa (41 ksi)

229 MPa (33 ksi)

275 MPa (40 ksi)

shift towards the 45-deg. locations, possibly due to the influence
of the delaminating 45-deg. plies. The variation of fringe order
and circumferential strain at the two characteristic locations on
the boundary of the hole is shown in Figure 94. The fringe
variation at the characteristic off-axis locations becomes non-
linear at a stress of approximately 131 MPa (19 ksi). The
maximum measured strain at the location of failure was approximately
19×10^{-3}. Failure in the form of cracking and delamination
initiated at three locations on the hole boundary, approximately
30-deg. off the horizontal and vertical axes (Figure 95). The
specimen failed at an applied biaxial stress of 299 MPa (43 ksi).

Specimen No. 6-9 had a 1.91 cm (0.75 in.) diameter hole
and was instrumented with strain gages and a 1.12 mm (0.044 in.)
thick photoelastic coating. Strains along the horizontal and
vertical axes are plotted in Figures 96 and 97 as a function of
effective far-field biaxial stress. Strains on the boundary of
the hole are linear up to an applied stress of 145 MPa (21 ksi).
Far-field strains are linear up to an applied stress of approxi-
mately 207 MPa (30 ksi). The specimen failed at an applied biaxial
stress of 261 MPa (38 ksi). Failure initiated at two points on
the hole boundary at two locations approximately 22.5-deg. off
the horizontal axis (Figure 98). In this case the laminate was
oriented with the outer fibers in the vertical direction.

Specimen No. 6-10 had a 1.27 cm (0.50 in.) diameter hole
and was instrumented with strain gages and a 0.51 mm (0.020 in.)
thick photoelastic coating. Strains along the horizontal and
vertical axes are plotted in Figures 99 and 100 as a function of
effective far-field biaxial stress. Strains on the boundary of
the hole become nonlinear at an applied stress of 145 MPa (21 ksi)
on the horizontal axis and a stress of 97 MPa (14 ksi) on the
vertical axis. Far-field strains are linear up to an applied

132

Figure 94.   Fringe Order and Circumferential Strain at Two Locations
on the Hole Boundary for [0/±45/90]$_s$ Graphite/Epoxy
Specimen with 1.91 cm (0.75 in.) Diameter Hole Under
Equal Biaxial Loading (Spec. No. 6-6).

133

Figure 95. Failure Pattern in $[0/\pm45/90]_s$ Graphite/Epoxy Specimen with 1.91 cm (0.75 in.) Diameter Hole Under Equal Biaxial Loading (Spec. No. 6-6).
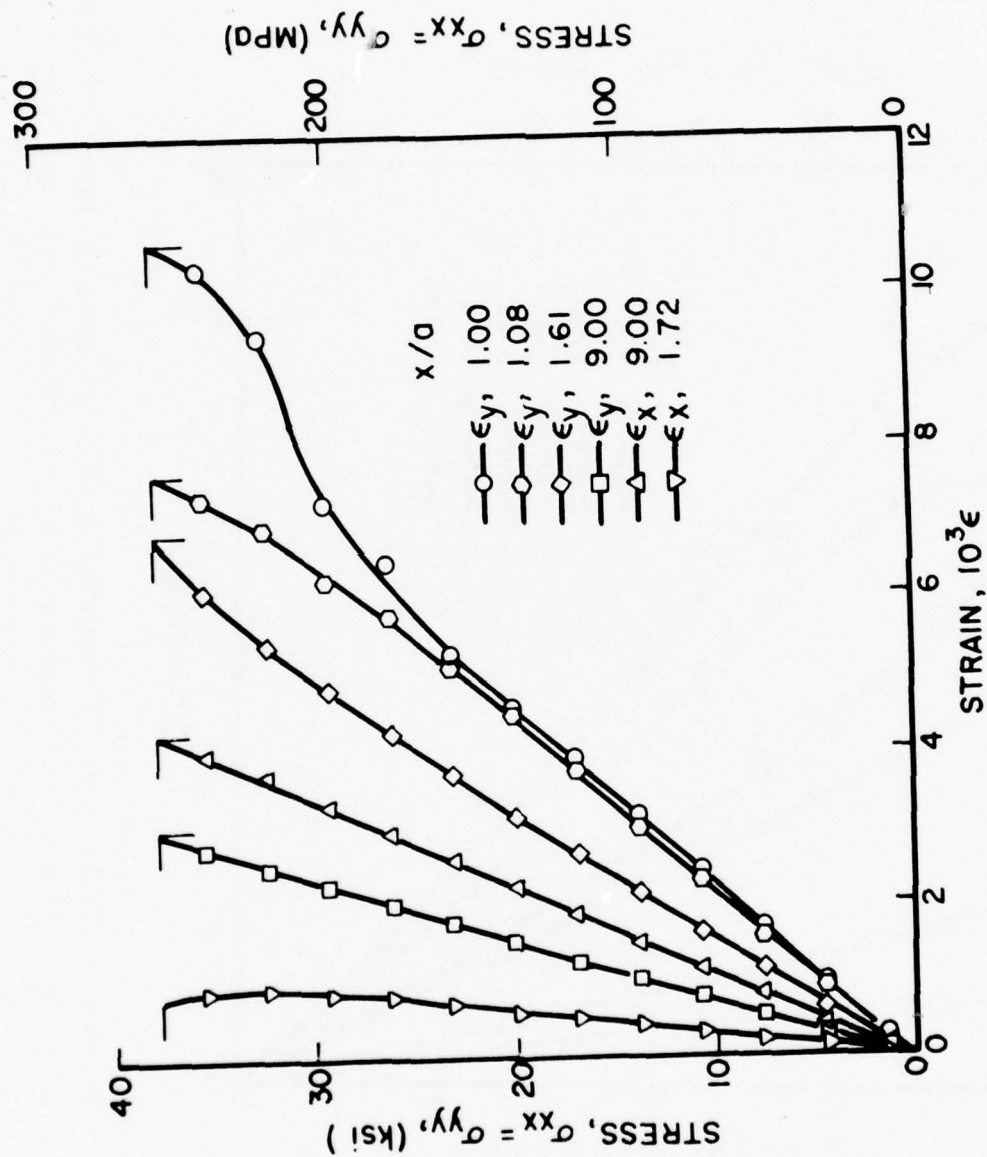
Figure 96. Strains on Horizontal Axis of $[0/\pm45/90]_s$ Graphite/Epoxy Specimen with 1.91 cm (0.75 in.) Diameter Hole Under Equal Biaxial Loading (Spec. No. 6-9).
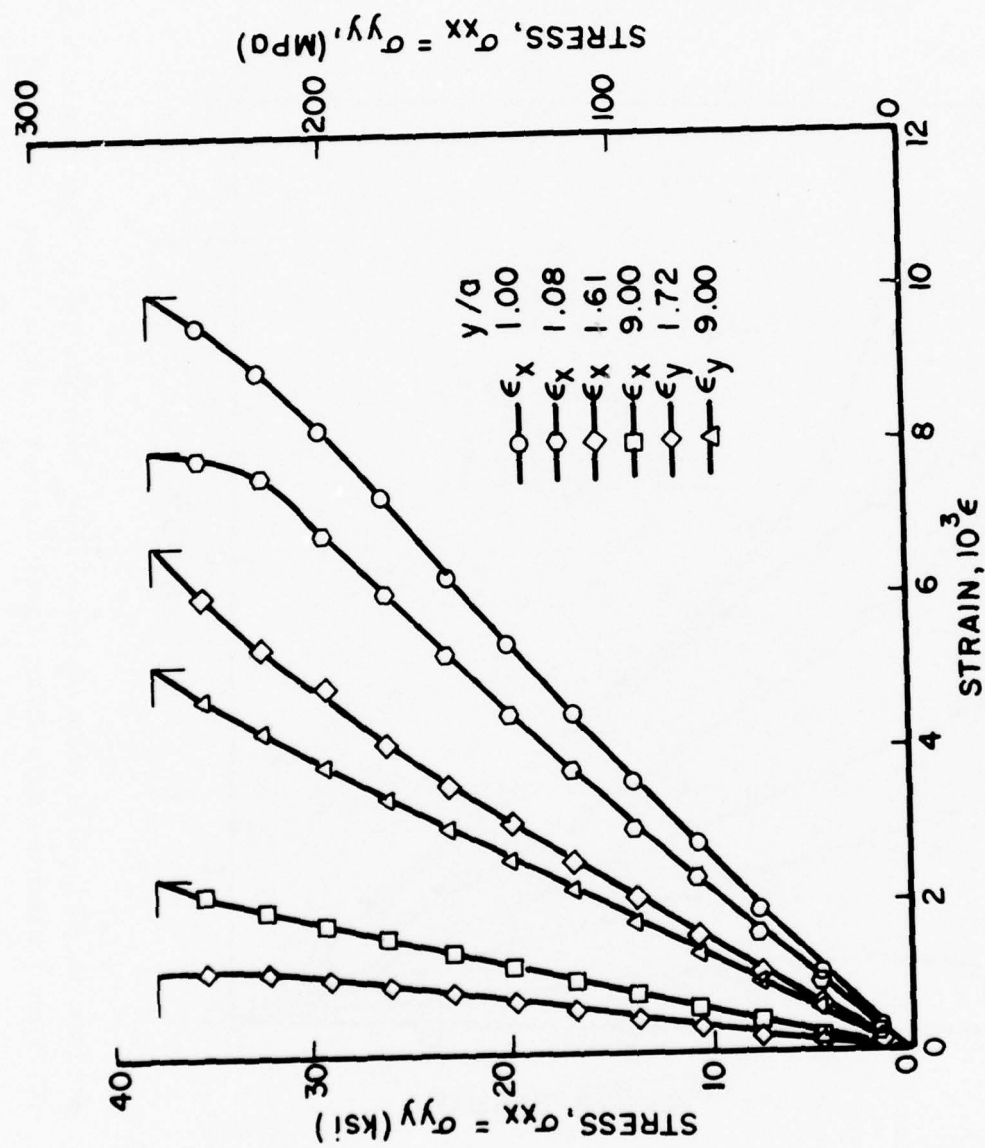
Figure 97. Strains on Vertical Axis of [0/±45/90]$_s$ Graphite/Epoxy Specimen with 1.91 cm (0.75 in.) Diameter Hole Under Equal Biaxial Loading (Spec. No. 6-9).
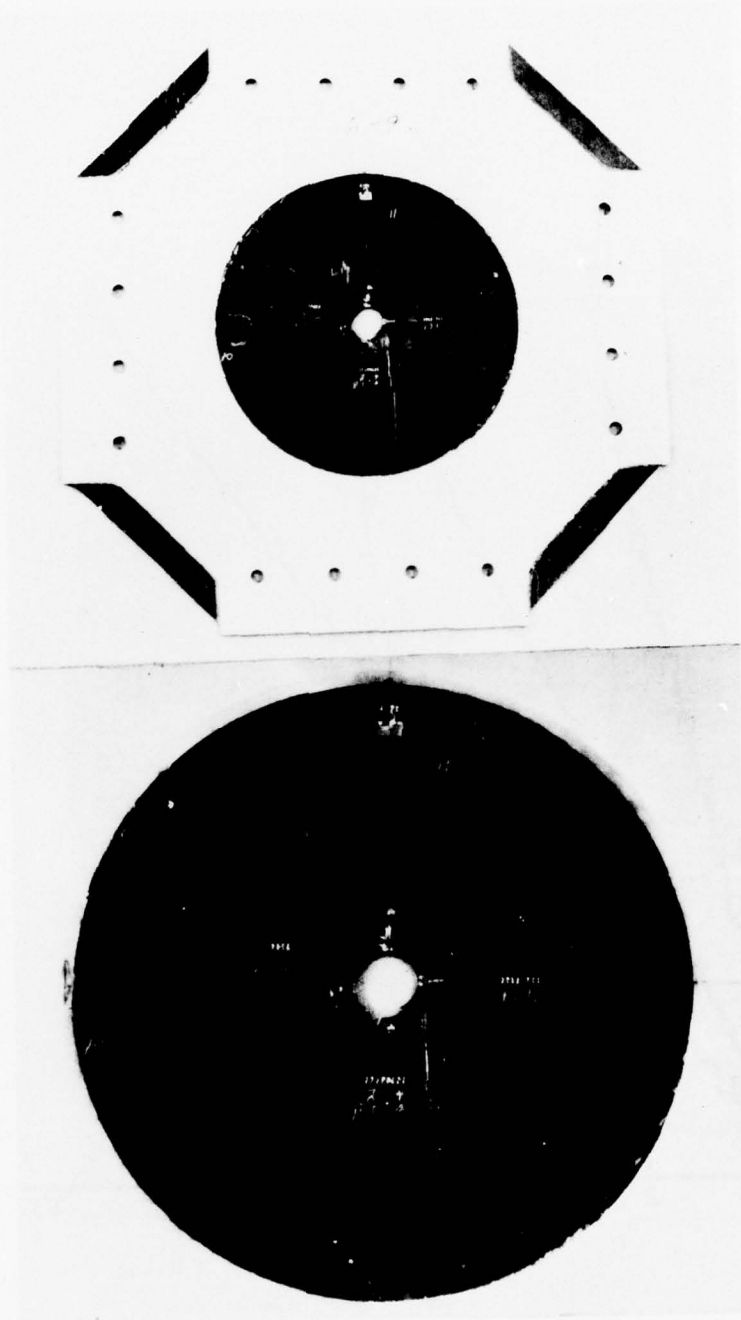
Figure 98. Failure Pattern in $[0/\pm45/90]_s$ Graphite/Epoxy Specimen
with 1.91 cm (0.75 in.) Diameter Hole Under Equal
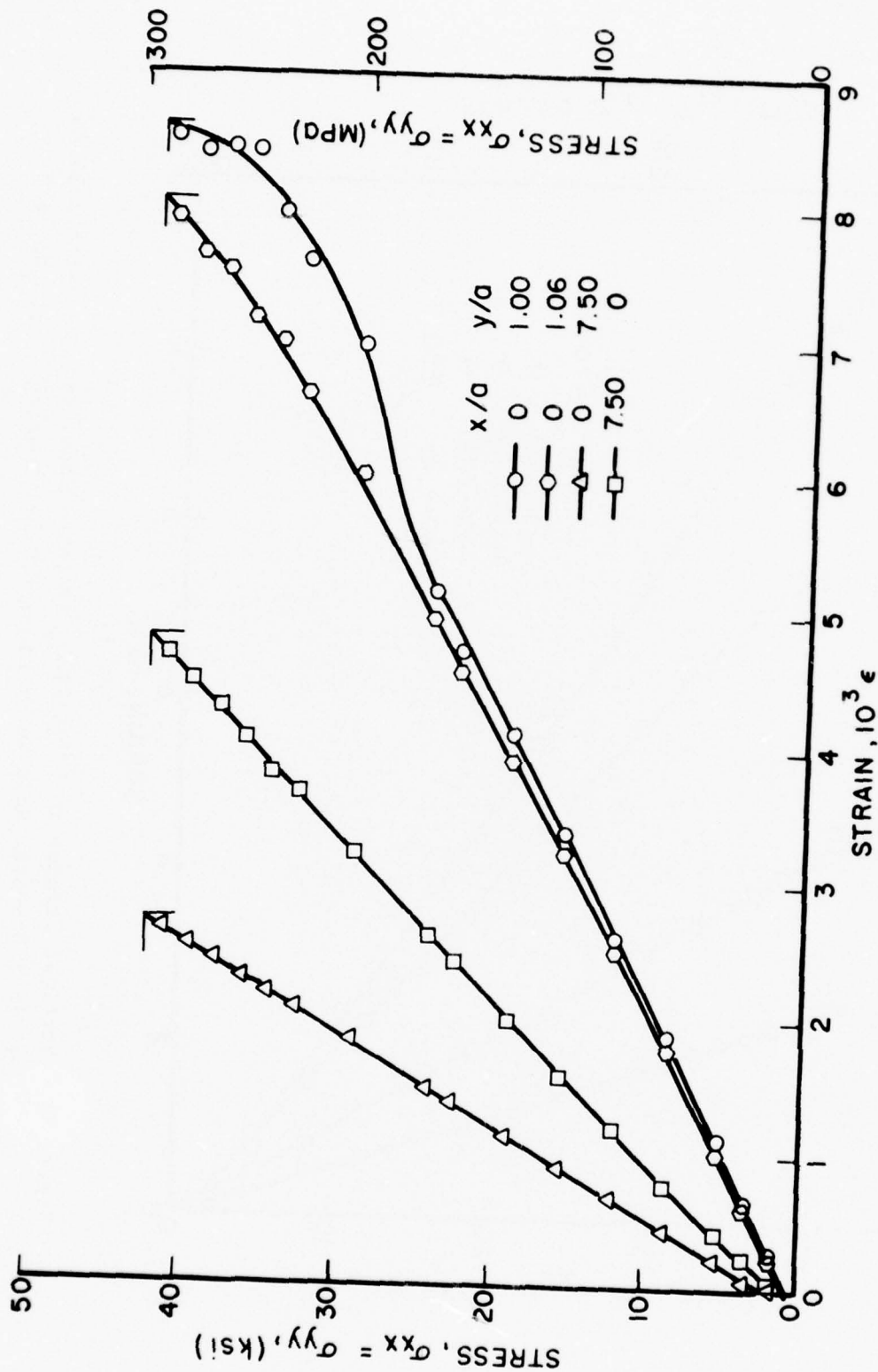Biaxial Loading (Spec. No. 6-9).

137
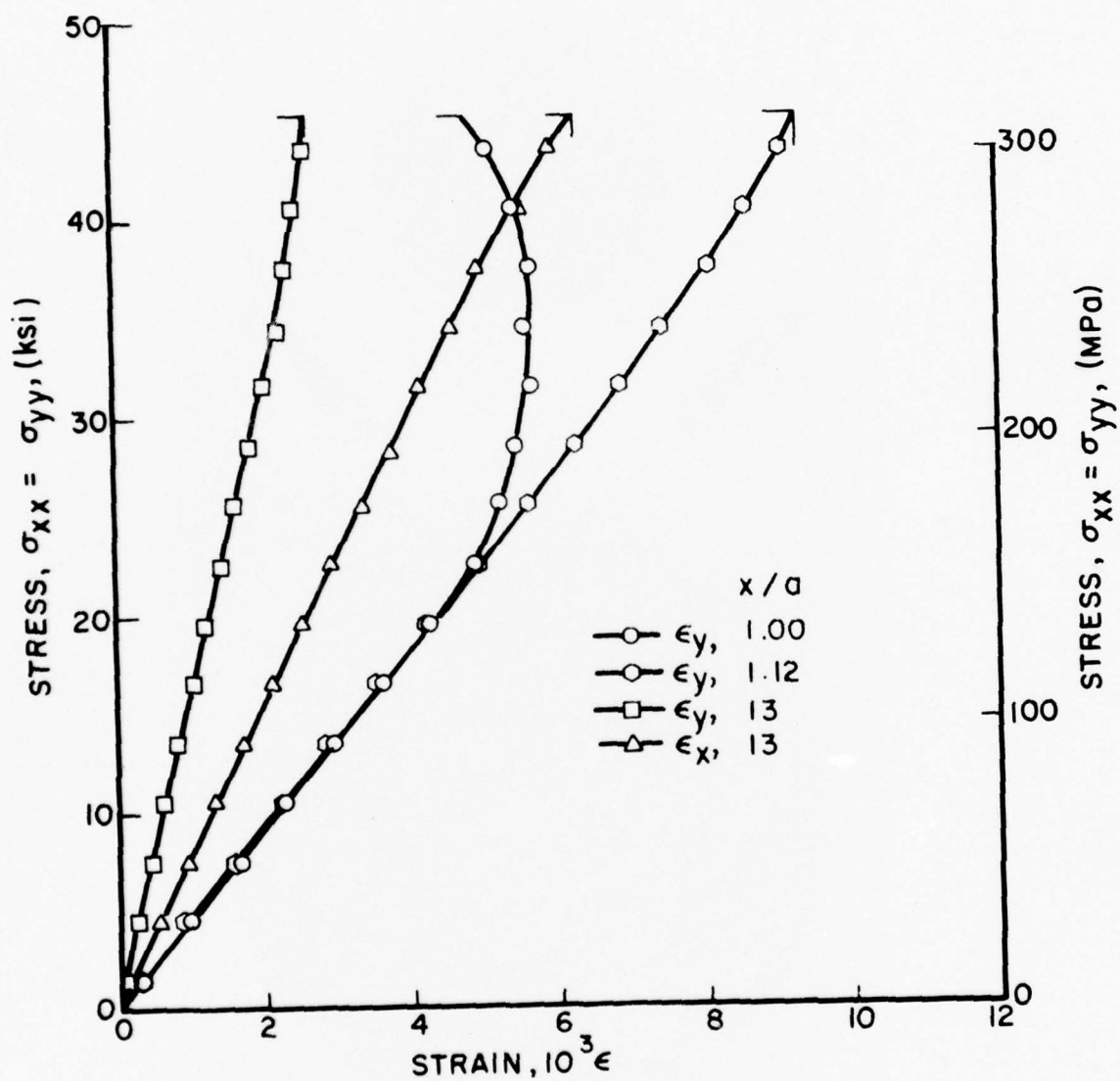
Figure 99. Strains on Horizontal Axis of $[0/\pm45/90]_s$ Graphite/Epoxy Specimen with 1.27 cm (0.50 in.) Diameter Hole Under Equal Biaxial Loading (Spec. No. 6-10).

138
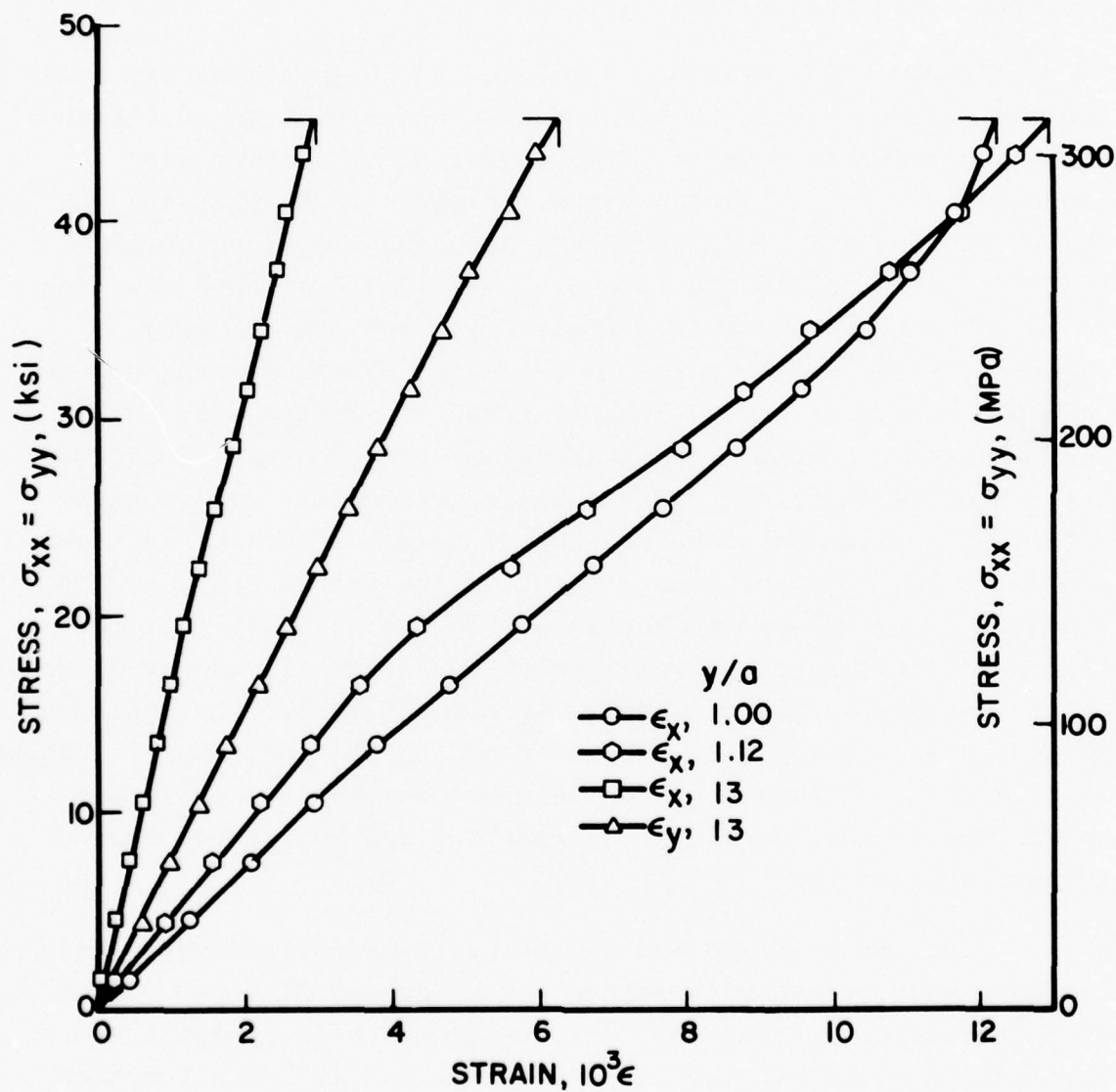
Figure 100. Strains on Vertical Axis of $[0/\pm45/90]_s$ Graphite/Epoxy
Specimen with 1.27 cm (0.50 in.) Diameter Hole Under
Equal Biaxial Loading (Spec. No. 6-10).

stress of approximately 214 MPa (31 ksi). The specimen failed
at an applied biaxial stress of 312 MPa (45.2 ksi). Failure
initiated at two points off the horizontal axis (Figure 101).
In this case also the outer fibers in the laminate were
oriented along the vertical direction.

Specimen No. 6-11 had a 1.27 cm (0.50 in.) diameter hole
and was instrumented with strain gages and a 0.51 mm (0.020 in.)
thick photoelastic coating. The variation of strains with
effective far-field biaxial stress is shown in Figures 102 and 103.
The strains on the boundary of the hole are linear up to an
applied stress of 110 MPa (16 ksi). Far-field strains are linear
up to an applied stress of approximately 260 MPa (38 ksi).
Isochromatic fringe patterns in the photoelastic coating around
the hole were similar to those observed previously with the
characteristic fringe concentrations at the 22.5-deg. locations.
The variation of fringe order and circumferential strain with
effective stress at the 0-deg. and 22.5-deg. locations is shown
in Figure 104. At the 0-deg. location the fringe order varies
linearly up to an applied stress of 276 MPa (40 ksi). At the
22.5-deg. location the fringe variation becomes nonlinear at an
applied stress of approximately 240 MPa (35 ksi). The specimen
failed at an applied biaxial stress of 328 MPa (47.5 ksi). Failure
initiated at two points on the hole boundary at two locations
approximately 22.5-deg. off the vertical and horizontal axes
(Figure 105).

Specimen No. 6-15 had a 0.64 cm (0.25 in.) diameter hole
and was instrumented with strain gages and a 0.51 mm (0.020 in.)
thick photoelastic coating. Strains along the horizontal and
vertical axes are plotted in Figures 106 and 107 as a function
of effective far-field biaxial stress. Strains on the boundary of
the hole are linear up to an applied stress of 104 MPa (15 ksi).

140
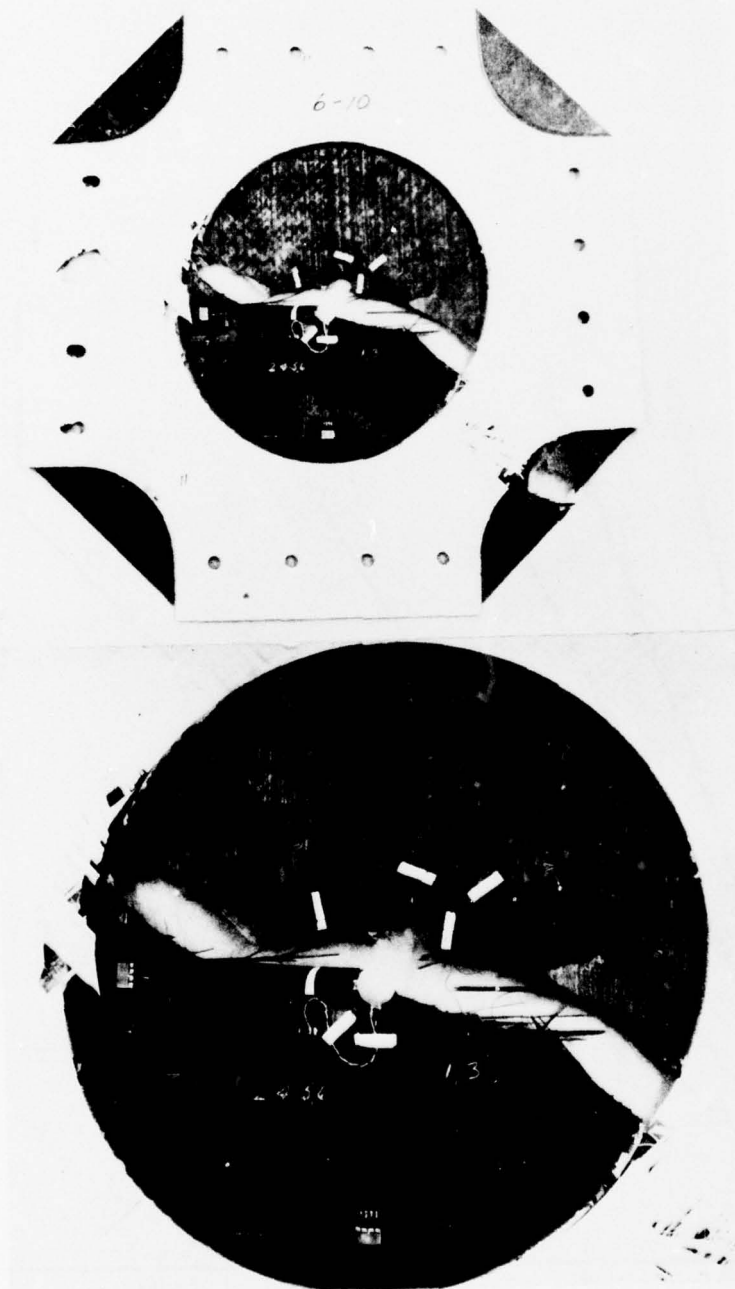
Figure 101. Failure Pattern in $[0/\pm45/90]_s$ Graphite/Epoxy Specimen
with 1.27 cm (0.50 in.) Diameter Hole Under Equal
Biaxial Loading (Spec. No. 6-10).

141
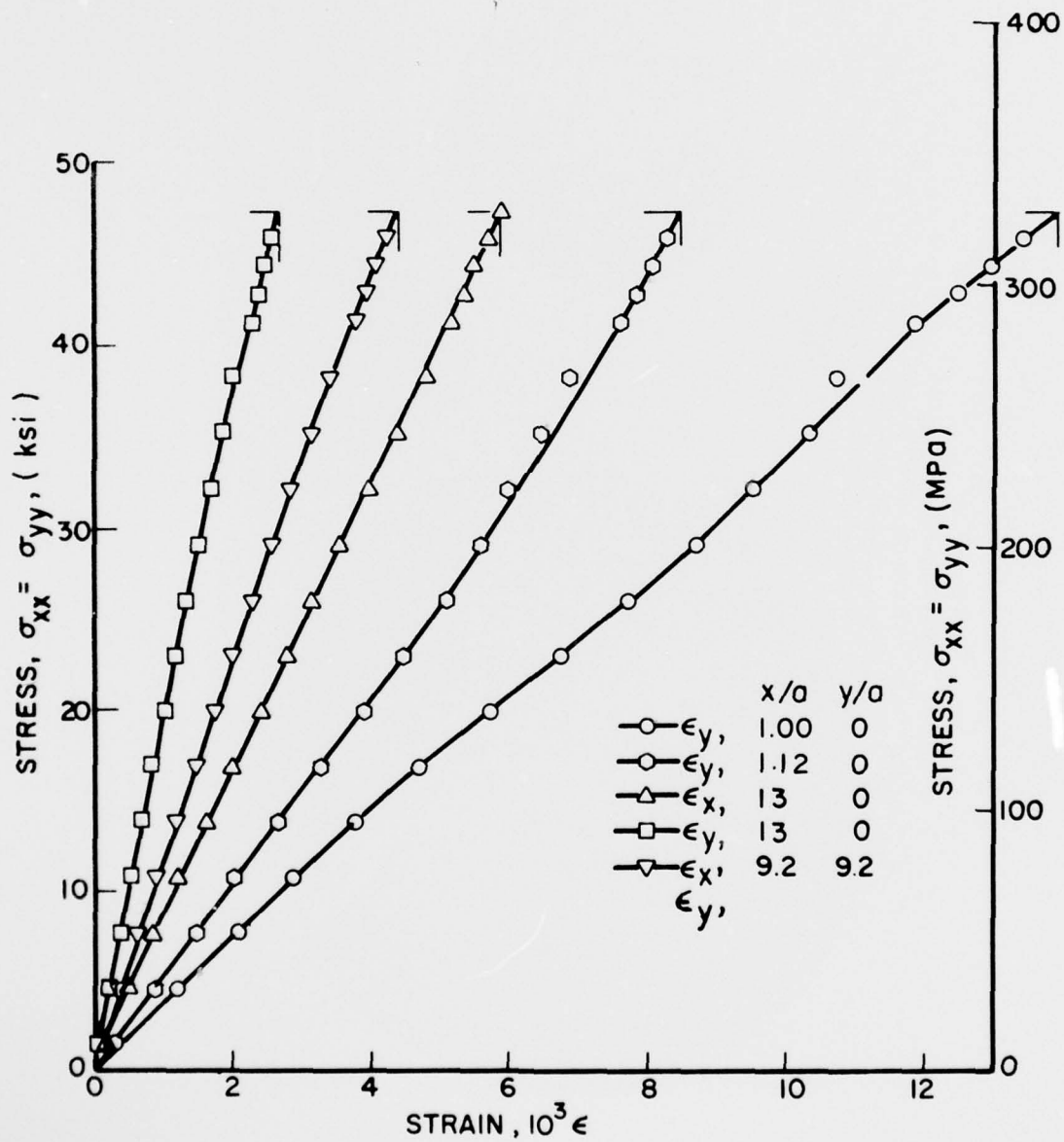
Figure 102.   Strains on Horizontal and Diagonal Axes of $[0/\pm45/90]_s$
Graphite/Epoxy Specimen with 1.27 cm (0.50 in.) Diameter
Hole Under Equal Biaxial Loading (Spec. No. 6-11).
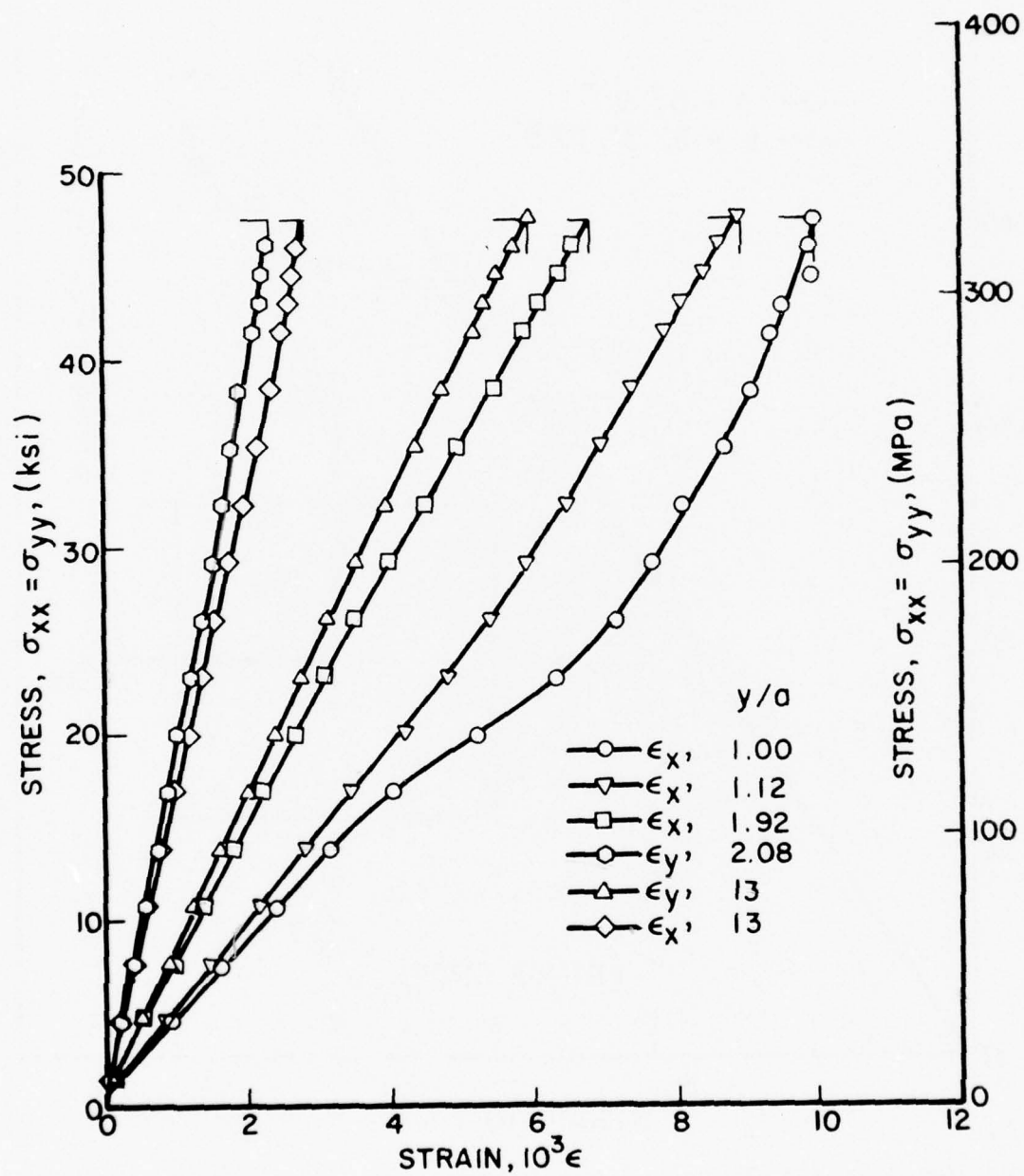
Figure 103. Strains on Vertical Axis of $[0/\pm45/90]_s$ Graphite/Epoxy
Specimen with 1.27 cm (0.50 in.) Diameter Hole Under
Equal Biaxial Loading (Spec. No. 6-11).

143
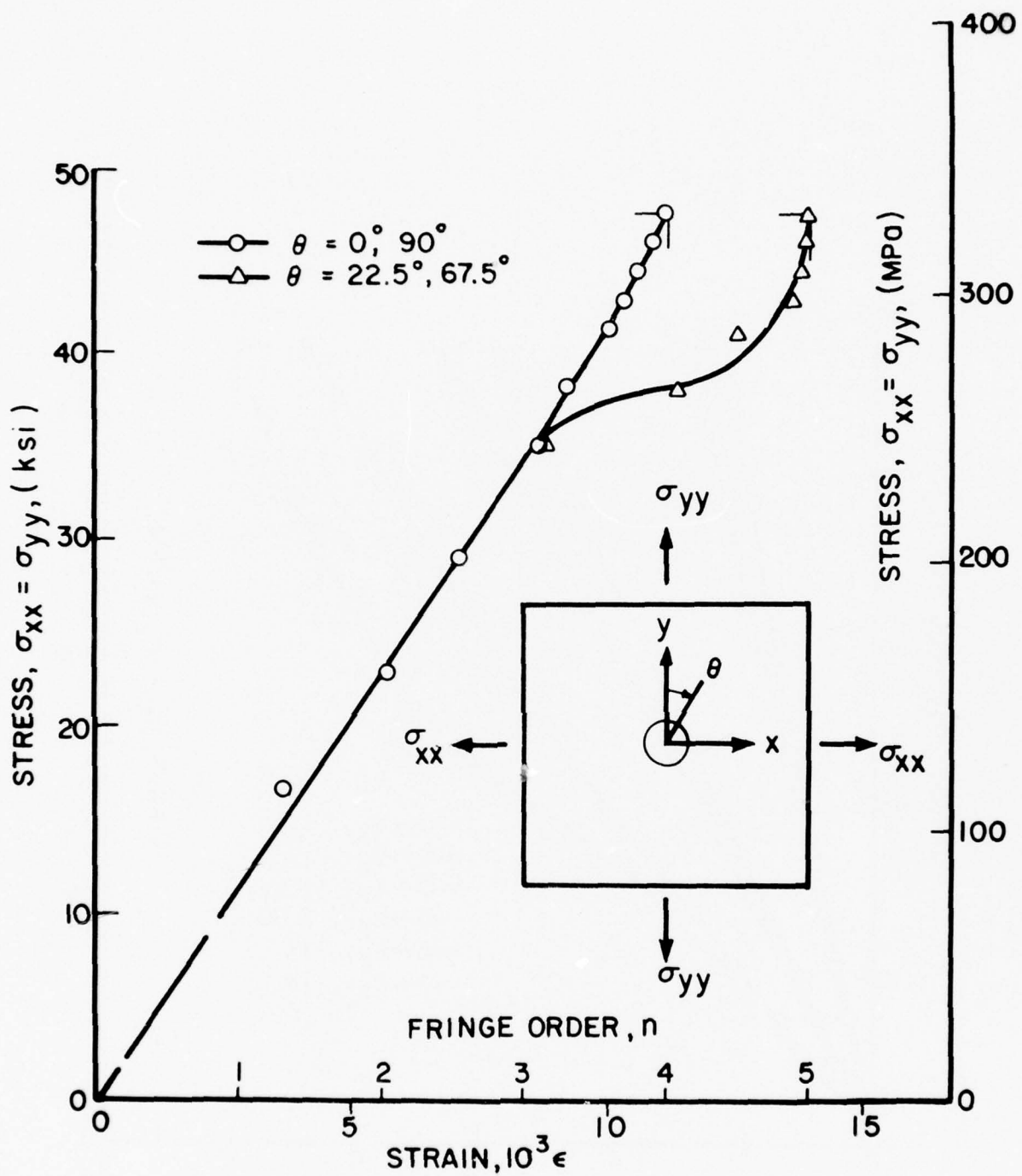
Figure 104. Fringe Order and Circumferential Strain at Two Locations on the Hole Boundary for $[0/\pm45/90]_s$ Graphite/Epoxy Specimen with 1.27 cm (0.50 in.) Diameter Hole Under Equal Biaxial Loading (Spec. No. 6-11).

144
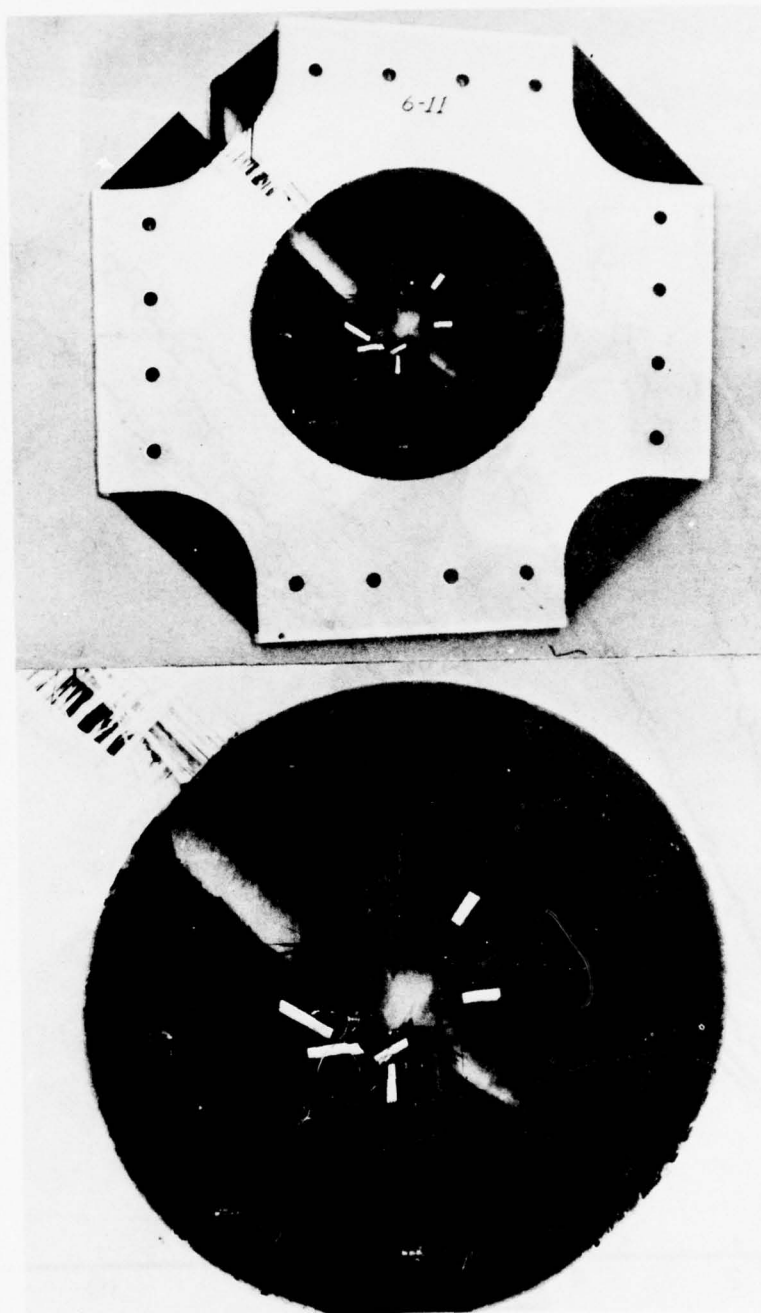
Figure 105.   Failure Pattern in $[0/\pm45/90]_s$ Graphite/Epoxy Specimen
with 1.27 cm (0.50 in.) Diameter Hole Under Equal
Biaxial Loading (Spec. No. 6-11).

145
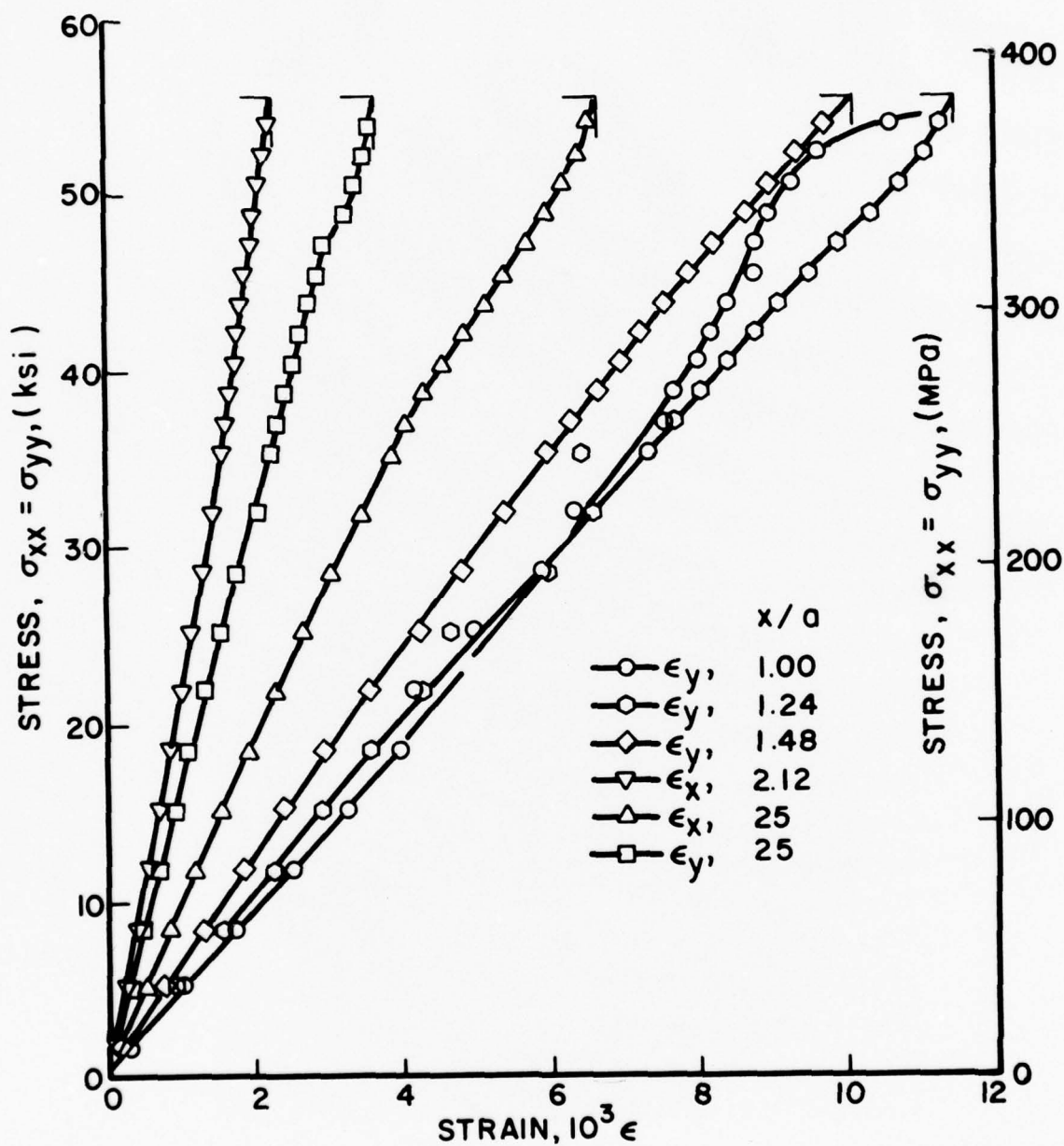
Figure 106.   Strains on Horizontal Axis of $[0/\pm45/90]_s$ Graphite/
Epoxy Specimen with 0.64 cm (0.25 in.) Diameter Hole
Under Equal Biaxial Loading (Spec. No. 6-15).

146
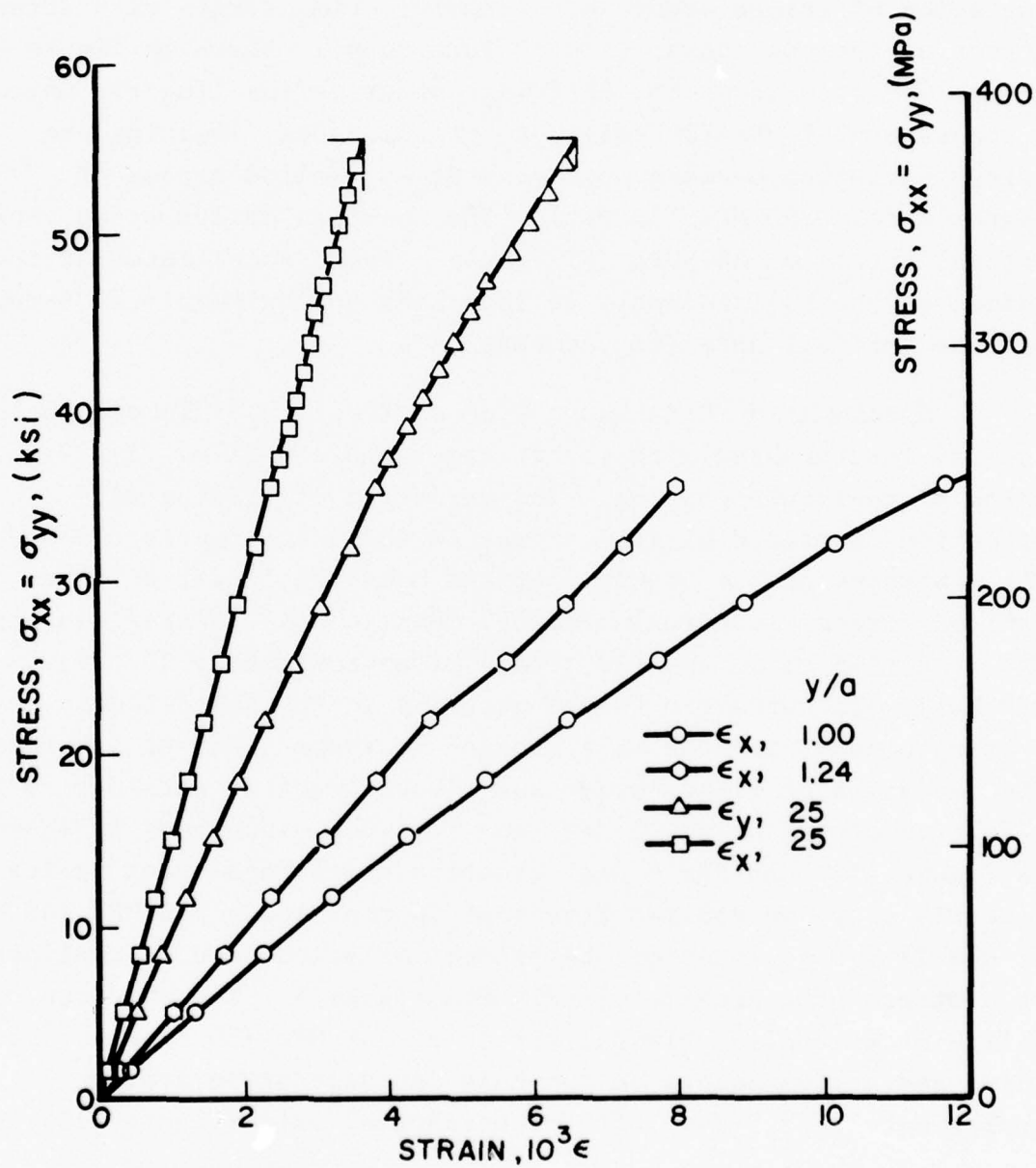
Figure 107. Strains on Vertical Axis of $[0/\pm45/90]_s$ Graphite/ Epoxy Specimen with 0.64 cm (0.25 in.) Diameter Hole Under Equal Biaxial Loading (Spec. No. 6-15).

147

Far-field strains are linear up to an applied stress of at least 145 MPa (21 ksi). Isochromatic fringe patterns in the photo-elastic coating around the hole were analyzed as before. The variation of fringe order and circumferential strain with effective stress at the two characteristic locations is shown in Figure 108. At the 0-degree location the fringe order varies linearly up to a stress of 269 MPa (39 ksi). At the 22.5-deg. location the fringe variation becomes nonlinear at an applied stress of approximately 200 MPa (29 ksi). The specimen failed at an applied biaxial stress of 383 MPa (55.5 ksi). Failure initiated at four points on the hole boundary at locations approximately 22.5-deg. off the vertical axis (Figure 109).

Specimen No. 6-22 had a 0.64 cm (0.25 in.) diameter hole and was instrumented with strain gages and a 0.51 mm (0.020 in.) thick photoelastic coating. The variation of strains with effective far-field biaxial stress is shown in Figures 110 and 111. Strains on the boundary of the hole are linear up to an applied stress of approximately 97 MPa (14 ksi). Far-field strains are linear up to an applied stress of approximately 207 MPa (30 ksi). Isochromatic fringe patterns in the photoelastic coating around the hole were similar to those observed previously. The variation of fringe order and circumferential strain with effective stress at the 0-deg. and 22.5-deg. locations is shown in Figure 112. At the 0-deg. location the fringe order varies linearly up to an applied stress of approximately 276 MPa (40 ksi). At the 22.5-deg. location the fringe variation becomes nonlinear at a stress of approximately 214 MPa (31 ksi). The specimen failed at an applied biaxial stress of 349 MPa (50.6 ksi). Failure initiated at two points on the hole boundary at locations approximately 22.5-deg. off the horizontal axis (Figure 113).

148
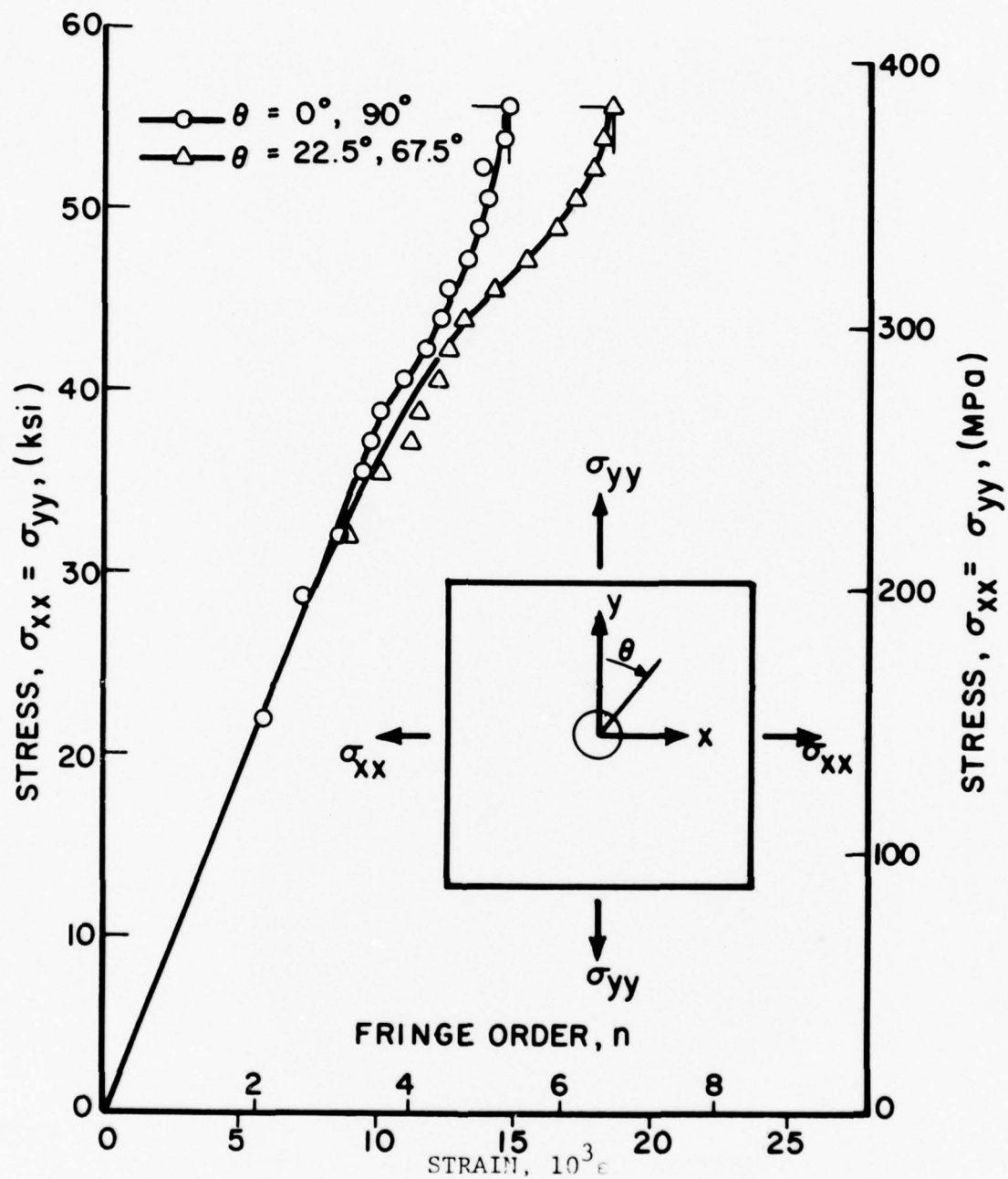
Figure 108. Fringe Order and Circumferential Strain at Two Locations on the Hole Boundary for $[0/\pm45/90]_s$ Graphite/Epoxy Specimen with 0.64 cm (0.25 in.) Diameter Hole Under Equal Biaxial Loading (Spec. No. 6-15).

149
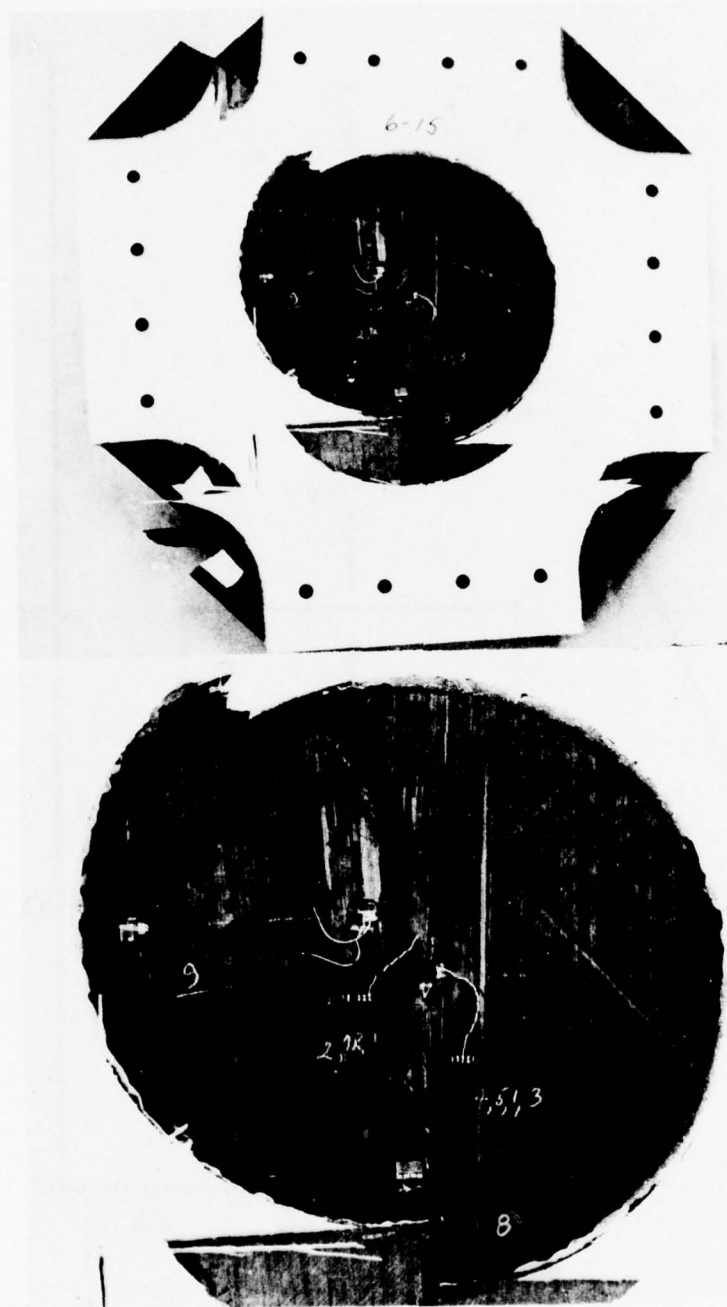
Figure 109.   Failure Pattern in $[0/\pm45/90]_s$ Graphite/Epoxy Specimen
with 0.64 cm (0.25 in.) Diameter Hole Under Equal
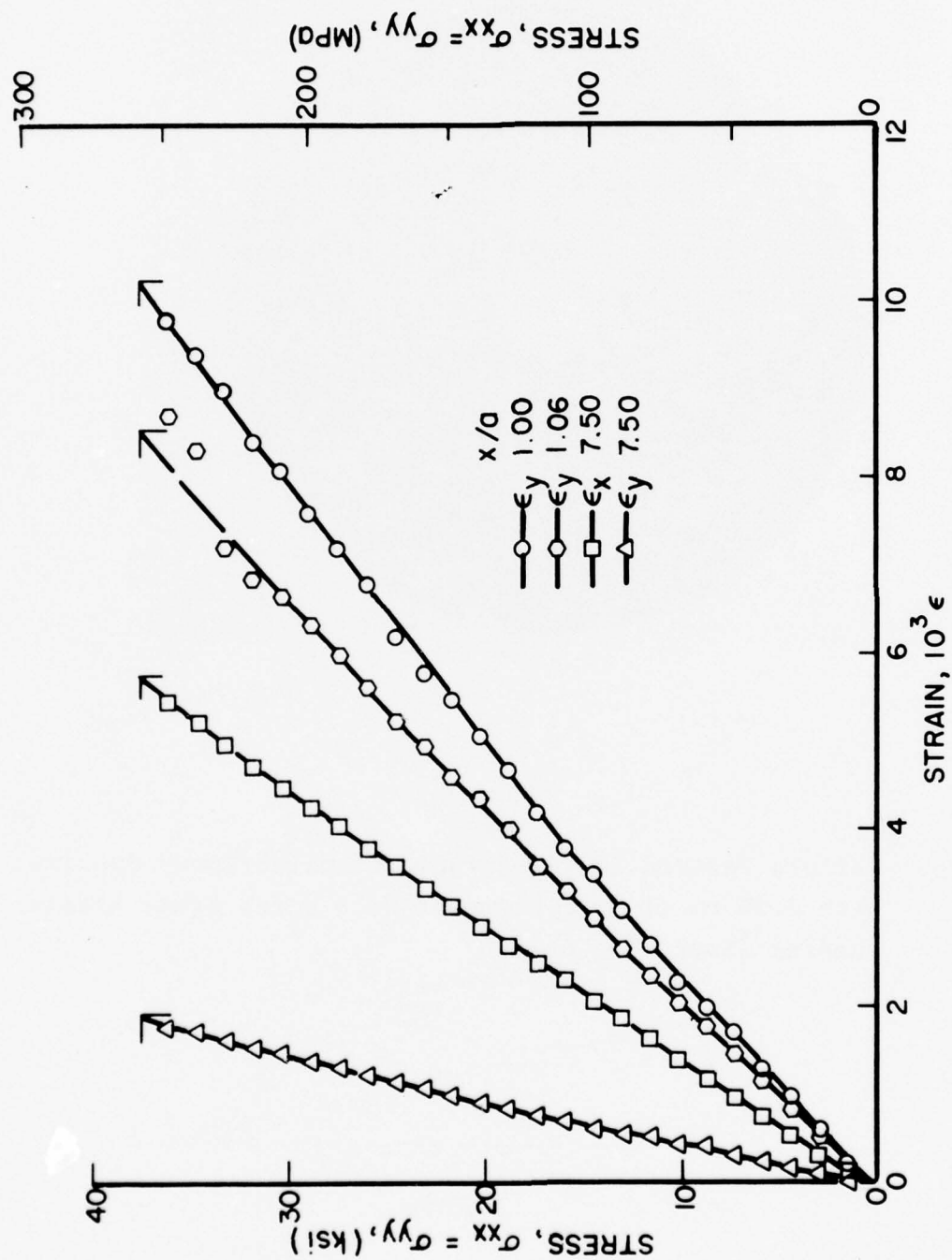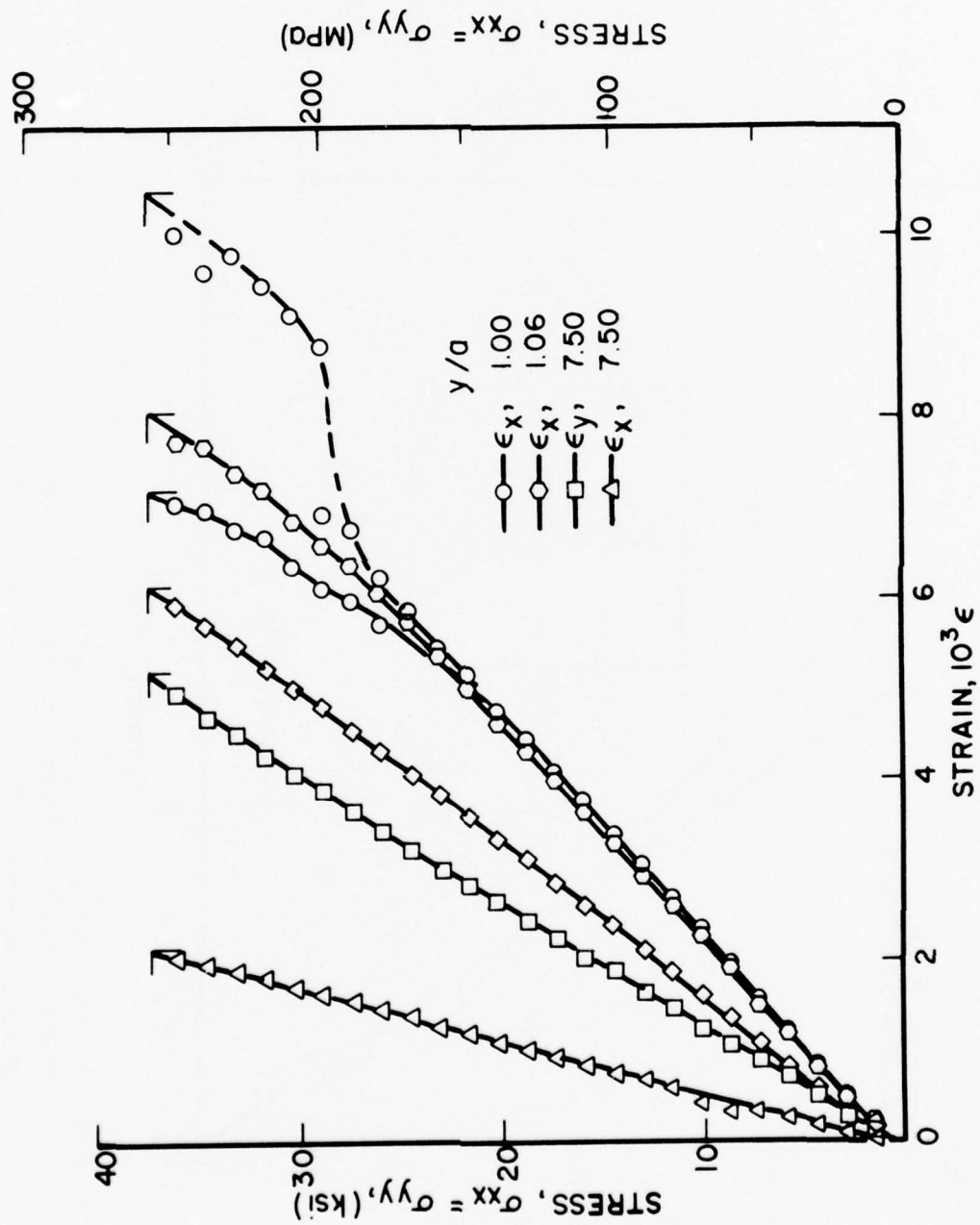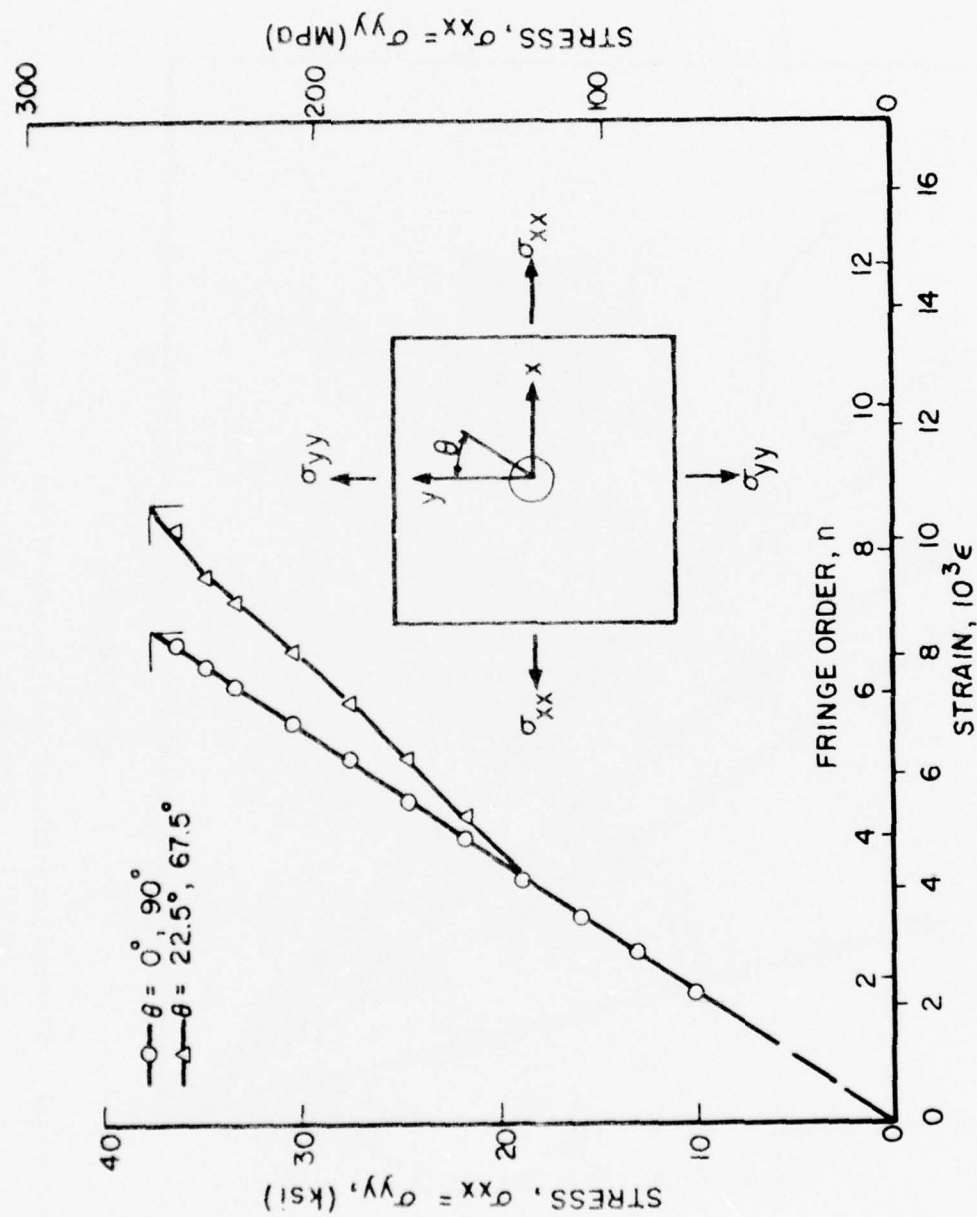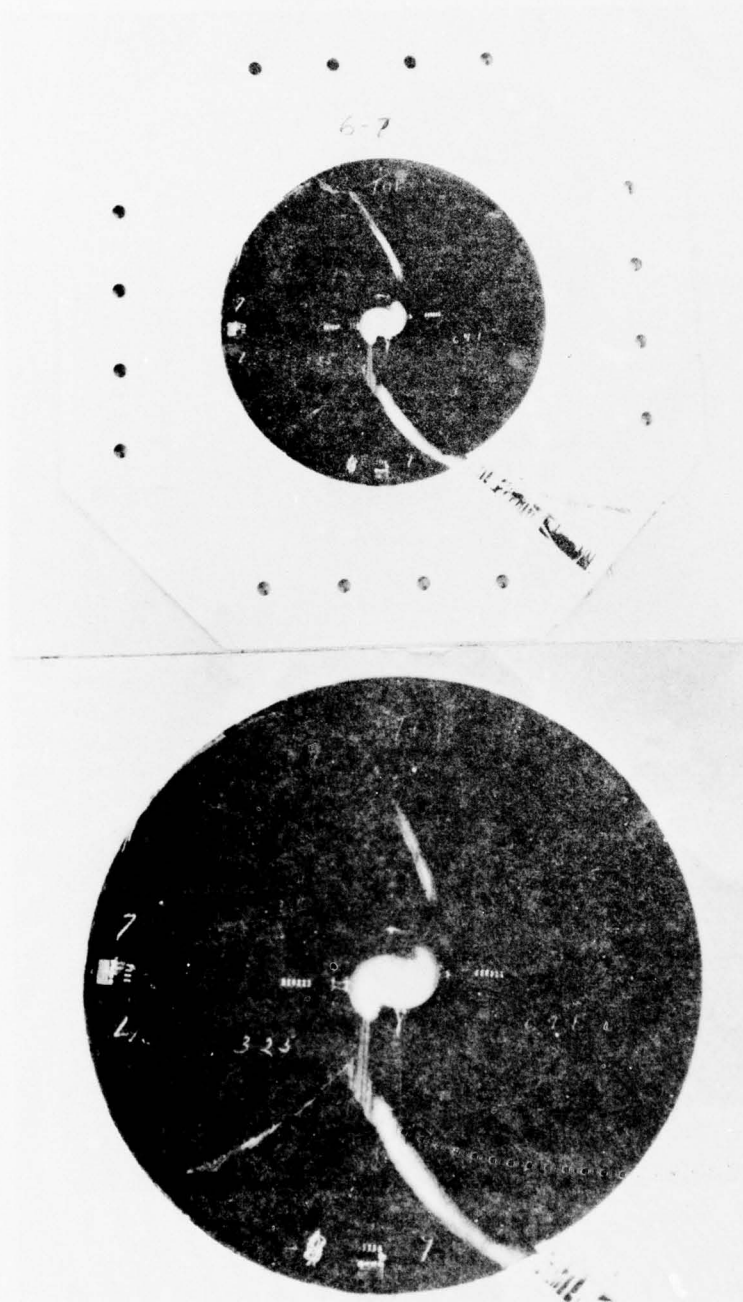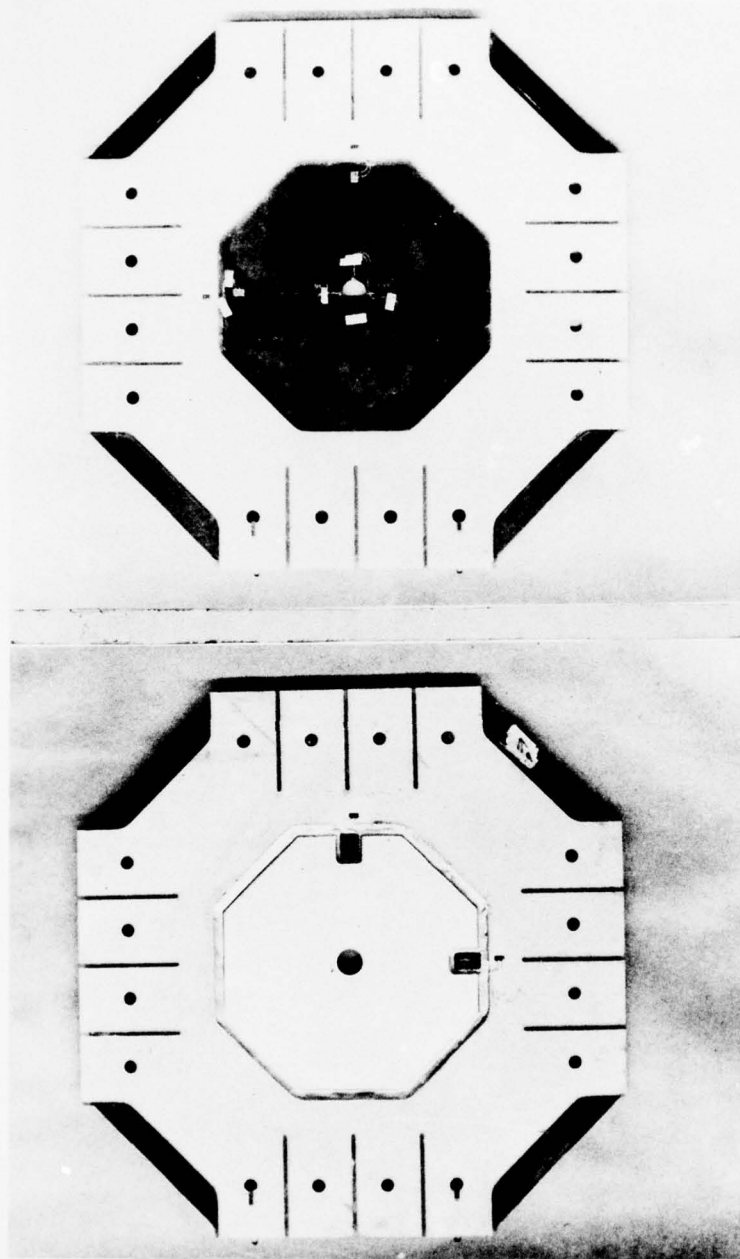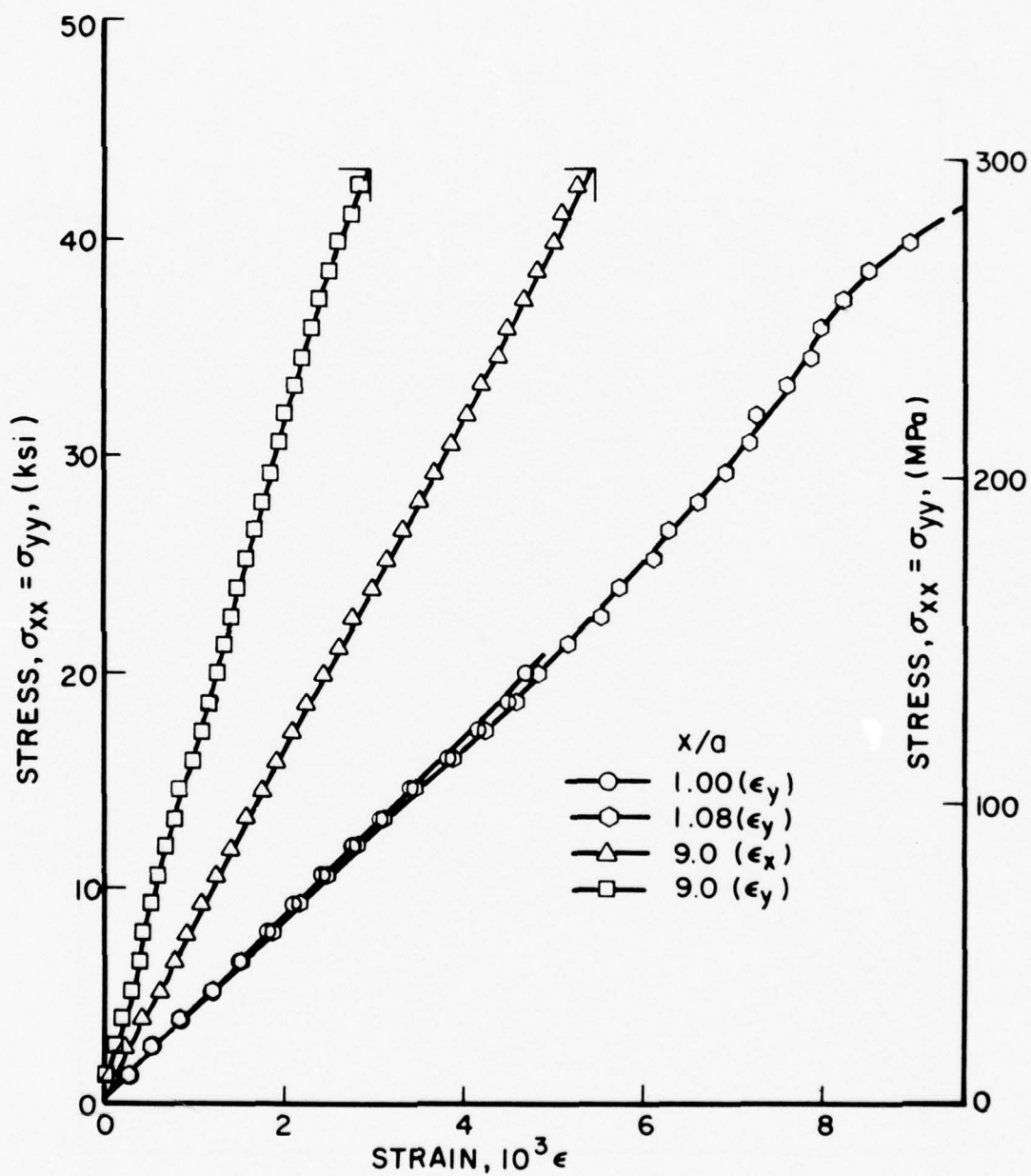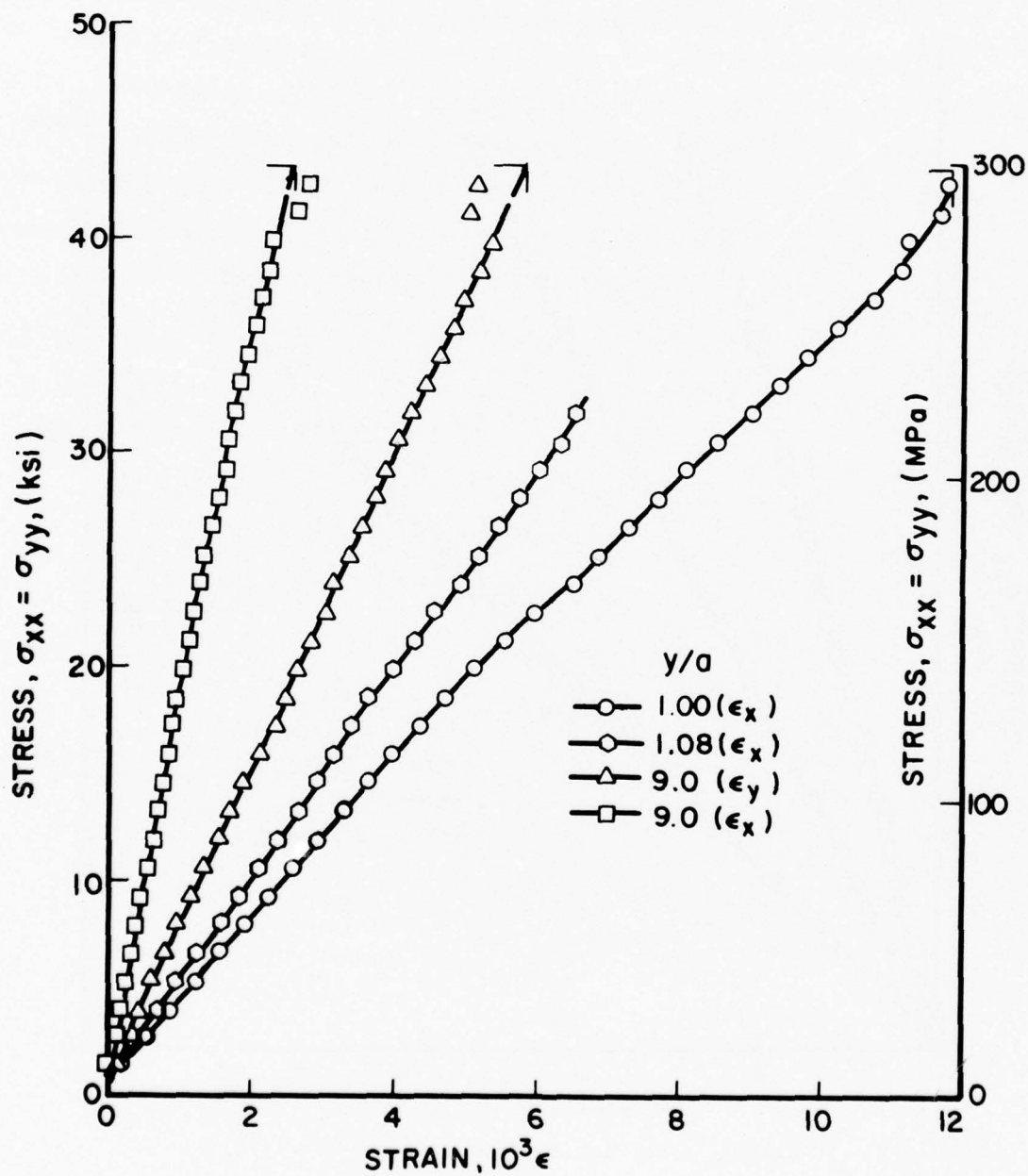Biaxial Loading (Spec. No. 6-15).
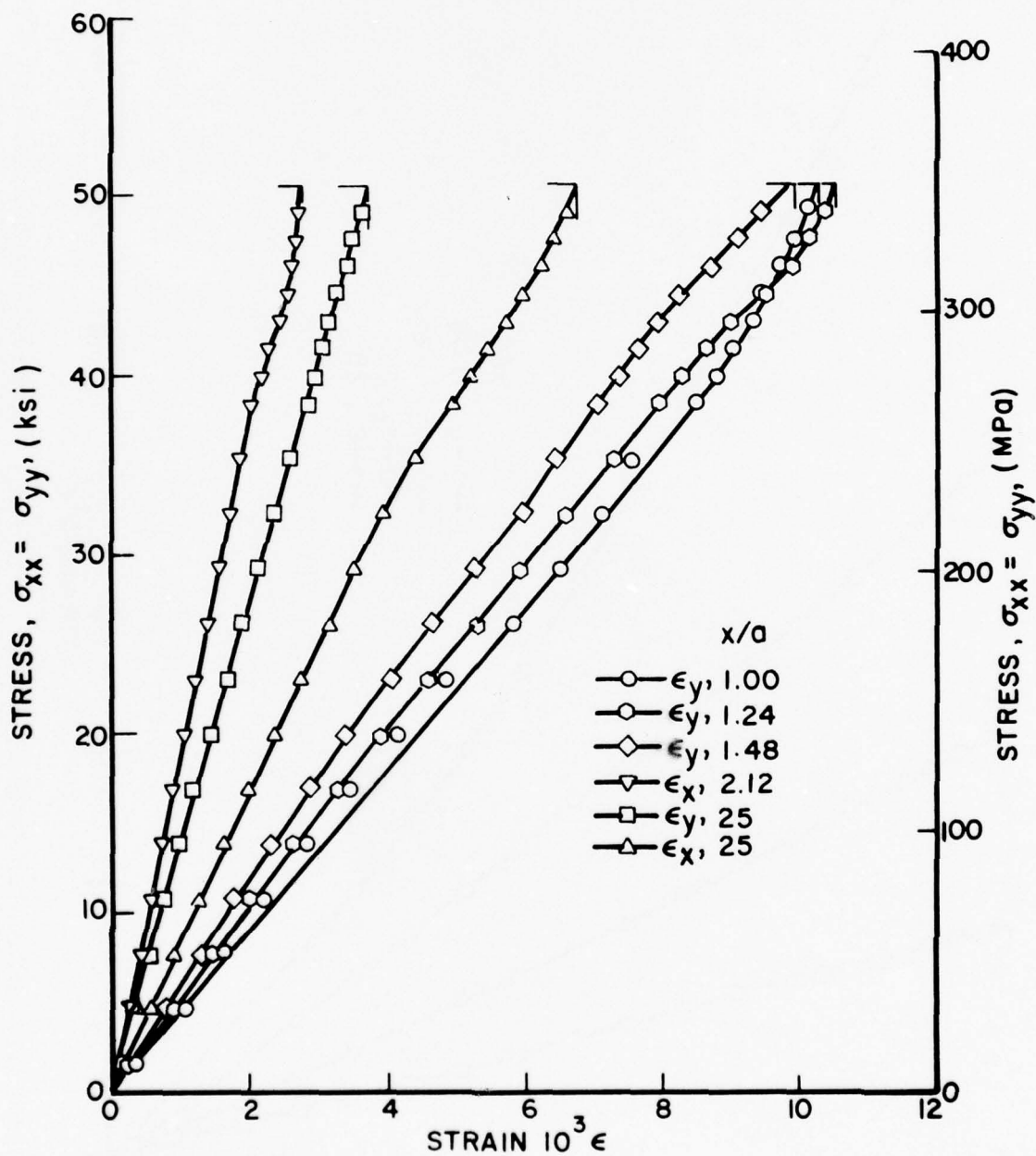
Figure 110. Strains on Horizontal Axis of [0/±45/90]$_s$ Graphite/
Epoxy Specimen with 0.64 cm (0.25 in.) Diameter Hole
Under Equal Biaxial Loading (Spec. No. 6-22).

151
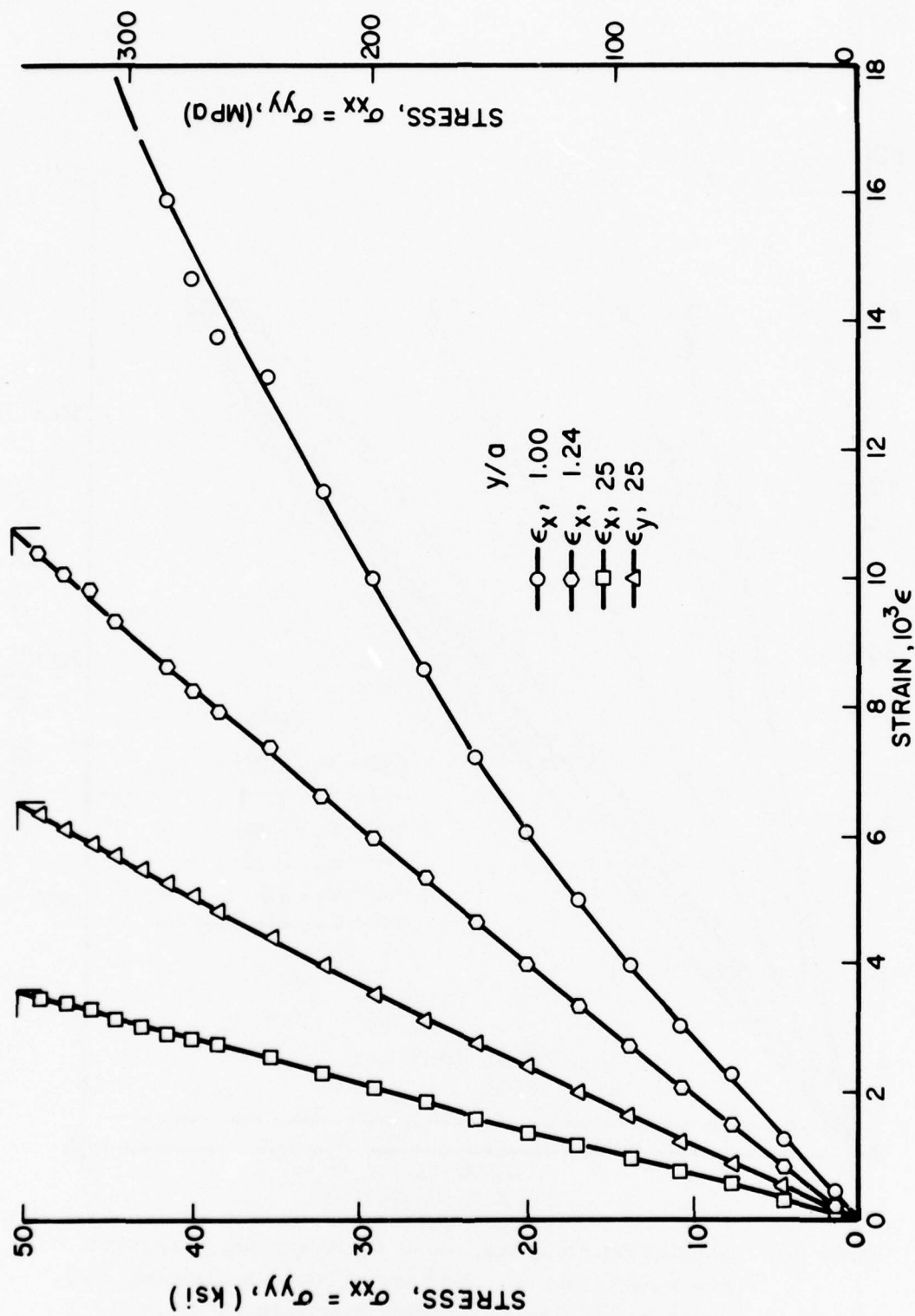
Figure 111. Strains on Vertical Axis of [0/+45/90]s Graphite/Epoxy Specimen with 0.64 mm (0.25 in.) Diameter Hole Under Equal Biaxial Loading (Spec. No. 6-22).

152
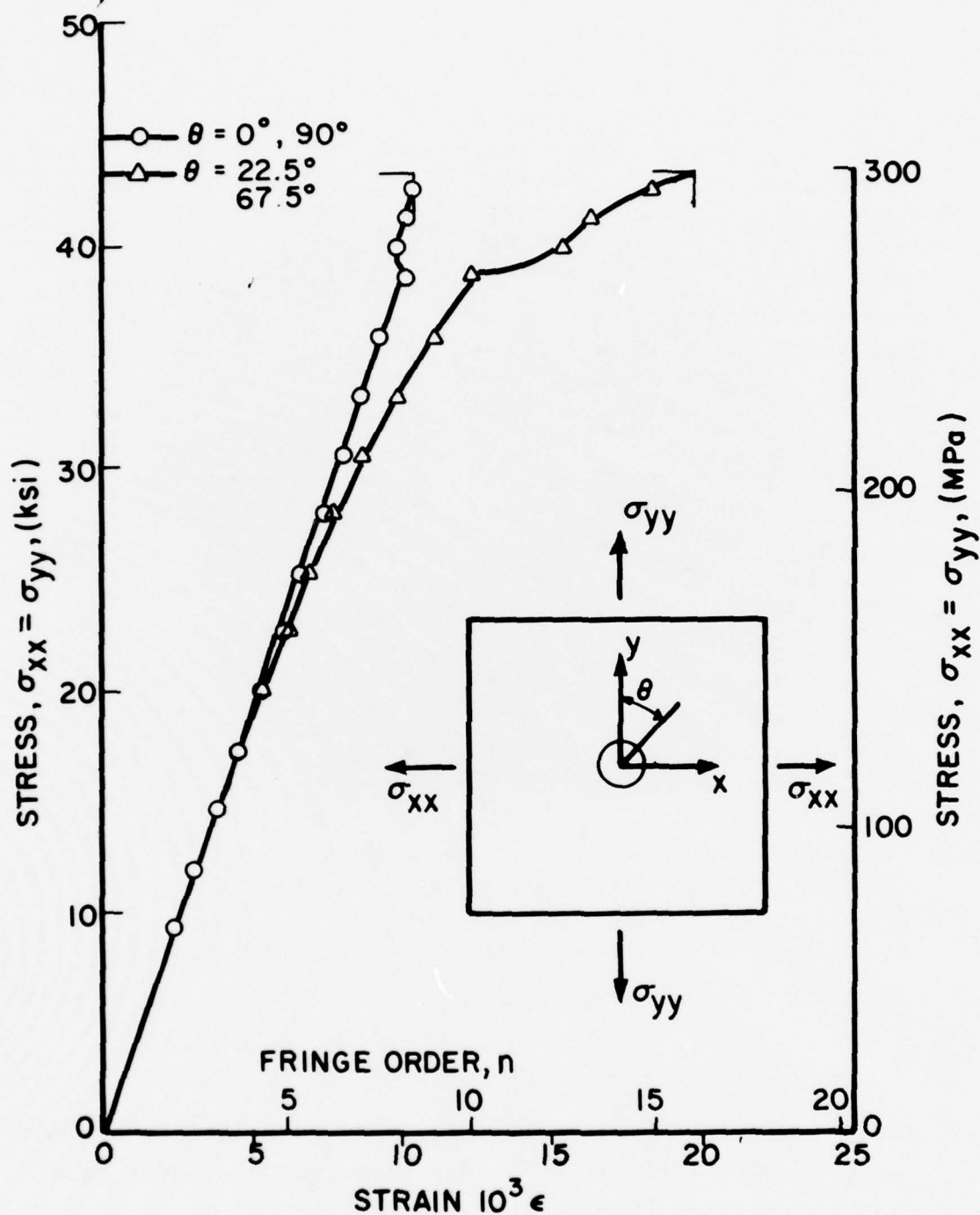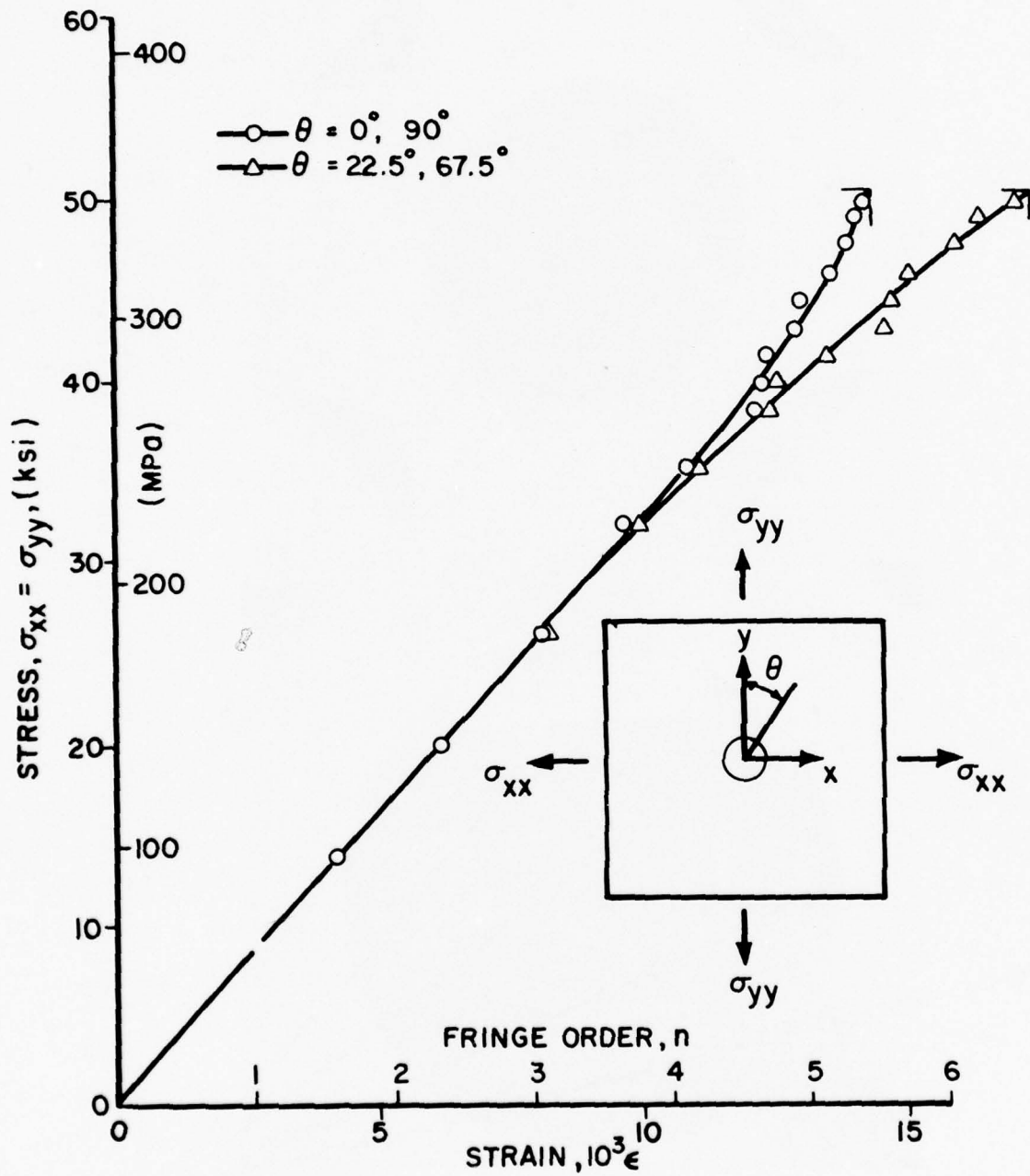
Figure 112. Fringe Order and Circumferential Strain at Two Locations on the Hole Boundary for [0/±45/90]$_s$ Graphite/Epoxy Specimen with 0.64 cm (0.25 in.) Diameter Hole Under Equal Biaxial Loading (Spec. No. 6-22).
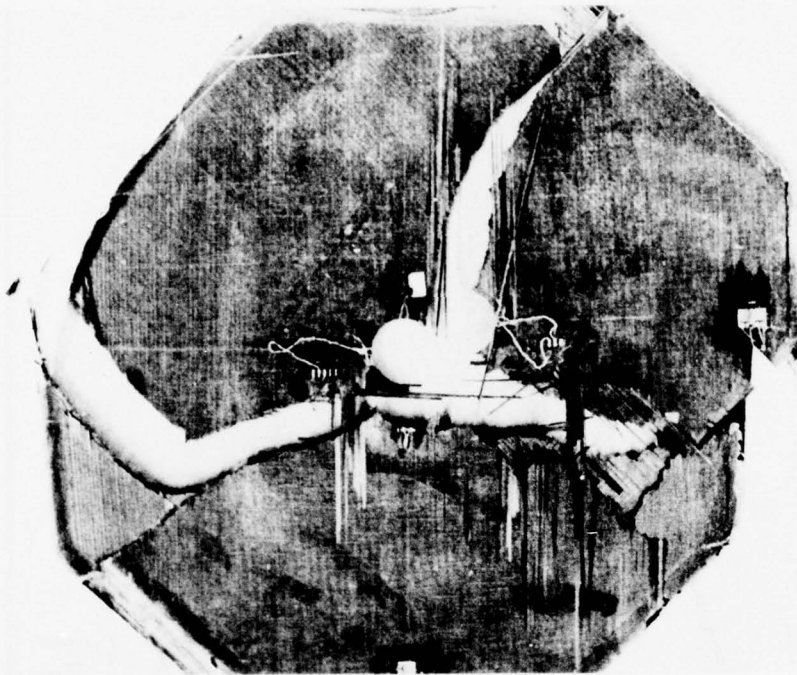
153

Figure 113.   Failure Pattern in $[0/\pm45/90]_s$ Graphite/Epoxy Specimen
with 0.64 cm (0.25 in.) Diameter Hole Under Equal Biaxial
Loading (Spec. No. 6-22).

154

5. EFFECT OF HOLE DIAMETER

Results for all specimens with holes loaded under equal biaxial tension are summarized in Table VII. The last column in this table shows the strength reduction ratio, i.e., the ratio of the stress at failure of the biaxial specimen to that of the unnotched uniaxial specimen. Additional testing of uniaxial unnotched specimens from the same batch of material used for the biaxial specimens gave an unnotched uniaxial strength of S_o = 483 MPa (70 ksi). Measured peak strains at failure reach values up to twice the uniaxial ultimate strain of the unnotched laminate.

The strength reduction ratio is plotted versus hole radius in Figure 114 where it is compared with the same ratio for uniaxially loaded plates with holes. The strength reduction ratio for biaxial loading exceeds that for uniaxial loading by approximately 30 percent. The average stress criterion, extended to a biaxial state of stress, was used to explain and predict the effect of hole diameter on the strength reduction ratio. The state of stress around the hole in an isotropic plate under equal biaxial loading σ_o is given by

$$\sigma_{rr} = \sigma_o \left[1 - \left(\frac{a}{r}\right)^2 \right]$$

$$\sigma_{\theta\theta} = \sigma_o \left[1 + \left(\frac{a}{r}\right)^2 \right]$$

where

$\sigma_{rr}, \sigma_{\theta\theta}$ = radial and circumferential stresses

a = hole radius

r = radial distance to point

These stresses averaged over an annulus between r = a and $r = a + a_o$ are

155

TABLE VII

BIAXIAL $[0/\pm45/90]_s$ LAMINATES WITH CIRCULAR HOLES

Spec. No.	Hole Diam. 2a cm (in.)	Failure Stress $S_{xxT} = S_{yyT}$ MPa (ksi)	Maximum Strain at Failure $(10^{-3}\varepsilon)$		Strength Reduction Ratio S_{xx}/S_o
			$\theta = 0°$	$\theta = 22.5°$	
6-7	2.54 (1.00)	293 (42)	10.0	17.5	0.600
6-8	2.54 (1.00)	258 (37)	10.2	10.7	0.529
6-6	1.91 (0.75)	299 (43)	10.0	19.5	0.614
6-9	1.91 (0.75)	261 (38)	10.3	11.8	0.543
6-10	1.27 (0.50)	312 (45)	12.2	-	0.643
6-11	1.27 (0.50)	328 (48)	12.0	14.9	0.686
6-15	0.64 (0.25)	383 (56)	15.0	18.5	0.800
6-22	0.64 (0.25)	349 (51)	14.3	17.3	0.729
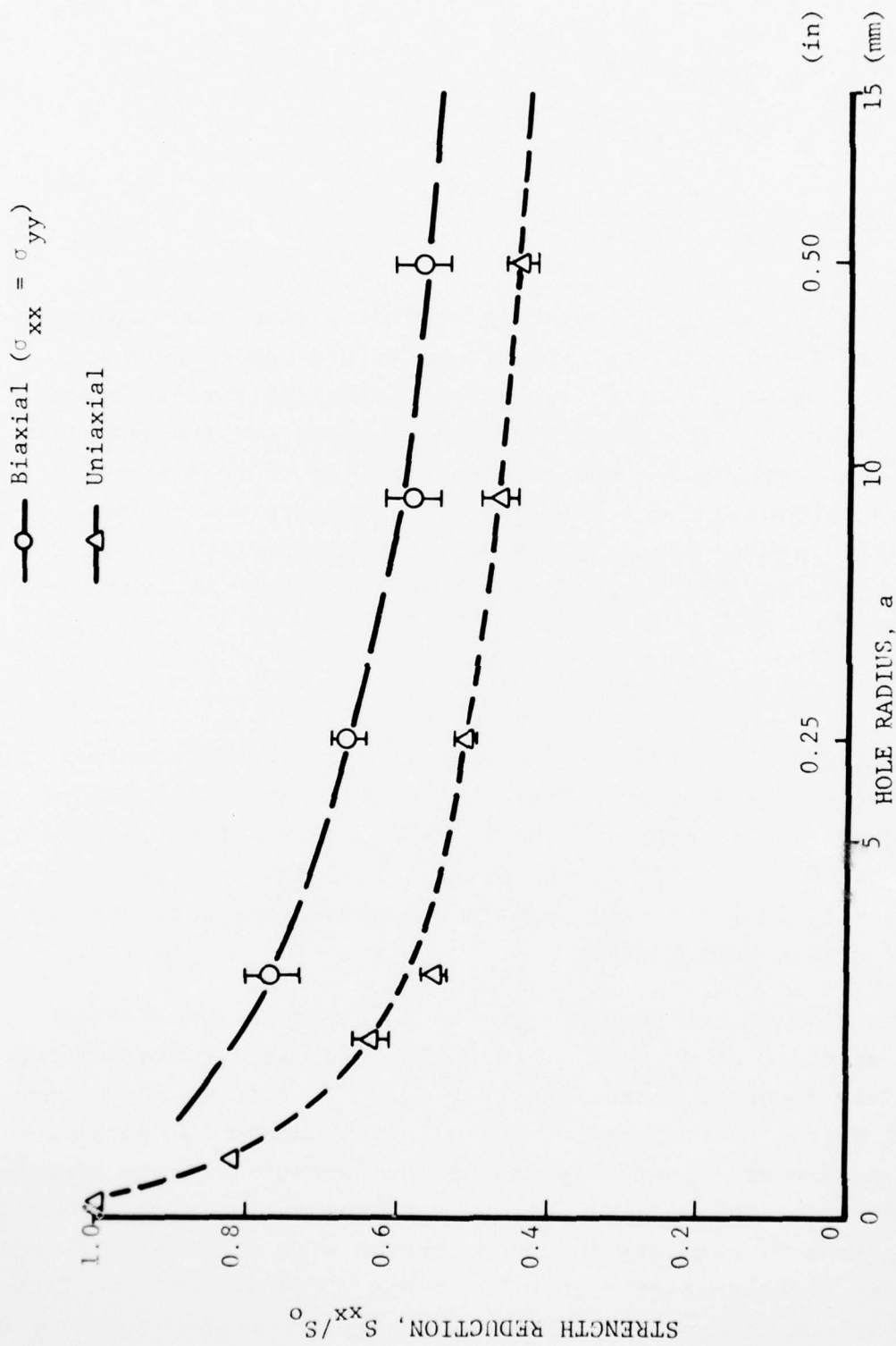
Figure 114. Strength Reduction as a Function of Hole Radius for $[0/\pm45/90]_s$ Graphite/Epoxy Plates With Circular Holes Under Uniaxial and 1:1 Biaxial Loading

157

$$\bar{\sigma}_{rr} = \sigma_o \left[1 - \frac{2}{\rho_1^2 - 1} \log \rho_1 \right]$$

$$\bar{\sigma}_{\theta\theta} = \sigma_o \left[1 + \frac{2}{\rho_1^2 - 1} \log \rho_1 \right]$$

where $\rho_1 = \dfrac{a+a_o}{a}$ and a_o = characteristic dimension. According to the biaxial stress failure criterion, failure occurs when the state of stress $\bar{\sigma}_{rr}$, $\bar{\sigma}_{\theta\theta}$ falls on the biaxial failure envelope for the laminate. The exact strength envelope for the laminate tested is not available. An envelope similar to that given by Sandhu (Reference 23) for a $[0/\pm45/90]_s$ laminate was assumed. Theoretical results thus obtained for a characteristic dimension a_o = 3 mm are in good agreement with experimental results (Figure 115).

6. SUMMARY AND CONCLUSIONS

An experimental study was conducted of the deformation and failure of $[0/\pm45/90]_s$ graphite/epoxy plates with holes loaded under equal biaxial tension. Hole diameters investigated were 2.54 cm (1.00 in.), 1.91 cm (0.75 in.), 1.27 cm (0.50 in.) and 0.64 cm (0.25 in.). Strain gages and birefringent coatings were used for strain measurement.

Strains on the boundary of the hole become nonlinear at applied stresses of $\sigma_{xx} = \sigma_{yy} \approx$ 120 MPa (17.5 ksi) corresponding to a strain level of approximately 4×10^{-3}. This is the strain level at which the response of the uniaxial unnotched specimens becomes nonlinear. Initially, the circumferential strain around the boundary of the hole is uniform. Subsequently, with increasing load, regions of high strain concentration with nonlinear response develop at eight characteristic locations 22.5-deg. off the fiber axes. Maximum strains at failure on the hole boundary reach values

158
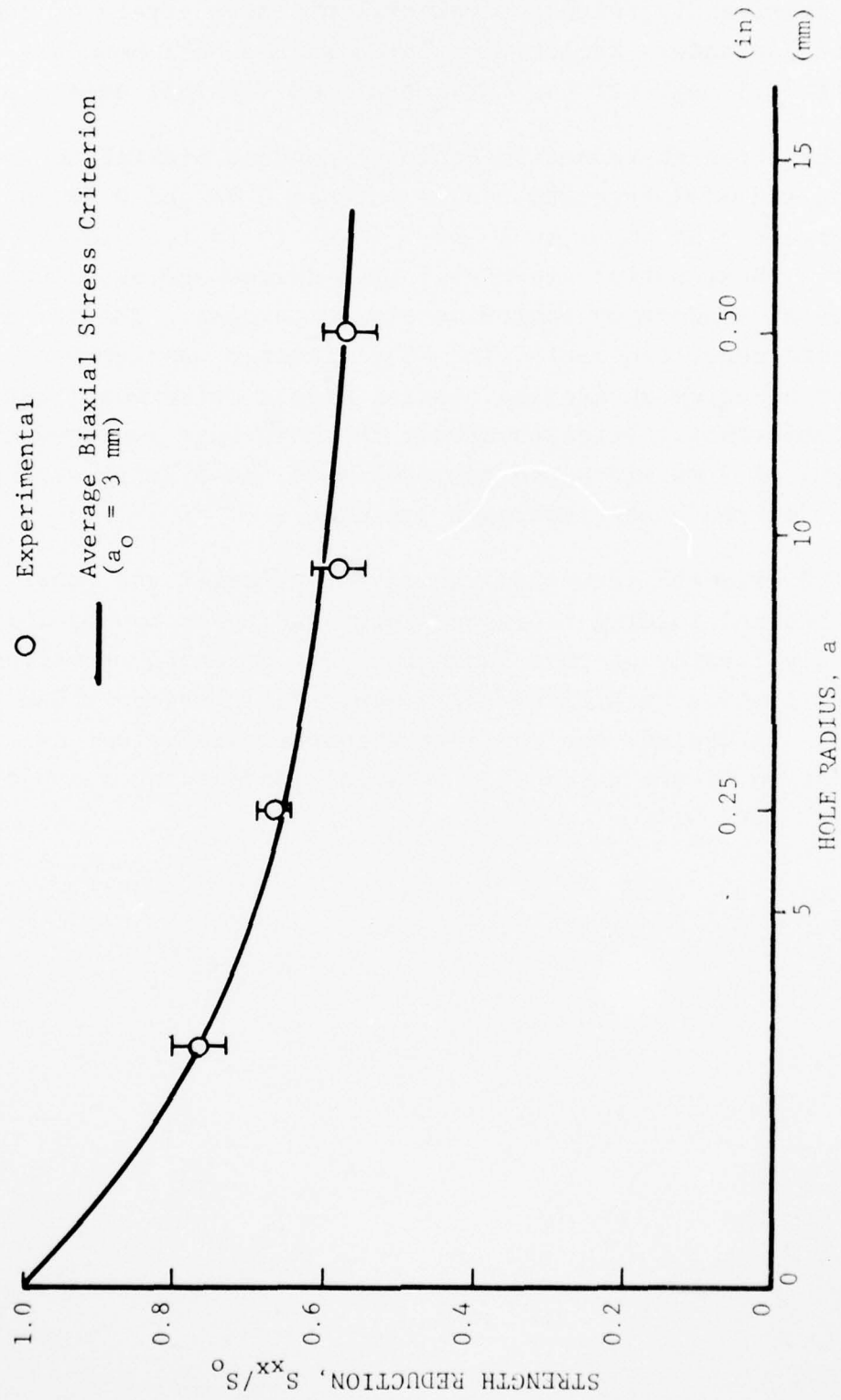
Figure 115. Strength Reduction as a Function of Hole Radius for [0/±45/90]$_s$ Graphite/Epoxy Plates With Circular Holes Under 1:1 Biaxial Tensile Loading

159

up to approximately twice the uniaxial ultimate strain of the
unnotched laminate. Failure initiates on the hole boundary
at points 22.5-deg. off the horizontal and vertical axes.

The strength reduction ratio of notched biaxial to
unnotched uniaxial strength ranges between 0.56 and 0.76 for
holes between 2.54 cm (1 in.) and 0.64 cm (0.25 in.) in
diameter. These ratios are higher than corresponding values
for uniaxial loading by approximately 30 percent. The variation
of strength reduction ratio with hole diameter was satisfactorily
described by using an average biaxial stress criterion. Radial
and circumferential stresses around the hole were averaged over
an annulus of 3 mm width and compared with the biaxial strength
envelope for the quasi-isotropic laminate.

The strength reduction ratios for uniaxial and equal
tensile biaxial loading represent lower and upper bounds for
any tensile loading of this laminate. The strength reduction for
any other tensile biaxiality ratio would fall between these two
extremes. In design, one can obtain approximate values by
interpolation or use values for uniaxial loading for a conservative
design.

SECTION VI

BIAXIAL TESTS OF PLATES WITH CRACKS

1. SPECIMENS

The specimens were 8-ply $[0/\pm45/90]_s$ plates 40 cm x 40 cm
(16 in. x 16 in.) with the 0-deg. fibers at 30-deg. with the
sides of the plate. They were tabbed with 5-ply crossply glass/
epoxy tabs with the outer fibers parallel to one side of the
plate, or at 30-deg. with the outer graphite plies. These tabs
had a circular cutout at the center of 20.3 cm (8 in.) diameter.
Cracks were machined ultrasonically in the center of these
specimens. The crack geometry was the same as in the uniaxial
specimens (Figure 20). The crack was oriented normally to the
outer fibers of the laminate, i.e., it was inclined at 30-deg. and
60-deg. with the sides of the specimen (Figure 116). Four crack
lengths were investigated, 2.54 cm (1.00 in.), 1.91 cm (0.75 in.),
1.27 cm (0.50 in.) and 0.64 cm (0.25 in.). Two specimens were
tested for each crack length.

2. STRAIN MEASUREMENT

Deformations and strains were measured using strain gages,
birefringent coatings and moiré grids. Miniature single gages
and rosettes were mounted near the crack tips along lines
perpendicular to the crack axis. Additional two- and three-gage
rosettes were mounted along the horizontal (x-) and vertical (y-)
axes of loading away from the crack. A typical gage layout is
shown in Figure 117. In most cases a birefringent coating 0.25 mm
(0.01 in.) thick was used around the crack. In some cases moiré
grids consisting of arrays of 400 lines per cm (1000 lines per
inch) parallel and normal to the crack were applied to the specimen

161
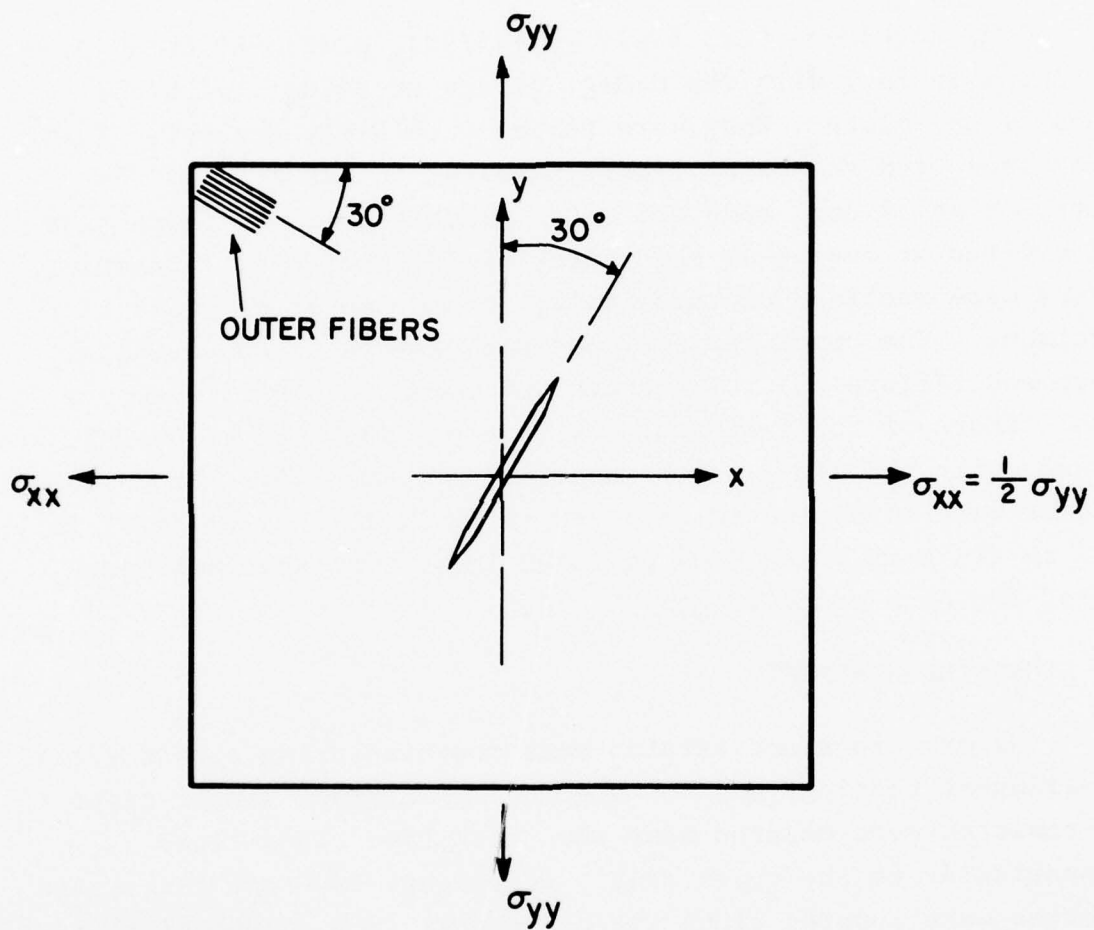
Figure 116. Biaxial Loading of $[0/\pm45/90]_s$ Graphite/ Epoxy Specimens with Cracks.
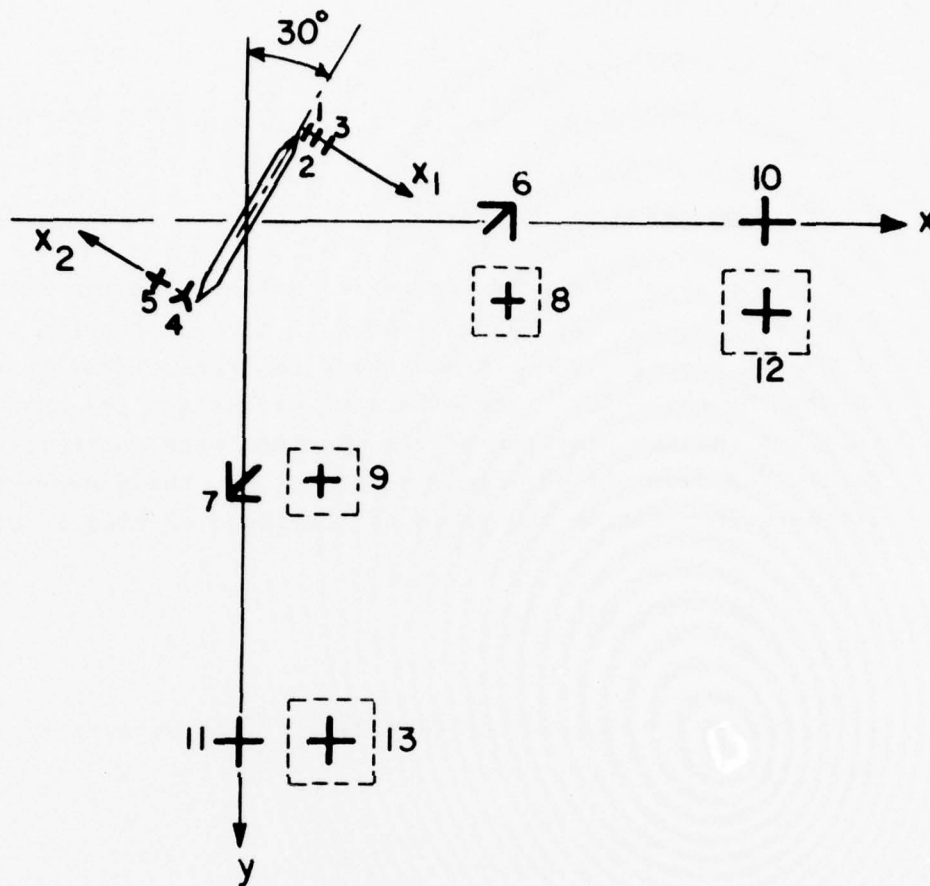
Gage No.	Location mm (in)		Type
1	x_1	= 0.76 (0.03)	EA-06-015DJ-120
2	x_1	= 2.54 (0.10)	EA-06-031DE-120
3	x_1	= 5.08 (0.20)	EA-06-031DE-120
4	x_2	= 1.78 (0.07)	WA-06-030WR-120
5	x_2	= 7.11 (0.28)	WA-06-030WT-120
6	x	= 38.1 (1.50)	EA-06-062RB-120
7	y	= 38.1 (1.50)	EA-06-062RB-120
8*	x	= 38.1 (1.50)	EA-06-062TT-120
9*	y	= 38.1 (1.50)	EA-06-062TT-120
10,12*	x	= 76.2 (3.00)	EA-06-125TM-120
11,13*	y	= 76.2 (3.00)	EA-06-125TM-120

*On opposite side of plate

Figure 117. Typical Gage Layout for Biaxially Loaded Specimens
with Cracks.

163

3. LOADING AND DATA RECORDING

The specimens were loaded in the same loading frame as those with holes. They were loaded in biaxial tension with the stress at 30-deg. to the crack twice as large as the stress at 60-deg. to the crack. The effective stress and the exact biaxiality ratio in the test section of the specimen were controlled and determined from the far-field strains. For the quasi-isotropic laminate in question the ratio of far-field strains is equal to

$$\frac{\varepsilon_{yy}}{\varepsilon_{xx}} = \frac{1 - k\nu}{k - \nu}$$

where $k = \frac{\sigma_{xx}}{\sigma_{yy}}$. The effective stress σ_{yy} is determined from the expression

$$\sigma_{yy} = \frac{E\varepsilon_{yy}}{1 - k\nu}$$

Values of the modulus and Poisson's ratio of the laminate in the direction of the applied loads were determined experimentally.

For the desired biaxiality $k = 0.5$ the required strain ratio is

$$\frac{\varepsilon_{yy}}{\varepsilon_{xx}} = 3.91$$

The ratio of applied loads was adjusted until the desired strain ratio was obtained. Thereafter, the load ratio was kept constant for the rest of the test.

The loads were applied in increments, the strain gages were recorded at every increment with the digital data acquisition system and photoelastic and moiré fringes were photographed.

164

4. RESULTS

Specimen No. 6-12 had a 2.54 cm (1.00 in.) long crack and was instrumented with strain gages and 400 lines/cm (1000 lines/in.) moire grids near the crack. A closeup of the gage layout around the crack is shown in Figure 118. The tabbed and instrumented specimen is shown in Figure 119. Strains in the vicinity of the crack tip and along the horizontal and vertical axes of the specimen are plotted as a function of effective vertical stress in Figures 120 and 121. In Figure 120 the gages nearest the crack tip do not read the highest strain initially because of their orientation. However, as the load is increased the damage (or crack) grows in the direction normal to the crack and these strains increase at a rapid rate and overtake the strains farther from the crack. The strain near the crack tip (gage 1 in Figure 120) at a distance of 0.76 mm (0.03 in.) from the tip is linear up to an applied vertical stress of approximately 76 MPa (11 ksi). The three gages near the crack tip, gages 1, 2 and 3 in Figure 120 at distances 0.76 mm (0.03 in.), 2.54 mm (0.10 in.) and 5.10 mm (0.20 in.), failed when the crack propagated through them at stresses of approximately 173 MPa (25 ksi), 207 MPa (30 ksi) and 240 MPa (35 ksi), respectively. In Figure 121 the strain read by the gage located at a distance of 1.52 mm (0.06 in.) from the crack tip is linear up to a stress of 69 MPa (10 ksi), thereafter, it increases rapidly up to the point when the crack propagates through the gage at an approximate stress of 186 MPa (27 ksi). The crack reaches the location of gages 4 and 5 (Figure 121) at a distance of 5.10 mm (0.20 in.) at a stress of approximately 228 MPa (33 ksi).

Moire fringe patterns around the crack are shown in Figure 122 for three load levels. The upper part of the pattern corresponds to displacements normal to the crack direction, the lower part to displacements parallel to it. By differentiating

165

Figure 118. Closeup of Gage Layout Near 2.54 cm
(1.00 in.) Crack of Spec. No. 6-12
(Smallest Division Shown is 0.01 in.)

166
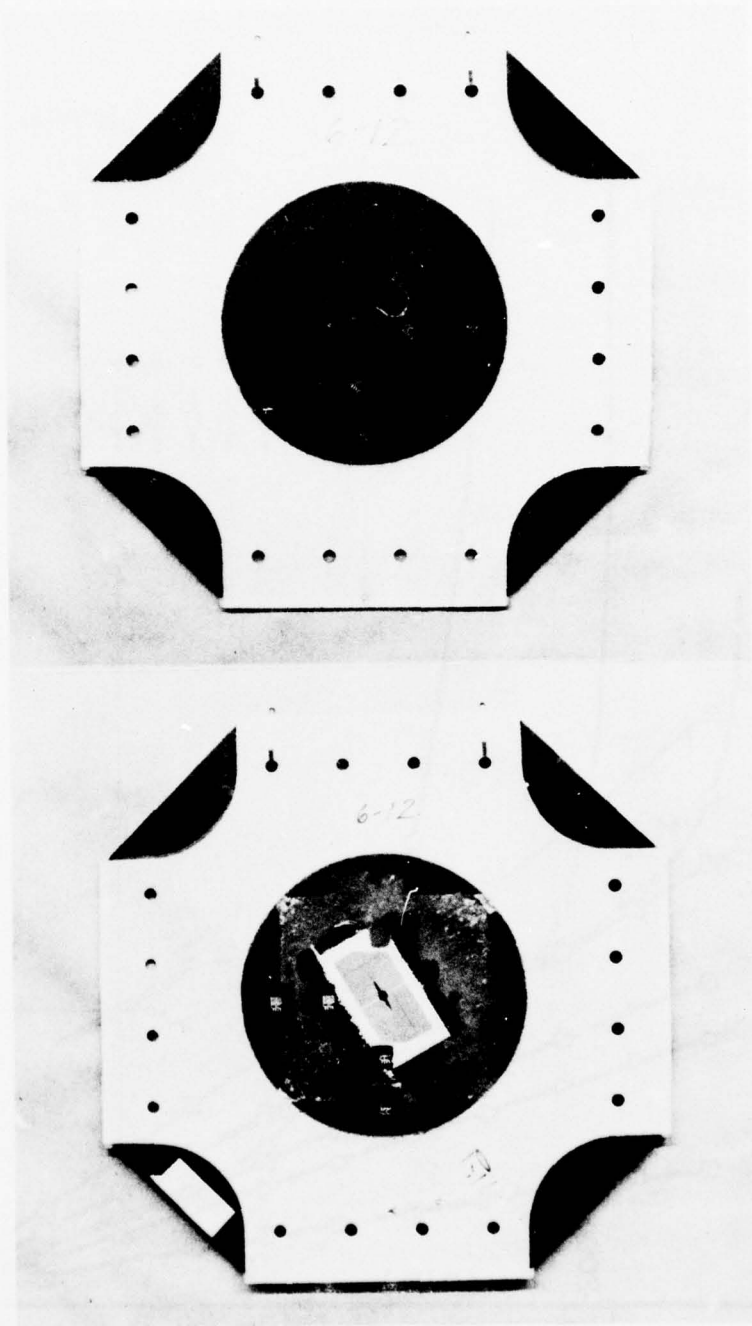
Figure 119.   Biaxial Specimen with 2.54 cm (1.00 in.)
Crack (Spec. No. 6-12)

167

Figure 120. Strains Near Crack Tip and Along Horizontal Axis of [0/±45/90]s Graphite/Epoxy Specimen with 2.54 cm (1 in.) Crack Under Biaxial Loading σ_{yy} = 1.98σ_{xx} at 30-Deg. with Crack Direction (Spec. No. 6-12)

Figure 121. Strains Near Crack Tip and Along Vertical Axis of [0/+45/90]s Graphite/Epoxy Specimen with 2.54 cm (1 in.) Crack Under Biaxial Loading $\sigma_{yy} = 1.98\sigma_{xx}$ at 30-Deg. With Crack Direction (Spec. No. 6-12)

END

DATE
FILMED
7-77

σ_{yy} = 214 MPa (31.0 ksi) σ_{yy} = 246 MPa (35.7) σ_{yy} = 257 MPa (37.2 ksi)
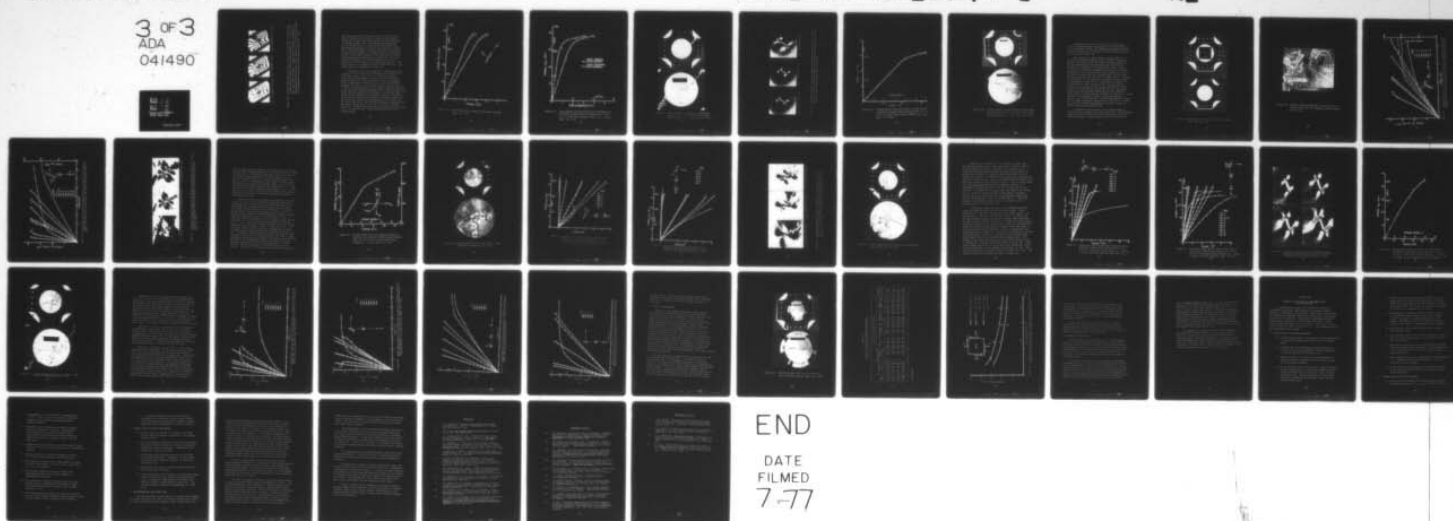
Figure 122.   Moiré Fringe Patterns Around 2.54 cm (1 in.) Crack in [0/±45/90]s Graphite/Epoxy Specimen Under Biaxial Loading σ_{yy} = 1.98σ_{xx} at 30-Deg. with Crack Direction.   (Upper part of pattern corresponds to displacements normal to the crack, lower part of pattern corresponds to displacements along the crack direction; Spec. No. 6-12).

170

the fringe patterns away from the crack the far-field strains
shown in Figure 123 were obtained. Relative displacements
between any two points can be obtained by the simple expedient
of counting fringes. Thus, the crack opening displacement
and the forward sliding or crack shearing displacement were
determined and plotted as a function of applied stress (Figure
124). These displacements are of the same order of magnitude
and they become nonlinear at an applied stress of approximately
172 MPa (25 ksi) which is close to the stress level of initial
crack propagation as detected by the strain gages. The crack
propagates normally to its initial direction or along the
outer fibers as illustrated by the moire fringe patterns. Total
failure occured at an applied stress of 264 MPa (38.3 ksi). The
failure pattern is illustrated in Figure 125.

Specimen No. 6-20A was a replicate of specimen 6-12 above.
It had a 2.54 cm (1.00 in.) long crack and was instrumented with
strain gages and a 0.25 mm (0.01 in.) photoelastic coating.
Isochromatic fringe patterns for three levels of loading are
shown in Figure 126. Failure starts at the tips at an applied
stress of approximately 167 MPa (24 ksi). The crack initially
propagates at 45-deg. to its original direction, then at one end
it turns to a direction normal to the original crack direction and
at the other end the damage propagates along a direction approximatel
25-deg. with the original crack direction, In the former case
damage consists primarily of subcracking parallel to the fibers of
the outer 0-deg. plies, in the latter case the damage seems to be
associated with subcracking and delamination of the interior 45-
deg. and 90-deg. plies. The variation of maximum birefringence and
approximate maximum strain at the tip of the crack is shown in
Figure 127. Ultimate failure occurred at an applied vertical stress
of σ_{yy} = 221 MPa (32 ksi). Figure 128 shows two views of the
failed specimen.

171
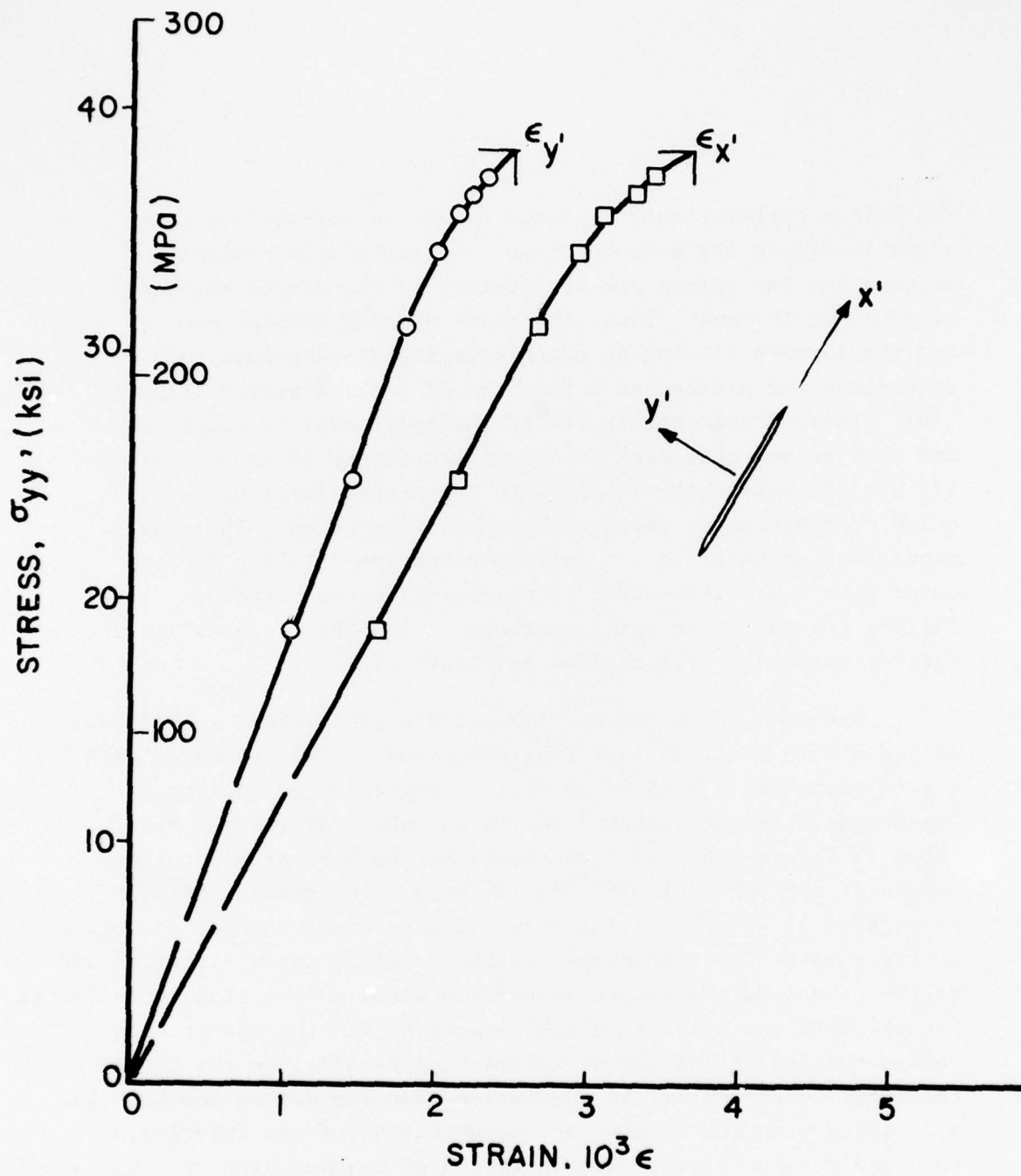
Figure 123. Far-Field Strains Obtained from Moiré Patterns
(Spec. No. 6-12)

172
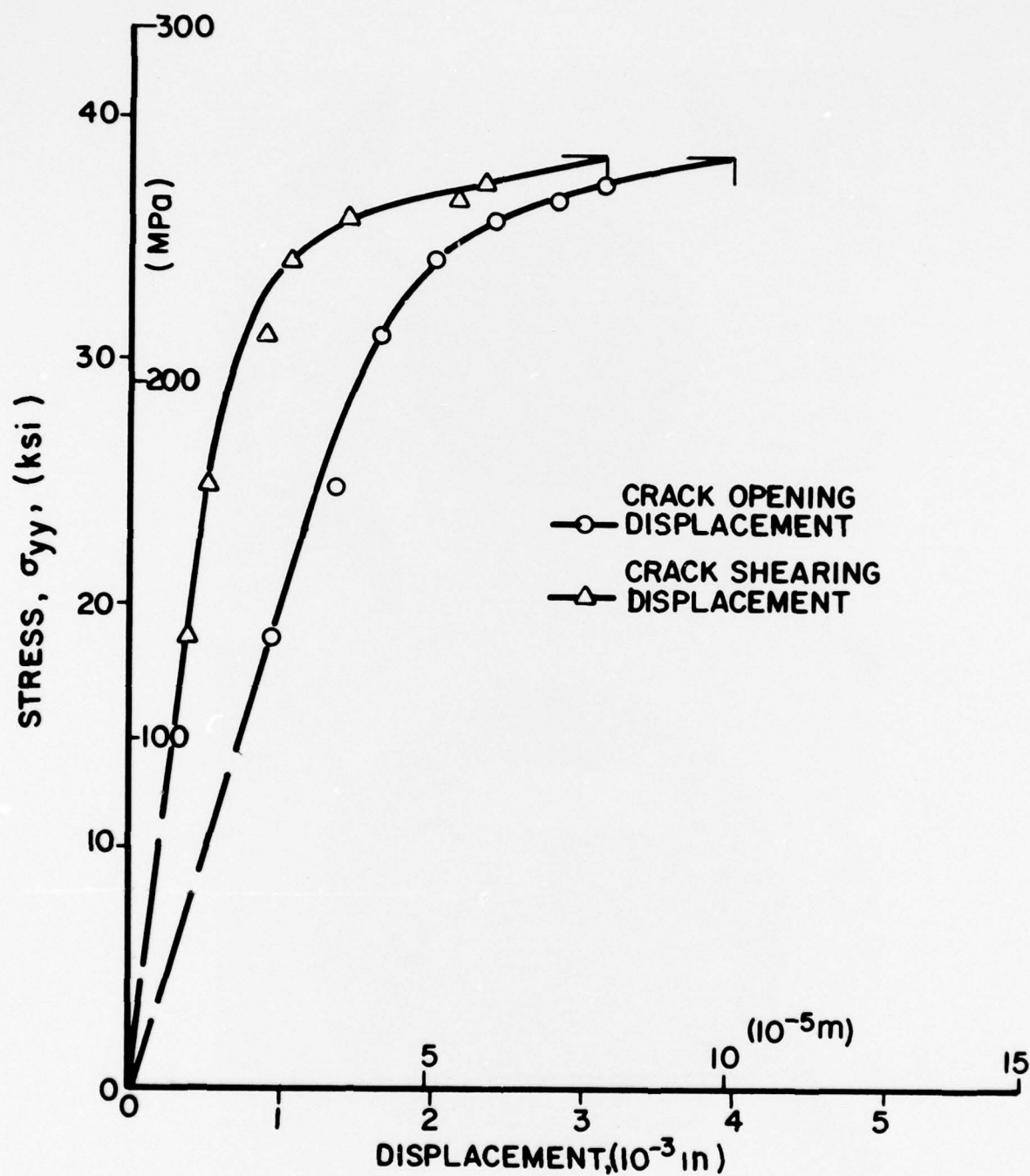
Figure 124. Crack Opening and Crack Shearing Displacements in
[0/±45/90]s Graphite/Epoxy Specimen with 2.54 cm
(1 in.) Crack Under Biaxial Loading $\sigma_{yy} = 1.98\sigma_{xx}$
(Spec. No. 6-12)

173

Figure 125.   Failure Pattern in $[0/\pm45/90]_s$ Graphite/Epoxy
Specimen with 2.54 cm (1.00 in.) Crack Under
Biaxial Loading $\sigma_{yy} = 1.98\sigma_{xx}$ (Spec. No. 6-12)

174

σ_{yy} = 167 MPa (24.2 ksi) σ_{yy} = 191 MPa (27.7 ksi) σ_{yy} = 215 MPa (31.1 ksi)
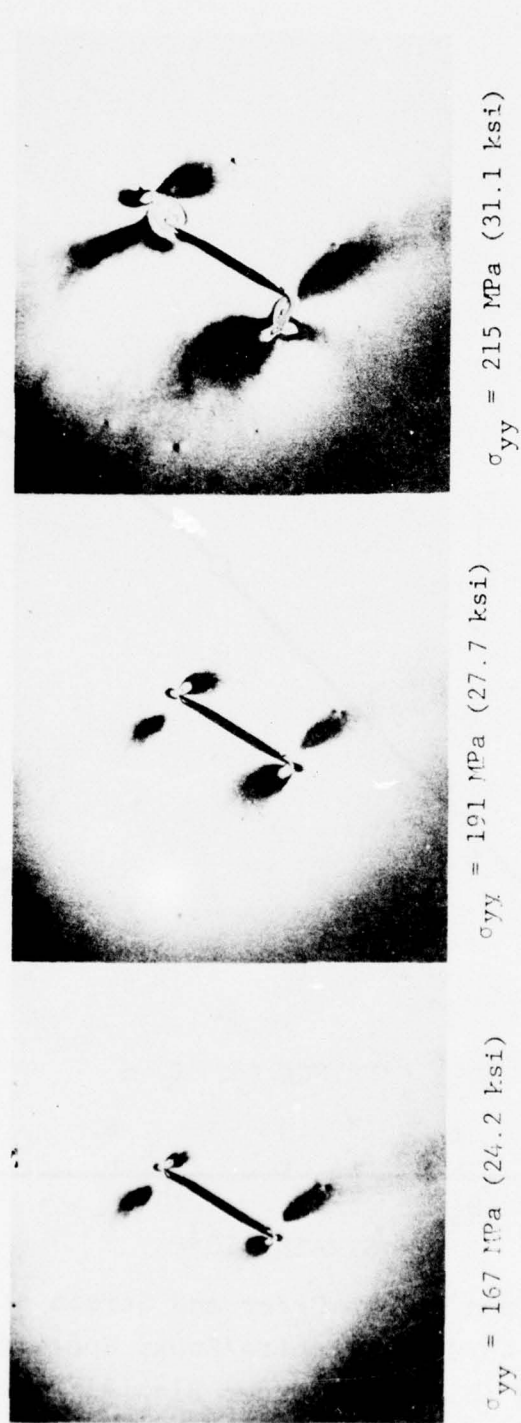
Figure 126. Isochromatic Fringe Patterns in Photoelastic Coating Around 2.54 cm (1.00 in.)
Crack In $[0/\pm45/90]_s$ Graphite/Epoxy Specimen Under Biaxial Loading $\sigma_{yy} = 2\sigma_{xx}$
at 30-Deg. with Crack Direction (Spec. No. 6-20A).

175
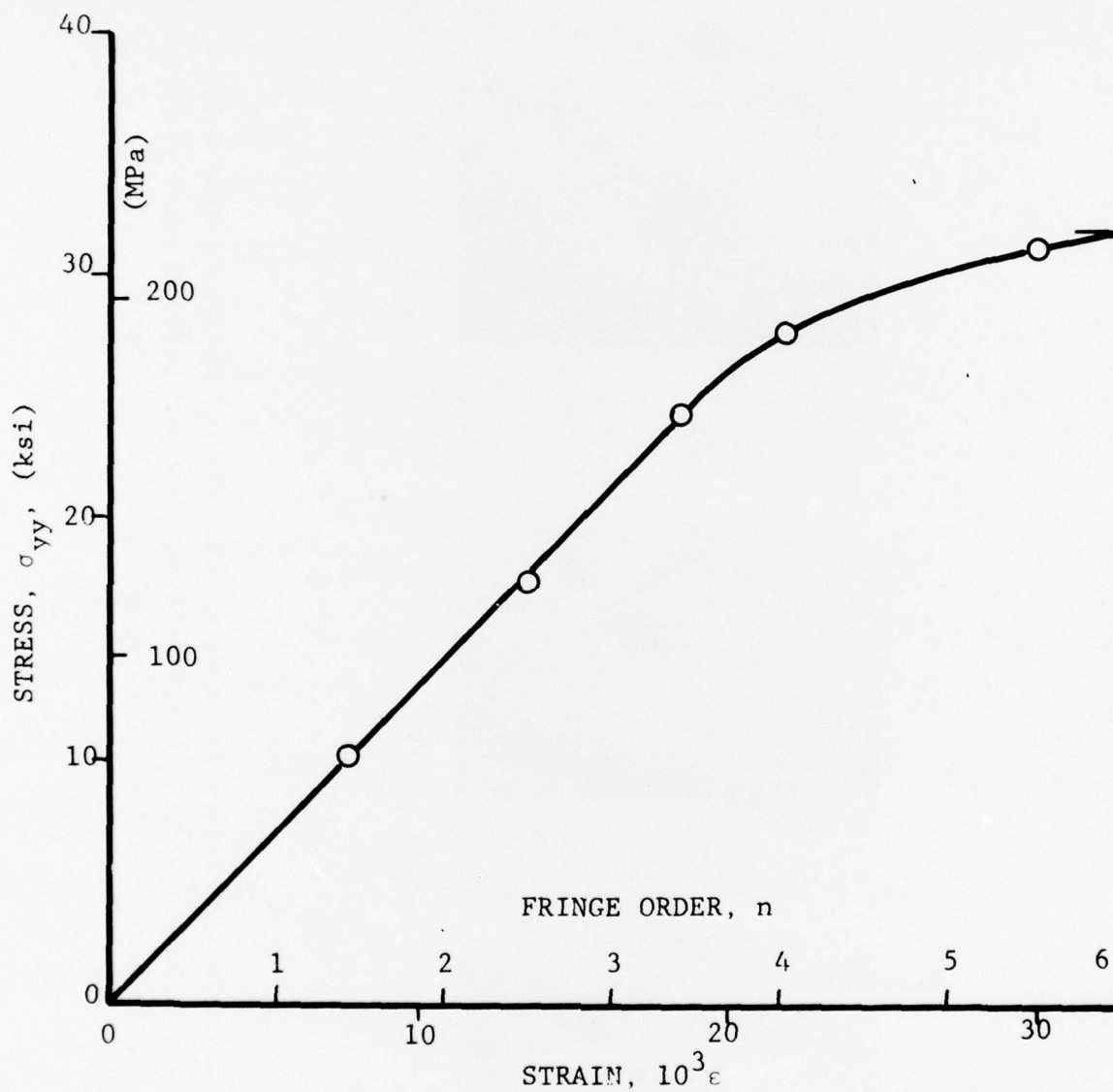
Figure 127. Maximum Fringe Order and Strain at Crack Tip of
[0/±45/90]$_s$ Graphite/Epoxy Specimen With 2.54 cm
(1.00 in.) Crack Under Biaxial Loading $\sigma_{yy} = 2\sigma_{xx}$
(Spec. No. 6-20A).

176
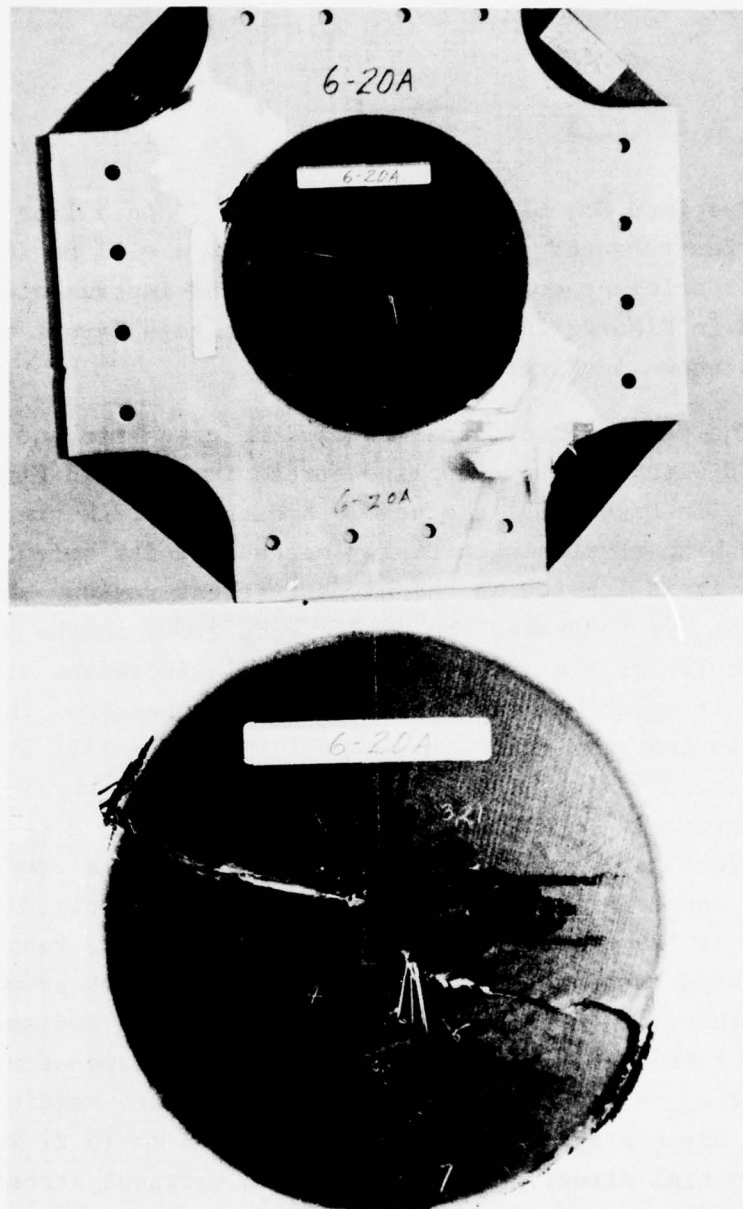
Figure 128. Failure Pattern in $[0/\pm45/90]_s$ Graphite/Epoxy
Specimen with 2.54 cm (1.00 in.) Crack Under
Biaxial Loading $\sigma_{yy} = 2\sigma_{xx}$ (Spec. No. 6-20A)

177

Specimen No. 6-13 had a 1.91 cm (0.75 in.) long crack and was instrumented with strain gages and a 0.51 mm (0.020 in.) thick birefringent coating. The tabbed and instrumented specimen is shown in Figure 129. A closeup of the gage layout around the crack is shown in Figure 130.

The variation of strains near the crack tip and in the far-field with effective applied stress is shown in Figures 131 and 132. In Figure 131 the gage nearest the crack tip does not read the highest strain initially because of its orientation, although it is located in the highest-stress region. However, as the load is increased the damage zone grows in the direction perpendicular to the crack and this strain increases at a faster rate and it overtakes the other strains farther from the crack. The strain near the crack tip (gage 1 in Figure 131) at a distance of 0.76 mm (0.03 in.) is linear up to an applied vertical stress of approximately 76 MPa (11 ksi). The strains at distances of 2.54 mm (0.10 in.) and 5.33 mm (0.21 in.) from the crack tip (gages 2 and 3 in Figure 131) are linear up to applied vertical stresses of 179 MPa (26 ksi) and 200 MPa (29 ksi), respectively. In all three cases the gages failed when the crack propagated through them. In Figure 132 gage 1 located at a distance of 1.78 mm (0.07 in.) from the crack tip shows a linear response up to a stress of σ_{yy} = 110 MPa (16 ksi). From the gage readings it seems that the crack propagated a distance of 5.33 mm (0.21 in.) normal to its initial direction between applied vertical stresses of 192 MPa (28 ksi) and 233 MPa (34 ksi).

Isochromatic fringe patterns in the coating around the crack are shown in Figure 133 for three load levels. They illustrate clearly the areas of high stress and the direction and extent of failure propagation. Failure seems to start at the tip of the

178
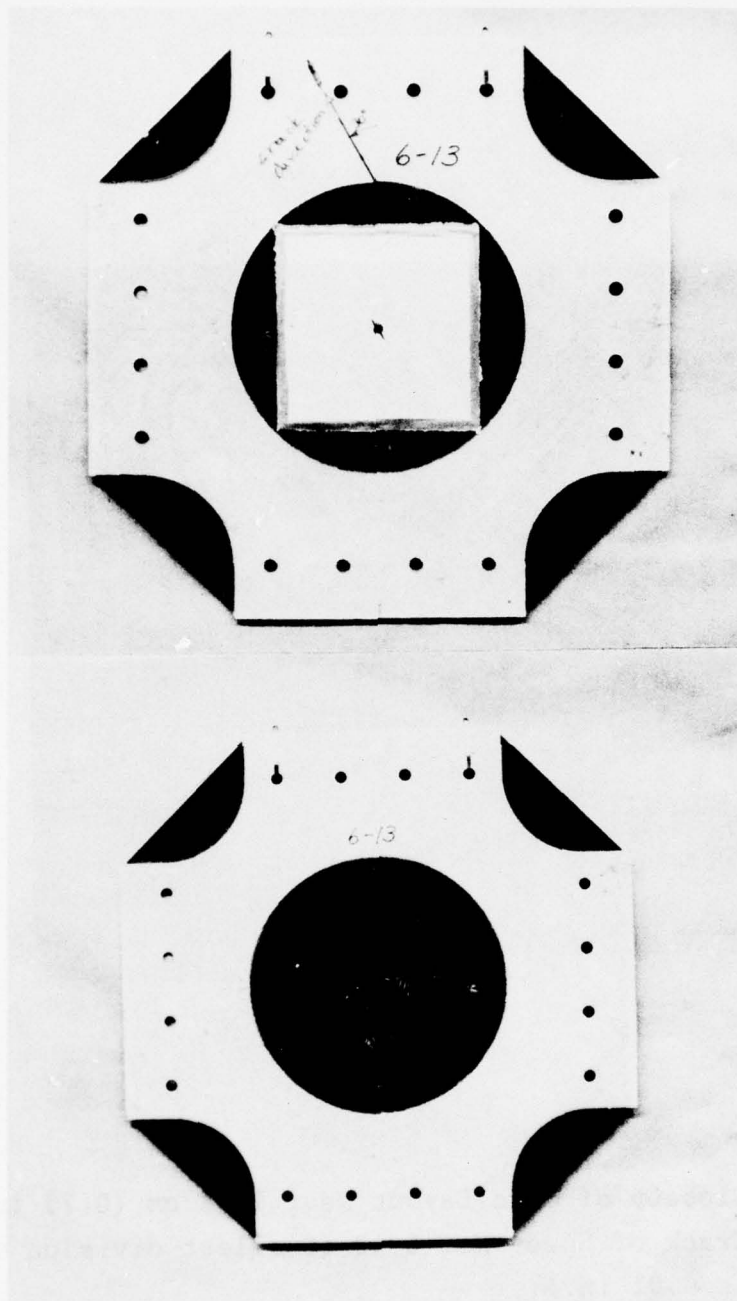
Figure 129. Biaxial Specimen with 1.91 cm (0.75 in.) Long
Crack (Spec. No. 6-13).

179
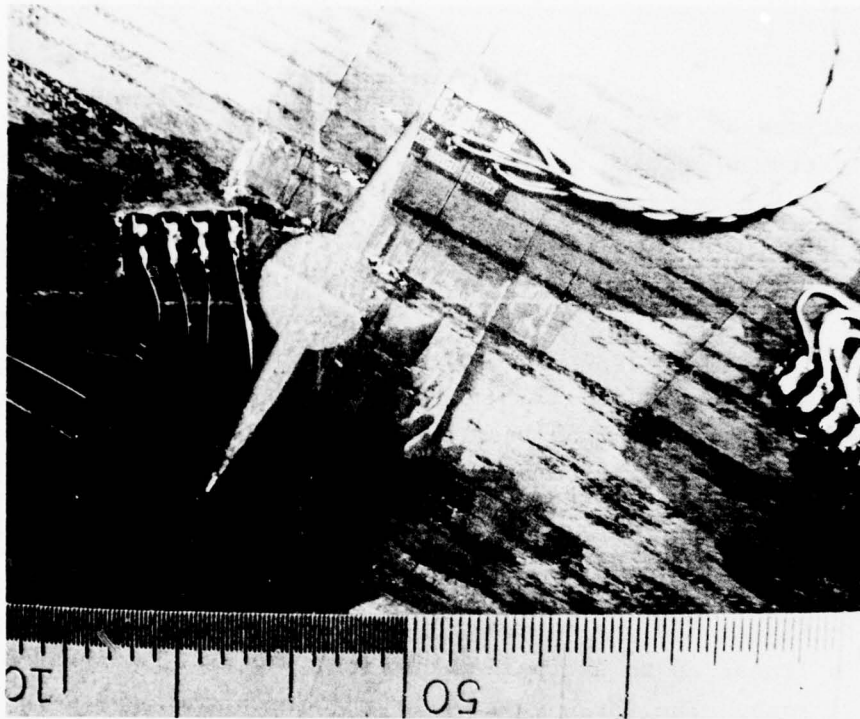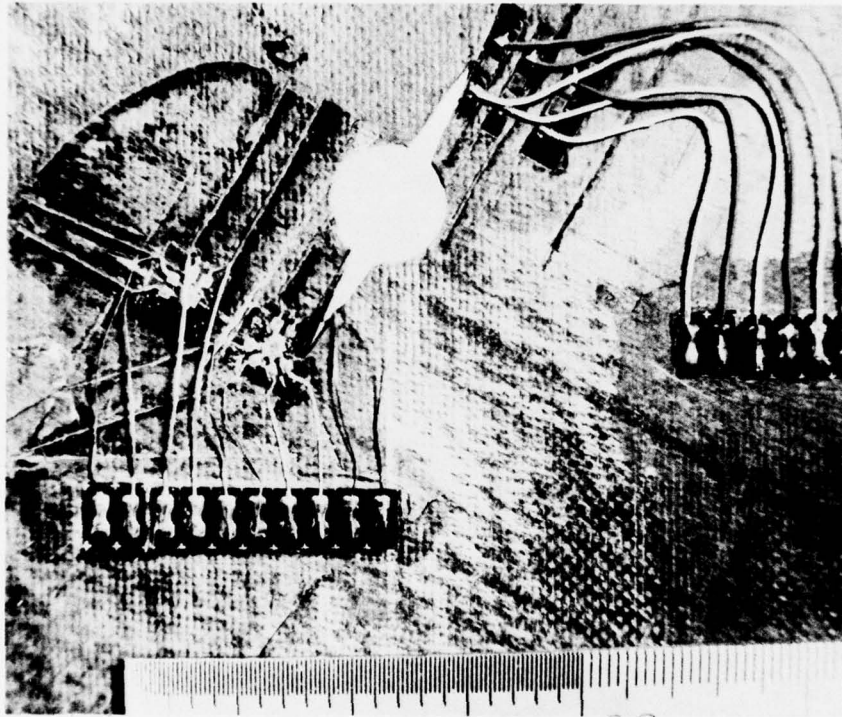
Figure 130.   Closeup of Gage Layout Near 1.91 cm (0.75 in.)
            Crack of Spec. No. 6-13 (Smallest division shown
            is 0.01 in.).
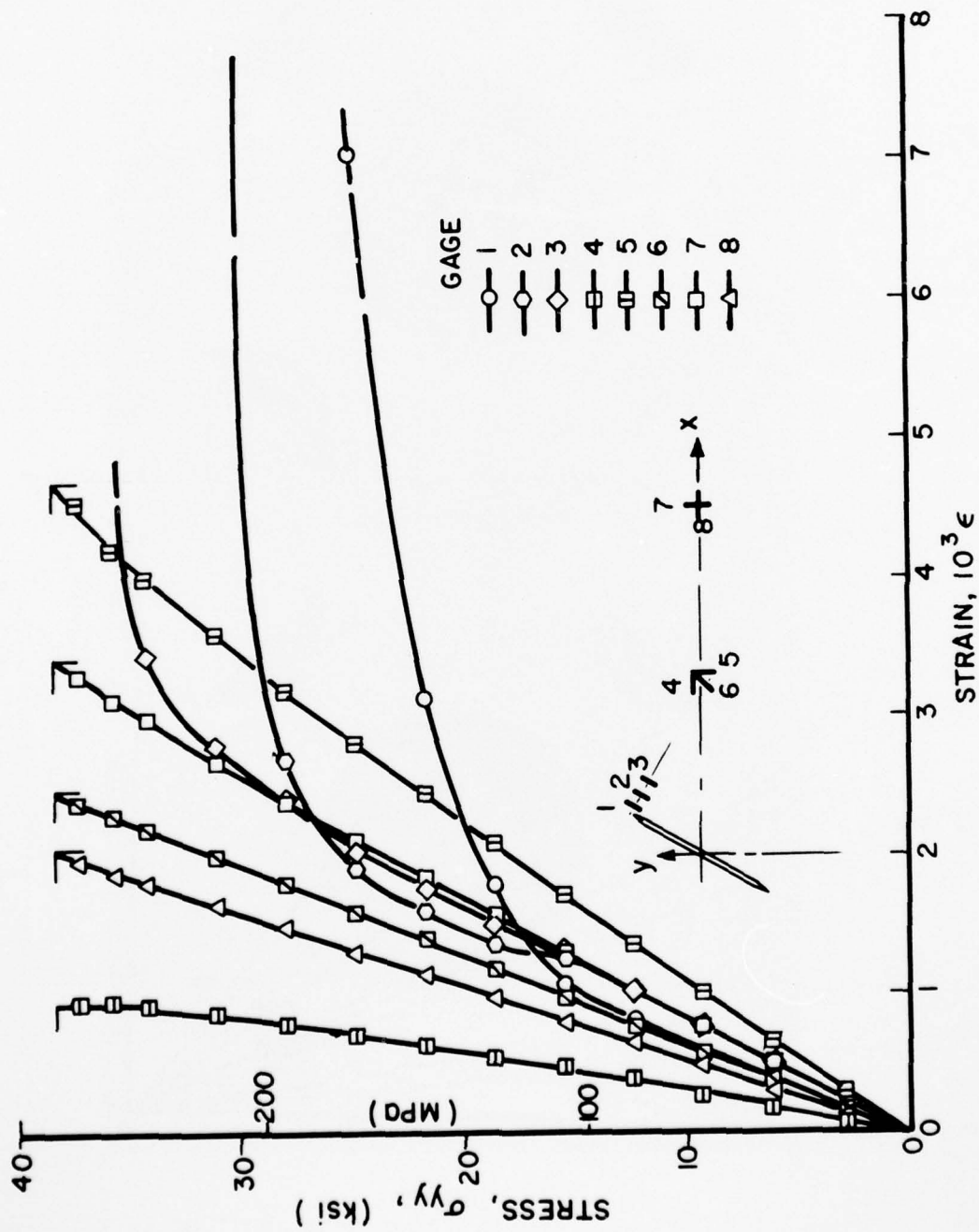
180

Figure 131. Strains Near Crack Tip and Along Horizontal Axis of [0/±45/90]s Graphite/Epoxy Specimen with 1.91 cm (0.75 in.) Crack Under Biaxial Loading σyy = 1.93σxx at 30-Deg. with Crack Direction and 60-Deg. with Outer Fiber Direction (Spec. No. 6-13).
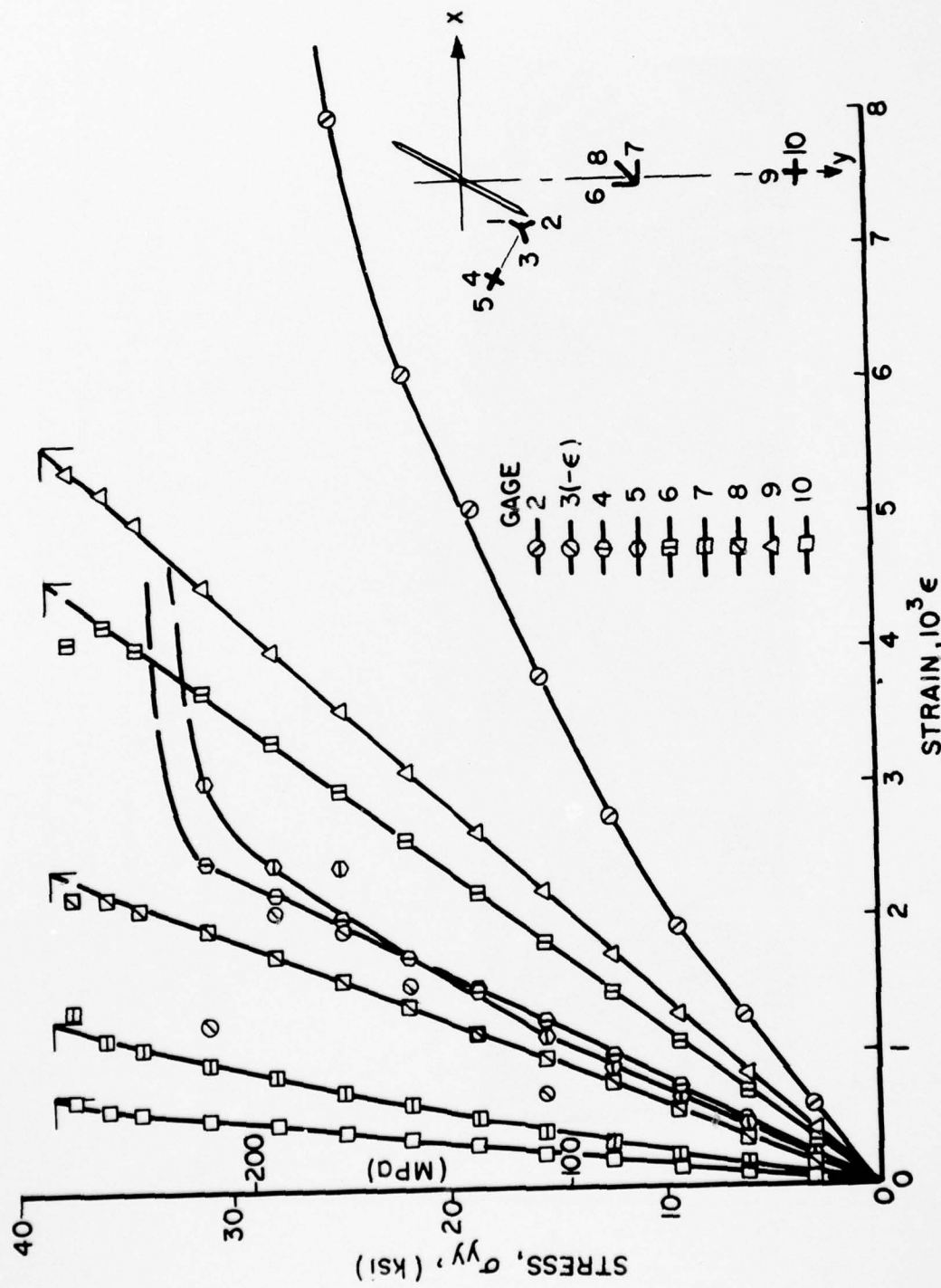
181

Figure 132. Strains Near Crack Tip and Along Vertical Axis of [0/+45/90]s Graphite/Epoxy Specimen with 1.91 cm (0.75 in.) Crack Under Biaxial Loading σ_{yy} = 1.93σ_{xx} at 30-Deg. with Crack Direction and 60-Deg. with Outer Fiber Direction (Spec. No. 6-13).

σ_{yy} = 182 MPa (26.4 ksi) $\bar{\sigma}_{yy}$ = 243 MPa (35.2 ksi) σ_{yy} = 253 MPa (36.7 ksi)
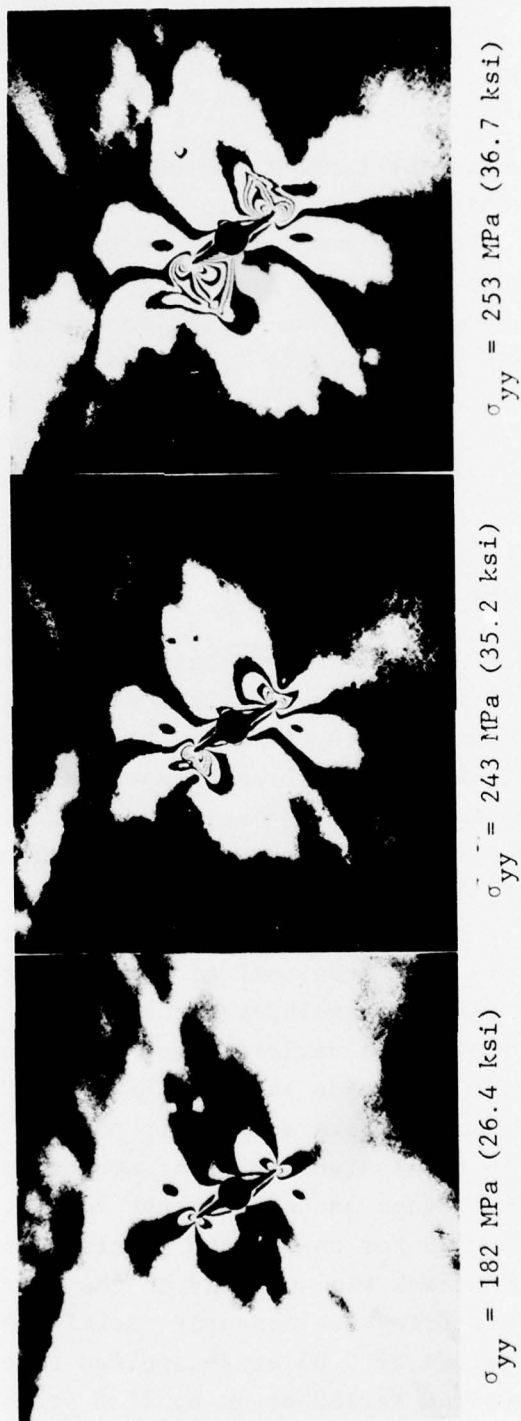
Figure 133. Isochromatic Fringe Patterns in Photoelastic Coating Around 1.91 cm (0.75 in.)
Crack in [0/±45/90]s Graphite/Epoxy Specimen Under Biaxial Loading σ_{yy} = 1.93σ_{xx}
at 30-Deg. with Crack Direction and 60-Deg. with Outer Fiber Direction
(Spec. No. 6-13).

183

crack at points where the tangent to the crack tip arc is vertical.
The crack then propagated normally to its initial direction or along
the outer fibers. The maximum fringe order at this point and the
corresponding tangential strain is plotted in Figure 134 as a
function of applied stress. The variation appears bilinear with a
knee at a strain of approximately 0.011, which is slightly higher
than the ultimate strain of an unnotched coupon of the same layup.
The computed stress concentration in the linear range is 3.2. The
maximum measured strain at failure, which occurred at σ_{yy} = 263 MPa
(38 ksi), is over 0.025. Two views of the failed specimen (Figure
135) show the direction of initial crack extension accompanied by
excessive delamination.

Specimen No. 6-14 was a replicate of specimen No. 6-13 above.
It had a 1.91 cm (0.75 in.) long crack and was instrumented with
strain gages and a 0.25 mm (0.010 in.) thick birefringent coating.
The specimen was loaded in the biaxial machine with a vertical
load exactly twice as high as the horizontal load. The effective
stress biaxiality ratio is not the same as the load input ratio
because of the influence of the glass/epoxy tab. Normally the input
loads were adjusted to yield a 2:1 stress biaxiality ratio. In
this case, which was the first test of its kind, the load ratio was
maintained at 2:1 and the resulting stress biaxiality ratio was
σ_{yy}/σ_{xx} = 3.57. The strain variation near the crack and in the far-
field with effective stress is shown in Figures 136 and 137. From
the strain readings near the crack tip it appears that the onset
of damage occurs at an applied stress of approximately 69 MPa (10
ksi). Isochromatic fringe patterns in the coating around the crack
are shown in Figure 138 for three load levels. The crack or damage
propagates from the crack tip normally to the initial crack direction.
According to the birefringence measured, strains near the tip of
the crack exceed values of 0.03 at an applied stress of 226 MPa
(33 ksi). The specimen failed at an applied stress of 305 MPa
(44 ksi). Two views of the failed specimen are shown in Figure 139.

184

Figure 134. Maximum Fringe Order and Tangential Strain at Crack Tip of $[0/\pm45/90]_s$ Graphite/Epoxy Specimen with 1.91 cm (0.75 in.) Crack Under Biaxial Loading $\sigma_{yy} = 1.93\sigma_{xx}$ (Spec. No. 6-13).

185

Figure 135. Biaxial Specimen with 1.91 cm (0.75 in.) Long
Crack After Failure (Spec. No. 6-13).

186

Figure 136. Strains Near Crack Tip and Along Horizontal Axis of
$[0/\pm45/90]_s$ Graphite/Epoxy Specimen with 1.91 cm
(0.75 in.) Crack Under Biaxial Loading $\sigma_{yy} = 3.57\sigma_{xx}$
at 30-Deg. with Crack Direction (Spec. No. 6-14).

187

Figure 137. Strains Near Crack Tip and Along Vertical Axis of [0/+45/90]s Graphite/Epoxy Specimen with 1.91 cm (0.75 in.) Crack Under Biaxial Loading $\sigma_{yy} = 3.57\sigma_{xx}$ at 30-Deg. with Crack Direction (Spec. No. 6-14).

σ_{yy} = 226 MPa (32.7 ksi)　　　σ_{yy} = 260 MPa (37.6 ksi)　　　σ_{yy} = 293 MPa (42.5 ksi)

Figure 138. Isochromatic Fringe Patterns in Photoelastic Coating Around 1.91 cm (0.75 in.) Crack in $[0/\pm 45/90]_s$ Graphite/Epoxy Specimen Under Biaxial Loading σ_{yy} = 3.57σ_{xx} at 30-Deg. with Crack Direction (Spec. No. 6-14).

189
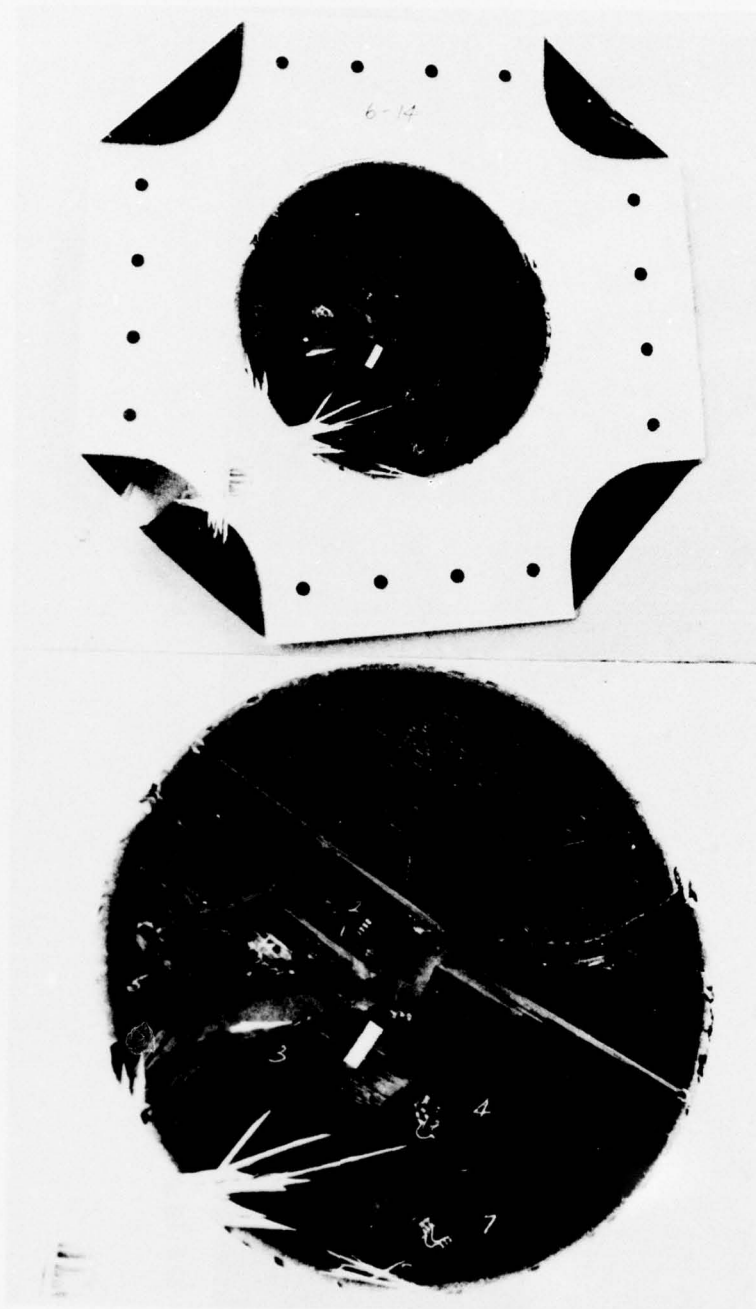
Figure 139. Biaxial Specimen with 1.91 cm (0.75 in.) Long Crack
After Failure (Spec. No. 6-14).

Specimen No. 6-16 had a 1.27 cm (0.50 in.) long crack and was instrumented with strain gages and a 0.25 mm (0.010 in.) thick photoelastic coating. Strains in the vicinity of the crack tip and along the horizontal and vertical directions are plotted as a function of effective applied vertical stress in Figures 140 and 141. In Figure 140 the strain near the crack tip (gage 1) is linear up to a stress of approximately 110 MPa (16 ksi The three gages near the crack tip (gages 1, 2 and 3) failed when the crack propagated through them at applied stresses of approximately 214 MPa (31 ksi), 269 MPa (39 ksi) and 276 MPa (40 ksi). In Figure 141 the strain near the crack tip is linear up to a stress of 104 MPa (15 ksi), thereafter it increases rapidly up to the point when the crack propagates through the gage at an approximate stress of 269 MPa (39 ksi). The crack reaches the location of gages 4 and 5 in Figure 141 at an applied stress of 290 MPa (42 ksi).

Isochromatic fringe patterns in the coating around the crack are shown in Figure 142 for four load levels. Crack propagation, in the direction normal to the crack, seems to be limited up to a stress of 260 MPa (37.7 ksi). An abrupt jump in crack extension seems to take place between this stress and the next level of 278 MPa (40.3 ksi). In addition to the primary propagation normal to the initial crack, there is crack extension along the original crack direction probably along the fibers of the central plies of the laminate. This is illustrated by the fringe patterns of Figure 142. There is also evidence of tertiary crack propagation normally to the initial crack direction but initiating at the tip of the subsurface extended crack. The maximum fringe order and strain at the tip of the initial crack is plotted as a function of applied stress in Figure 143. Rapid crack propagation occurs in the stress range 220-262 MPa (32-38 ksi) corresponding to peak strains of the order of 0.030. Total failure occurred at an applied stress of 313 MPa (45.3 ksi). Two views of the failed specimen are shown in Figure 144.
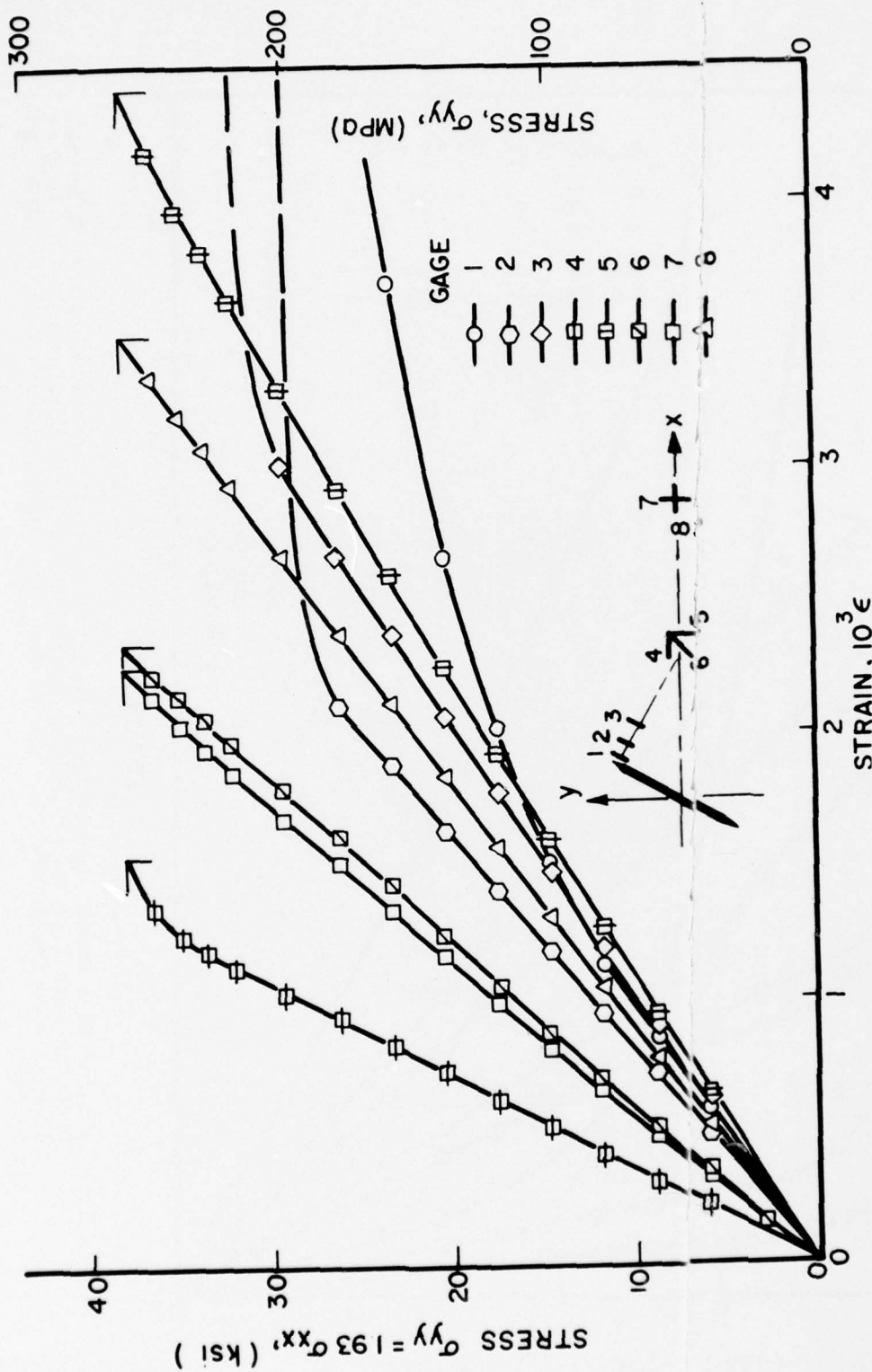
191

Figure 140. Strains Near Crack Tip and Along Horizontal Axis of
[0/±45/90]$_s$ Graphite/Epoxy Specimen with 1.27 cm
(0.50 in.) Crack Under Biaxial Loading $\sigma_{yy} = 2.03\sigma_{xx}$
at 30-Deg. with Crack Direction (Spec. No. 6-16).
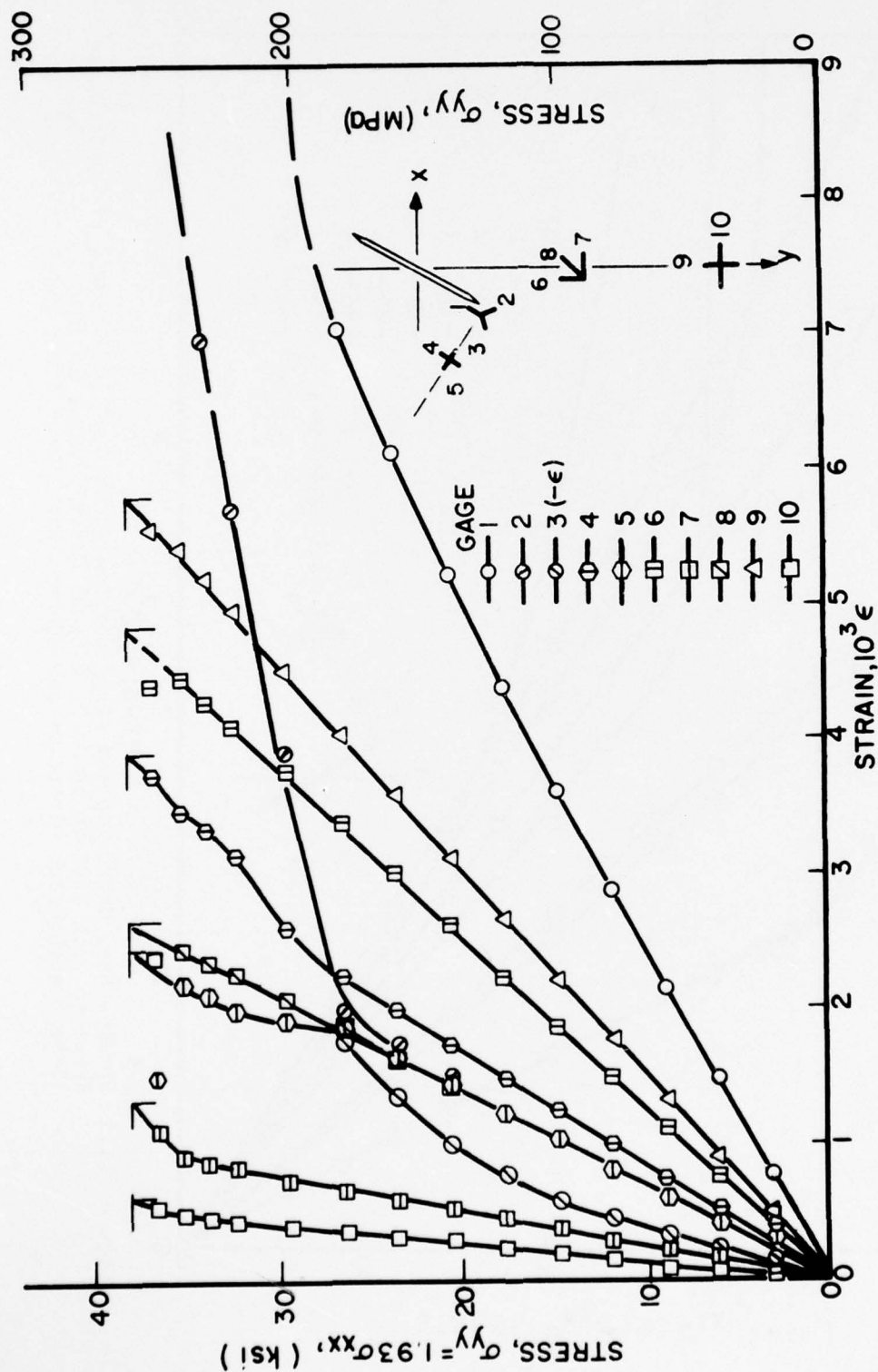
192

Figure 141.   Strains Near Crack Tip and Along Vertical Axis of
[0/±45/90]$_s$ Graphite/Epoxy Specimen with 1.27 cm
(0.50 in.) Crack Under Biaxial Loading $\sigma_{yy} = 2.03\sigma_{xx}$
at 30-Deg. with Crack Direction (Spec. No. 6-16).

193

σ_{yy} = 260 MPa (37.7 ksi) σ_{yy} = 278 MPa (40.3 ksi)

σ_{yy} = 292 MPa (42.4 ksi) σ_{yy} = 303 MPa (43.9 ksi)

Figure 142.   Isochromatic Fringe Patterns in Photoelastic Coating
Around 1.27 cm (0.5 in.) Crack in $[0/\underline{+}45/90]_s$ Graphite/
Epoxy Specimen Under Biaxial Loading, $\overline{\sigma}_{yy}$ = $2.03\sigma_{xx}$
at 30-Deg. with Crack Direction (Spec. No. 6-16).

194
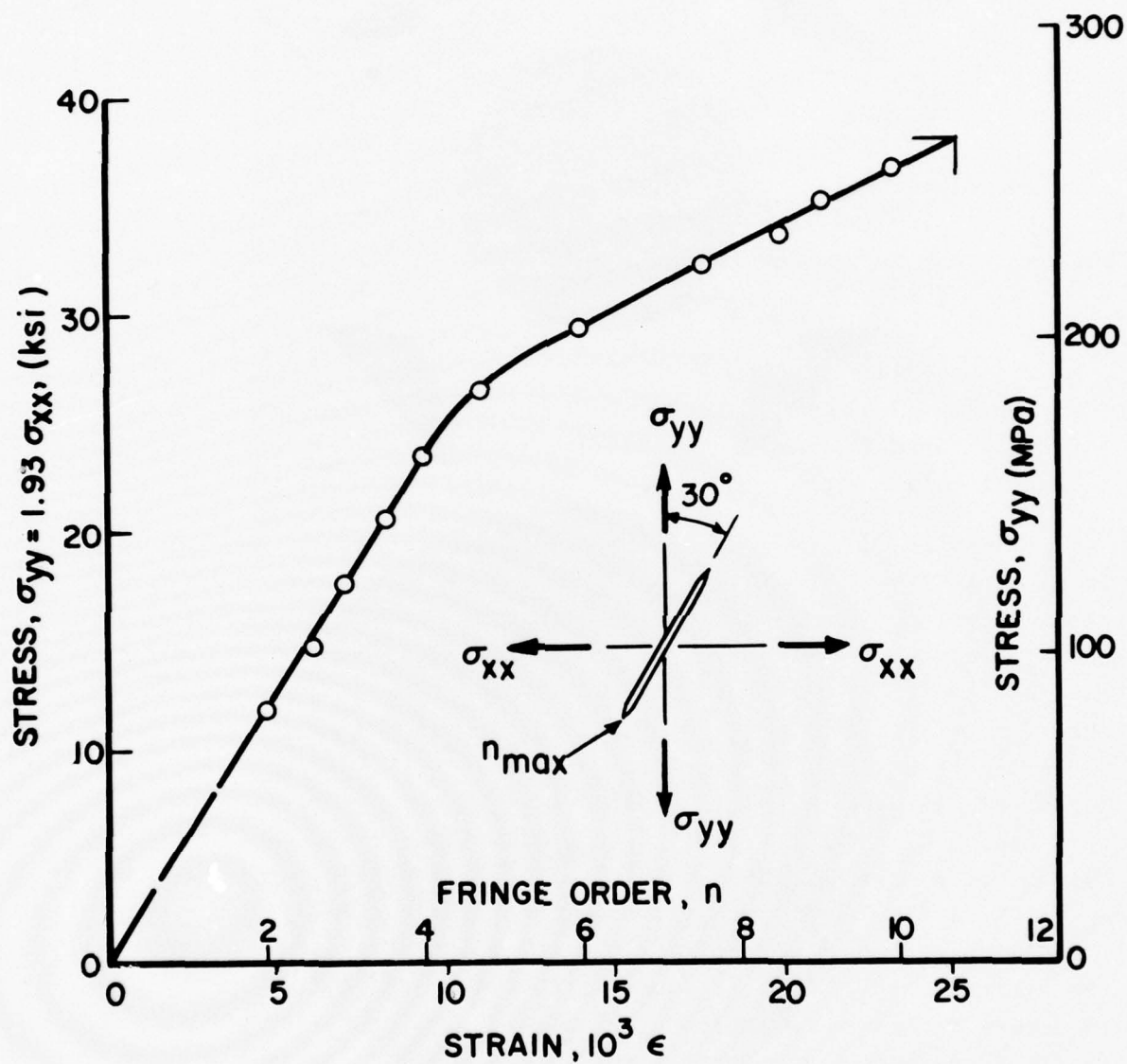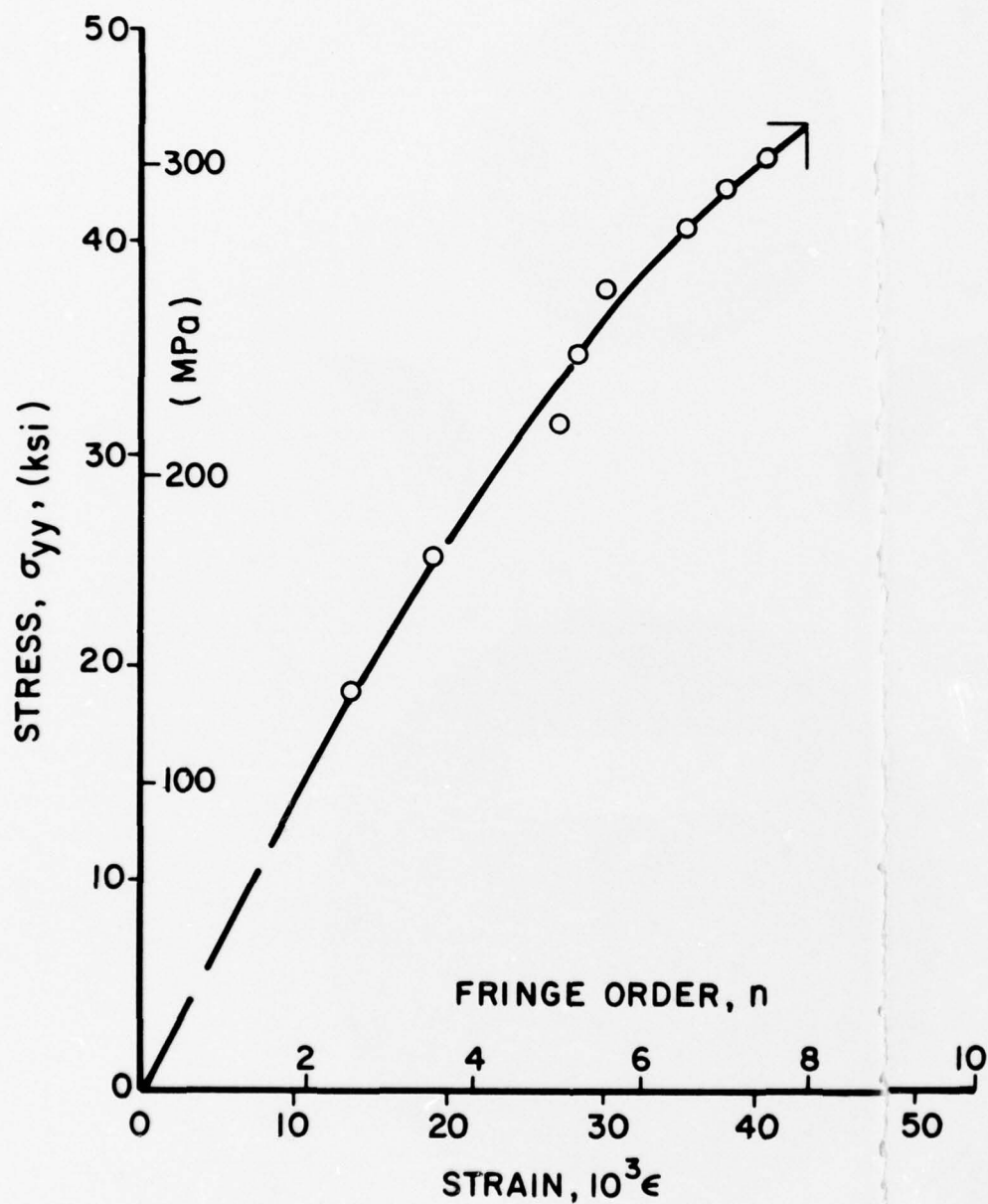
Figure 143. Maximum Fringe Order and Strain at Crack Tip of $[0/\pm45/90]_s$ Graphite/Epoxy Specimen with 1.27 cm (0.50 in.) Crack Under Biaxial Loading $\sigma_{yy} = 2.03\sigma_{xx}$ at 30-Deg. to Crack Direction (Spec. No. 6-16).

195
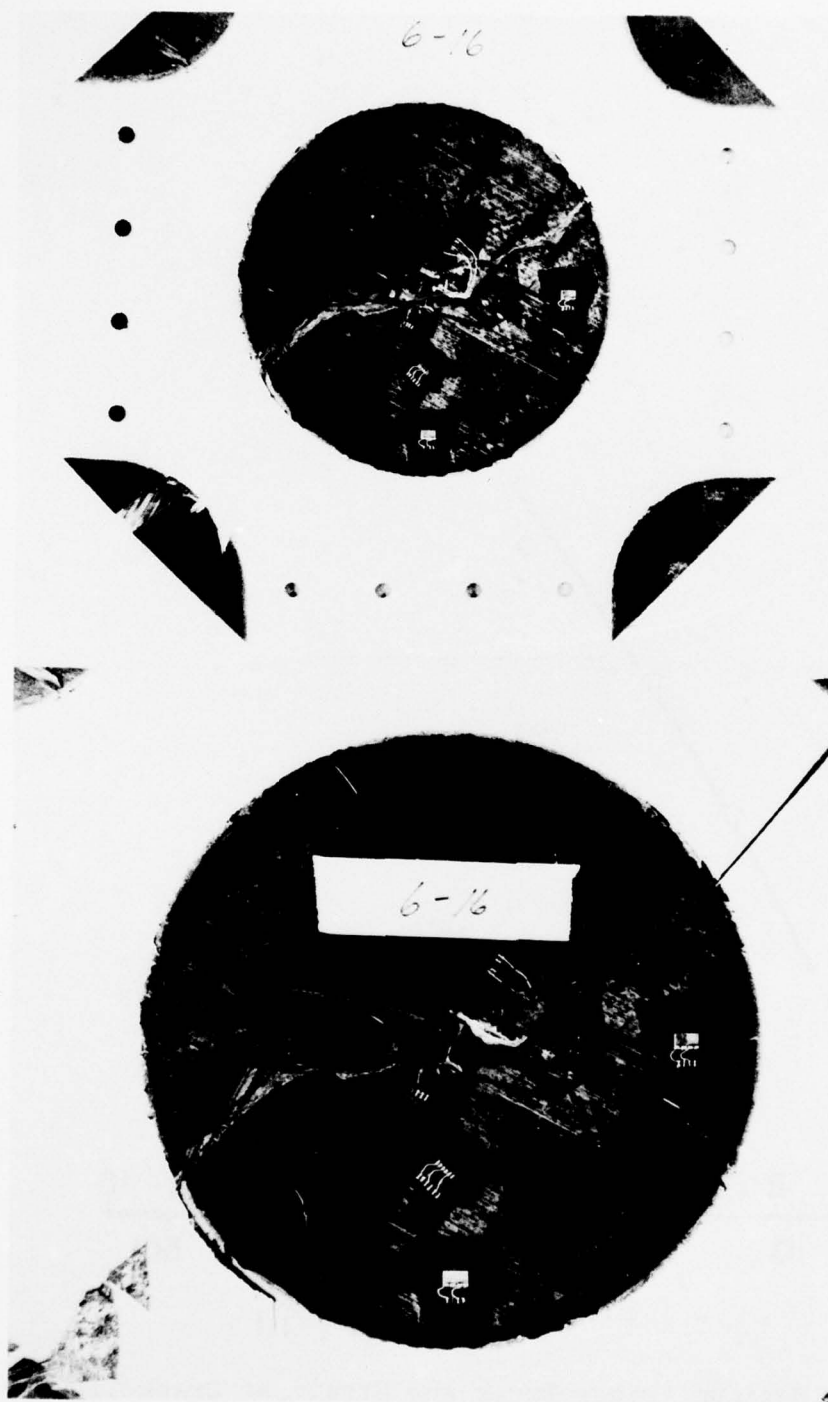
Figure 144. Biaxial Specimen with 1.27 cm (0.50 in.) Long
Crack After Failure (Spec. No. 6-16).

Specimen No. 6-17A was a replicate of the specimen above. It had a 1.27 cm (0.50 in.) long crack and was instrumented with strain gages. The strain variations near the crack tip and along the horizontal and vertical axes are shown in Figures 145 and 146. The strain near the crack tip in Figure 145 (gage 1) appears nonlinear throughout the loading range up to the stress level of 186 MPa (27 ksi) when the crack propagates through the gage. The damage zone reaches the gages farther from the crack tip at a stress level of approximately 290 MPa (42 ksi). Although the damage zone had propagated more than 2.5 mm (0.1 in.) from the crack tip final failure did not occur through the crack but away from it near the tab. This failure occurred at a stress of 343 MPa (49.8 ksi)

Specimen No. 6-18A had a 0.64 cm (0.25 in.) crack and was instrumented with strain gages and a 0.25 mm (0.01 in.) photo-elastic coating. The strain near the crack tip was nonlinear throughout up to the stress level of 258 MPa (37 ksi) when the damage extended through the strain gage. The photoelastic fringe patterns confirm that visible damage initiation and extension occurred at the stress level above. The specimen failed prematurely away from the crack near the tab at a stress of 332 MPa (48.1 ksi).

Specimen No. 6-19A had a 0.64 cm (0.25 in.) crack and was instrumented with strain gages. The specimen was initially tabbed with 5-ply crossply glass/epoxy with the outer fiber parallel to the y-direction or the direction of the highest load. Subsequently three additional layers of resin-impregnated glass cloth (style No. 1581) were laid over each side of the original tab and cured in a vacuum bag at room temperature. This overlay extended up to a 15.2 cm (6 in.) diameter circle in the middle of the specimen. Strains near the crack tip and along the horizontal and vertical axes are shown in Figures 147 and 148. The strain at a distance of 0.5 mm (0.02 in.) from the crack tip is linear up to a stress of approximately 97 MPa (14 ksi) corresponding to a local strain of 0.002. The crack tip damage reaches this point at a stress of

197
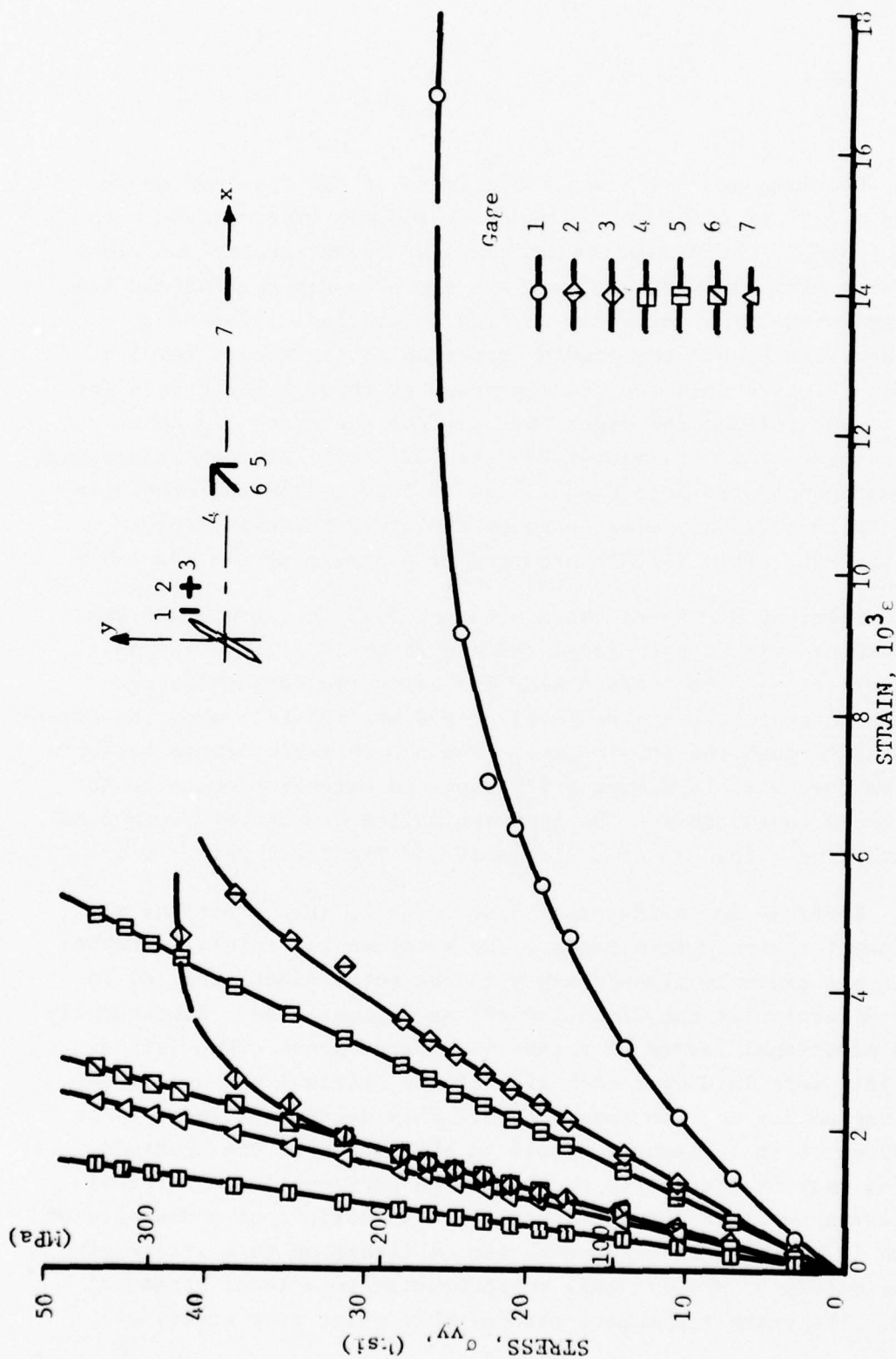
Figure 145. Strains Near Crack Tip and Along Horizontal Axis of $[0/\pm 45/90]_s$ Graphite/Epoxy Specimen With 1.27 cm (0.50 in.) Crack Under Biaxial Loading $\sigma_{yy} = 2.0\sigma_{xx}$ at 30-Deg. With Crack Direction (Spec. No. 6-17A).
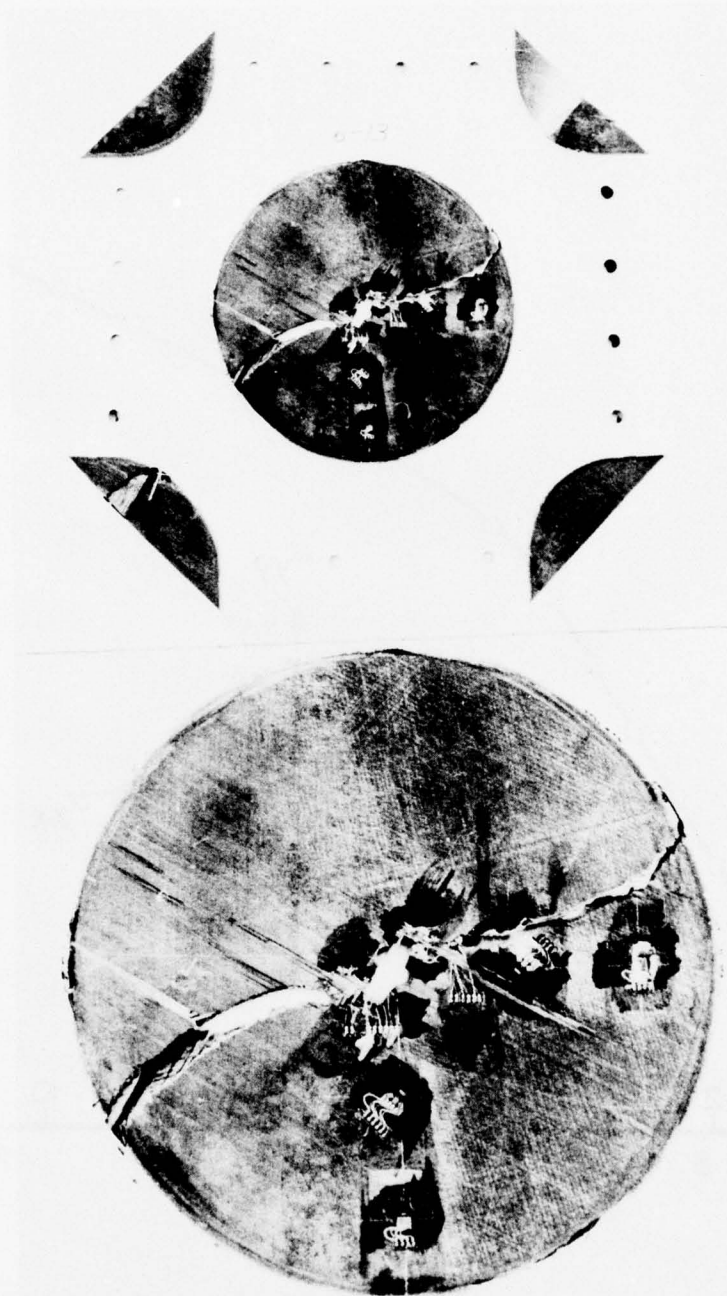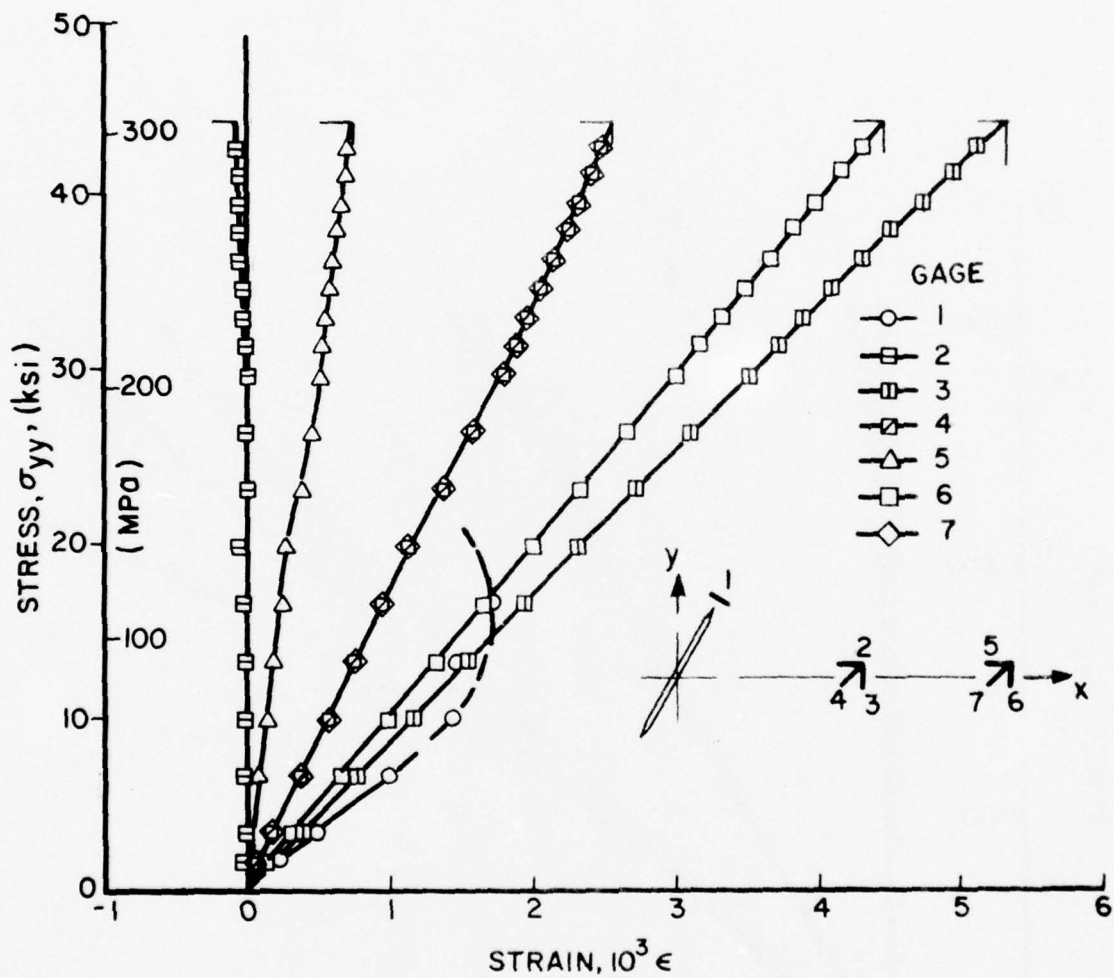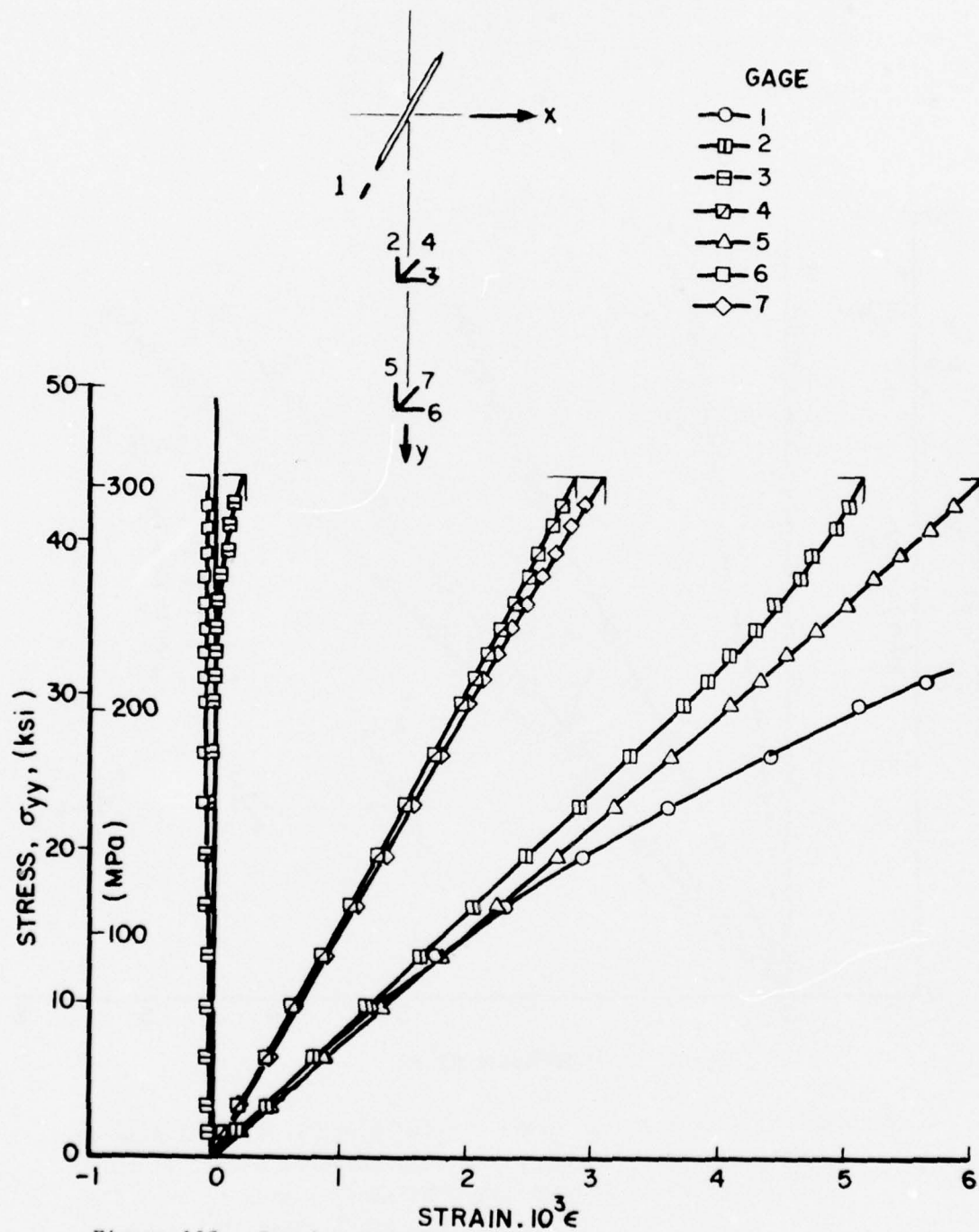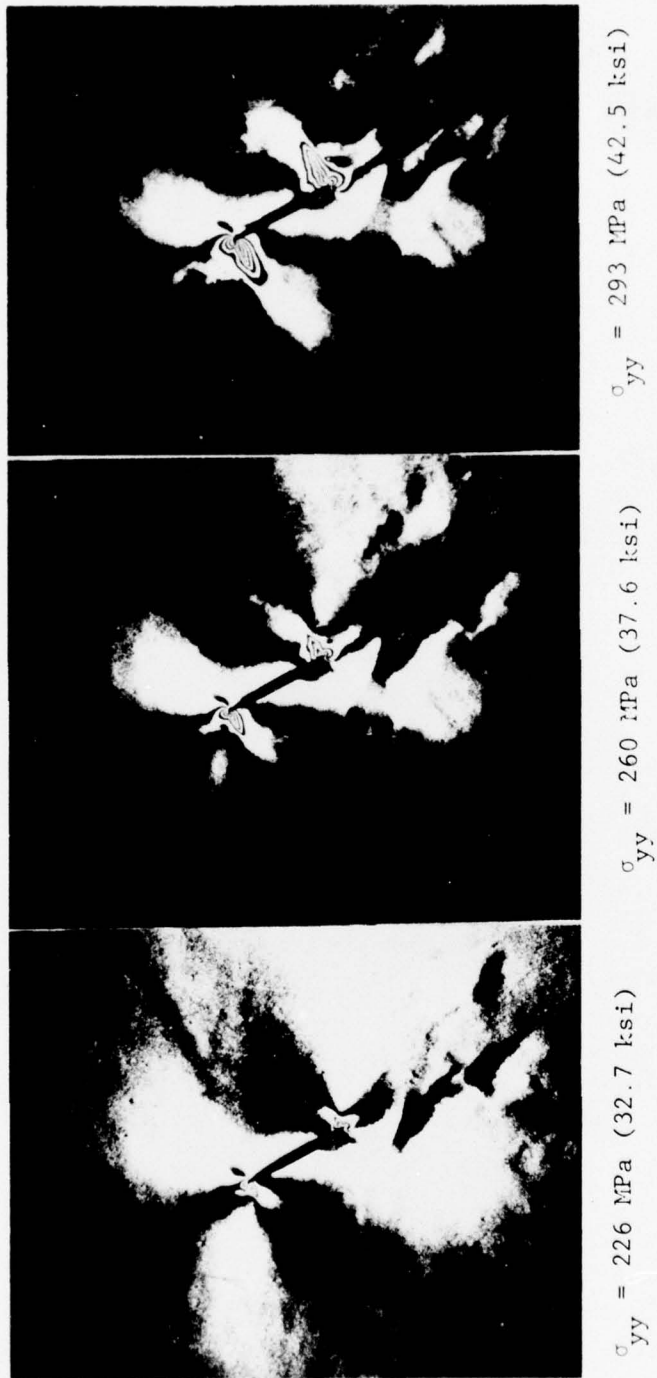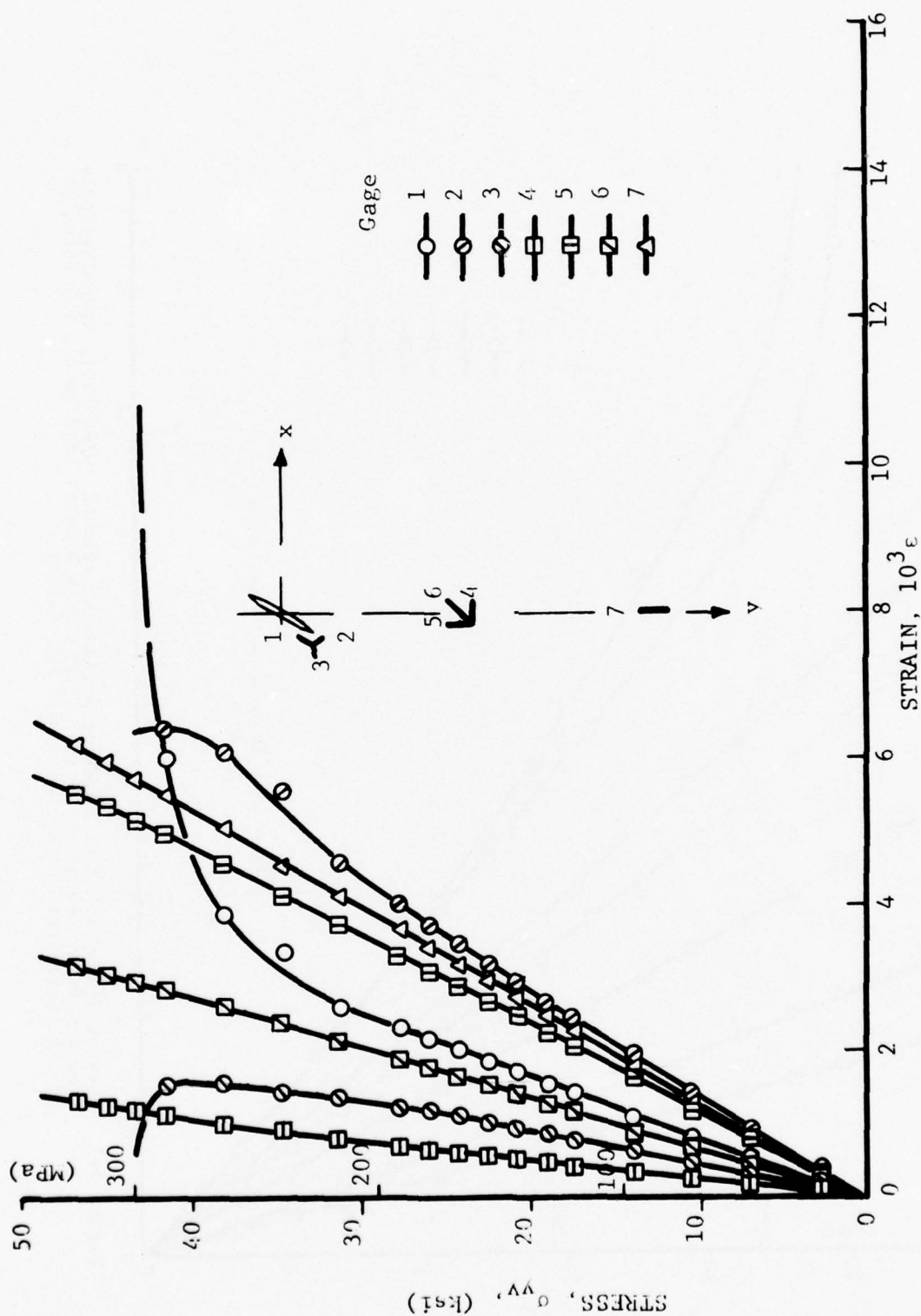
Figure 146. Strains Near Crack Tip and Along Vertical Axis of [0/+45/90]s Graphite/Epoxy Specimen With 1.27 cm (0.50 in.) Crack Under Biaxial Loading σ_{yy} = 2.0σ_{xx} at 30-Deg. With Crack Direction (Spec. No. 6-17A).

199
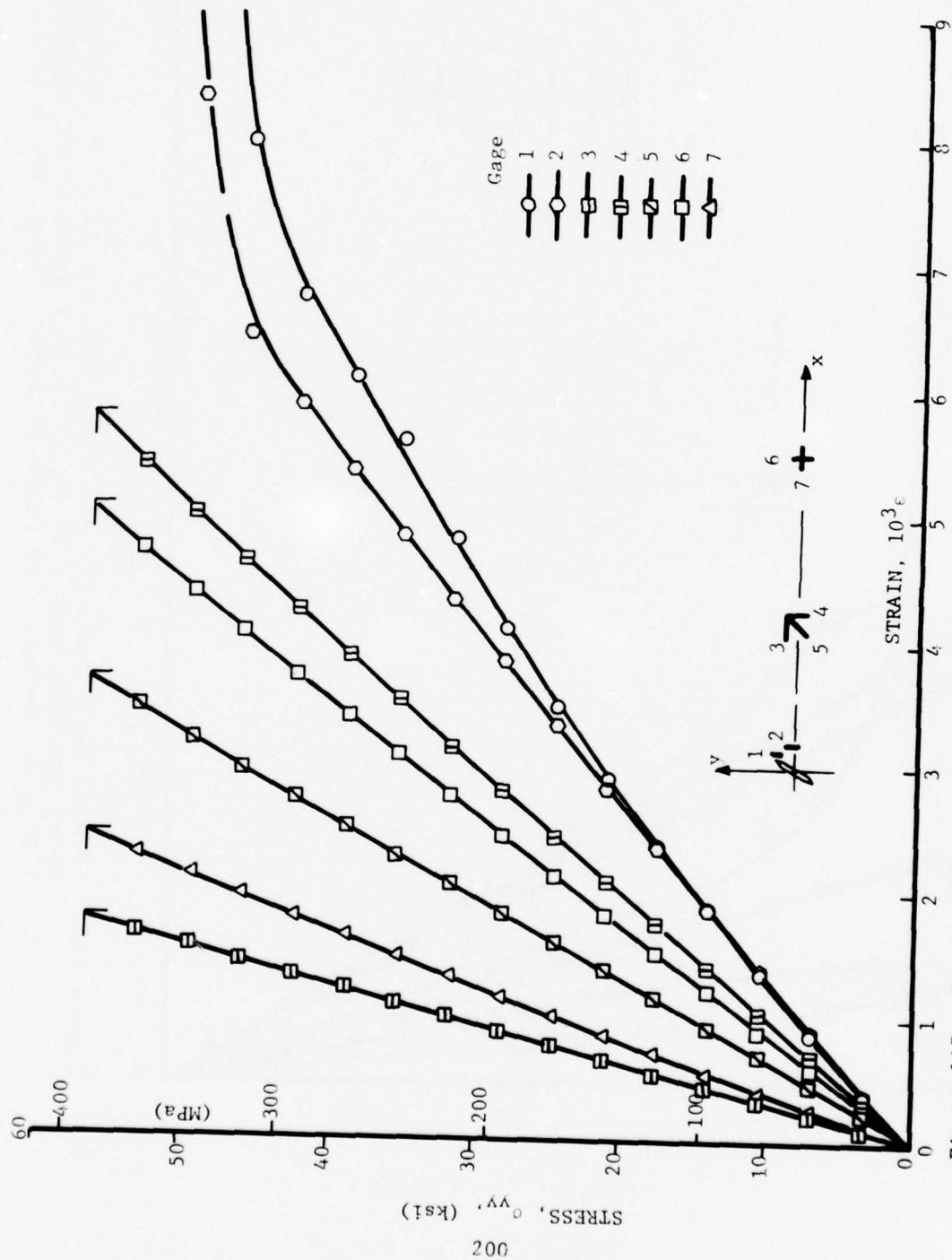
Figure 147. Strains Near Crack Tip and Along Horizontal Axis of [0/+45/90]s Graphite/Epoxy Specimen With 0.64 cm (0.25 in.) Crack Under Biaxial Loading $\sigma_{yy} = 1.96\sigma_{xx}$ at 30-Deg. With Crack Direction (Spec. No. 6-19A).
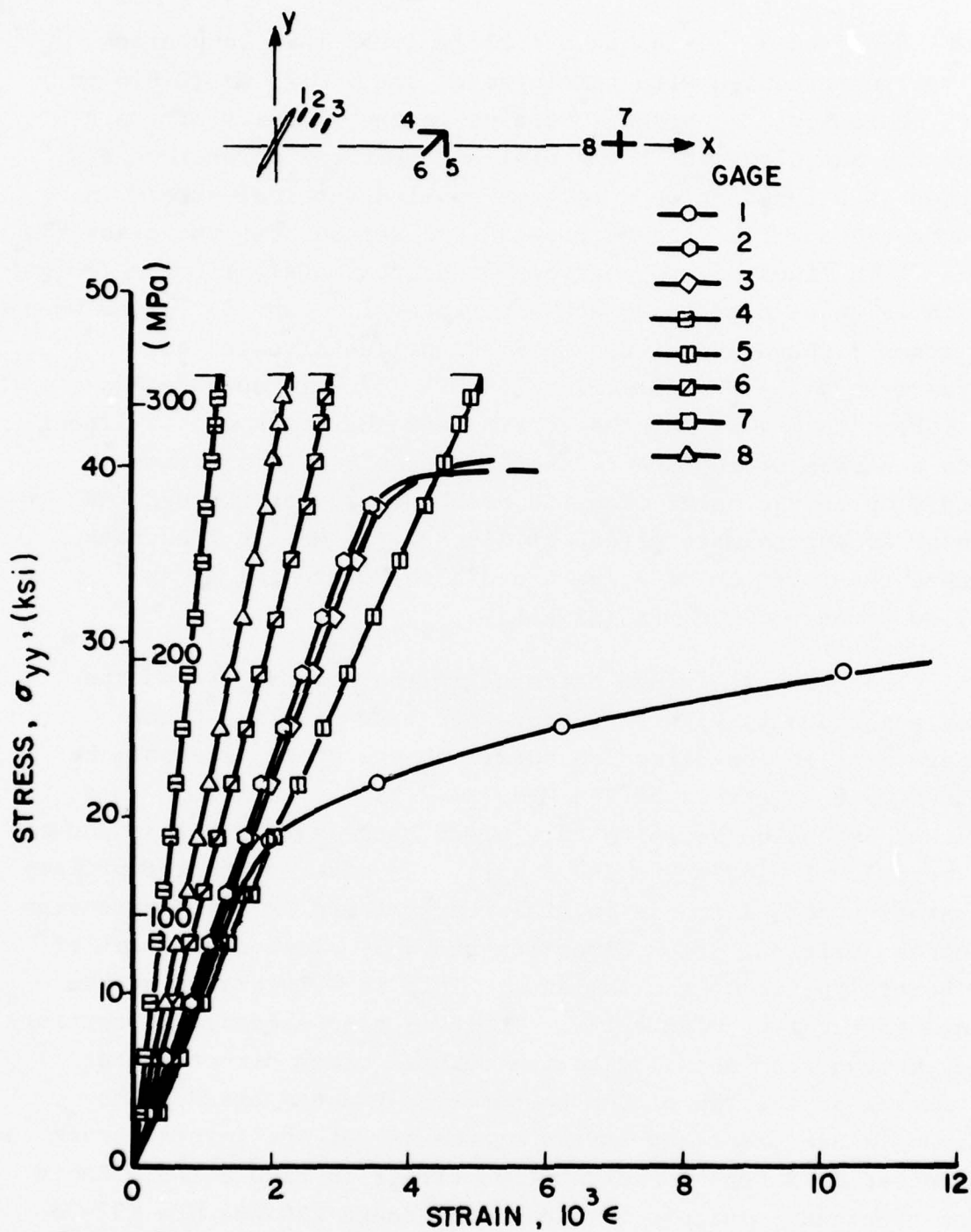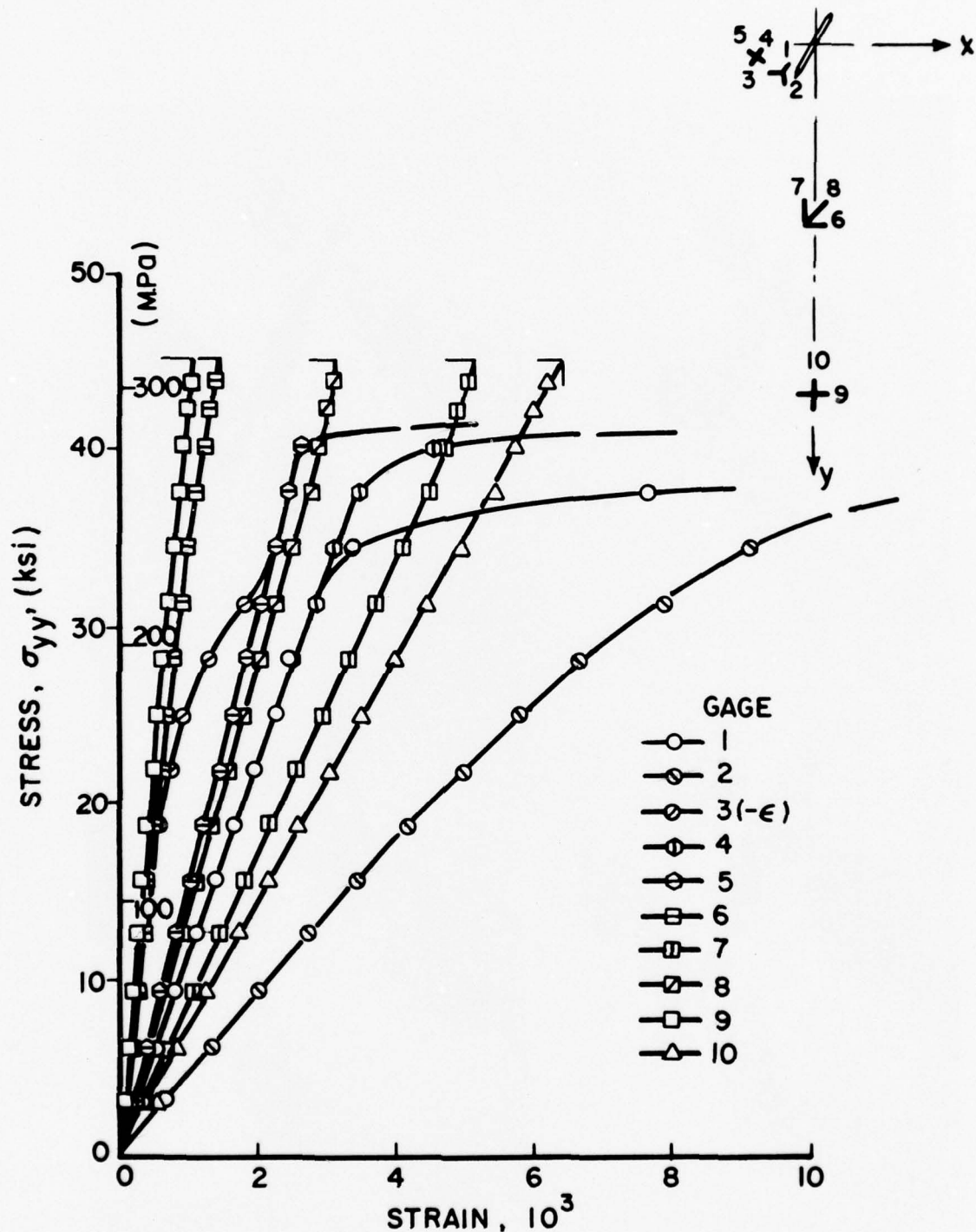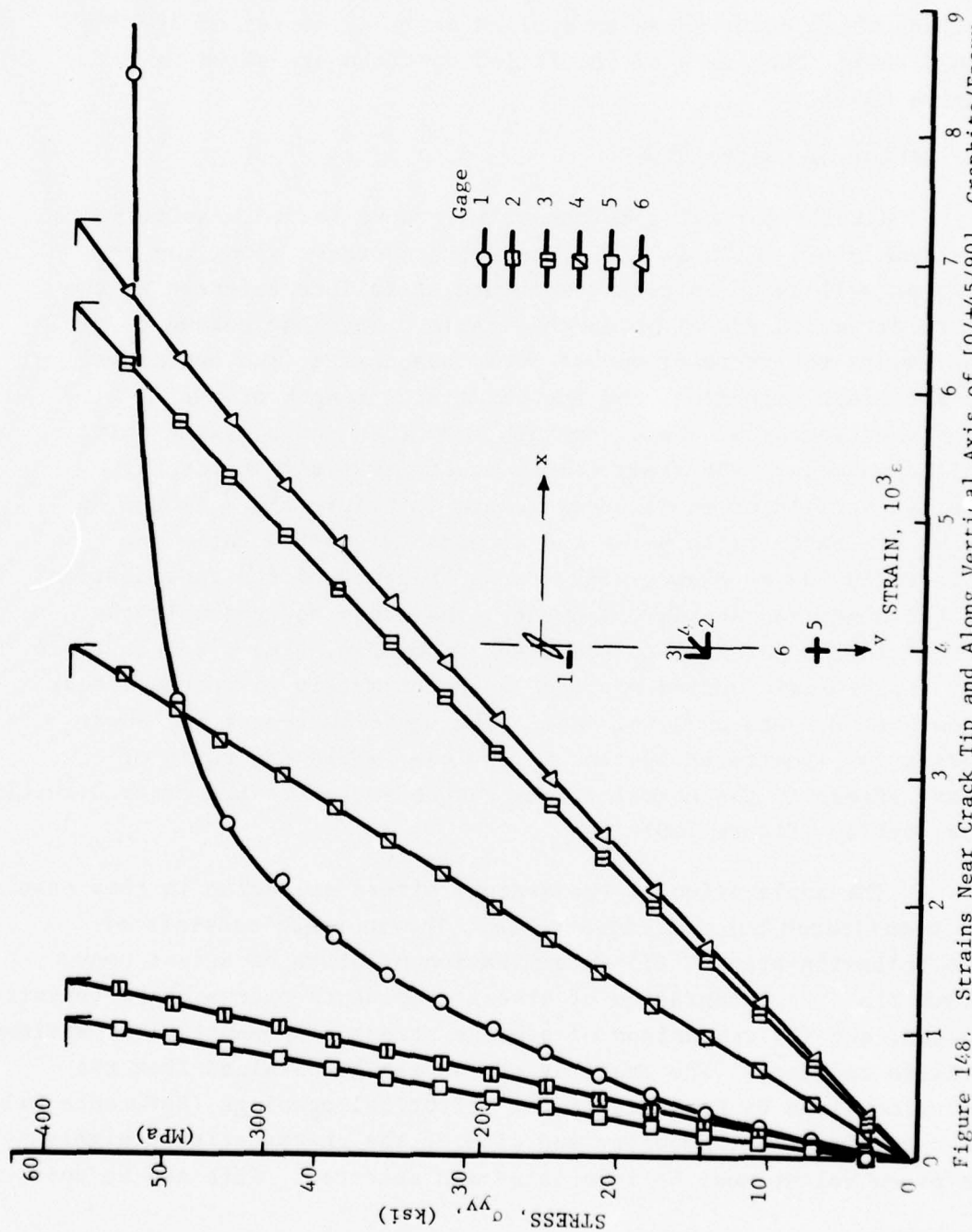
Figure 148. Strains Near Crack Tip and Along Vertical Axis of [0/±45/90]s Graphite/Epoxy Specimen With 0.64 cm (0.25 in.) Crack Under Biaxial Loading σ_{yy} = 1.96σ_{xx} at 30-Deg. With Crack Direction (Spec. No. 6-19A).
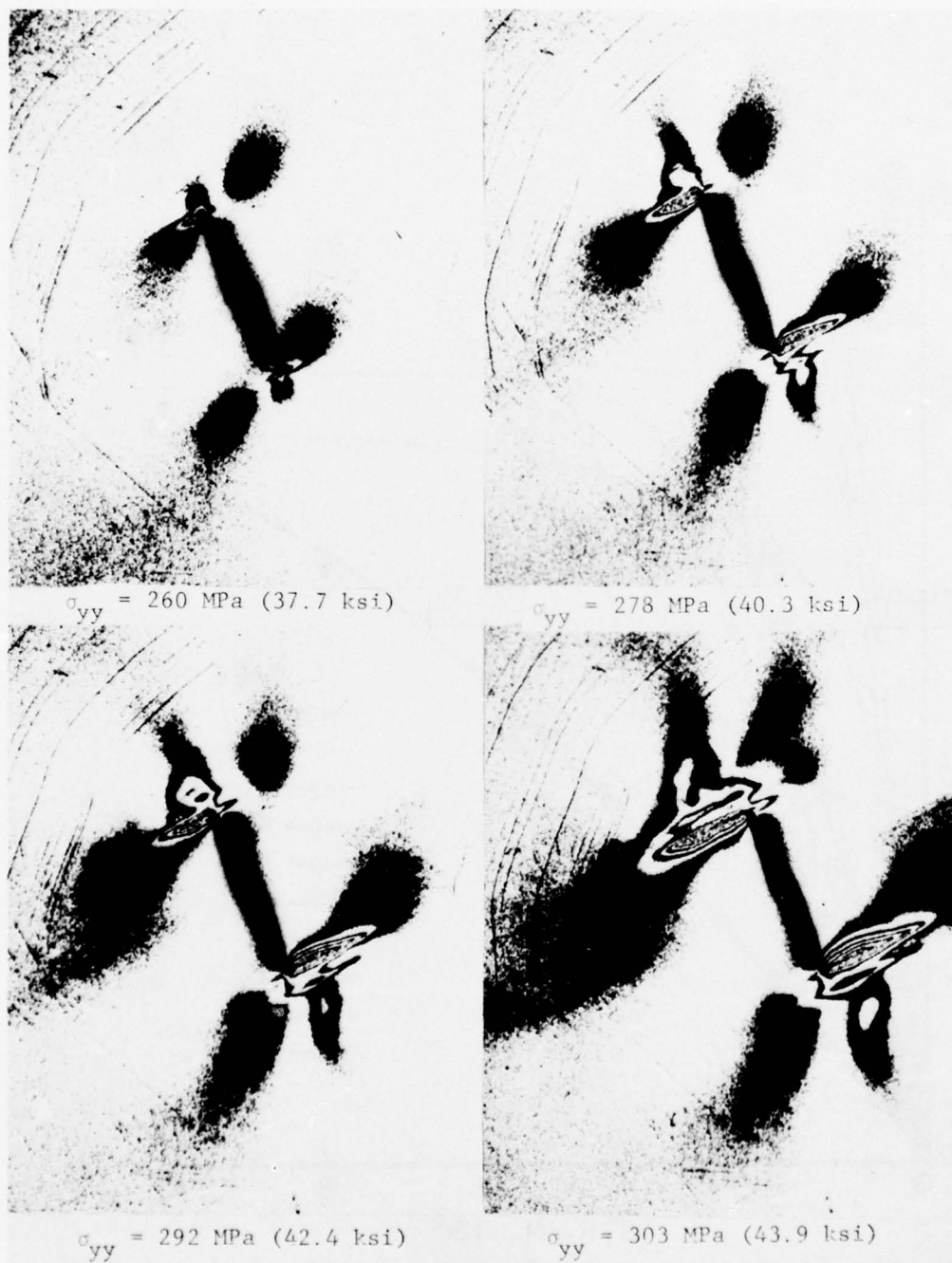
330 MPa (48 ksi). Far-field strains remained nearly linear to
failure which occurred at an applied vertical stress of 390 MPa
(56.5 ksi). Two views of the failed specimen are shown in
Figure 149.

5. EFFECT OF CRACK LENGTH

Results for all specimens with cracks loaded biaxially
are summarized in Table VIII. The failure stress along the y-
axis as well as the stress components at failure referred to the
crack direction are given in this table. The last column
represents the ratio of one of these components (the one normal
to the crack direction) and the uniaxial strength of the
unnotched laminate. This strength reduction ratio, based only
on the normal to the crack component of far-field stress, is
plotted as a function of crack length in Figure 150. As can be
seen this ratio falls below the strength reduction ratio for
uniaxially loaded plates with cracks, because of the contribution
of the other two stress components, the shear and possibly the
normal stress parallel to the crack direction. The strength ratio
for the biaxial loading applied is approximately 21 percent lower
than that for the uniaxial case. The contribution of the shear
stress is illustrated further in one case where the ratio of
shear stress to the normal stress perpendicular to the crack direction
was doubled (Figure 150).

The application of the average stress criterion in this case
is complicated but not intractable. The approach consists of
the following steps: (1) determination of state of stress near
crack tip, (2) integration of stress components over a characteristic
volume, and (3) comparison of average stress components with pertinent
failure envelope. The state of stress can be obtained from the
solution given by Lekhnitskii for elliptical openings (Reference 24).
Then the location, geometry and size of the characteristic highly
stressed volume must be identified and selected. This can be done

202
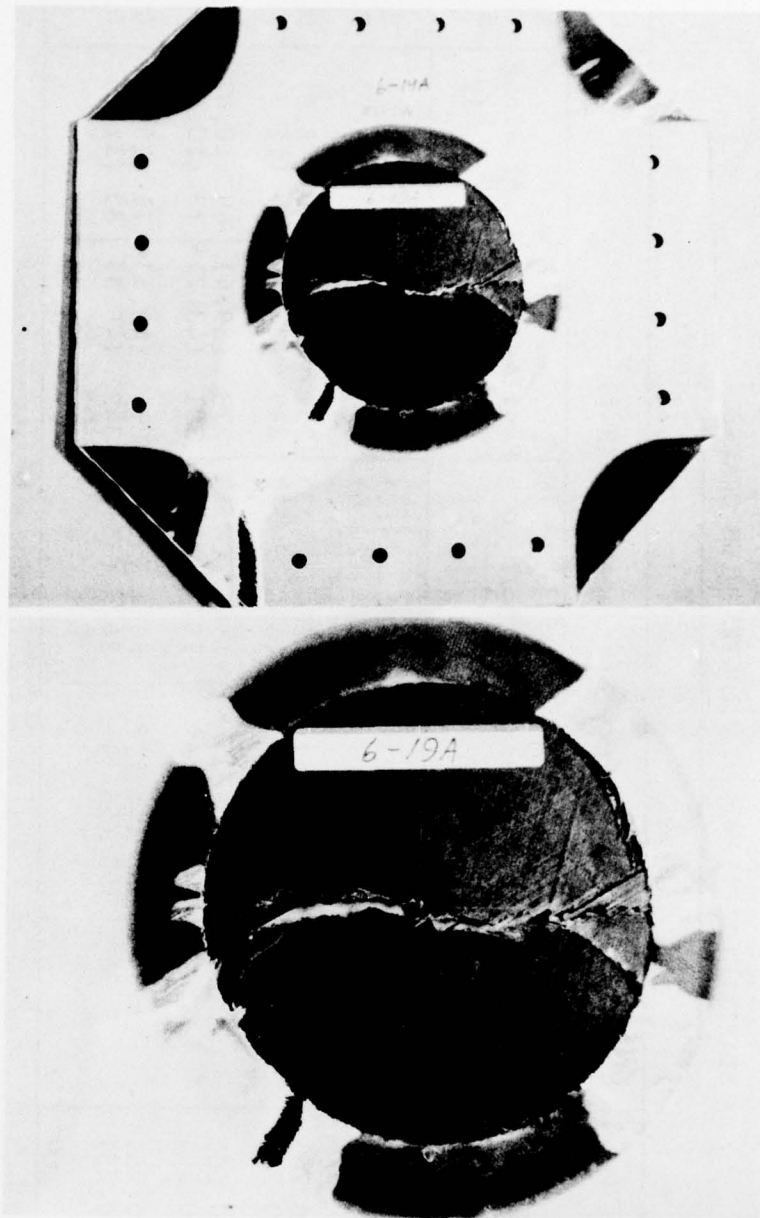
Figure 149. Biaxial Specimen with 0.64 cm (0.25 in.)
Long Crack After Failure (Spec. No. 6-19A).

TABLE VIII

BIAXIAL [0/±45/90]$_s$ LAMINATES WITH CRACKS

Spec. No.	Crack Length 2a cm (in.)	Biaxiality Ratio, σ_{yy}/σ_{xx}	Failure Stresses, MPa (ksi)				Stress Ratio, S_{11}/S_o
			Along y-axis S_{yy}	Normal to Crack, S_{11}	Parallel to Crack, S_{22}	Shear Along Crack, S_{12}	
6-12	2.54 (1.00)	1.98	264 (38.3)	165 (24.0)	232 (33.6)	57 (8.2)	0.343
6-20A	2.54 (1.00)	2.00	221 (32.0)	138 (20.0)	193 (28.0)	48 (6.9)	0.286
6-13	1.91 (0.75)	1.93	263 (38.1)	168 (24.3)	231 (33.5)	55 (8.0)	0.347
6-14	1.91 (0.75)	3.57	305 (44.0)	140 (20.2)	249 (36.1)	95 (13.7)	0.289
6-16	1.27 (0.50)	2.03	313 (45.3)	194 (28.1)	273 (39.6)	69 (10.0)	0.402
6-17A	1.27 (0.50)	1.97	343 (49.8)*	217 (31.4)*	301 (43.7)*	73 (10.6)*	0.449
6-18A	0.64 (0.25)	1.98	332 (48.1)*	208 (30.1)*	291 (42.1)*	71 (10.3)*	0.430
6-19A	0.64 (0.25)	1.96	390 (56.5)	247 (35.7)	342 (49.6)	83 (12.0)	0.510

* Tab Failure

204
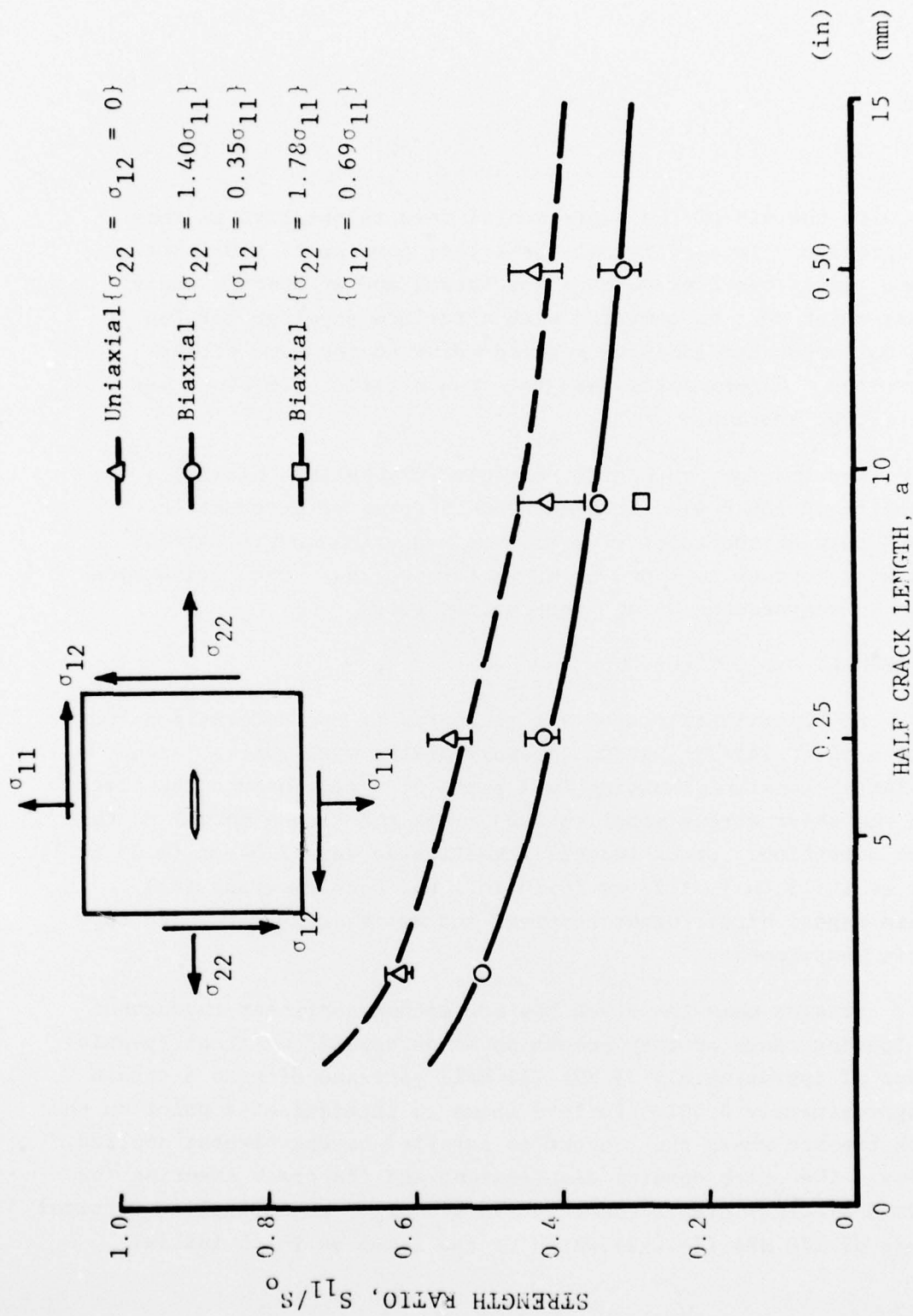
Figure 150. Strength Ratios as a Function of Crack Length for [0/+45/90]s Graphite/Epoxy Plates With Cracks Under Uniaxial and Biaxial Loading.

also with the aid of the experimental results obtained in this test program. Integration of the stress components over this volume yields two average normal stresses and an average shear stress which must be compared with a failure envelope for the same but unnotched laminate corresponding to the same stress conditions. Experimental data for such a failure envelope are not readily available.

Results for arbitrarily oriented cracks in a biaxial stress field could also be presented in terms of interaction curves between the critical symmetric and antisymmetric stress intensity factors as shown by Wu (Reference 25). Each crack size would be represented by one interaction curve.

6. SUMMARY AND CONCLUSIONS

An experimental study was conducted of the deformation and failure of $[0/\pm45/90]_s$ graphite/epoxy plates with cracks loaded in biaxial tension resulting in a state of stress around the crack with the shear stress equal to 0.35 times the stress normal to the crack direction. Crack lengths investigated were 2.54 cm (1.00 in.), 1.91 cm (0.75 in.), 1.27 cm (0.50 in.) and 0.64 cm (0.25 in.). Strain gages, birefringent coatings and moiré grids were used for strain measurement.

Strains near the crack tip are either nonlinear throughout the loading range or they become so at an applied vertical (y-axis) stress of approximately 75 MPa (11 ksi) corresponding to a strain of approximately 0.001. Failure seems to initiate at a point on the crack tip arc where the tangent is parallel to the highest applied stress. The crack opening displacement and the crack shearing (or forward sliding) displacement remain linear up to an applied vertical stress of 172 MPa (25 ksi) which is the level at which initial

206

crack or damage propagation takes place. At this level the crack
opening and crack shearing displacements begin to increase at a
much faster rate. The initial crack extension seems to be at
45-deg. to the original crack direction. Thereafter, the damage
zone consisting of subcracks parallel to the fibers of the various
plies propagates normally to the crack direction in most cases.
In one case crack propagation was observed at 25-deg. with the
crack direction and in another case damage propagation occurred
both parallel and normal to the crack direction. In those cases
where the peak strain near the crack tip was recorded up to failure,
it exceeded values of the order of 0.03.

The components of far-field stress at failure referred to
the crack direction were determined. Results were presented in
terms of the ratio of the normal to the crack stress and the
unnotched tensile strength of the laminate. This ratio was found
to be approximately 21 percent below that for uniaxially loaded
plates with transverse cracks, indicating an appreciable contribution
to failure of the shear stress. This percentage of strength ratio
reduction remained nearly the same for all crack sizes.

SECTION VII

SUMMARY, CONCLUSIONS AND RECOMMENDATIONS
FOR FUTURE WORK

An experimental program was conducted to study the
deformation and failure under uniaxial and biaxial tensile
loading of $[0/\pm45/90]_s$ graphite/epoxy plates with circular holes
and through-the-thickness cracks and to determine the influence
of notch size on failure. Experimental techniques used were
strain gages, photoelastic coatings and moire' grids. Notch
sizes investigated were 2.54 cm (1.00 in.), 1.91 cm (0.75 in.),
1.27 cm (0.50 in.) and 0.64 cm (0.25 in.). The following results
and conclusions were reached:

1. UNIAXIAL TESTS OF NOTCHED LAMINATES

   a) In the elastic range, the measured stress concentration
      is close to the theoretical value of 3 for circular
      holes.

   b) Strains near the discontinuity become nonlinear at
      a strain level of approximately 0.006 corresponding
      to initial failure of the 90-deg. plies.

   c) Maximum strains at failure on the hole boundary or
      near the crack tip exceed twice the ultimate strain
      of the unnotched laminate.

   d) In the specimens with circular holes, regions of high
      strain concentration with nonlinear response develop
      at four characteristic locations 22.5-deg. off the
      horizontal axis. Failure initiates at these points
      where the interlaminar and membrane shear stresses
      reach maximum values.

208

e) Failure at the tip of the crack takes the form of a damage zone consisting of ply subcracking and local delamination with occasional fiber breakage. Failure initiates off the very tip of the crack and propagates at an angle to it (approximately 40-deg).

f) The damage zone increases linearly with the square of the stress intensity factor K_I^2 up to a certain value of K_I, which is nearly constant with crack length. Thereafter, this zone increases linearly at a faster rate, which is independent of crack length.

g) Final failure occurs when the damage zone reaches some critical size.

h) The strength reduction ratio ranged between 0.40 and 0.64 for notch sizes between 2.54 cm (1.00 in.) and 0.64 cm (0.25 in.).

i) The effect of notch size was satisfactorily described using the average stress criterion. The average stress over a distance of 4 to 5 mm from the notch seems to give the best fit.

j) The strength reduction was independent of notch geometry, i.e., specimens with holes and cracks of the same size had the same strength.

k) In the case of circular holes it was found that there is a critical size below which the laminate becomes notch-insensitive.

2. BIAXIAL TESTS OF PLATES WITH HOLES

a) Strains on the boundary of the hole become nonlinear at applied stresses of $\sigma_{xx} = \sigma_{yy} \cong 120$ MPa (17.5 ksi)

corresponding to a strain level of approximately 4×10^{-3}. This is the strain level at which the response of the uniaxial unnotched specimens becomes nonlinear.

b) Initially, the circumferential strain is uniform around the boundary of the hole. Subsequently, with increasing load, regions of high strain concentration with nonlinear response develop at eight characteristic locations 22.5-deg. off the fiber axes.

c) Maximum strains at failure on the hole boundary reach values up to twice the ultimate strain of the unnotched laminate.

d) Failure initiates on the hole boundary at points 22.5 deg. off the horizontal and vertical axes.

e) The strength reduction ratio ranges between 0.56 and 0.76 for holes between 2.54 cm (1.00 in.) and 0.64 cm (0.25 in.) in diameter.

f) The strength reduction ratios are higher than corresponding values for uniaxial loading by approximately 30 percent.

g) The variation of strength reduction ratio with hole diameter can be satisfactorily described by using an average biaxial stress criterion over a radial distance of 3 mm.

h) The strength reduction ratios for uniaxial and equal tensile biaxial loading represent lower and upper bounds for any biaxial tensile loading of this laminate.

210

i) Quasi-isotropic laminates with circular cutouts subjected to any arbitrary biaxial tensile loading can be designed conservatively by assuming strength reduction ratios corresponding to uniaxial loading.

3. BIAXIAL TESTS OF PLATES WITH CRACKS

a) Failure seems to initiate at a point on the crack tip arc where the tangent is parallel to the highest applied stress.

b) The crack opening displacement and the crack shearing displacement remain linear up to the point where the damage zone begins to propagate. Thereafter, they increase at a much faster rate.

c) The initial crack extension seems to be at 45-deg. to the crack direction. Thereafter, in most cases, the damage zone propagates normally to the initial crack direction.

d) Peak strains as high as 0.03 were measured near the tip of the crack at failure.

e) A far-field shear stress equal to 0.35 times the stress normal to the crack (σ_{11}) reduces the normal stress (σ_{11}) at failure by approximately 21 percent from that for uniaxial loading normal to the crack. This relative strength reduction is independent of crack size.

4. RECOMMENDATIONS FOR FUTURE WORK

The work described in this report has already been extended to include a study of the effect of laminate construction. Plates of a more anisotropic layup, $[0_2/\pm45]_s$, with circular holes are

211

being tested under uniaxial and biaxial tensile loading. The
failure criteria that proved successful for the quasi-isotropic
laminate will be investigated in the angle-ply laminate above.
Testing of this layup with cracks is not currently planned, but
it would be of interest to study any peculiar damage zone growth
associated with this laminate. It is generally assumed in the
case of a crack in a biaxial stress field that the normal stress
in the direction of the crack has no influence on crack extension.
A task to investigate this hypothesis is currently being conducted.
Uniaxial tensile tests are conducted with cracks oriented with
respect to the load so that they produce the same ratio of shear
stress to the stress normal to the crack as in the case of the
biaxially loaded specimens discussed in Section VI. The only
difference between these two sets of tests will be the relative
magnitude of the normal stress in the direction of the crack.

One of the conclusions listed before is that, for the
quasi-isotropic laminate with circular holes, the strength reduction
ratios obtained by uniaxial and equal biaxial loading represent
lower and upper bounds. To check this conclusion and help obtain
interpolation curves for other biaxiality ratios it is recommended
that some limited biaxial testing be conducted for other biaxiality
ratios such as 2:1, 4:1 and 6:1.

The task of expressing an explicit failure criterion around
a crack in a general biaxial stress field remains to be done. This
is not hampered only by the complexity of computations but also by
the lack of adequate failure data under a general biaxial stress
field for the various laminates. The task can begin by establishing
reliable failure envelopes for the laminate in question for the
general biaxial state of stress. The procedure for establishing
an average stress criterion outlined before in Section VI could
be followed successfully. Additional testing is recommended with
cracks in biaxial fields of varying ratios of shear stress to

212

normal stress perpendicular to the crack to establish interaction
curves between the symmetric and antisymmetric stress intensity
factors. The variation of these interaction curves with crack
size could then be studied.

The observation of strain buildup and failure initiation
at 22.5-deg. locations off the fiber axes has been emphasized. In
all these cases the principal far-field stresses were oriented
along fiber directions. It has been suggested that some testing
of panels with holes be conducted with the loading at 22.5-deg.
to fiber axes. It will be of interest to see whether the points
of fracture initiation would still shift from the axes of loading
symmetry.

All work completed and planned currently deals with fiber
dominated laminates. It would be useful to extend the study of
notch stress concentration and notch size on matrix-dominated
laminates.

A great deal of emphasis is being placed and a great deal
of work is being done on the environmental effects of temperature
and moisture on composite laminates. A logical and most important
step would be to study these environmental effects on the behavior
of laminates with notches (holes and cracks) including the notch
size effect. The experimental stress analysis in these tests
need not be as extensive as that reported in this report.

Finally, another logical sequence of the static biaxial
testing conducted here would be to study the behavior of notched
laminates under cyclic biaxial loading. Modification of the
existing biaxial loading system to apply cyclic biaxial loading
is not very difficult.

REFERENCES

1. S.G. Lekhnitskii, Theory of Anisotropic Elastic Body,
   Translated by P. Fern, J.J. Brandstatter, ed., Holden-
   Day, San Francisco, 1963.

2. G.N. Savin, Stress Concentrations Around Holes, Pergamon
   Press, New York, London, 1961.

3. L.M. Lackman and R.M. Ault, "Mollifying Stress Fields
   by Using Filamentary Composite Materials," Advances in
   Structural Composites, SAMPE, Vol. 12, October 1967.

4. G.J. Wennagel, P.W. Mason and J.D. Rosenbaum, "Ideas,
   Integrated Design and Analysis System," Paper No. 680728,
   Soc. Auto. Engrs., Aeronautical and Space Engineering and
   Manufacturing Meeting, Los Angeles, Calif., Oct. 7-11, 1968.

5. A. Puppo and J. Haener, "Application of Micromechanics to
   Joints and Cutouts," U.S. Army Aviation Material Laboratory,
   Report No. 69-25, April 1969.

6. A. Levy, H. Armen and J.B. Whiteside, "Elastic and
   Plastic Interlaminar Shear Deformation in Laminated
   Composites Under Generalized Plane Stress," Presented at
   Air Force Third Conference on Matrix Methods in Structural
   Mechanics, WPAFB, Ohio, October 1971.

7. E.F. Rybicki and A.T. Hopper, "Analytical Investigation
   of Stress Concentrations Due to Holes in Fiber-Reinforced
   Plastic Laminated Plates; Three-Dimensional Models,"
   Air Force Materials Lab. Report, AFML-TR-73-100, June 1973.

8. J.B. Whiteside, I.M. Daniel and R.E. Rowlands, "The Behavior
   of Advanced Filamentary Composite Plates with Cutouts,"
   AFFDL-TR-73-48, June 1973.

9. I.M. Daniel and R.E. Rowlands, "Determination of Strain
   Concentration in Composites by Moiré Techniques," Journal
   Composite Materials, Vol. 5, April 1971, pp. 250-254.

10. R.E. Rowlands, I.M. Daniel and J.B. Whiteside, "Stress
    and Failure Analysis of a Glass-Epoxy Plate with a Hole,"
    Experimental Mechanics, Vol. 13, pp. 31-37, Jan. 1973.

11. I.M. Daniel, R.E. Rowlands, and J.B. Whiteside, "Deformation
    and Failure of Boron-Epoxy Plate with Circular Hole,"
    Analysis of the Test Methods for High Modulus Fibers and
    Composites, ASTM STP 521, American Society for Testing and
    Materials, pp. 143-164, 1973.

REFERENCES (Cont'd)

12.   R.E. Rowlands, I.M. Daniel, and J.B. Whiteside, "Mechanical Behavior of a Graphite-Epoxy Laminate Containing a Hole," _Proceedings of Sixth St. Louis Symposium on Composite Materials_, St. Louis, Missouri, 1972.

13.   I.M. Daniel, R.E. Rowlands, and J.B. Whiteside, "Effects of Material and Stacking Sequence on Behavior of Composite Plates with Holes, " _Experimental Mechanics_, Vol. 14, pp. 1-9, Jan. 1974.

14.   R.E. Rowlands, I.M.Daniel, and J.B. Whiteside, "Geometric and Loading Effects on Strength of Composite Plates with Cutouts," _Composite Materials: Testing and Design_ (Third Conference), ASTM STP 546, American Society for Testing and Materials, pp. 361-375, 1974.

15.   L.B. Greszczuk, "Stress Concentrations and Failure Criteria for Orthotropic and Anisotropic Composite Plates with Circular Openings," _Composite Materials; Testing and Design_ (Second Conference), ASTM, STP 497 (1972).

16.   M.E. Waddoups, J.R. Eisenmann and B.E. Kaminski, "Macroscopic Fracture Mechanisms of Advanced Composite Materials," _J. of Composite Materials_, Vol. 5, Oct. 1971, pp. 446-454.

17.   T.A. Cruse, "Tensile Strength of Notched Composites," _J. of Composite Materials_, Vol. 7, 1973, p. 218.

18.   J.M. Whitney and R.J. Nuismer, "Stress Fracture Criteria for Laminated Composites Containing Stress Concentrations," _J. Composite Materials_, Vol. 8, July 1974, pp. 253-265.

19.   I.M. Daniel, R.E. Rowlands and D. Post, "Strain Analysis of Composites by Moire Methods," _Experimental Mechanics_, Vol. 13, June 1973, pp. 246-252.

20.   J.F. Mandell, Su-Su Wang and F.J. McGarry, "The Extension of Crack Tip Damage Zones in Fiber Reinforced Plastic Laminates," _J. Composite Materials_, Vol. 9, July 1975, pp. 266-287.

21.   W. Elber, "Mechanical Modification of Fracture Toughness Properties of Graphite/Epoxy Composites," to be presented at Gordon Conference on "Deformation and Failure Mechanisms in Polymer Composites," Jan. 3-10, 1977, Santa Barbara, California.

REFERENCES (Cont'd)

22. J.M. Whitney, "Durability of Fiber Reinforced Resin
     Matrix Composites," Mechanics of Composites Review,
     Air Force Materials Laboratory, 26-28 October 1976,
     Dayton, Ohio.

23. R.S. Sandhu, "Ultimate Strength Analysis of Symmetric
     Laminates," Air Force Flight Dynamics Laboratory,
     AFFDL-TR-73-137, Feb. 1974.

24. S.G. Lekhnitskii, Anisotropic Plates, Translated from
     Second Russian Edition by S.W. Tsai and T. Cheron,
     Gordon and Breach, Science Publishers, Inc., New York,
     1968.

25. E.M. Wu, "Fracture Mechanics of Anisotropic Plates,"
     in Composite Materials Workshop, edited by S.W. Tsai,
     J.C. Halpin and N.J. Pagano, Technomic Publishing Co.
     Inc., Stamford, Conn., 1968.